ENGINEERING PROPERTIES AND STRUCTURAL BEHAVIOUR OF HIGH STRENGTH REINFORCED CONCRETE BEAMS

BY

Osama K. Adwan, BSc (Hons)

Thesis submitted to the

University of Abertay Dundee

in Candidature for The Degree of

Doctor of Philosophy

July 1997

I certify that this thesis is the true and accurate version of the thesis approved by the exami[redacted]

Signe[redacted] ..... Date ..12/9/97.....

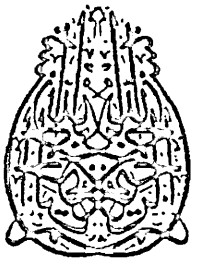

IN THE NAME OF GOD, MOST GRACIOUS MOST MERCIFUL

They Ask Thee Concerning the Spirit (of Inspiration).

Say: " The Spirit (Cometh) by Command of my Lord:

of Knowledge It is Only a Little that is Communicated to You,

(O Men!)"

The Holy Qur'an Verse 85,Chapter 17

Dedication

This thesis is dedicated to

my Mum and Dad

With gratitude, love and thanks for all the sacrifices they have made to help me succeed

Osama

DECLARATION

I, the undersigned hereby declare that, the work contained in this thesis was carried out by myself at the University of Abertay Dundee, in the School of Construction & Environment, under the supervision of Professor Susanta Sarkar.

I also wish to declare that, except where for commonly understood ideas, or where due stated acknowledgement is made, this work presented herein has not been submitted previously in any application for a higher degree.

Singe[redacted]Osama. K. Adwan)

Date.....22/07/1997.....

ACKNOWLEDGEMENTS

Firstly, the author wishes to express his deep gratitude to Professor Susanta Sarkar, chairman of his supervisory committee of this research study, for his invaluable guidance and supervision throughout the entire study. The author is deeply grateful to Dr. John Munday for his valuable comments, suggestion and also serving on his supervisory committee. The author is greatly indebted to Dr. Ali Shaat for the abundance of help and guidance at the early stage of this research programme.

The author is also indebted to the technical staff namely Messrs Alex Thomson, Moir Smart and Jerry Duncan of School of Construction & Environment at the University of Abertay Dundee, for their co-operation, and assistance in batching, testing and setting up the experiments. Special thanks go to the head technician Mr. Galloway for his assistance and commitment.

The help which UAD *Research Committee* has given by financing me at the School of Construction and Environment is greatly appreciated, without it the study could not have been undertaken.

Finally, it is a great privilege to have this opportunity to sign out the author's heartfelt indebtedness and gratitude to his parents (Professor Kamel Adwan and Mrs Fatema Adwan) and sisters (Sabah and Sawsan) whose support, blessings and constant encouragement tided him over this study.

ABSTRACT

High Strength Concrete (HSC) has become a viable alternative to lower strength concrete. However, its utilisation is increasing faster than the development of suitable design recommendations. This is because limited and diverse investigations have been carried out concerning engineering properties and structural behaviour of HSC. The experimental investigation and theoretical considerations described in this thesis have been undertaken as an attempt to start to remedy this problem.

As part of the investigation into the structural behaviour of HSC beams, a series of 18 different concrete mixes were tested in order to optimise HSC mixes using local aggregates. The effect of different factors such as w/c ratios, silica fume and superplasticizer dosages on compressive strength and splitting tensile strengths in the range of 80 to 120 N/mm^2 (MPa) were studied. Additionally, new mathematical expressions were developed to replace some of the currently used relationships concerning HSC as a material, for a wide range of concrete mixes.

The second part of this investigation concerned the structural behaviour of singly reinforced HSC beams in flexure. A total of 13 beams were manufactured using selected concrete mixes obtained from the first part of the investigation, i.e., 80, 100 and 120 MPa respectively. The size of the beam specimens was determined in order to make the beam fail in flexure, and also to be sufficiently large to simulate a real structural element of HSC. There were three beams in each of four groups, with the exception of group two which had four. For each group of beams the tensile reinforcement ratios were 1.03%, 1.42%, 1.94%, and 4.04% respectively. The test variables were thus the concrete strength and the longitudinal reinforcement ratio.

The third part of this investigation concerned the structural behaviour of doubly reinforced HSC beams in flexure. Four beams were cast and tested using the same

criteria of the singly reinforced beams. The variables considered were tensile and compressive reinforcement ratios.

All beams in flexure were tested in a closed-loop testing machine under incrementally increased loading. Based on experimental evaluations and analytical considerations, the results are presented in terms of load-deflection characteristics, moment-rotation relationship, flexural strength capacity of high strength reinforced concrete (HSRC) beams, sectional ductility, crack patterns and surface crack width. Further, theoretical analyses were undertaken to idealise the nature of the concrete stress block developed in HSRC beams from elastic to ultimate load condition. In other words, proper idealisations of stress blocks were suggested in order to calculate the ultimate flexural capacity of HSRC members in good accuracy with experimental data obtained. The proposed equations have demonstrated rigorous outcomes on the flexural design of HSRC beams, providing a means of determining the internal forces in the context of compatibility of strains and equilibrium conditions of concrete. Additionally, the existing code of practice recommendations (BS 8110) were critically examined at ultimate strength capacity for HSRC beams having concrete strengths far beyond the limits normally considered in the code.

The fourth part of this investigation concerned the shear capacity of HSRC beams. A total of 23 reinforced concrete beams,with and without shear reinforcement, were tested to determine their diagonal cracking and ultimate shear capacities. In beams without web reinforcement the shear span/ depth ratio was kept constant at 2 whilst concrete strength and flexural reinforcement ratio were varied. The concrete strength was varied from 40 to about 120 MPa while the steel reinforcement ratios were 1.94%, 2.92% and 4.04%. In beams with web reinforcement the variables were the same as beams without web reinforcement but in addition the a/d ratio was varied as 1.5, 1.75, 2 and 2.6. One series of beams were cast with a preformed smooth inclined crack in order to remove aggregate interlock capacity. The effect of different parameters on shear capacity,

structural behaviour in terms of load-deflection response, shear contribution carried by different mechanisms and shear ductility of HSRC beams were studied. In addition, an evaluation of some existing expressions from codes of practice used in calculating the shear stress were carried out to determine their applicability to HSRC beams. From this, new design equations have been developed to predict the ultimate shear stress of HSRC beams.

CONTENTS

3 EXPERIMENTAL PROGRAMME IN FLEXURE

4 PRESENTATION OF EXPERIMENTAL RESULTS IN FLEXURE

5 THEORETICAL CONSIDERATIONS AND COMPARISON WITH EXPERIMENTAL RESULTS IN FLEXURE

LIST OF FIGURES

LIST OF TABLES

APPENDICES TABLES

LIST OF SYMBOLS

f_{cu}	= compressive strength of concrete cubes, *MPa*
f_c	= compressive strength of concrete cylinder, *MPa*
f_r	= modulus of rupture, *MPa*
f_{sp}	= splitting cylinder tensile strength, *MPa*
E_c	= modulus of elasticity of concrete, *MPa*
k_1, k_2, k_3	= coefficient pertaining to amount and position of internal compressive force
β	= plasticity ratio
θ	= rotation, radians
ε_u	= strain at extreme compression fibre
k_d	= neutral axis depth in, *mm*
d_1	= Demec-gauge distance 200 *mm*
I_{cr}	= moment of inertia of the cracked transformed area, mm^4
I_g	= moment of inertia of gross-section, mm^4
Ie	= effective moment of inertia, mm^4
x	= neutral axis for a cracked section
m	= modular ratio (E_s / E_c)
M_u	= measured ultimate moment capacity, *kNm*
M_n	= nominal ultimate moment capacity, *kNm*
M_{cr}	= cracked moment, *kNm*
y	= distance from centroid axis of cross section neglecting reinforcement, *mm*
δ_1	= deflection at midspan due to life loads, *mm*
l	= beam span between two supports, 3240 *mm*
a	= distance from end support to one loading point, 1320 *mm*
a / d	= shear span to depth ratio
C	= the area of compression force, *kN*

ζ = the location of centroid from neutral axis, *mm*

λ = the distance from the extreme compression fibre to the resultant force, *mm*

$\bar{x}$ = centre distance from extreme compression fibre, *mm*

d = distance from extreme compression fibre to centroid of tension reinforcement, *mm*

b = width of beam, 150 *mm*

A_s = area of flexural reinforcement, mm^2

ψ_u = curvature at ultimate stage, *radian/mm*

ψ_y = curvature at yield stage, *radian/mm*

μ_c = curvature ductility index, ψ_u / ψ_y

ρ = flexural steel ratio, $A_s / b\,d$

ρ_v = shear reinforcement ratio, $A_w / b\,s$

s = spacing of shear reinforcement, *mm*

W_{avg} = average crack width at the level of tensile reinforcement, *mm*

f_y = yield point stress of reinforcement, *MPa*

S_m = average final spacing between cracks, *mm*

v_{cr} = shear capacity at inclined cracking load of a beam, *MPa*

v_u = ultimate shear stress of a beam, *MPa*

v_a = shear stress carried by aggregate interlock, *MPa*

ρ_r = A_s / A_e for computation of crack spacings.

CHAPTER 1

INTRODUCTION

1.1 General

In general terms, as the review suggests high strength concrete (HSC) may be defined as any concrete which satisfies performance criteria not usually achieved by concrete ordinarily available. Meanwhile, concrete which provides substantially improved resistance to environmental influences, i.e., durability under service conditions, or substantially enhanced mechanical properties is indeed high performance concrete. HSC can be produced using relatively high cement contents, or using admixtures such as superplasticizer and supplementary cementitious materials such as silica fume. Moreover, the production of such concrete requires special attention to be paid to the mix ingredients. A survey of available literature addressing the characteristics of HSC mixes indicates that while there has been a significant amount of research conducted, the research lacks coherence.

During the past few years, HSC has been generating increasing interest amongst civil and structural engineers. The commercial use of this new material is expanding steadily, and this can be explained partially by the life cycle cost-performance ratio it offers, as well as its outstanding engineering properties[84]. These outstanding properties justify its use in structures in a number of cases in spite of its somewhat higher initial cost than normal strength concrete (NSC). In short, HSC is now being considered for a much wider range of structural applications[97]. However, from the literature it is clear that while a number of international research investigations are currently being undertaken with the aim of spreading its applications, only limited research is being undertaken in the UK.

The flexural design recommendations in codes of practice are derived from research conducted essentially on NSC up to 50 *MPa* compressive strength. Also, recent studies[4,9] dealing with the concrete stress-strain behaviour have shown that significant differences exist between normal and high strength concretes. In view of this, the current design recommendations of BS 8110 must be assessed in relation to high-strength members in flexure.

A survey of the published literature addressing the flexural behaviour of high strength reinforced concrete (HSRC) members has shown that most of the previous studies have been limited to strengths of up to only 80 *MPa*, and were aimed to verify the ACI code recommendations. Accordingly there appears to be no existing research work which has been carried out to verify the BS 8110 design recommendations for HSC beams under flexure. An assessment of design requirements for HSRC beams having strengths in excess of 80 *MPa* is required to supplement the provisions of the code of practice.

Additionally, despite the amount of research work that has been carried out on HSC as a material, additional work on the behaviour of structural elements using HSRC subjected to shear is required. Information regarding the shear ductility, shear contribution of different elements and failure mode mechanisms for HSRC beams is almost non- existent.

Overall, the research reported herein is an attempt to bridge some of these gaps and remedy some problems related to the engineering properties and structural behaviour of HSRC beams in flexure and shear.

1.2 Definition of High Strength Concrete

High strength concrete is a term related to the obvious and dramatic changes in the field of concrete technology with such material and the associated potential of novel forms of construction over the past few decades.

Normal weight HSC has been defined as concrete with density of about 2400 kg/m^3 having compressive strengths in the range of 55 to 85 *MPa*. Concrete with compressive strength varying between 35 to 55 *MPa* is defined as medium strength concrete (MSC), and that with concrete compressive strength below 35 *MPa* as low strength concrete (LSC). The definition of HSC adopted in this research investigation is '*a workable concrete with cube compressive strengths in the range of 75 to 120 MPa at 28 days*'. One must remember, that to achieve concrete strength in this range implies the use of two additives, namely superplasticizer and silica fume.

1.3 Objectives of the Investigation

The overall purpose of this investigation was to go some-way towards determining information which fills the present gaps in fundamental engineering knowledge of HSC in a manner which is directly useful in the field of concrete technology and structures. The objectives can be stated as follows:

1. To optimise the constituents of concrete mixes having compressive strength in the range of 70 to 120 *MPa* following a trial batch programme techniques by studying the effect of different factors such as w/c ratio, cement content, silica fume and superplasticizer on the compressive strength and splitting cylinder strength of HSC mixes.
2. On the basis of the experimental results and using the statistical analysis, the existing relationships between the compressive strength and the splitting cylinder

strength will be evaluated for HSC. An attempt will be made to develop a new relationship for a wide range of HSC mixes.

3. On the basis of the experimental results and the available literature a mathematical expression will be developed in order to predict the compressive strength of HSC mixes in terms of their constituents proportions.
4. To evaluate HSC as a material for use in a typical civil engineering structure,i.e., beams under flexure, through a substantial experimental and theoretical investigation. A comparison will be made between the experimental and theoretical results of load-deflection, moment-rotation, surface cracking patterns and surface crack width of HSRC beams. In addition, the ductility of HSRC beams will be evaluated in the context of the data obtained.
5. On the basis of experimental data and theoretical analysis made, the current design ultimate limit state stress block of BS 8110 will be evaluated for HSRC beams in flexure. If appropriate alternative idealisations of the stress block will be suggested in order to predict the ultimate moment capacity of HSRC beams.
6. To evaluate the shear capacity of HSRC beams through a programme of experimental and theoretical investigation including the effects of different parameters on the shear strength, e.g., concrete compressive strength (f_{cu}), longitudinal reinforcement ratio (ρ) and shear span to depth ratio (a/d). The structural behaviour in terms of load-deflection response, the shear ductility and ductility index of HSRC beams and the shear contribution which is provided by different mechanisms, e.g., the aggregate interlock, compression zone and dowel action will also be studied.

   Various expressions from existing codes of practice used in estimating the shear capacity of beams will be considered to determine if changes are necessary for safe and economical use of HSC, leading to the development of design equations in order to predict the ultimate shear capacity of HSRC beams.

7. In the context of above study, the physical mechanism of the diagonal shear crack by which failure is initiated, and the behaviour of the diagonal shear crack by which failure is propagated will be studied in some details.

1.4 Scope and Format

The state of current knowledge, determined through a comprehensive review of past research work related to HSC ,particularly materials, behaviour of reinforced concrete members in flexure and shear capacity of reinforced concrete beams is presented in Chapter 2. The programme of work for HSC in flexure is described in Chapter 3 to 5.

Chapter 3 describes in detail the development of HSC mixes and the manufacture and testing procedures of reinforced concrete specimens in flexure. All the experimental results in flexure are presented in Chapter 4 while Chapter 5 deals with theoretical considerations and comparison with experimental results related to HSC as a mix as well as HSRC beams in flexure. This includes load-deflection characteristics, analysis for ultimate flexural strength of HSRC beams, ductility and ductility indices and surface crack width.

The experimental programme in shear is presented in Chapter 6 which includes the specimen details, testing procedure and material used. Chapter 7 provides an analysis of all the experimental results on shear, including the effect of different variables on shear stress, load-deflection behaviour, crack pattern development, estimation of shear transfer contribution carried by different mechanisms and shear ductility of HSRC beams. Chapter 8 deals with theoretical considerations in shear and considers the mechanism of beam shear failure, propagation mechanism of diagonal shear crack and the analysis methods of shear transfer mechanism.

The overall conclusions and recommendations for further research needed are given in chapter 9.

Five appendices are also included in this thesis. Appendix A contains tables of load-flexural strains at mid-span along depth of all beams tested. Appendix B incudes tables of characteristic mid-span load deflection curves for both experimental and analytical data. Appendix C contains tables pertaining to the characteristic mid-span moment-rotation curves while Appendix D presents the load-strain curves of tensile reinforcements, pictorial views of cracking patterns of HSRC beams at different load stages, sample calculations of ultimate moment capacity of a typical beam and the calculated versus measured shear stress of HSRC beams .

CHAPTER 2

LITERATURE REVIEW

In this chapter the results of the review of extensive published literature of high strength concrete are presented in four sections:

Section one deals with the properties of high strength concrete incorporating silica fume.

Section two deals with the structural behaviour of high strength concrete beams in flexure.

Section three reports on shear capacity of reinforced concrete beams.

Section four presents the main conclusions drawn from the literature reviewed on high strength concrete from both materials and structural behaviour point of view.

2.1 Section One: Properties of High Strength Concrete

2.1.1 Effect of silica fume on high strength concrete

a. Strength

Yogendran *et al.*[149] investigated the efficiency of silica fume in influencing the strength of HSC at different water-cement ratios and dosages of silica fume. A high strength concrete mix with no air entrainment was designed to achieve a 28 day compressive strength in the range of 50 to 70 *MPa* by optimising some of the factors that affect the compressive strength. The mix parameters for the HSC's were selected after several trial mixes without using either silica fume or superplasticizer,i.e., control mix. In all the concrete tested, the silica fume replacement percentages by weight were varied from 0 to 30 percent. Aggregate-cement ratios by weight for all the concretes varied from 3.0 to 3.5. Three main series of concrete were tested: **series 1** contained concretes in which the quantity of mixing water was adjusted to maintain a constant slump of 50 mm for each silica fume replacement; in **series 2** water-

cement ratio was kept constant at 0.34 as silica fume contents were varied; **series 3** consisted of concretes with water-cement ratios of 0.34 and 0.28. The slump in series 1 was maintained at 50 *mm* by varying the dosage of superplasticizer. The test specimens were 300 x 150 *mm* cylinders for compressive strength. The main conclusions were: for **series 1** concretes with 5 to 30 % replacement of cement by silica fume there was no increase in water demand for up to 5% replacement. A 5 % replacement produced the highest compressive strength at 7 and 28 days,i.e., optimum level of cement replacement. Silica fume dosages of 25 and 30 percent produced lower strengths at all test ages. For **series 2** concretes with a constant water-cement ratio, and 5 % of silica fume replacement, no change in slump was observed compared to that of the control mix. The compressive strengths at 7, 28, and 56 days of concrete with 5% replacement were slightly higher compared with those of the control mix. For **series 3** it was concluded that with 0.34 w/c ratio the amount of superplasticizer required to maintain the slump of 50 *mm* increased linearly for 10 to 30% replacement, while at 5 % replacement no superplasticizer was required. Similar conclusions were drawn by Hjorth[63] from a similar experimental programme. Furthermore, the maximum compressive strength of mixes with a w/c ratio of 0.34 was at 15 % silica fume replacement at all ages tested. However, for concrete with a w/c ratio of 0.28 and 5, 10 and 15% silica fume replacement level, the strength at 28, 56 and 91 days decreased compared to control concretes even at 5% replacement, as shown in Fig. 2.1. It was further noted that with silica fume replacement at 20% much lower compressive strengths were observed. Similar results were also obtained by Tu[140] and Gjorv[57] who reported that the inclusion of silica fume increased the cohesiveness and stability of fresh concrete and moreover, that even a small amount of silica fume generally improved the mechanical properties of concrete.

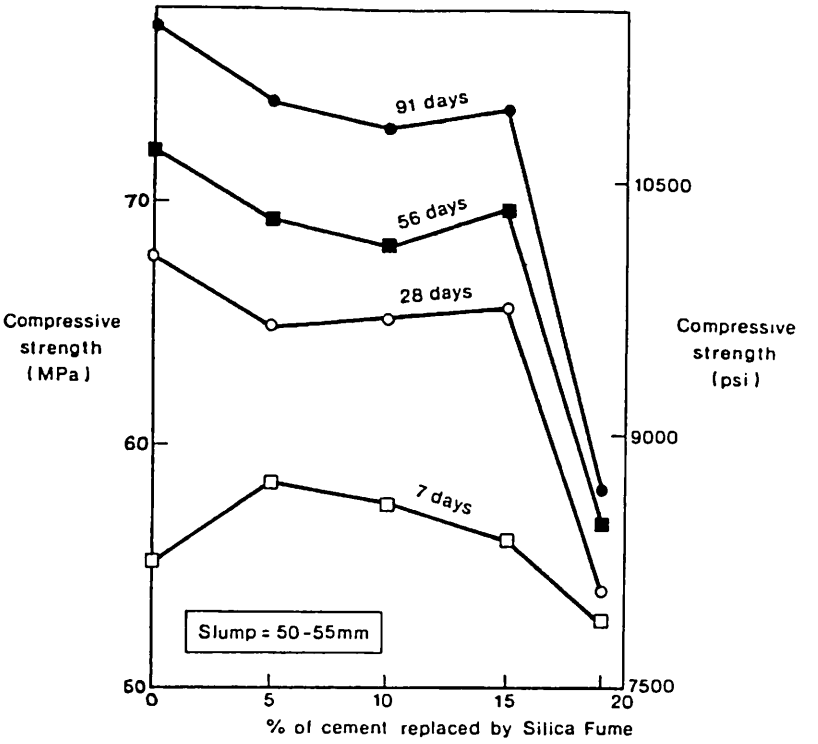

Fig. 2.1- Effect of silica fume and age on strength at 0.28 w/c ratio. [149]

Bentur and Goldman[22] investigated the effect of curing on the strength and physical properties of high strength silica fume concretes. The results were evaluated and compared with reference to Portland cement concrete, having either the same cement content as the silica fume concrete or the same w/c ratio. They concluded that: in the presence of silica fume, the concrete compressive strength increased markedly, especially at 28 days. This observation was recently confirmed by Novokshchenov[102] for silica fume dosage of 20%, and by Mak *et al.*[85] at 8% of silica fume dosage.

Aitcin and Laplante[14] investigated the long-term compressive strength of silica fume concrete. They reported the results of compressive strength tests on 4 to 6 years old cores obtained from well documented field experiments where both silica fume and non-silica fume concrete mixes were used. All the concrete specimens were exposed to freeze and thawing cycles and heavy de-icing salt applications. The results clearly showed that silica fume field concretes did not experience any strength loss compared to the non-silica fume concretes. Also, the compressive strength test results obtained from concrete cores taken after a 4-year period from an experimental column built with a very high strength concrete confirmed that there was no tendency for strength loss in silica-fume concretes. On the other hand, a study carried out by Carette[32] on the long term strength of silica fume concretes contradicted the above. He concluded that losses in compressive strength occurred between 90 days and 4 years on silica fume high strength concretes cured in air. This latter result was confirmed by De Larrad *et al.*[46] , on silica fume concretes having 28 day strength of 100 *MPa* when tested at 4 years.

Recently research work has been carried out by Cong *et al.*[42] which aimed to investigate the role of silica fume in influencing the compressive strength of the constituent phases of cement paste, mortar and concrete. They put forward an explanation for the role of silica fume in influencing the strength of concrete in terms

of its observed ability to strengthen the bond between cement paste and aggregate. Their tests were accomplished using concretes with w/c ratio ranging from 0.30 to 0.39 in mixes incorporating (i) no admixtures, (ii) a superplasticizer only and (iii) silica fume and a superplasticizer. They concluded that a partial replacement of cement by silica fume exhibits an increased compressive strength, which was due to the improved strength characteristic of its cement paste. They also concluded that a reduction in the strength of the concrete mix occurred at higher dosages of superplasticizer due to segregation.

Mor *et al.*[93] studied the fatigue of HSRC. Both lightweight and normal weight aggregate concretes were tested under reversible loading under both submerged and air dry conditions. Fatigue capacity of light weight aggregate concrete was similar to or better than that of normal weight aggregate concrete of similar strength properties. They found that fatigue capacity of HSRC directly related to the bond between concrete and reinforcement and not to any other strength property. Moreover, the addition of silica fume to light weight aggregate concrete improved its bond by 100 % and its fatigue life by over 60 %. On the other hand, no significant improvement was observed when silica fume was added to normal weight aggregate concrete.

b. Durability

Cabrerra and Claisse[30] studied the chloride penetration into silica fume concrete as chloride induced corrosion of reinforcement is a major factor affecting the service life of concrete structures. The likely effect of using silica fume to reduce chloride penetration was measured by using a ponding type experiment and by an electrical method. They concluded that due to the special nature of the silica fume HSC mixes the electrical tests were not a reliable way of measuring the effect of chloride penetration. However, they observed that HSC mixes were less permeable than the OPC mixes. Chloride penetration and corrosion of reinforcement in concrete containing silica fume was also investigated by Kazuyuki *et al.*[74]. They concluded

that the use of silica fume could effectively reduce the chloride penetration of concrete and improve the protective function of concrete against the chloride corrosion of steel bars. The recommended replacement ratio of silica fume was approximately 10% by weight of cement. This replacement dosage was supported by Tachibana *et al.*[130] who reported freezing and thawing test results which showed that HSC containing 10% silica fume was durable with almost no scaling observed. Furthermore, it was confirmed by Tachibana[130] and Benturand and Goldman[22] that silica fume HSC exhibited less drying shrinkage than conventional OPC; the creep coefficients were also significantly smaller compared with those of non-silica fume concretes. Figs. 2.3, and 2.4 show the significant effect of silica fume on creep, and drying shrinkage of HSC.

Bickley *et al.*[23] investigated the permeability and strength of in-situ HSC in the 68 storey Scotia Plaza in Toronto. With the thought of strength loss of silica fume concretes after long exposure to humidity the strength and quality of the concrete in-situ at ages up to 2 years were determined. The compressive strength of cores drilled from columns were compared with compressive strength of standard cylinder tests. A total of 16 core specimens were collected. Eight of the cores were tested in air dry condition at an age of approximately 1 year. The other eight cores were sealed at 1 year and tested in an air dry condition at an age of approximately 2 years. For permeability tests: three specimens were tested at approximately 1 year of age to determine water, and chloride permeability in accordance with AASHTO T277. Three other specimens were similarly tested at an age of approximately 2 years. Throughout the test period satisfactory concrete of low permeability to water and chloride was obtained. Also, a petrographic examination showed that the concrete at 1 and 2 years was sound and free of any evidence of developing deleterious reaction,i.e., micro cracking. The latter result was also confirmed elsewhere by Sarkar *et al.*[117] for HSC's. The compressive strength test results showed that the strength of the in-situ cores was less than the standard cured cylinders by about 15%.

On the other hand, the core strengths at the age of 2 years were slightly higher than those at the age of 1 year.

Another investigation carried by Wolsiefer[148] '*concerning strength and durability of silica fume high strength concrete'* concluded that the useful dosage rate of silica fume is 20% by weight of cement as f_{cu} is concerned. On the other hand, freeze-thaw, abrasion resistance, and de-icer scaling tests were also conducted in order to investigate the durability of HSC. It was concluded that high strength concrete exhibited low expansion and weight loss percentages along with a high durability factor, low abrasion resistance, and low scaling rating. Moreover, HSC was found to be much more resistant to attack by ammonium nitrate solution when silica fume was incorporated in the mix. Overall it was emphasised by Wolsiefer[148] that HSC is a superior product than ordinary concrete, with enhanced engineering properties of the concrete mixes.

Bunett[28] studied the performance characteristics of silica fume concrete in a variety of HSC structures. The significant benefits and potential of silica fume concretes were clearly proven throughout the high level of construction activity in Melbourne which provided the impetus to spur the development of silica fume concrete for different applications,i.e., shotcrete for site retention, high strength and very high strength concrete, pumped concrete for tall buildings, increased resistance to aggressive ground water, tunnel linings and precast concrete piles. It was concluded by Burnett that the need and market for silica fume concrete was strong for the many possible applications,e.g., reduction in construction costs, faster construction, different construction methods, improved resistance to attack by chemicals and aggressive water, reduction in corrosion of the reinforcement, and improvement in durability and permeability.

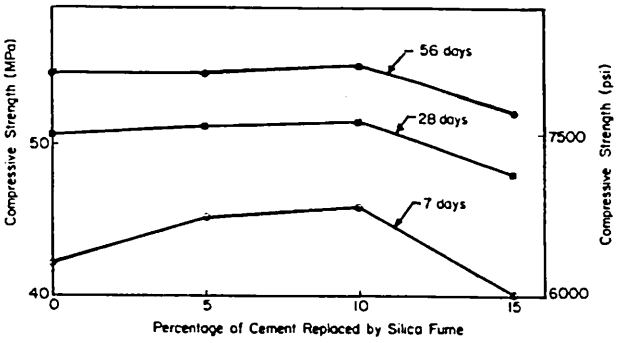

Fig. 2.2- Variation of compressive strength at constant slump. [149]

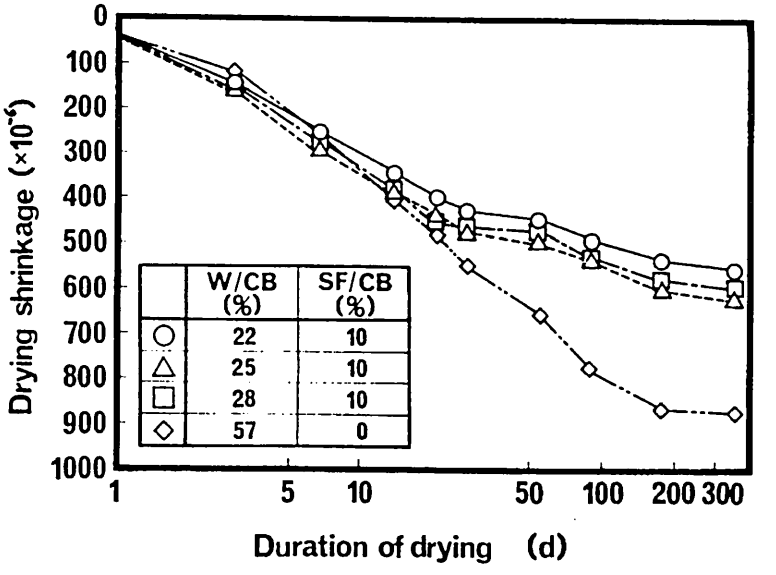

Fig. 2.3- Change in length due to drying shrinkage. [130]

2.1.2 Effect of superplasticizer

Supeplasticizers have become an essential component in the production of HSC and a majority of the references in this review reports their use. They scatter flocs of fine cementitious particles and lower the viscosity of cement paste in concrete as reported by Sarkar *et al.*[118], Detwiler *et al.*[48] and Aitcin [15].

Superplasticizers allow workable concretes to be produced even with water/binder ratio of 0.22, as reported by Mak *et al.*[82]. On the other hand, they do not increase the compressive strength of concrete when used at a constant water/binder ratio, as reported by Jerath and Yamane.[67]. The efficiency of superplasticizer may depend upon the specific cementitious binder with which it is used for HSC's.

Investigators such as Nagataki[96] and Aitcin *et al.*[11] suggested that sulphonated naphthalene superplasticizers were more efficient than those with a melamine base. However, it was recommended to select the most effective combination of superplasticizer and cementitious binder based on testing.

Watanabe[145] and Adwan *et al.*[3] also observed that the loss of workability that generally occurs with time after the addition of superplasticizers can be recovered by a second addition of about 30% of the initial dosage without affecting the concrete strength. On the other hand, Aictin[11] reported that it was necessary to use a retarder accompanied by a superplasticizer to obtain a slump of 75 to 100 *mm* after one hour for a 100 *MPa* concrete strength; moreover, it was necessary to use a second addition of superplasticizer prior to placing. Consequently, Watanabe concluded that for a given slump, superplasicized HSC might require periods of vibration two or three times longer than those for normal strength concrete.

2.1.3 Effect of aggregate

The reviewed publications showed that a wide range of coarse, natural aggregates can be used in the production of HSC. Moreover, it was frequently stated that the highest concrete strengths were obtained with crushed rocks as reported by

Saucier[120], Aitcin[10] and ACI 363 report[16], whilst there are reports of gravel and rounded aggregates producing strengths up to 140 *MPa* as reported by Burge[29] and Godfrey[58].

Ezeldin *et al.*[52] studied the effect of coarse aggregate types on the compressive strength, flexural strength, and flexural strength/compressive strength ratio of normal and HSC. They found that for normal strength concrete the coarse aggregate did not greatly influence the mechanical properties. However, the HSC containing limestone aggregates (Type C) produced higher compressive strength than the concrete containing either gravel aggregates (Type A & B) or granite aggregates (Type D), see Fig. 2.5. According to this investigation the flexural strength of HSC was not affected by the aggregate type, see Fig 2.6. Further, it is worth noting that from test investigations made by Mak *et al.*[82], the compressive strength of HSC is highly dependent on both type and grading of aggregates.

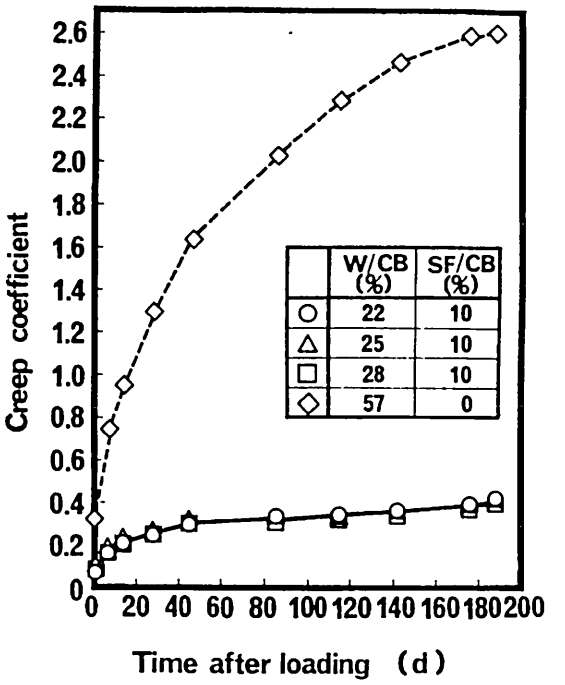

Fig. 2.4- Creep characteristics of HSC.[130]

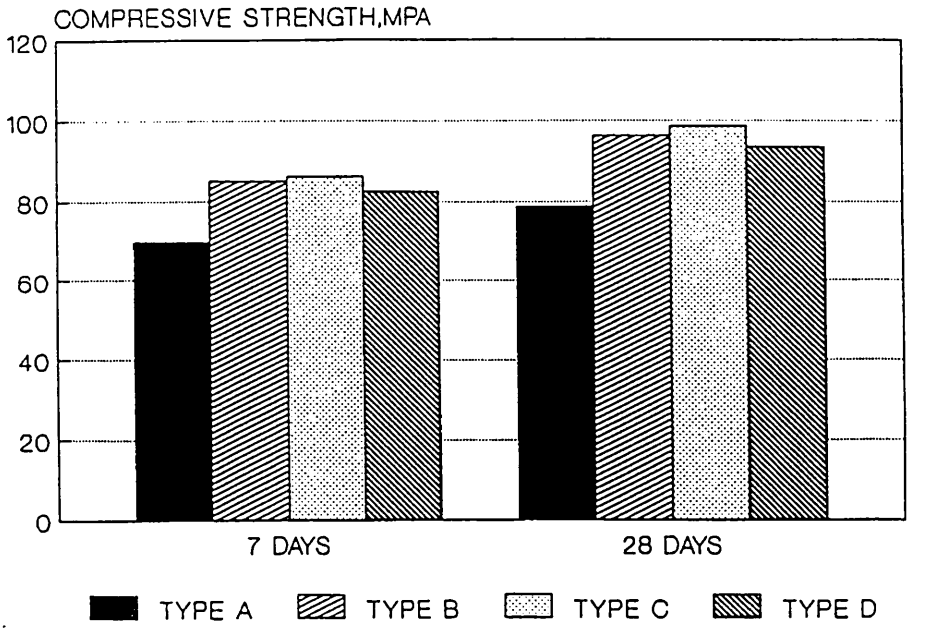

Fig. 2.5- Aggregate type effect on compressive strength. [52]

Baalbaki *et al.*[19] studied the influence of coarse aggregate on elastic properties of HSC. All the concrete mixes were made with different types of crushed rocks,i.e.,Limestone, Quartzite, and Sandstone. From the experimental results it was found that the highest strength was reached by sandstone concrete and the lowest by quartzite concrete at any given age. The elastic moduli of lime and quartzite concretes were very similar and higher than the elastic modulus of sandstone concrete, see Fig. 2.7. The shape of the loading -unloading stress-strain curve of lime and quartzite concrete is similar to that found by Aitcin and Mehta[13]. The higher porosity of sandstone, the mineralogy, and the texture may also have influenced the elastic modulus and played a certain role on the observed non-linear behaviour of the loading stress-strain curve. Baalbaki *et al.* concluded that the elastic modulus of HSC is strongly influenced by the elastic properties of coarse aggregates and that the present formula relating the elastic modulus E_c to the compressive strength,i.e., $E_c = 3320\sqrt{f_c} + 6900$ as quoted by ACI Committee 363 is not valid as far as HSC is concerned. Fig .2.7 shows some existing relationship between the elastic modulus and concrete strength for different aggregate types. Consequently, a new formula relating E_c and f_c is needed for HSC taking into account the elastic modulus of the parent rock from which the coarse aggregate was obtained.

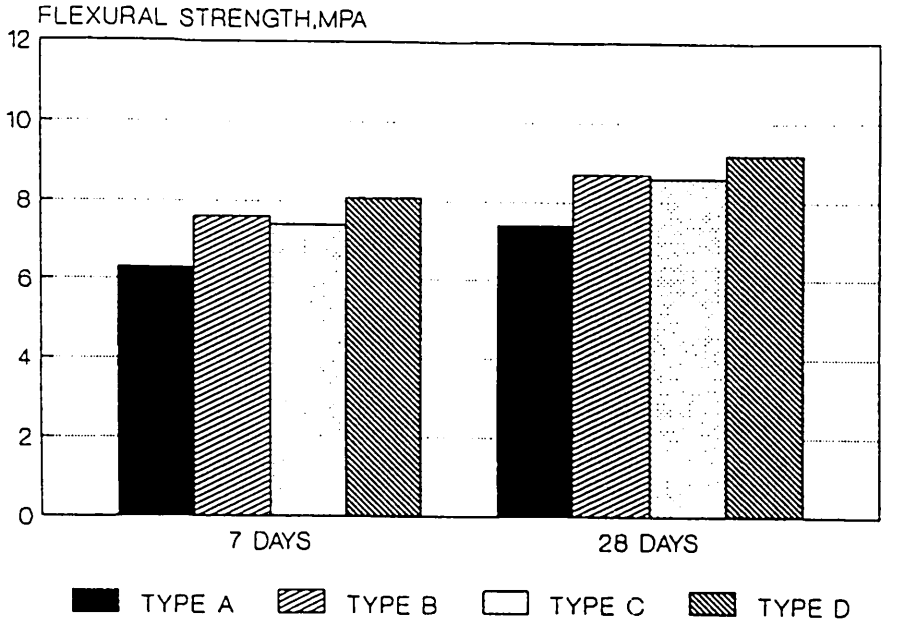

Fig. 2.6- Aggregate type effect on flexural strength. [52]

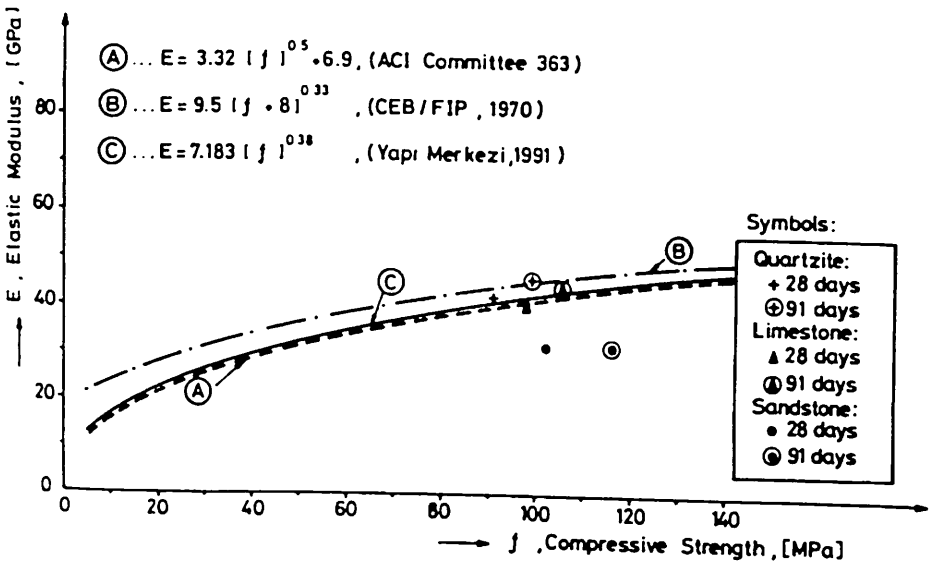

Fig. 2.7- Comparison of various relationships between the elastic modulus of concrete and compressive strength. [19]

2.1.4 Proportioning of high strength concrete

In the light of the reviewed literature it is clear that the material selection and mix proportioning of a HSC are a more critical process than the design of normal strength concrete mixes. Each material, namely, cement, sand, coarse aggregate, chemical and mineral admixtures,i.e., superplasticizer and silica fume, must be evaluated as to type, strength characteristics, gradation, fineness, and interaction in combination with each others. In short many trial mix optimisations are required to generate the optimum materials and their proportions. Only then an optimum concrete strength mix at a specified age could be achieved. Moreover, the proportion of water to cement binder ratio seemed to be the most dominant factor in the design of HSC mixes.

De Larrard[45] presented an empirical method for proportioning HSC mixes. In this method, it was assumed that the optimal concrete would have a low cement paste and a high admixture content and that the coarse aggregate was stronger than the paste. The concretes obtained by this method exhibited good qualities. The following formula was derived for HSC mixes using Portland cement, silica fume and superplasticizer:

$$fc = \frac{kg.Rc}{\left(1+\frac{3.1w/c}{1.4-0.4e^{(-11s/c)}}\right)^2} \qquad 2.1$$

where,

f_c = compressive strength of concrete cylinders at 28 days, *MPa*

w, c, s = the mass of water, cement , and condensed silica fume for a unit volume of fresh concrete, respectively, *kg*

kg = a parameter depending on the aggregate type,i.e., a value of 4.91 applies or river gravel.

Rc = the strength of cement at 28 days, in *MPa*, i.e.,ISO mortar containing three parts of sand for each part of cement and one -half part of water.

The aforementioned empirical formula was recommended for use to determine the composition of a concrete mix having a given strength and workability with a minimal number of trial concrete batches. The main assumption of the method concerning the use of the saturation amount of superplasticizer leads to concretes with good secondary properties even if they are more expensive than others containing more cement and less admixture.

2.1.5 Effect of curing

Asselanis *et al.*[18] investigated the influence of curing conditions on the properties of HSC,i.e.,compressive strength, elastic modulus and stress-strain behaviour. Twenty-four 100 x 200 *mm* cylindrical specimens were made, kept in moulds for 1 day, and then subjected to three different curing conditions. The curing conditions comprised continuous moist curing at 100% RH in a fog room at 23°C ± 3, moist curing for 7 or 28 days followed by air curing until the test age. Water-cement ratio of 0.31 was selected in order to produce a HSC mix.

It was concluded from the test results, that a 7-day moist curing period instead of 28 days is enough for the development of potential concrete strength,e.g., compare group 3 and 4 in Fig. 2.8. In other words, moist curing beyond this period was not substantially needed to enhance the compressive strength and elastic modulus of concrete. However, curing in air after the initial 7-days moist curing caused considerable improvement in the compressive strength,i.e., almost 30% increase in f_c, see Fig. 2.8. This is because the concrete have become impervious,i.e., retained sufficient moisture internally for further hydration of cement during the 7 to 28-days air curing period.

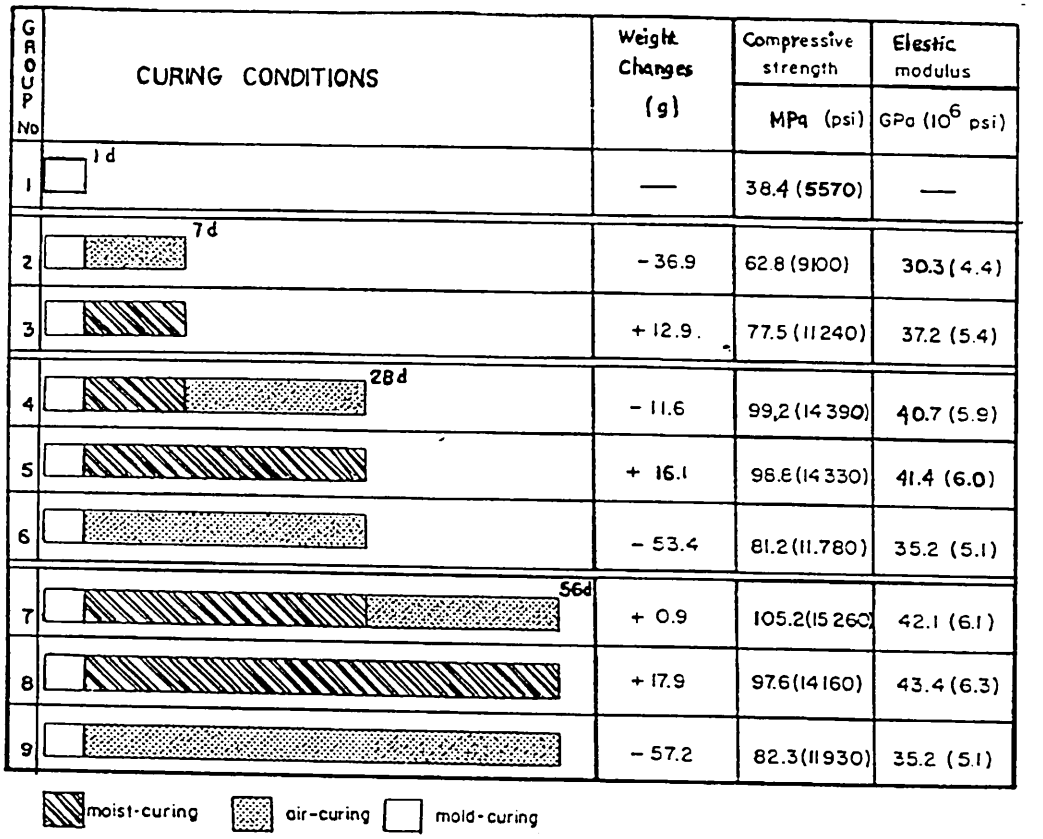

Fig. 2.8- Changes in compressive strength, elastic modulus with different curing conditions.[18]

2.1.6 Engineering relationships

Setunge *et al.*[122] investigated the engineering properties of HSC with compressive strength in the range of 80 to 120 *MPa*. The study included the determination of the static modulus of elasticity, Poisson's ratio, tensile strength,i.e., split cylinder tensile strength and modulus of rupture of HSC, and direct tensile strength of reinforced concrete using silica fume in the concrete mixes, locally available aggregate, cement and superplasticizers. The authors suggested that very little work had been done on the properties of HSC at such concrete grade using pozzolanic additives. So their investigation aimed to provide data for the better understanding of the behaviour of HSC by measuring some basic mechanical properties. Test results were obtained at 7, 28, and 56 days for the static modulus of elasticity, Poisson's ratio, modulus of rupture and split cylinder tensile strength. All these tests were carried out following AS 1012 recommended procedures for normal strength concrete. All specimens were moist cured until the day of test. It was concluded from the test results obtained that: the equation proposed by Carrasquillo *et al.*[33] and later modified by Nilson[101] ,i.e., $E_c = (3320\sqrt{f_c} + 6900)(\rho / 2320)^{1.5}$ for concrete compressive strength in the range of 20 to 83 *MPa* may be used to predict the mean static modulus of elasticity, E_c of silica fume concrete. On the other hand statistical analysis of the results indicated that there was a possibility of E_c values for HSC falling below the -20 % limit associated with AS 3600 formula $E_c = 0.04\rho^{1.5}\sqrt{f_c}$, see Fig 2.9. It was suggested that the AS 3600 formula should not be used to predict the E_c for HSC. The Poisson's ratio of HSC at 56 days is generally about 0.2. It was observed that Poisson's ratio increased with the age of the concrete. For tensile strength results, the equation: $fsp = 0.54\sqrt{f_c}$ proposed by Carrasquillo *et al.*[33] for concrete strength up to 83 *MPa* can be used to calculate the mean split cylinder tensile strength of HSC. The AS 3600 formula $fsp = 0.4\sqrt{f_c}$ gave a reasonable estimate to the characteristic splitting tensile strength, see Fig. 2.11. It was also concluded that the equation, $fr = 0.94\sqrt{f_c}$, proposed by Carrasquillo *et al.*[33] and the equation, $fr = 1.15\sqrt{f_c}$ proposed by Aitcin *et al.*[12] overestimated the value of the mean

modulus of rupture obtained for the HSC tested in the study, see Fig. 2.10. The latter two equations are based on the results obtained by testing 100 x 100 x 300 *mm* prism specimens, while the investigation reported Setunge *et al.*[122] were obtained from testing larger prism specimens,i.e., 150 x 150 x 450 mm. The lower strengths could be explained as a size effect which should receive further investigation. The AS 3600 formula, $fr = 0.6\sqrt{fc}$ gives a conservative estimate for the modulus of rupture of HSC.

Shah and Ahmad[123] stated that there was not enough information available on the structural properties of HSC. Moreover, the current ultimate strength design practice is based on experimental information obtained from concretes with compressive strength of 21 to 42 *MPa*. They investigated the engineering properties of HSC ,i.e., stress-strain relationship, secant modulus of elasticity, tensile strength, Poisson's ratio and shear strength up to 80 *MPa*, in order to develop a satisfactory procedure for the structural design of HSC. The authors highlighted that additional consideration, validation or modification of existing strength design methods may be necessary.

They proposed empirical expressions to substitute some of the currently used relationships. The main conclusions were: there were significant differences in the compressive stress-strain curves of normal and high strength concretes,i.e., for HSC the shape of the ascending part of the curve is more linear and steeper, the strain at maximum stress is slightly higher, and the slope of the descending part is steeper, as compared with normal strength concrete, see Fig 2.12. The ACI[16] equation for estimating the secant modulus of elasticity, $E_c = 33W^{1.5}\sqrt{f_c}$ *psi* , predicts values as much as 20 percent too high for concretes with compressive strength in the range of 84 *MPa*. They proposed an expression which correlates the modulus of elasticity and the compressive strength, $E_c = W^{2.5}(\sqrt{f_c})^{0.65}$ *psi*. The split cylinder strength for low and high strength was conservatively represented by the expression,

$fsp = 6\sqrt{f_c}$ *psi*. Also, the ACI code current expression for modulus of rupture, $fr = 7.5\sqrt{f_c}$ *psi* may be too conservative for HSC and an alternative expression, $fr = 2\,(f_c)^{2/3}$ *psi*, appeared to be more representative of the test data,see Fig .2.10.

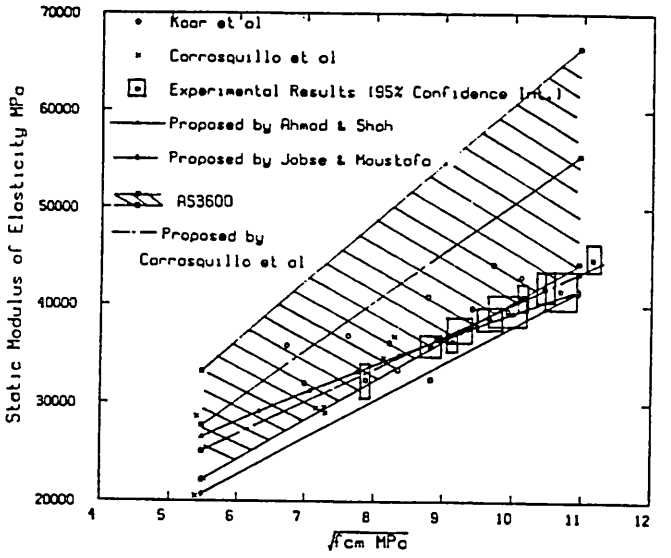

Fig. 2.9- Static modulus of elasticity. [122]

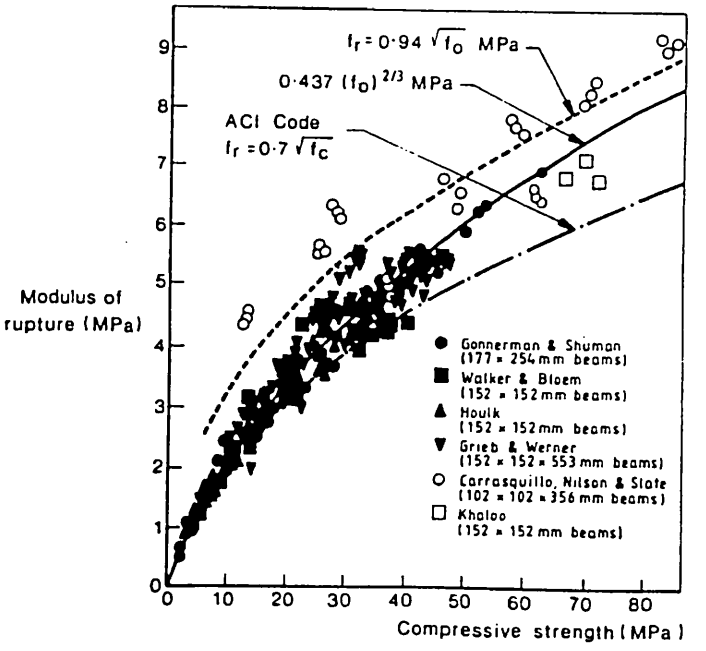

Fig. 2.10- Flexural tensile strength of HSC.[4]

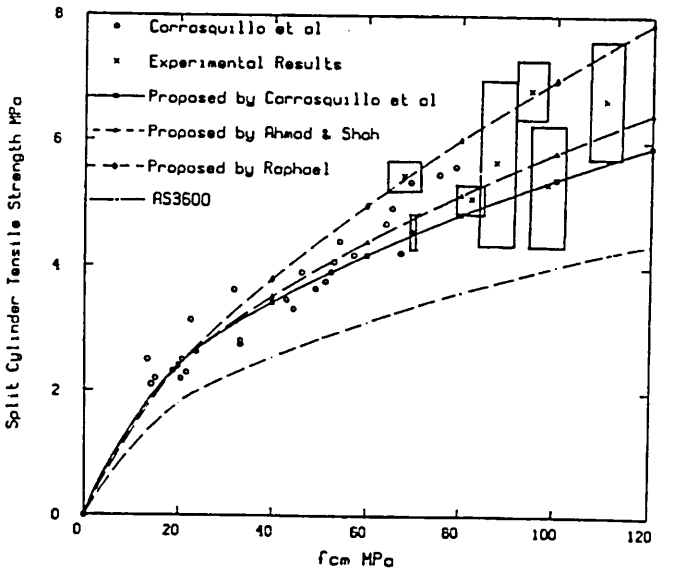

Fig. 2.11- Splitting tensile strength of HSC.[122]

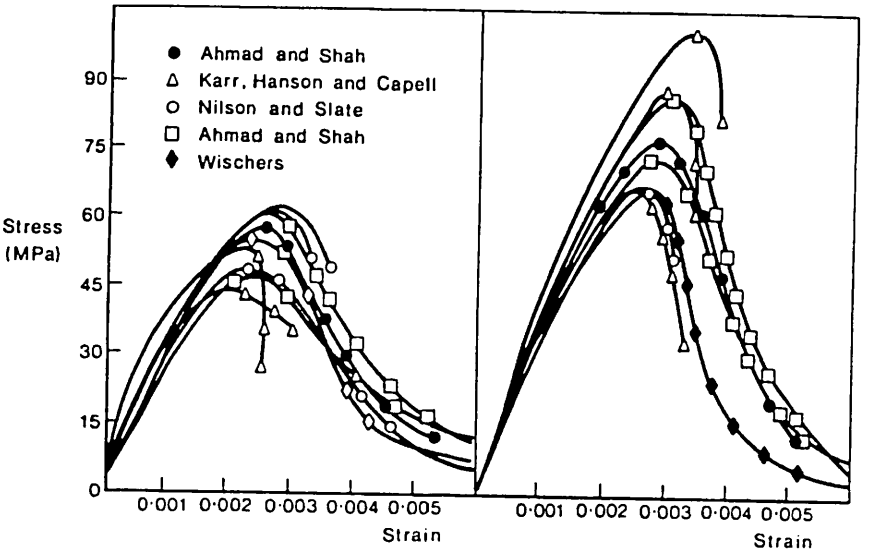

Fig. 2.12- Stress-strain curves for medium and HSC's. [123]

2.2 Section Two: Structural Behaviour of HSRC Beams in Flexure

Three important aspects related to the design and behaviour of HSRC beams have recently been investigated: stress-strain relationships, ductility and load-deflection characteristic. The findings from the available literature are reviewed below.

2.2.1 Stress- strain relationship

One of the most important characteristics in designing a reinforced concrete flexural member is the stress-strain relationship of the concrete.

The design procedures which are currently used in both BS 8110[27] and ACI 318[1] codes are primarily based on work by Mattock *et al.*[86]. The primary aim of their investigation was to find a suitable approximation of the non-linear, and highly variable stress-strain relationship of reinforced concrete at ultimate strength. As a result of this, there have been many proposed simplifications, the most popular ones being those currently used in both the ACI 318-83, and BS 8110 codes. The actual stress distribution is replaced by an equivalent rectangular stress distribution of an average intensity equal to $0.85 f_c$ in the ACI code and $0.45 f_{cu}$ in the BS code. These simplifying assumptions are based essentially on test results of beams made from concrete of 3000 to 6000 *psi* (21 to 42 *MPa*) compressive strength.

At the present time, only a few reports of investigations are available which verify the use of the ACI code rectangular stress block for concretes with strength above 55 *MPa* in spite of the different behaviour of HSC specimens under uniaxial compression, as shown earlier, see Fig. 2.12 .

Based on the analysis of the stress-strain curves obtained from tests, Leslie *et al.*[78] concluded that the ACI rectangular stress block did not accurately predict the behaviour of beams having cylinder compressive strength above 8000 *psi* (55 *MPa*). They recommended the use of a triangular stress block with the maximum compressive strength at the extreme fibre, and zero stress at the neutral axis as a

conservative model for predicting the ultimate flexural strength of beams having concrete strength above 55 *MPa*.

Kaar *et al.*[70] studied the change in shape of the stress-strain curve, based on reinforced concrete members ranging from 6500 *psi* to 14850 *psi* (45 to 102 *MPa*). The test data were compared with the ACI 318-71 code recommendations pertaining to the flexural constants for strength design k_1, k_2 and k_3. They showed that the geometry of the stress block in the compression zone of flexural members should be adjusted at higher levels of compressive strength with a suitable flexural coefficient. This could be accomplished by adjusting the area and the centroid position of a simple rectangular stress block, see Fig. 2.13.

Another research investigation carried out by Zia[151] suggested the revision of the design parameters for flexural reinforcement of higher strength concrete. These design parameters are the elastic modulus, modulus of rupture, and the minimum reinforcement volume. Moreover, Zia tried to verify the idealised trapezoidal stress-strain curve involving the concept of plasticity ratio β , see Fig. 2.14 which was originally suggested by Jensen[66], and confirmed by the Cornell university researchers as stated elsewhere[16]. He concluded that, it might be suitable to use the trapezoidal stress-strain curve for application over the full range of concrete strengths. As a result, an equivalent rectangular stress block for such a stress-strain relationship can be defined by the design parameters k_1 and k_3 given by the following relationships:

$$\beta = 1 - \frac{fc}{E_c \varepsilon_c} \qquad 2.2$$

$$k_1 = \frac{1+\beta}{2k_3} = \frac{2\left(1+\beta+\beta^2\right)}{3(1+\beta)} \qquad 2.3$$

$$k3 = \frac{3(1+\beta)^2}{4(1+\beta+\beta^2)} \qquad 2.4$$

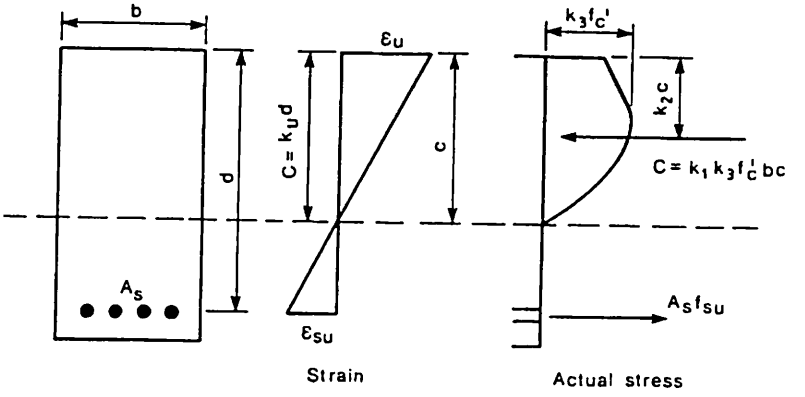

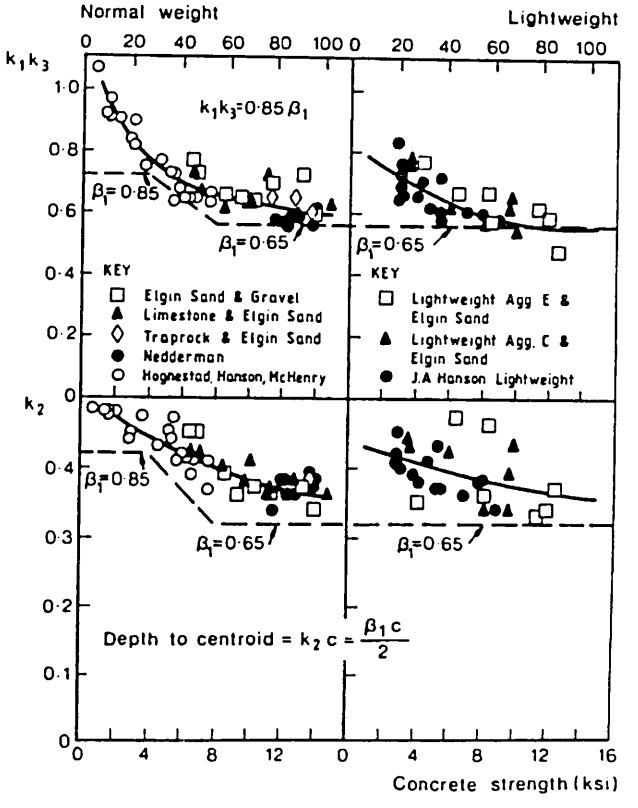

Fig. 2.13- Effect of compressive strength on k_1, k_2 and k_3 that describe the geometry of stress block. [70]

where, $E_c = 40000\sqrt{f_c} + 1000\ psi$ for $3000 < f_c < 12000\ psi$

$E_c = 3320\sqrt{f_c} + 6900\ \ MPa$ for $21 < f_c < 83\ MPa$

In contrast with the above mentioned investigations, Wang *et al.*[144] concluded: "*Rectangular stress distribution gives sufficiently accurate prediction of ultimate loads and moments of reinforced concrete beams and columns made with HSC* ". In their research study beams with varying amount of tension and compression reinforcement and concrete strengths between 3000 to 13000 *psi* (21 to 90 *MPa*) were considered. In short Wang *et al.* were able to make close prediction of the test results obtained by Leslie *et al.*[78].

However, according to the author's best knowledge,on the basis of an up to date literature review, there is no report of work available that has been done to evaluate or assess the BS recommendations in predicting ultimate strength of HSRC beams in flexure. Thence, it is clear that there is a strong need to investigate the performance of HSC members in flexure with associated reassessment of the recommendations in BS 8110.

2.2.2 Ductility

Many studies have been carried out to investigate the ductility of HSC for both materials and reinforced concrete members. The view reported herein will highlight some of this work on the ductility of HSC beams.

Wang *et al.*[144] have shown that the maximum concrete strain, ε_{cu}, in beams does not only depend on the concrete strength but also on the amount of tension and compression reinforcement. They concluded that while the value of the maximum strain, ε_{cu}, of concrete in compression decreases rapidly as the concrete strength increases, it increases when compressive strength increases for a singly under-reinforced beam. The flexural ductility factor increased markedly by the addition of

compression steel and the reduction of tensile steel. Moreover, it would also increase with increasing concrete strength. It was also noted that ultimate concrete compressive strain was always higher than 0.003.

Another investigation carried by Sing *et al.*[126] on the ductility, μ_d, of HSC members ($\mu_d = \Delta_u / \Delta_y$,where μ_d =displacement ductility index, Δ_y = deflection at first yield of tensile reinforcement and Δ_u = deflection at ultimate load) confirmed that the ductility of HSC was generally higher than that of beams with moderate concrete strength. Also, the ductility index decreased dramatically as the tensile strength ratio, ρ, increased. This fact was also confirmed by Nilson[101] and Tognon *et al.*[139] who showed that the ductility index was almost independent of the concrete compressive strength, see Fig. 2.15.

Zia[151] reported that the moment capacity, and the mode of failure, of HSC sections were affected significantly by the ultimate concrete stain, ε_{cu}, value when a section is reinforced with higher percentages of steel. For ordinary concrete strength the moment capacity of a section is not sensitive to the value of ultimate concrete strain, ε_{cu}.

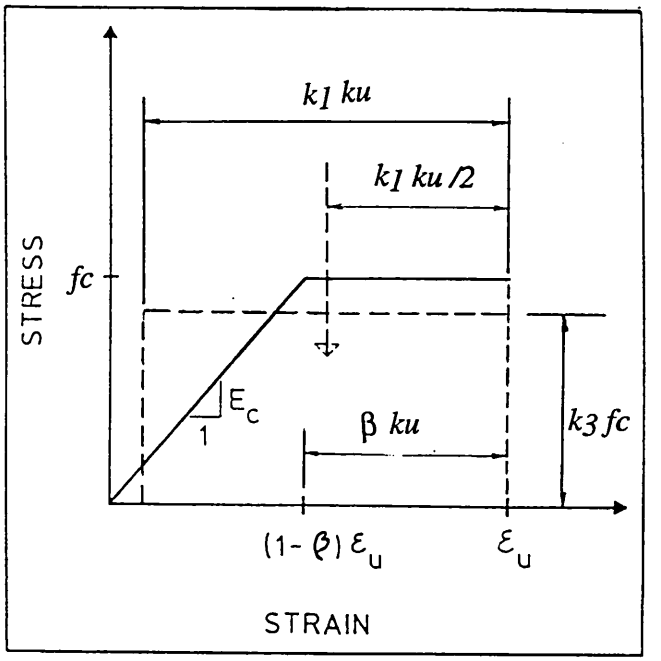

Fig. 2.14- Idealised stress-strain curve for concrete in compression. [151]

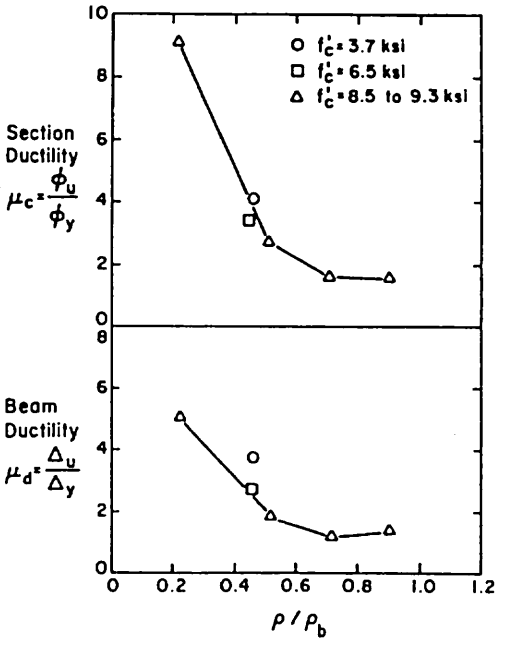

Fig. 2.15- Ductility index versus steel ratio.[101]

2.2.3 Load-Deflection Behaviour of HSC beams in flexure

Very few research investigations have been conducted concerning the load-deflection behaviour of HSC beams; the following summarises some work that has come to the notice of the writer.

Leslie *et al.*[78] conducted flexure tests on HSC rectangular beams with compressive strength ranging between 64 to 81 *MPa*. For all beams, in order to prevent shear failure, heavy stirrups were provided in the shear spans. The main variable was tensile reinforcement ratio,i.e.,$1\% < \rho < 3\%$. They concluded that beams with lower reinforcement ratio are much more ductile than the beams with the higher reinforcement ratios, see Fig. 2.17. Similar behaviour was also obtained from test investigation carried by Ahmad *et al.*[7,8] with lightweight HSC beams.

Another investigation addressing the shear span to depth ratio (a/d) on the load-deflection behaviour of HSC beams was carried out by Ahmad *et al.*[8]. The variables were the tensile reinforcement ratio,i.e., $0.35\% < \rho < 6.64\%$, and the shear span to depth ratio,i.e., $1 < a/d < 4$. The compressive concrete strength varied from 63 to 70 *MPa*. It was concluded that beams with $a/d < 2.5$ exhibited a brittle behaviour, with some reserve in strength after the formation of the diagonal crack. The failure mode was sudden and catastrophic. For beams with $a/d > 2.5$, vertical flexure crack initiated at mid-span; on further loading, additional vertical cracks along with diagonal cracks developed at sections away from the mid span. The crack pattern of these beams indicated a predominantly flexural behaviour. The failure was sudden and occurred soon after the formation of the inclined cracking, see Fig. 2.16.

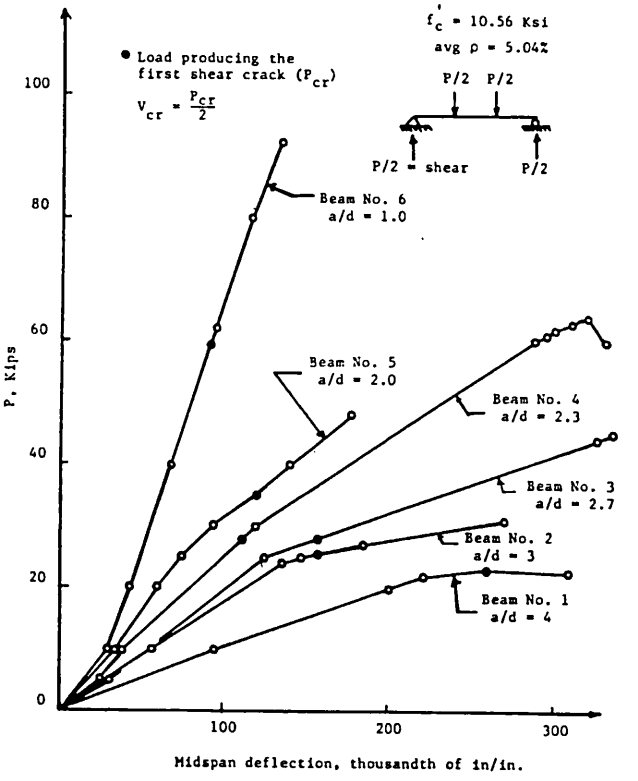

Fig. 2.16- Load-deflection curves. [6]

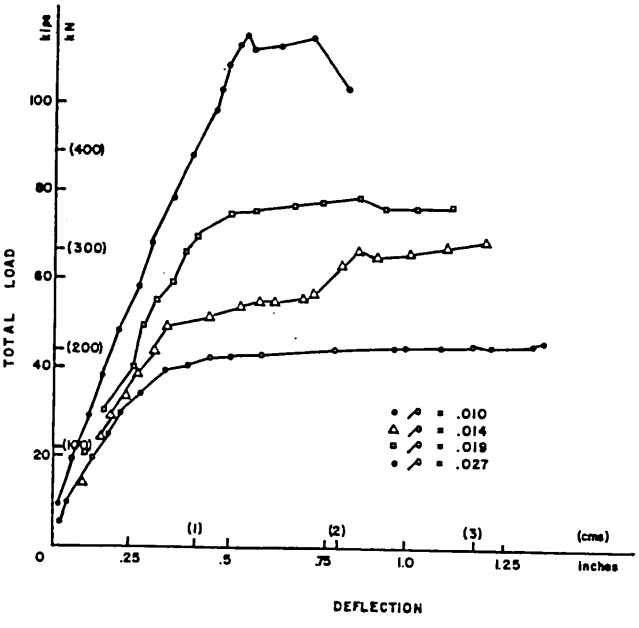

Fig. 2.17- Load-deflection curves.[6]

2.3 Section Three: Shear Capacity of Reinforced Concrete Beams

This section reports the review of technical literature related to beam shear capacity with particular emphasis on results relating the influence of concrete strength, reinforcement ratio, shear span to depth ratio and aggregate interlock on shear capacity of HSRC beams. The majority of studies have been undertaken to investigate the contribution of the individual component to the shear capacity of ordinary reinforced concrete beams. However, some of the works reported relate to HSC concrete as well.

2.3.1 Shear transfer in reinforced concrete beams without shear reinforcement

The mechanism of shear transfer in reinforced concrete beams is not yet completely understood. However, it is now generally accepted that when a reinforced concrete beam cracks as a result of diagonal tension stress, the internal forces are generally redistributed. Thus, the total shear force at a section is carried by three principal mechanisms, see Fig. 2.18 :

(i) By the uncracked concrete compressive zone, V_{cz}.

(ii) By the vertical component of the force developed due to interlocking of aggregates a cross the inclined crack, V_a.

(iii) By the transverse force developed by the main reinforcement due to dowel action, V_d.

It was previously assumed that all the shear force at a section was carried by the uncracked concrete in the compression zone and by dowel action of main reinforcement, and aggregate interlock was ignored. Fenwick and Paulay[53] and Taylor[135] examined the relative contribution of each of the above mentioned mechanisms. They concluded that aggregate interlock contributed significantly to the shear strength and reported that the uncracked concrete, V_{cz}, aggregate interlock, V_a and dowel action,V_d could contribute approximately 20%, 60% and 20%

respectively to the total shear force carried by the concrete section in beams without shear reinforcement.

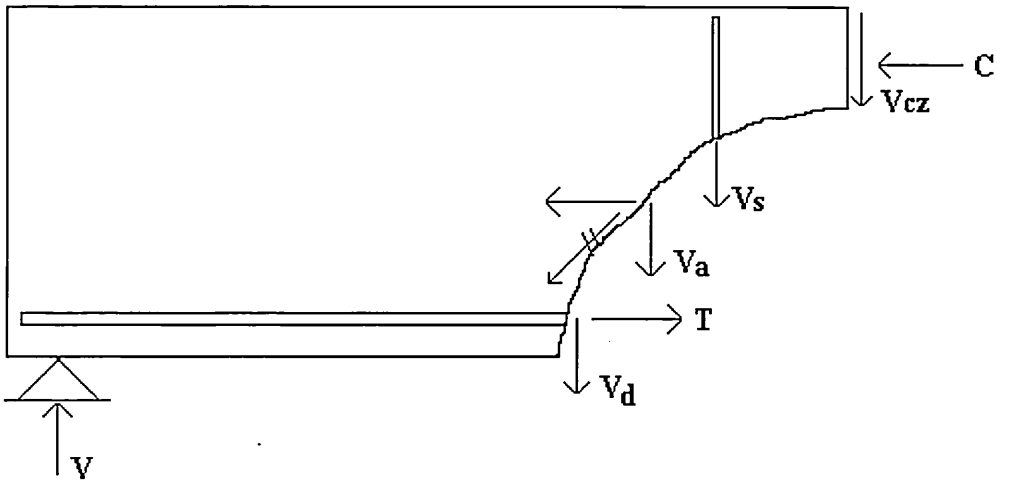

Fig. 2.18- Mechanisms of shear transfer

2.3.2 Shear transfer in beams with shear reinforcement

It is commonly accepted that shear reinforcements assist in carrying shear. A study by Swamy and Andriopoulos[128] showed that the shear carried by the concrete section remains fairly constant in magnitude even when the amount of shear reinforcement is increased. They also studied the effects of aggregate interlock and dowel action on the shear strength of reinforced concrete beams which were provided with a minimum amount of shear reinforcement. The percentage contribution of V_a and V_d were found to be 48% and 33% respectively in beams with shear span/depth ratio of 3.

The ACI-ASCE-Committee[2] reported that there is an interaction between the stirrups and the aggregate interlock. Furthermore, the stirrups contribute significantly to the capacity of the member by increasing or maintaining the shear transferred by the aggregate interlock.

Fenwick and Paulay[53] reported that the capacity of the aggregate interlock decreased with increasing crack width. They also concluded that, stirrups assist the aggregate interlock mechanism by restricting the widths of diagonal cracks, thus maintaining bearing of aggregate across the crack. Also, the ultimate dowel strength is significantly increased if the longitudinal reinforcement is provided by stirrups as reported by Swamy and Bahia[129].

2.3.3 Factors affecting shear strength

The factors influencing the shear strength of reinforced concrete beams are numerous and complex according to the report of ACI-ASCE committee 426[2], the major factors being:

(i) Concrete strength.

(ii) Shear span to depth ratio (a / d or M / Vd).

(iii) Details of longitudinal reinforcement,i.e., steel ratio, yield strength and surface condition.

(iv) Shear reinforcement ratio.

Most current codes provide equations relating the shear capacity of beams mainly in terms of concrete compressive strength, f_c, flexural reinforcement ratio, ρ , and span/ depth ratio, a / d .

2.3.3.1 Effect of concrete strength

Mphonde and Frantz[95] reported results of shear tests of high and low strength concrete beams. They concluded that the current ACI code 318-83[1] equation for shear design was conservative which is;

$$v_c = 0.16\sqrt{f_c} + 17.25\rho \frac{Vud}{Mu} \qquad 2.5$$

However, they found that the ratio of test/ predicted capacity using the ACI code decreased from 1.64 to 1.2 as the concrete strength increased from 21 to 104 *MPa*. They proposed the following equation to predict the shear strength of reinforced concrete beams without stirrups and having an a/d ratio of 3.6;

$$v_u = 0.366\sqrt[3]{f_c} + 0.49 \qquad 2.6$$

They also tested beams with a/d ratios of 2.5 and 1.5, and concluded that the effect of concrete strength on shear capacity becomes more significant as a/d ratio decreased. Moreover, they reported that failure becomes more sudden and explosive as the concrete strength increased particularly at lower a/d ratio.

Elzanaty *et al.*[50] also tested several beams to study the effect of concrete strength on shear capacity. They concluded that ACI 318-83[1] code equation overestimates the shear strength by 10 to 30%, particularly for beams with higher concrete strength combined with normal to high shear-span ratios and relatively low longitudinal reinforcement ratios, see Fig. 2.23. On the other hand, for beams with shear reinforcement, all test strengths exceeded those predicted by ACI code. They pointed out that the effect of concrete strength on shear capacity changed with the a/d ratio.

BS 8110 allows for increases in the design concrete shear capacity as the concrete compressive strength increases. However, this increase is limited to a value of 1 *MPa* for any concrete strength above 35 *MPa*. Moreover, the BS 8110: Part1 ignores the effect of compressive strength of concrete greater than 40 *MPa* in the evaluation of shear capacity of beams without web reinforcement. Also, it does not allow for any increase in shear capacity for the main reinforcement ratio, ρ, and effective depth of beam, d, greater than 0.03 and 400 *mm* respectively.

Clarke[38] reported that further work was required on shear capacity of HSRC beams. However, he concluded, based on tests on beams made of concrete having a cube strength of 70 *MPa*, that the equation given in BS 8110 for the design shear stress could be extended to take account of the higher strengths. It would lead to an increase of 20 to 45 % in the design shear stress for the concrete strengths considered.

Hansoun[61] tested a series of five lightweight concrete beams with concrete strength varying from 26 to 74 *MPa*. For all the beams tested he estimated the ratio of measured shear to the calculated shear capacity at diagonal cracking using the ACI code equation. He concluded that the ratio varied from 1.11 to 1.26. Moreover, the ratio decreased as concrete strength increased,i.e., ratio of 1.17 for 55 *MPa* concrete strength and 1.1 for 74 *MPa* concrete strength.

Taylor[134] and Van der Berg[142] conducted a series of tests on rectangular concrete beams without shear reinforcement. The concrete strength varied from 14 *MPa* (2000 *psi*) to 66 *MPa* (9500 *psi*). They concluded that both the diagonal cracking load and ultimate shear capacity increased with increase in the concrete strength. They also concluded that the beam ultimate shear capacity did not increase as rapidly as the concrete compressive strength. For example, if the shear strength was proportional to $(f_c)^{0.5}$, then the results plotted in Fig. 2.19 must lie on a straight line through the origin. It should be noted almost all the values for concrete strength over 35 *MPa* (5000 *psi*) are below the line, see Fig. 2.19. This indicates that for f_c above 35 MPa, the shear strength increases less rapidly than $(f_c)^{0.5}$ proportion predicts.

Zsutty[152] used a combination of dimensional and statistical regression analysis to show the relation between the concrete compressive strength to the shear strength. He concluded, both the diagonal cracking and the ultimate shear strengths are

directly proportional to $(f_c)^{1/3}$. He derived the following equation to predict the ultimate shear stress of reinforced concrete beams:

$$v_n = 2.18 \left(f_c \rho \frac{d}{a}\right)^{1/3} \quad , MPa \qquad 2.7$$

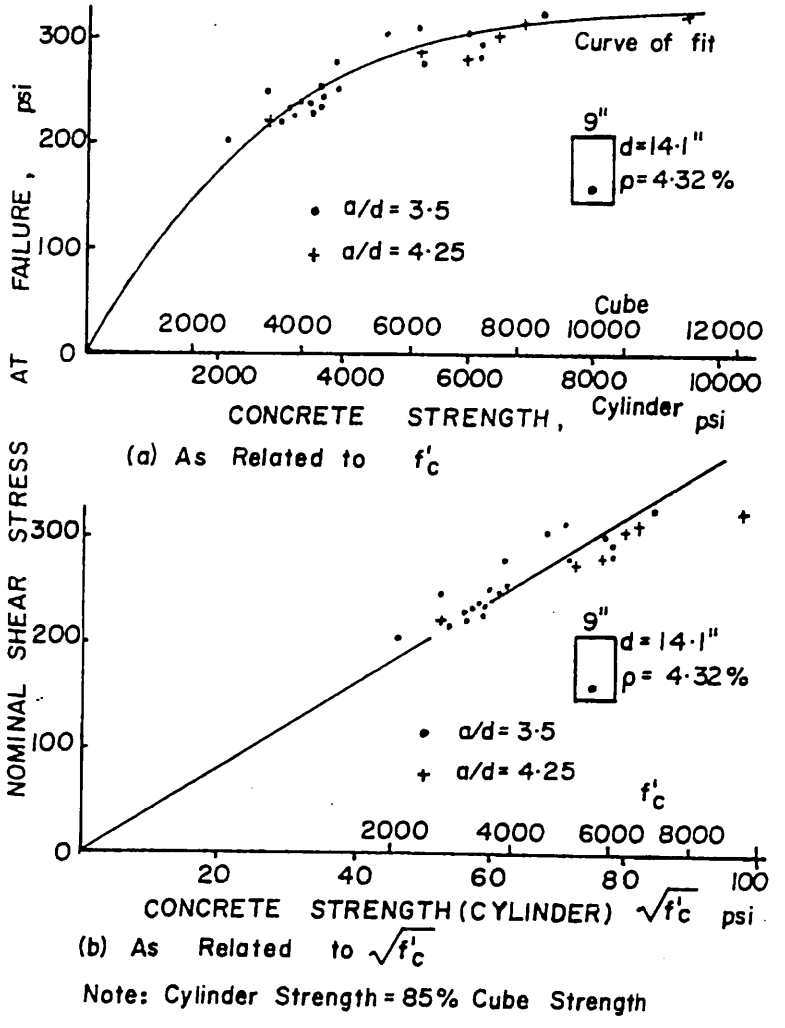

Fig. 2.19- Effect of concrete strength on beam shear capacity.[142]

Recently, Sarsam and Al-Musawi[119] tested 14 beams with concrete strength up to 80 *MPa* and with shear reinforcement. They critically examined the existing code expressions for calculating the shear capacity of high and normal strength concrete beams with shear reinforcement and proposed an empirical formula for calculating the shear capacity of beams with shear reinforcement:

$$vu = 0.85\left[1.8\left(fc\,\rho\frac{Vud}{Mu}\right)+\frac{Avfy}{b\,s}\right] \qquad 2.8$$

They concluded that the ACI code, the proposed expression and the Canadian code design equations were conservative for estimating the shear strength capacity of reinforced beams up to 80 *MPa*, whereas the New Zealand code, the British code and Zsutty's methods were less conservative compared with those mentioned above.

2.3.3.2 Shear span / depth ratio

It is well recognised that shear span to depth ratio has a very important influence on the shear capacity of reinforced concrete beams and on the type of failure that occurs. Iyengar *et al.*[64] and Kani[72] reported results on beams tested to investigate the influence of a/d ratio on the shear capacity of reinforced concrete beams. The concrete compressive strength was 26 *MPa*. The tensile reinforcement ratio, ρ, varied between 0.8% to 2.88%. They concluded that the shear capacity increases as *a/d* ratio decreases. This phenomenon is more pronounced for a/d ratios less than 2.5.

Salandra and Ahmad[112] investigated the shear capacity of reinforced lightweight HSC beams. The variables in their test programme were concrete strength,i.e., 54 and 73 *MPa*, a/d ratio,i.e., 0.56, 1.56, 2.56 and 3.63 and shear reinforcement which was 0.76%. They concluded that the ACI building code equation was optimistic for

lightweight concrete beams. Also, beams with smaller a/d ratio exhibited more reserve capacity after cracking as compared to beams with larger a/d ratio.

Elzanaty *et al.*[50] tested the shear strength of reinforced concrete beams using concrete with compressive strength ranging from 21 to 83 *MPa*. A total of 18 beams were tested. The variables were concrete strength, longitudinal steel ratio, ρ, and shear span to depth ratio. The results were compared with strengths predicted using ACI 318-83 expression. They concluded that the ACI expression overestimates shear strength by 10 to 30 % particularly for HSC combined with normal to high shear-span ratios and relatively low longitudinal steel ratios. The shear strength decreased markedly with increase of a/d, see Fig. 2.20. Moreover, the ACI 318-83 expression was unconservative for beams with *a/d* equal to 6 for even high ρ.

Kim and Park[77] tested 20 reinforced concrete beams, having strength of 54 *MPa*, in order to investigate their behaviour and to determine their ultimate shear capacity. The test results were analysed and compared with the strength predicted by different codes of practice. They concluded that for beams with a/d equal to or greater than 3, the ratio of measured to predicted shear strength using BS 8110 equation was decreased with increasing a/d. Meanwhile, the ACI code equation underestimates the effect of a/d, see Fig. 2.21. Recent investigation carried out by Ashour *et al.*[17] on the shear capacity of high strength fibre reinforced concrete beams confirmed the same aspects.

Generally, It can be observed from the investigations reported above which were carried out on the effect of a/d ratio upon the shear capacity of beams that: when a/d ratio exceeds approximately 2.5 the diagonal cracking, V_{cr}, may represent the ultimate shear capacity, V_u ,i.e., there is no reserve strength beyond cracking load. For a/d ratio smaller than about 2.5, V_u is greater than V_{cr} and the reserve capacity

(V_u - V_{cr}) becomes higher as a/d decreases. Furthermore, as a/d increases, both the diagonal cracking and the ultimate shear capacity become smaller.

To account for this behaviour the BS 8110 shear equation for ordinary beams was modified by a factor which shows the influence of the a/d ratio on the ultimate shear capacity. The BS 8110 code equation for v_c, the allowable shear strength of concrete:

For $a/d \geq 2$ $$v_c = \frac{0.79}{\gamma_m}(100\rho)^{1/3}\left(\frac{400}{d}\right)^{1/4}\left(\frac{f_{cu}}{25}\right)^{1/3} \qquad 2.8$$

A modified equation, which forms the basis for shear design of deep beams (i.e., $a/d < 2$), is obtained by multiplying the above equation by a factor of $2d/a$.

Zsutty[152] also modified his equation for ordinary reinforced concrete beams with a factor which shows the strong influence of a/d ratio. He presented the following equation for the ultimate shear capacity of deep beams loaded on the compression face and supported on the tension face:

$$v_c = 2.18\left(2.5\ {}^{d}\!/_{a}\right)\left(f_c\rho\ {}^{d}\!/_{a}\right)^{1/3} \qquad 2.9$$

2.3.3.3 Effect of longitudinal reinforcement

Batchelor and Kwun[20] and Heger and McGrath[62] reported that the longitudinal steel ratio, ρ, has a significant effect on the shear capacity. It is a well known fact that as the percentage of the longitudinal reinforcement ratio increases the mode of failure of beams changes from flexure to shear. Moody *et al.*[91] concluded that increasing the percentage of longitudinal reinforcement ratio increased the ultimate shear capacity of the beams. This was confirmed by Diaz de Cossio and Siess[49] as they reported that the shear capacity of reinforced concrete beams was roughly a linear function of tensile reinforcement ratio.

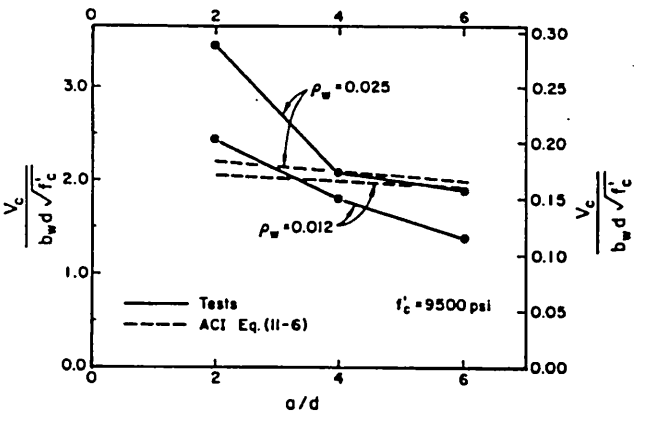

Fig. 2.20- Effect of a/d on shear strength of beams.[50]

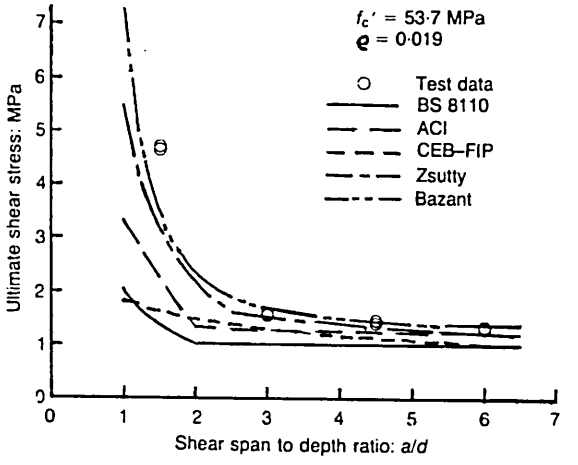

Fig. 2.21- Effect of a/d on shear strength of beams.[50]

Zsutty[152] in his proposed equation which was derived from a statistical analysis showed that the shear strength is proportional to $(\rho)^{1/3}$. This was confirmed by Kim and Park[77] as they stated *"from nonlinear regression analysis with data, it is shown that the shear strength is nearly proportional to 1/3 power of* ρ ".

Elzanaty *et al.*[50] and Ahmad *et al.*[5] concluded that the ACI equation underestimates the effect of the longitudinal reinforcement, i.e., Fig. 2.22. Also, the ratio of measured to predicted shear strength increases with the increase of ρ, whereas, for beams with ρ of 0.01 the margin of safety in the ACI equation may disappear. The effect of low steel ratio was explained by the fact that the flexural cracks extend higher and wider, reducing both the shear capacity of the compression zone and the interface shear transfer.

2.3.3.4 Shear reinforcement ratio

Stirrups not only carry shear themselves but also enhance the strength of the other shear transfer mechanisms. The stirrups provide support for the longitudinal steel and thus prevent them from splitting the surrounding concrete. Thus, they greatly increase the strength of the dowel action. They also help to contain the cracks, limiting their propagation and keeping their width small. These effects increase both the shear carried by aggregate interlock and the shear strength of the uncracked compression zone. Stirrups also increase the strength of compression concrete by providing confinement. Although stirrups do not affect the diagonal cracking load, they enhance the concrete contribution by increasing the capacity of the different shear transfer mechanisms.

Haddadin *et al.*[59] studied the behaviour of shear reinforcement in reinforced concrete beams. The primary variables were the amount of web reinforcement, the concrete strength and shear span to depth ratio. They concluded that the effect of low to moderate amounts of shear reinforcement on the shear capacity of beams is approximately 75% higher than the strength calculated using the ACI 318

expression. Figs. 2.24 and 2.25 show their results. It can be seen that the relationship between shear stress, v_u and shear reinforcement ratio rf_y is similar for both groups of beams.

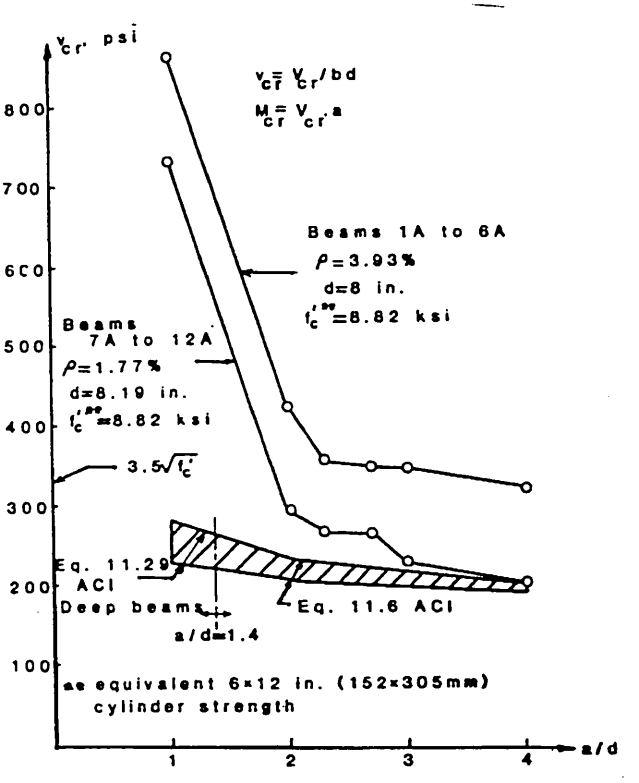

Fig. 2.22- Effect of ρ *and a/d on diagonal cracking stress.* [5]

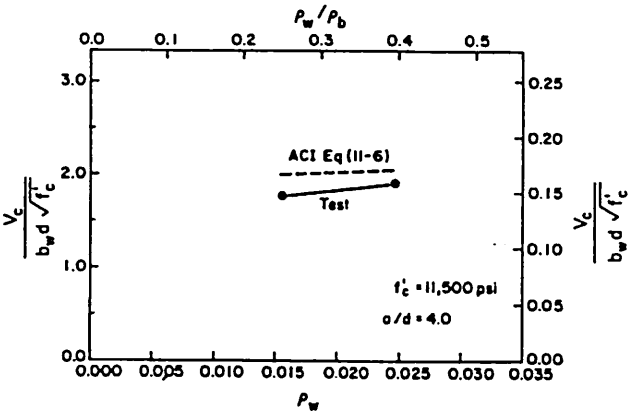

Fig. 2.23- Effect of ρ on shear strength of beams.[50]

The results were represented closely by two straight lines, one with a slope of 1.75 extending to rf_y of 1.38 *MPa* (200 *psi*), and the second line with a slope of 0.5 extending from rf_y of 1.38 *MPa* (200 *psi*). The change in slope appears to correspond to a change in failure mode from diagonal tension failures in beams with small to medium amounts of shear reinforcement to shear compression failures in beams with larger amounts of shear reinforcement. They also found that the stirrups had no effect on diagonal cracking load and were more efficient at low to moderate values of rf_y than at high values. This phenomenon was also confirmed by Bresler and Scordelis[24] and De Pavia[47].

Palaskas *et al.*[104] tested 15 reinforced concrete T-beams. The major variables were the amount of flexural and shear reinforcement. The flexural reinforcement varied from 0.5 to 1% and the shear reinforcement varied from 0 to 0.75 *MPa*. They concluded that the contribution of the shear reinforcement to shear strength was 50% higher than that obtained by using ACI 318-83 equation. They suggested that the higher values reported by Haddadin *et al.*[59] may be due to the higher longitudinal reinforcement ratio used in that study.

It should be mentioned that the BS 8110 equation of beams with shear reinforcement is based on the following equation: $vn = vc + vs$,where $vs = {Vs}/{bd}$ and $Vs = {Avfy\,d}/{s}$.

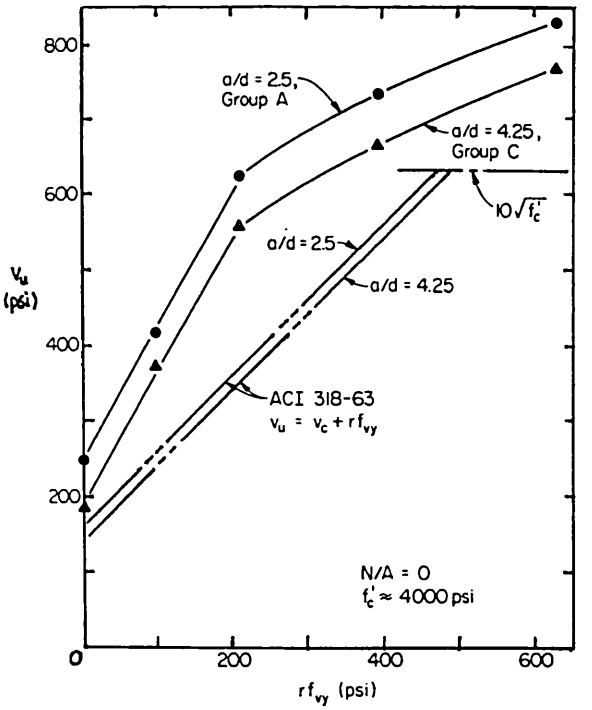

Fig. 2.24- Effect of variation in a/d on relationship between vu and rfy. [59]

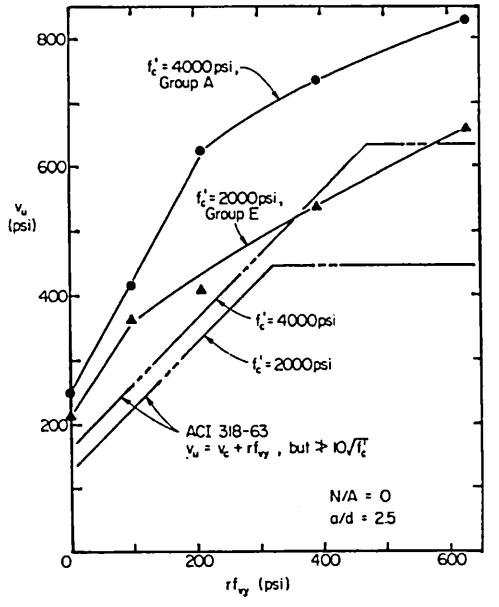

Fig. 2.25- Effect of variation in fc on relationship between vu and rfy.[59]

2.3.3.5 Aggregate interlock

Design codes assume that the shear force required to initiate diagonal cracking can be carried by the concrete section after cracking. It is important to know the ultimate concrete shear strength after diagonal cracking.

Taylor[132,133] developed a method to compute the shear stresses in the compression zone of reinforced concrete beams. The method involves an analysis of the longitudinal strains of the beam compression zone. Longitudinal strain readings at different levels through the depth along one vertical line were used to calculate the shear in the compression zone. In his beam tests, he integrated the shear stresses from the compression face down to the neutral axis which was located below the inclined crack. The amount of shear carried by the compression zone was determined. He came to a conclusion that the shear force carried by a beam without stirrups is shared approximately 20 to 40% by the compression zone, 33 to 50% by aggregate interlock and 15 to 25% by dowel action.

Swamy and Andriopoulos[128] carried out 87 beam tests with and without shear reinforcement in order to investigate the contribution of aggregate interlock and dowel forces to the shear capacity of reinforced concrete beams. They concluded that the maximum aggregate interlock and dowel force contributions: $\frac{(V_a + V_d)}{V}$ in beams without shear reinforcement was varied from approximately 90% for a beam failing by strut action with $a/d = 2$, to approximately 50% for a beam failing in diagonal tension with $a/d = 6$. For beams with shear reinforcement, $\frac{(V_a + V_d)}{V}$ varied from approximately 20% to 75% at $a/d = 2$ depending on the shear reinforcement ratio. They also came to a conclusion that the shear carried by the aggregate interlock mechanism may decrease significantly with the provision of a high amount of shear reinforcement.

Gergeley[56] estimated that the contribution of the aggregate interlock force to the beam shear capacity was approximately 45%.

Overall, a significant amount of difference was seen between the results obtained by these investigators. It should be noted that the concrete compressive strength, the shear reinforcement ratio and the a/d ratio were assumed to have no effect on the contribution of the various mechanisms in Taylor's[132] and Gergeley's[56] investigations ,whereas, Swamy and Andriopoulos[128] did consider the effect of shear reinforcement and a/d ratio. Table-2.1 shows the individual contribution of different shear transfer mechanisms to the beam strength as reported by different investigators.

Table 2.1- Distribution of shear force in reinforced concrete beams

Investigator (s)	Percentage of Total Shear Carried by		
	Aggregate Interlock	Dowel Action	Compression Zone
Taylor[132]	33% to 50%	15% to 25%	20% to 40%
Swamy and Andriopoulos[128]	90 % at a/d=2 and for rfy=0 50% at a/d=6 and for rfy=0 20% to 75% at a/d=2 and for $rfy \neq 0$		-
Gergeley[56]	45%	-	-

2.3.4 Shear failure modes

According to many investigations, such as ACI-ASCE Committee 426[2], Kani[72] and Ferguson[54], one of the most significant factors influencing failure modes in rectangular simply supported reinforced concrete beams is the shear span to depth ratio, a/d. In this sub-section, generally observed failure modes of the beams are reviewed in relation to one condition that only a/d is varied.

(i). Short beams ($1< a/d <2.5$)

In this range of shear span an inclined shear crack is generally the result of a principal tensile crack. The diagonal shear crack appears relatively clearly and forms in the region of the shear span. Once the crack reaches the compression zone, the lower end of the crack propagates downwards to extend along the reinforcement for a short distance towards the support. After reaching approximately above the neutral axis of the beam, the tip of the inclined shear crack propagates gradually towards the load point and finally accompanied with crushing of concrete above the crack into the reduced section. This failure mode is conventionally called *Shear-compression failure*. It is also found that, in these beams the ultimate shear capacity significantly exceeds the inclined crack capacity.

(ii). Intermediate long beams ($2.5< a/d < 6$)

In this range of shear span the crack is known as flexural-shear crack. The first crack forms due to flexural tension at the cross section of maximum moment. As the load on the beam is increased the flexural cracks gradually spread to regions of lesser moment. At some stage of loading, before the beam's full flexural capacity is developed, an inclined shear crack forms suddenly starting at or near an existing flexural crack and rapidly extending both toward the support and the load point. The sudden formation of the inclined shear crack is immediately followed by complete collapse of the beam. The inclined shear crack extends directly to the top of the beam with little change in direction resulting in separation of the beam into two parts. A

number of failures have been seen where the thin segment remaining above the crack fails by spalling upward without any evidence of crushing. This failure mode is usually called *a diagonal tension failure*, as reported by many researchers such as Heger *et al.*[62] , Bresler *et al.*[25], Morrow *et al.*[94],Taylor[132] and Chana[36].

(iii). Long beams ($a/d \geq 6$)

Beyond a certain value of a/d, inclined shear cracks do not develop before the beam fails in flexure. The limiting value of a/d may be a function of such beam characteristics as amount of longitudinal reinforcement,yield strength of main reinforcement and strength of concrete. With such criteria beams usually fail in bending and the failure mode is usually called *a flexural failure*. Fig. 2.25 shows the variation in shear capacity with a/d ratios for rectangular beams.

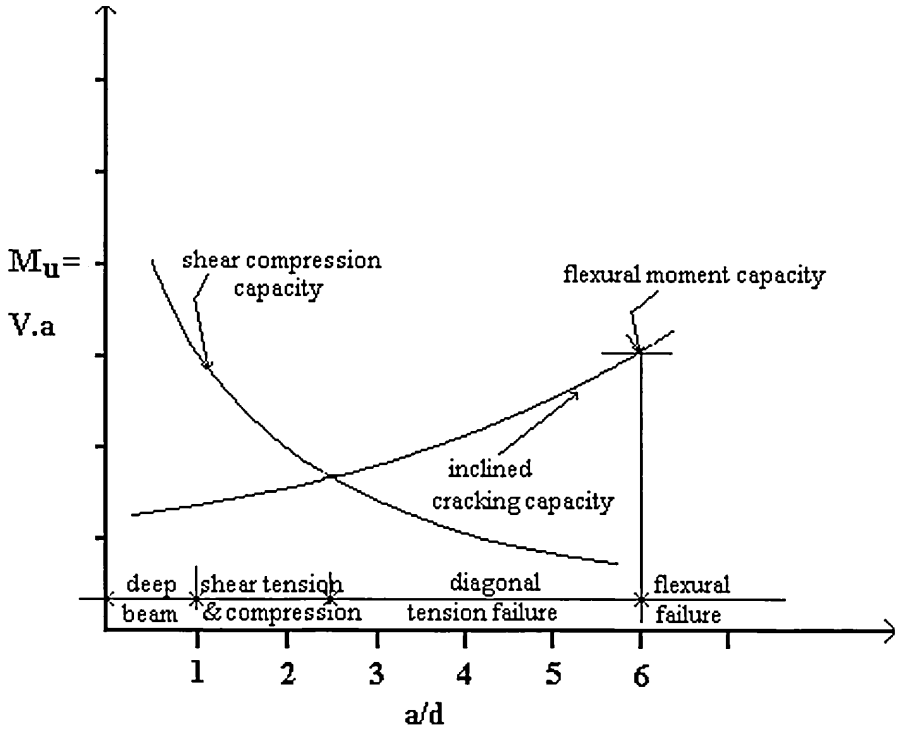

Fig. 2.26- Variation in shear capacity with a/d for R.R.C beams

2.4 Section Four: Main Conclusions

The main conclusions from the aforementioned literature review on normal and HSC are as follows:

2.4.1 High strength concrete materials

1. It is necessary to use a low water / binder ratio and a strong aggregate that bonds well with the matrix to obtain high compressive strength. A superplasticizer needs to be used to ensure adequate workability for these concrete mixes in particular for very low water/binder ratio,e.g., 0.22. Furthermore, superplasticizers should be added to the concrete mix shortly before placing to extend concrete workability, as the effectiveness of superplasticizer diminishes with time after the first dosing.
2. Most of publications advocate the use of mineral admixtures ,*in particular,* silica fume because of the higher concrete strengths which could be obtained compared with other mineral admixtures like ground blast furnace slag or pulverised fuel ash. Moreover, using such admixtures enhance the concrete compressive strength at early ages. On the other hand, it appears that the optimum percentage of silica fume is somewhat obscure,i.e., varied silica fume dosages were recommended by researchers in the reviewed publications, but generally most of the investigations recommended the dosages between 8% to 12% by weight of cement. Also, silica fume in slurry form was reported to be convenient to use and gave predictable results, while the powder form of silica fume was found to be more difficult to use ,*in particular,* for ready mixed concrete.
3. The compressive strength of HSC varied significantly with type and grading of aggregates used.
4. The production and proportioning of HSC is a more critical process compared with that of normal strength concrete. Many trial concrete mixes are required

after the evaluation process of all concrete constituents to detremine the optimum mix.

5. The tensile splitting strength, and elastic modulus of HSC are closely correlated with the compressive strength as illustrated in Fig. 2.9 and Fig. 2.11.
6. The shape of the stress-strain curve of HSC is different from normal strength concrete as shown in Fig. 2.12 ,i.e., there is only a small increase in maximum strain at the maximum stress.
7. HSC is more durable than NSC. It has also, less permeability, drying shrinkage and creep coefficient compared with normal strength concrete particularly when silica fume is included in the concrete mix. Overall, HSC is a superior product with enhanced engineering properties.

2.4.2 High strength concrete members in flexure

1. It is noted that most of the studies on design and analysis of reinforced HSC beams have significantly followed the same proposed simplification of NSC technique, i.e., simplified stress block. It appears that these assumptions led most of the time to conservative results. Moreover, most of these investigations have been limited to compressive strengths of up to 80 *MPa*, and they have not been able completely to clarify the structural behaviour of members made from concrete with compressive strength in access of 80 *MPa*.
2. It was concluded that the ductility of HSC members were generally higher than that of beams with lower strength concrete. Moreover, the ductility index is almost independent of concrete compressive strength.
3. The maximum tensile reinforcement amount which can be used in a reinforced concrete beam is significantly influenced by the concrete compressive strength, f_c, the yield stress, f_y, of the reinforcement, and the ultimate compressive strain of concrete, ε_{cu}.

2.4.3 Shear capacity of reinforced concrete beams

From the review of research presented on the shear capacity of reinforced concrete beams, it is realised that the number of parameters that influence the shear capacity of reinforced beams are large. Unfortunately they do not act independently of each other. The primary factors that influence the shear capacity of a reinforced concrete beam are concrete strength, shear span to depth ratio, flexural reinforcement ratio and shear reinforcement ratio. The following summarise the effect of each parameter on the shear capacity:

1. The shear capacity of reinforced concrete beams increases as the concrete compressive strength increases; however, the rate of increase is not proportional to the increase of the concrete strength value.
2. The shear capacity increases significantly as a/d decreases. Also, the a/d ratio has significant influence on the type of failure that occurs.
3. The flexural reinforcement ratio has a significant influence on the shear capacity of reinforced concrete beams and the failure mode,i.e., the shear capacity increases as the flexural reinforcement ratio increases.
4. Stirrups significantly increase the shear capacity and affect the mode of failure. Moreover, they are more efficient at low and moderate longitudinal steel ratio than at high ratio.

CHAPTER 3

EXPERIMENTAL PROGRAMME IN FLEXURE

This chapter deals with the details and manufacture of specimens tested in flexure. Testing procedures and results of tests of plain concrete specimens obtained from trial mixes of higher strength concretes, and reinforced concrete beams are presented.

3.1 Materials Used

(i) Cement

For this research investigation Portland cement was used with a compressive strength of 57.5 *MPa* at 28 days tested according to the European Standard EN 196. The initial and final setting times were 100 and 150 minutes respectively.

(ii) Fine and Coarse aggregates

The fine aggregate was natural sand with a relative density of 2.61 at the saturated surface dry condition. The coarse aggregates, 10 *mm* and 20 *mm*, were crushed stone obtained from a local quarry. The selection of this aggregate was made after a detailed analysis of aggregate from three local quarries. The results of sieve analysis, and other properties for the sand and the aggregates used in the project are shown in Table-3.1, and Fig. 3.1 to 3.3. All coarse aggregates were washed and sieved in order to get rid of dust.

(iii) Admixture

Two chemical materials were used in order to achieve HSC mixes, Silica fume and Superplasticizer. The former was in a slurry form supplied by Elkem company,i.e., product name EMSAC 500 S while the latter was in the form of an aqueous solution, supplied by Cormix,i.e., product name S 10 naphthalene-based

superplasticizer, and was used to reduce the w/c ratio and to adjust the slump of the concrete mix. The ranges of silica fume and superplasticizer dosages were 5 to 11.5%, and 0.67 to 2% respectively by weight of cement as a solid content. Table 3.2 shows their physical properties.

(iv) Reinforcing steel for the beams

High yield deformed steel of 12 and 20 *mm* diameter were used in this part of the investigation. For beams having 12 *mm* reinforcement the bars were bent at the end according to BS 4466 clause 3.12.8.4. Tension tests were carried out for the steel reinforcements according to EN 10002 part one using Denison universal testing machine of 250 *kN* capacity. The Stress-Strain characteristics of the reinforcement are shown in Fig. 3.4 and Table 3.3.

Table- 3.1 Properties of Coarse Aggregate

Size	*Absorption %*	*ACV %*
10 *mm*	4.39	-
20 *mm*	2.98	-
10 -14 *mm*	-	14.52

Table- 3.2 Properties of Superplasticizer & Silica fume

Item	*Superplasticizer*	*Silica fume*
Appearance	dark brown liquid	grey slurry
Specific gravity	1.19	1.4
Air entrainment	1% to 2%	-
Water content	60 % by weight	50 % by weight

Table 3.3 - Properties of Tensile Steel Reinforcement

Bar Size ϕ *mm*	$f_{y\bullet}$, *MPa*	f_u* *MPa*	E_s, *kN/mm²*	ε_y, *mm/mm*
12	470	610	192	0.0024
20	442	631	211	0.0020

$f_{y\bullet}$= Average yield stress

f_u*= Average ultimate stress

Fig. 3.1- Sieve Analysis of the Sand

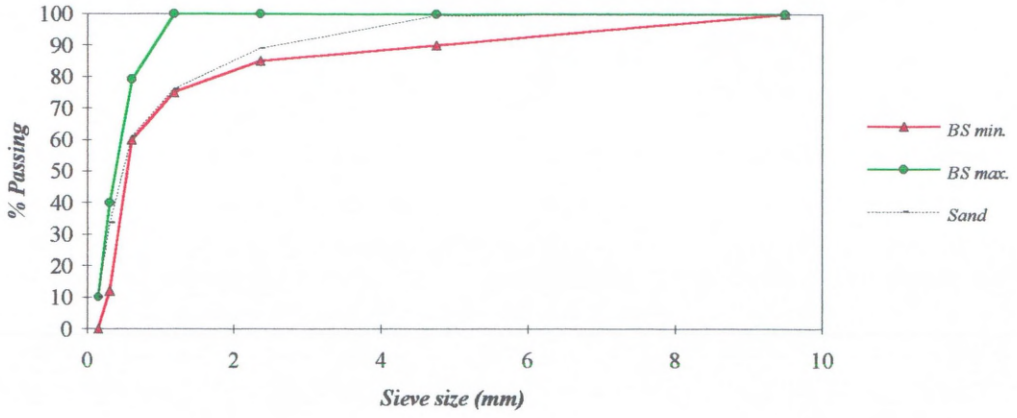

Fig. 3.2- Grading of 10 mm Aggregate

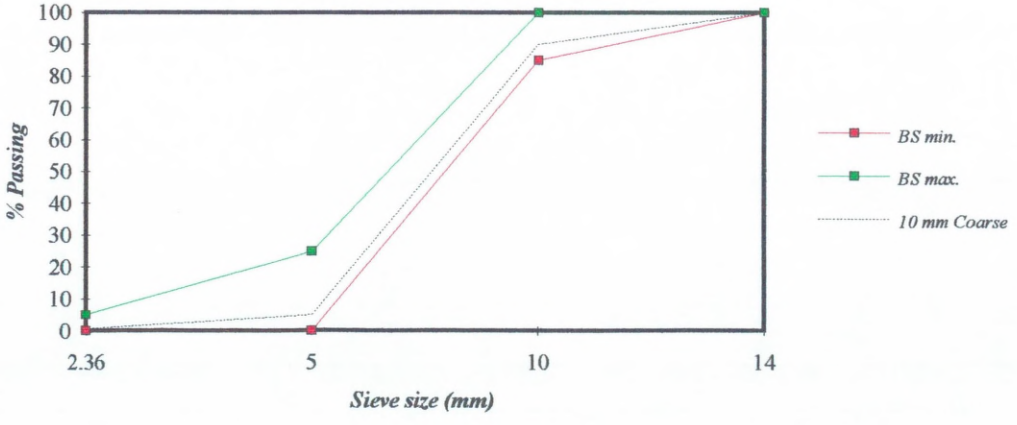

Fig. 3.3- Grading of 20 mm Aggregate

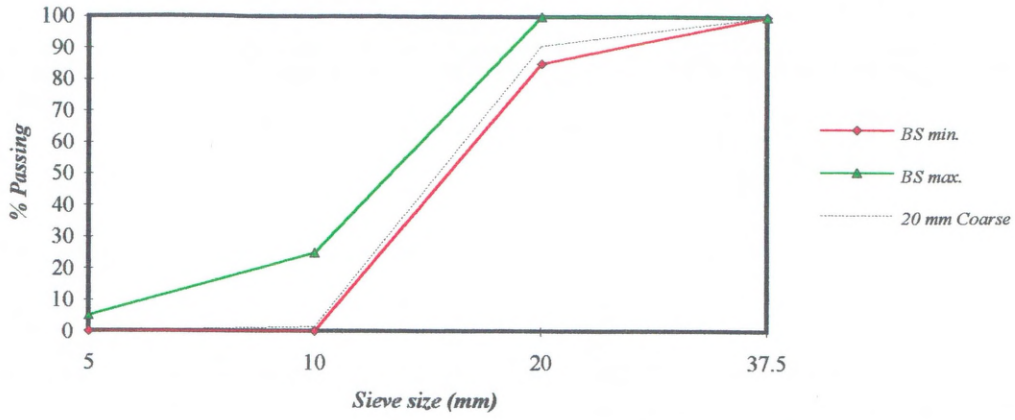

Fig. 3.4 - Typical Stress -Strain relationship for 12 mm &20 mm reinforcements

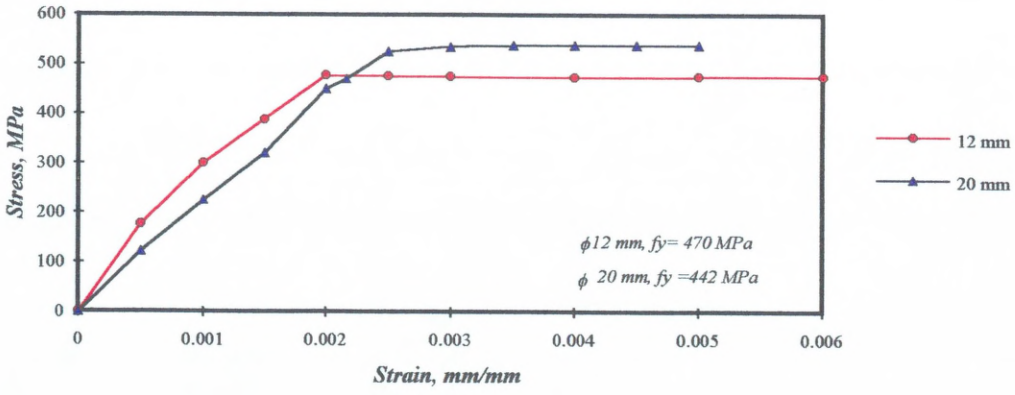

3.2 Mix Proportions and Experimental Procedures

3.2.1 Mix proportions-trial Mixes

The literature review revealed that higher strength concrete technology is relatively new and, therefore conventional mix design methods were not applicable for higher strength concrete. A trial batch programme was considered to be the most effective method for determining the suitability of the materials and their proportions for a specific batch, in order to get the optimum concrete mix.

In this study the mix proportioning was primarily based on known facts of designing concrete mixes. Throughout the experimental work, the fine aggregate to total aggregate ratio was kept at 0.425, the cement content was between 430 to 450 kg/m^3. The major variables were Silica fume and Superplasticizer dosages, while the cement content was the minor variable. A total of 18 trial concrete mixes were used until the required range of compressive strength was achieved. Table-3.4 illustrates the compositions of these concrete mixes.

A summary of the results from the trial mixes is shown in Table 3.5. The results of these mix trials are discussed in full in chapter four. At this point it is sufficient to note that the range of strength required for the beam tests for the beam tests for the main experimental work could be achieved using mix designations **3, 13 and 16.** These were then used to cast the beams, the actual details of mixes used are shown in the Tables 3.4 and 3.5 which give the beam designations.

Table 3.4- Compositions of High Strength Concrete Mixes

Mix	*C* kg/m^3	*S* kg/m^3	*CA* kg/m^3	*SF* L/m^3	*SP* L/m^3	*W** L/m^3	*W/C*	*W/(C+SF)*
1	450.0	566.5	1333.5	61	9.5	136.50	0.303	0.277
2	450.0	566.5	1333.5	61	11	128.68	0.286	0.261
3	450.0	566.5	1333.5	61	12	126.18	0.280	0.256
4	450.0	566.5	1333.5	48	11	124.85	0.277	0.258
5	450.0	566.5	1333.5	73.5	11	132.70	0.295	0.265
6	450.0	566.5	1333.5	73.5	12	130.42	0.290	0.260
7	428.5	566.5	1333.5	30.7	7.2	159.40	0.372	0.354
8	428.5	566.5	1333.5	49	18	137.90	0.322	0.299
9	428.5	566.5	1333.5	36.7	7.2	173.46	0.400	0.382
10	428.5	566.5	1333.5	61	6.75	169.20	0.390	0.360
11	428.5	566.5	1333.5	61	7.65	166.45	0.388	0.353
12	428.5	566.5	1333.5	61	7.75	151.90	0.355	0.329
13	428.5	566.5	1333.5	61	6	197.10	0.460	0.418
14	428.5	566.5	1333.5	61	8.5	155.85	0.364	0.330
15	428.5	566.5	1333.5	61	9.5	135.65	0.317	0.288
16	428.5	566.5	1333.5	61	10.5	123.30	0.288	0.262
17	428.5	566.5	1333.5	49	10.5	125.05	0.292	0.270
18	428.5	566.5	1333.5	36.8	10.5	119.93	0.280	0.264

C= Cement S= Sand CA= Coarse aggregate SP = Superplasticizer SF = Silica fume W=Water

* This includes water in Silica fume, Superplasticizer, and Sand.

Table 3.5- Experimental results of Compressive strength of HSC mixes

Mix	*W/C*	f_{cu}, *MPa* *1 day*	f_{cu}, *MPa* *7 days*	f_{cu}, *MPa* *28 days*	f_{cu}, *MPa* *90 days*
1	0.303	46.9	84.50	114.50	114.50
2	0.286	51.6	90.00	110.00	113.00
3	**0.280**	**50.9**	**94.00**	**114.50**	**120.00**
4	0.277	51.0	90.50	109.50	115.50
5	0.295	50.9	90.50	99.00	106.50
6	0.290	40.5	87.00	101.00	114.50
7	0.372	25.6	68.00	80.00	92.50
8	0.322	23.3	70.25	80.50	90.00
9	0.400	39.4	80.00	93.00	96.00
10	0.390	37.8	66.50	91.50	93.00
11	0.388	37.6	56.00	92.00	106.00
12	0.355	37.6	72.00	98.00	100.00
13	**0.460**	**28.4**	**60.50**	**78.00**	**88.00**
14	0.364	41.1	80.00	99.50	107.00
15	0.317	44.4	82.50	90.00	105.00
16	**0.288**	**46.9**	**91.00**	**100.50**	**111.00**
17	0.292	47.4	90.00	109.00	110.00
18	0.280	36.1	93.00	109.50	110.00

Mixes 3, 13 and 16 were selected for casting the flexural reinforced concrete beams

3.2.2 Beam test specimens

The beam dimensions were chosen in order to make the beams fail in flexure,i.e., the shear span to depth ratio (a/d) was 6, and to ensure that the specimens were sufficiently large so as to represent real structural element of high strength concrete. With these considerations in mind a specimen of cross section of 150 *mm* by 250 *mm* deep, and a span of 3240 *mm* was chosen; the overall length of the beams was 3440 *mm*. A typical beam specimen is illustrated in Fig. 3.5-a. The specimens were tested under two-point loading which subjected a considerable length of the beams to pure flexure.

For singly reinforced beams four sets of three specimens each were manufactured, using mixes to give three concrete compressive strengths,i.e., 85, 100, and 115 *MPa* as selected from the first stage of this research investigation. The longitudinal reinforcement ratios were 1.03%, 1.42%,1.94% and 4.04% respectively. Four doubly reinforced specimens were also manufactured using the highest concrete compressive strength mix,i.e., 115 *MPa*. In this series the variables were the tensile reinforcement ratio,ρ, and the compression reinforcement ratio,ρ'. The ρ values were 4.04 and 4.4% whereas the ρ' values were 0.504 and 0.727% respectively. For all sets, nominal shear reinforcement was provided at a spacing of 150 *mm* according to BS 8110 clause 3.4.5.4 so as to avoid shear failure. Two 8 *mm* diameter hanger bars outside the flexural test zone were used to support the links. Figs. 3.5b and 3.5c illustrate the reinforcement details.

Each beam was designated by three letters, and two numerals, such as HSC1-1. The first numeral indicates the percentage of the longitudinal reinforcing bars, the second numeral the grade of concrete strength. The details of beams in flexure are listed in Table- 3.6 and Table-3.7.

Table -3.6- Designation and Properties of Singly Reinforced HSC Beams

Beam No.	*Beam+ Mark*	f_{cu} *, MPa	*h, mm*	*b, mm*	*d, mm*	E_c, *MPa*	*Rin-forcing bars*	A_s, mm^2	ρ %
1	HSC1-1	107	250	150	220	40640	3 ϕ12	339	1.03
2	HSC1-2	97	250	150	220	41000	3 ϕ12	339	1.03
3	HSC1-3	85	250	150	220	38550	3 ϕ12	339	1.03
4	HSC2-1	105	250	150	212.5	49650	4 ϕ12	452	1.42
5	HSC2-2	100	250	150	212.5	43600	4 ϕ12	452	1.42
6	HSC2-3	78	250	150	212.5	34000	4 ϕ12	452	1.42
7	HSC2-4	90	250	150	212.5	40487	4 ϕ12	452	1.42
8	HSC3-1	107	250	150	215	53000	2ϕ 20	628	1.94
9	HSC3-2	85	250	150	215	39000	2ϕ 20	628	1.94
10	HSC3-3	78	250	150	215	34005	2ϕ 20	628	1.94
11	HSC4-1	101	250	150	207.5	41200	4ϕ 20	1257	4.04
12	HSC4-2	87	250	150	207.5	38855	4ϕ 20	1257	4.04
13	HSC4-3	82	250	150	207.5	41130	4ϕ 20	1257	4.04

* From 100 x 100 *mm* cubes

+ Beam nomenclature: for HSC indicates High strength singly section, "1-1" the lowest ρ, and the highest f_{cu} grade in each group respectively.

Table-3.7- Designation and properties of doubly reinforced HSC beams

Beam	f_{cu} *, *MPa*	*h*, *mm*	*b*, *mm*	*d*, *mm*	E_c, *MPa*	*Rin-forcing bars*	A_s, mm^2	ρ %	A'_s, mm^2	ρ' %
DHSC1-1	107	250	150	207.5	41000	4 ϕ20 1ϕ12	1370	4.4	157	0.5
DHSC1-2	100	250	150	207.5	40000	4 ϕ20	1257	4.04	157	0.5
DHSC1-3	100	250	150	207.5	40500	4 ϕ20 1ϕ12	1370	4.4	226	0.73
DHSC1-4	100	250	150	207.5	40500	4 ϕ20	1257	4.04	226	0.73

* From 100 x 100 *mm* cubes

3.2.3 Casting and curing

(i) Small test specimens

Concrete was mixed in a 0.05 m^3 pan-type revolving mixer. For all the mixes, coarse aggregate and sand were introduced into the mixer and mixed for a minute. About 1/3 of the estimated water was then added and mixed for two minutes. The cement was introduced with some mixing water and mixed to ensure the uniformity of the mix. The rest of the ingredients, including silica fume slurry, and superplasticizer were added while the mixer was running for about 2.5 minutes. The slump was measured, the rest of the mixing water then added if necessary to adjust the slump in the range of 50 to 100 *mm*. Before casting control specimens, the slump was determined. For each concrete batch a set of eight 100 *mm* x 100 *mm* cubes, and two 100 *mm* x 300 *mm* cylinders in steel moulds were cast. The specimens were demoulded on the following day and moist-cured at 20 ± 1° C in a water tank. The concrete cube specimens were tested at 1, 7 , 28 and 90 days for compressive strength, while the cylinder specimens were tested at 28 days for the splitting tensile strength. For each test the average strength of two specimens was determined and the results were used in the analysis.

(ii) Beam specimens

The concrete for the beams was mixed in a 0.1 m^3 revolving mixer. The steel beam mould was oiled before the cage was placed in position. Chairs were used to ensure appropriate cover for the reinforcement. Concrete was placed in the moulds in two layers and was internally vibrated by a poker vibrator. Two concrete batches were required to cast one beam. Two cubes of 100 x 100 *mm*, and one cylinder of 100 x 300 *mm* were cast from each batch to determine the strength, and the stress-strain characteristics of the concrete at the age of beam test. When casting was completed, the beam, cubes, and cylinders were completely wrapped with wet hessian and polyethylene sheets to prevent moisture loss. The cubes and cylinders were stripped after 24 hours, while the beam was stripped one day later. The control cubes and

cylinders were placed in a water tank with an average temperature of approximately 20° C. The beams were wrapped in wet hessian and polythene which was regularly re-wetted for a period of 28 days, after which the beams were allowed to dry in the laboratory air until the day of testing. All beams were given a coat of thin white-wash prior to testing to facilitate the observation of cracks during the tests.

3.3 Mounting of Strain Gauges

(i) Longitudinal bars

For all the specimens the two outermost longitudinal bars were provided with strain gauge at top and bottom surfaces at the mid length of the bars to monitor steel strains during the progress of the test; additional strain gauges were used in the specimens which had two layers of reinforcement. All the gauges used were FLK-6-11, with a resistance of 120 Ω, and an active grid length of approximately 6 *mm*. To facilitate mounting of these gauges, the bar deformations were ground off over a length of approximately 35 *mm*. After mounting on the bars, the gauges were given a coating of a water proofing compound to prevent damage during and after casting.

(ii) Concrete surface

Seven pairs of demec-gauge studs were placed on each vertical face of the beams, the gauge length being 200 *mm*. In order to measure the maximum compression strains two demec-gauges were mounted as close to the top surface as possible. The other six gauges were mounted on each side along the depth of the beam at 30 *mm*, 60 *mm*, 90 *mm*, 120 *mm*, 150 *mm* from the top, and at the centric line of the longitudinal reinforcements. Fig. 3.5-a shows the locations of the demec- gauges.

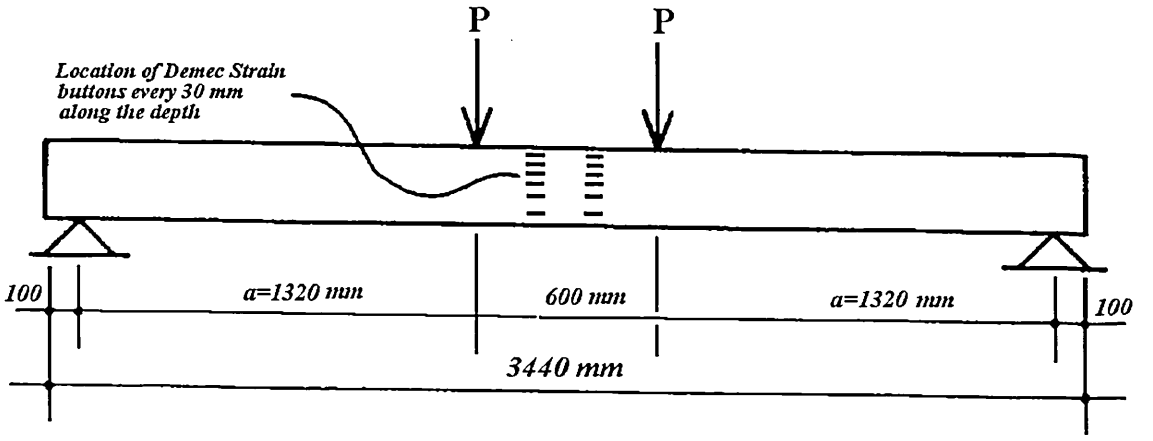

Fig.3.5 a- Loading Configuration for the Test Specimen

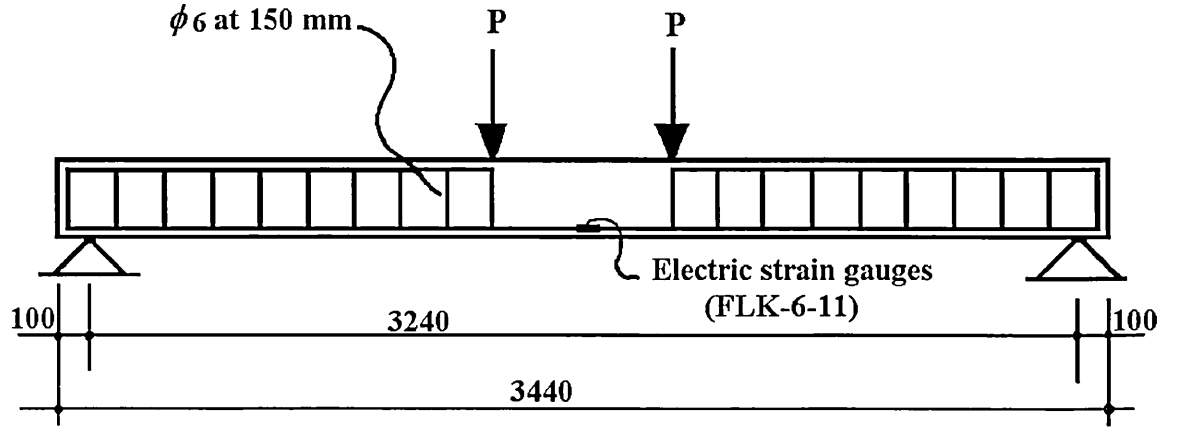

Fig.3.5 b-Reinforcement Details for the Singly Reinforced Test Specimens

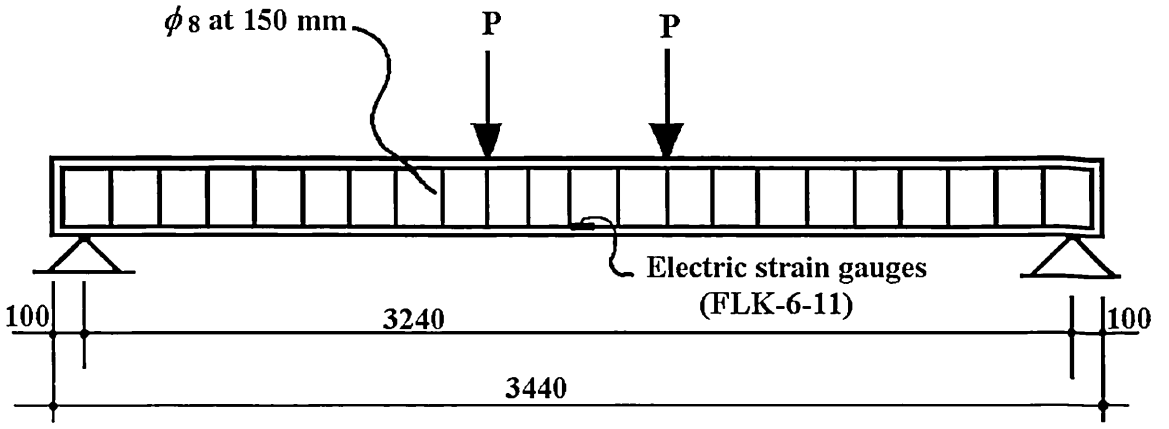

Fig.3.5 d-Reinforcement Details for the Doubly Reinforced Test Specimens

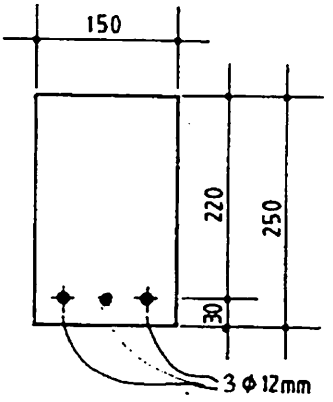

Beam 1, 2 and 3

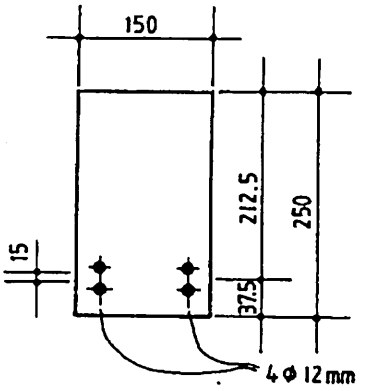

Beam 4, 5, 6 and 7

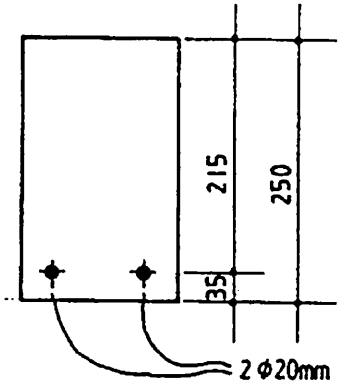

Beam 8, 9 and 10

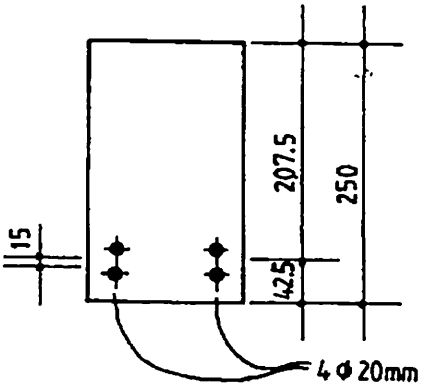

Beam 11, 12 and 13

Fig.3.5 c- Cross-Section Specimens Details

3.4 Tests on Hardened HSC

The strength tests performed on the small concrete cylinder and cube specimens were compressive strength and splitting tensile strength tests. Modulus of elasticity tests were performed on separate cylindrical specimens from the concrete mixes used in casting the beam specimens.

3.4.1 Compressive strength test

Compressive strength tests were performed in accordance with BS 1881: part 116: 1983 for compressive strength of cube specimens using an Avery-Denison testing machine with a maximum capacity of 3000 *kN*. The compressive strength was calculated as follows:

$$f_{cu} = P/A \qquad 3.1$$

where,

f_{cu} = Cube compressive strength, *MPa*

P = Maximum load carried by the specimen, N

A = Average cross-section area of the specimen, mm^2

3.4.2 Splitting tensile strength test

To determine the splitting tensile strength of the concrete mixes used in this investigation an Avery-Denison testing machine with a capacity of 1250 *kN* was used. The cylinders were loaded on two diametrically opposite edges with two plywood strips used to apply line loads, at a constant rate of 2.1 *kN/sec*, until the failure of the specimen in accordance with BS 1881: part 117:1983.

The splitting tensile strength of each cylinder calculated as follows:

$$f_{sp} = \frac{2P}{\pi l d} \qquad 3.2$$

where,

f_{sp} = Splitting cylinder tensile strength, *MPa*

P = Applied load at failure of specimen by splitting, *N*

l = Length, *mm*

d = Diameter of cylinder, *mm*

3.4.3 Modulus of elasticity and Poisson's ratio

The modulus of elasticity of concrete was calculated from the stress-strain diagram of cylinder specimens cast from the concrete mixes corresponding to each beam specimen. The Avery-Denison testing machine mentioned above was used for this purpose at a constant load rate of 1.88 *kN/sec*, according to the BS 1818: part 121:1983 recommendation.

Cylindrical specimens measuring 100 x 300 *mm* were used. The longitudinal, and the traverse strain deformations were measured using electric resistance strain gauges PL-60-11, with gauge length of 60 *mm*, and gauge resistance of 120 ± 0.3 Ω. For every cylinder specimen two longitudinal, and two traverse strains gauges were used and reading were taken using a multi-channel digital strain indicator.

The load was applied up to about 45% of the expected ultimate compressive strength while all strain readings were taken, then unloaded to the initial strain values.
The processes of loading and unloading were repeated until consistent strain values were attained between the lower and upper stress limits.
The secant modulus of elasticity was calculated as follows:

$$E_c = \frac{(\sigma_2 - \sigma_1)}{(\varepsilon_2 - \varepsilon_1)} \qquad 3.3$$

where,

E_c = Secant modulus of elasticity, *MPa*

σ_2 = Stress corresponding to 45% of ultimate load, *MPa*

σ_1 = Stress corresponding to initial load, *MPa*, and

$\varepsilon_1, \varepsilon_2$ = longitudinal strains produced by stresses σ_1, σ_2.

The Poisson's ratio was calculated for every test specimen, at every load stage according to the following equation:

$$\mu = \frac{\varepsilon t}{\varepsilon l} \qquad 3.4$$

where,

μ = Poisson's ratio,

εt = Average transverse strain at mid-height of the specimen, and

εl = Average longitudinal strain at mid-height of the specimen.

3.5 Testing Arrangements for HSC Beam Tests

All beam specimens were tested using a static screw- head jack. The applied load was measured by a load cell of a maximum capacity of 1000 *kN* connected to a data logger as shown in Fig. 3.7-a.

3.5.1 Measurement of deflections

Three linear voltage displacement transformers (LVDT) were placed under each member at the centre of the beam span, and at the two loading points, to measure the deflections within the region of pure bending. The full displacement range of the LVDT used was ± 100 *mm*. In addition to the LVDT's, one dial gauge with a displacement range of 50 *mm*, and a least count of 0.01 *mm*, was used to measure the deflection at the top of mid-span as a secondary check.

3.5.2 Measurement of strains

As stated earlier, the tensile strains in the tension steel were measured using electrical foil strain gauges with an accuracy of one micro-strain. Compressive strains on concrete were measured by using the mechanical demec-gauges on both faces of the beams. All recording systems were calibrated before testing.

3.5.3 End support

All beam specimens were supported at each end by means of steel saddles which were designed to prevent bearing failure of the test specimens. Each saddle was stiffened and provided with a 15 mm steel plate. All the beams were supported on steel bars of 40 mm diameter on both ends. Details and dimensions of these supports are shown in Fig. 3.6.

3.5.4 Test procedure for beam specimens

All the tests in this part of research programme were performed using the static screw-jack as shown in Fig. 3.7-b, through a single point, transferred to the concrete member through a universal steel spreader beam,i.e., W 254 x 146 with a total length of 1200 *mm*, designed and fabricated for the test purpose. The steel spreader beam was supported on two bearing plates 200 x 150 x 30 *mm* resting on steel rollers, covering the entire width of the beam, and placed symmetrically with respect to the mid-span section at a distance of 600 *mm*.

Loads were increased incrementally, until ultimate load capacity was reached,i.e.,the maximum load-carrying capacity beyond which the beam deflection started to increase in an unstable manner. For groups one and two the load increments were kept relatively constant at 5 *kN* while for groups three and four the incremental loads were at 10 *kN*. The application of each load increment, and taking of all measurements, i.e., deflections, strain deformations and crack width at mid-span zone required about 5 to 10 minutes. The entire testing of one beam specimen

required about 3-hours. On the day a beam was tested auxiliary tests were carried out to determine the concrete compressive strength and the stress-strain characteristics of the concrete.

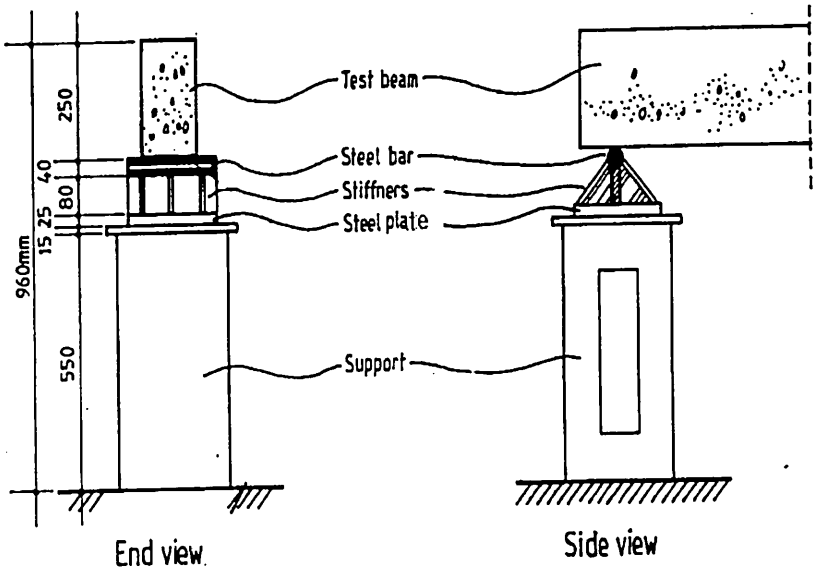

Fig.3.6- End Support Details

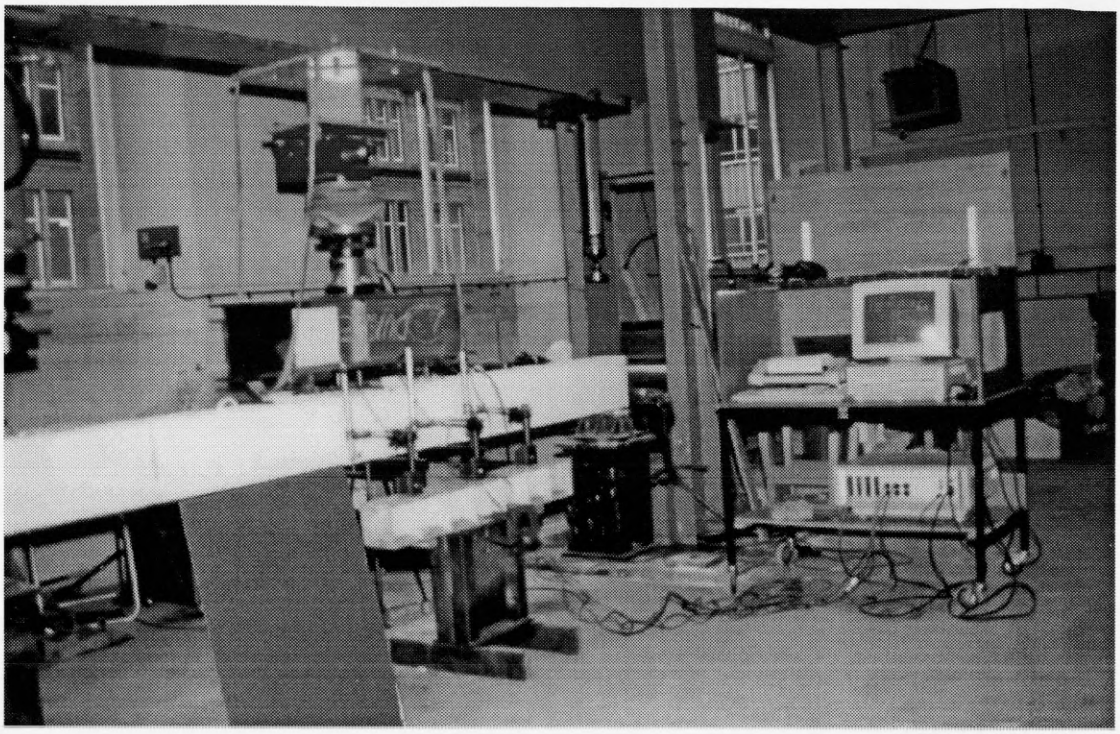

Fig.3.7a- Test arrangement for the beam specimen in flexure

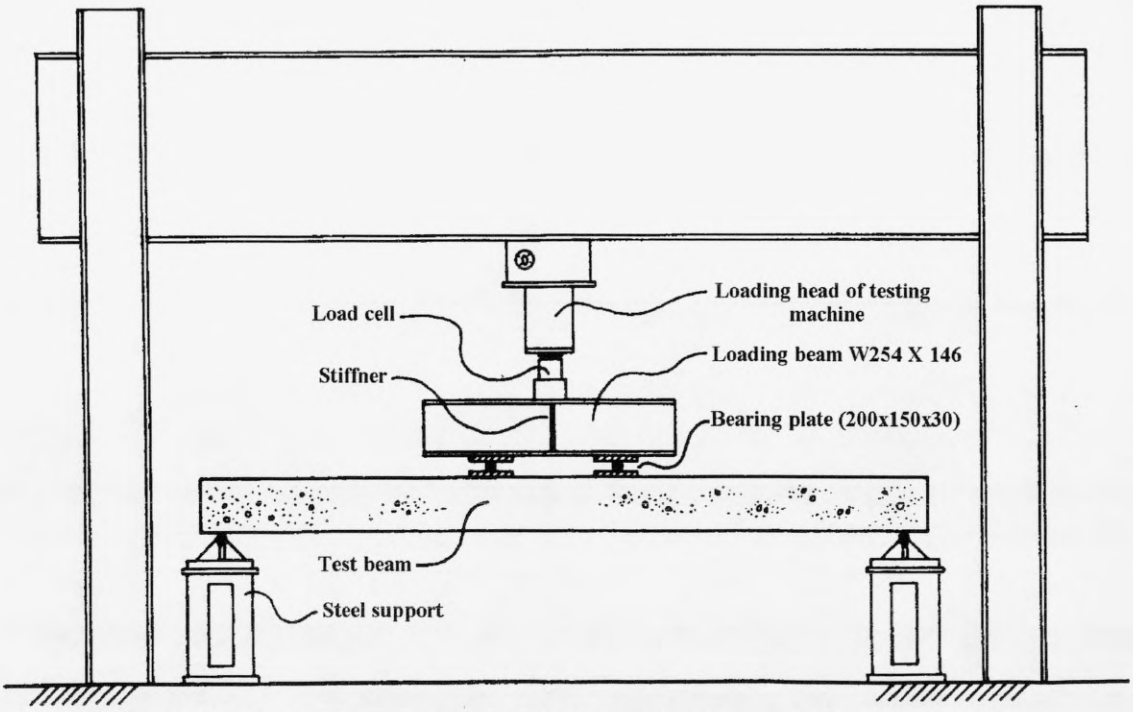

Fig. 3.7b- Test arrangement for the beam specimen in flexure

CHAPTER 4

PRESENTATION OF EXPERIMENTAL RESULTS IN FLEXURE

4.1 Introduction

This chapter has been presented in two parts. The first part presents the experimental results concerning the properties of HSC mixes, including the effect of superplasticizer on the workability and the influence of silica fume on both concrete compressive strength and splitting tensile strength. Data on the static modulus of elasticity and Poisson's ratio of HSC mixes are also presented.

The second part presents the results of tests reinforced HSC beams in flexure. These include load-deflection behaviour, moment-rotation characteristics, ductility and crack patterns.

4.2 Properties of HSC

4.2.1 Workability of HSC mixes

As mentioned earlier the use of superplasticizer is essential in order to produce a workable HSC mix with a low w/c ratio, in some cases as low as w/c = 0.27. Superplasticizers disperse flocs of fine cement particles, and lower the viscosity of the cement paste to produce the enhanced workability. Fig. 4.1 shows the effect of different superplasticizer dosages on the workability of HSC mixes at a constant w/c ratio. At w/c ratio of 0.4 and a superplasticizer dosage of 0.75% by weight of cement the slump was only 46 *mm* (as seen in mix 10; Fig. 4.1). When the superplasticizer dosage was increased only slightly to 0.8%, the slump increased markedly by 30% (60 *mm*) as shown in Fig. 4.1 for mix 9. At w/c ratio of 0.29 the slump was also increased significantly when superplasticizer dosages were increased, e.g, compare mix 1 and mix 6 in Fig. 4.1. This indicates the beneficial effect of superplasticizer on the workability of concrete.

4.2.2 Compressive strength

The compressive cube strengths, f_{cu}, at ages 1, 7, 28, and 90 days are presented in Table 4.1. Two major factors, the silica fume content and the W/(C+SF) ratio, and their effect on the concrete compressive strength are discussed below.

(i) Effect of silica fume

It is well known that silica fume can be used either as a partial replacement for cement or as an additive in concrete. Because of its fineness, it can fit into spaces between cement grains in the same way as sand fills the spaces between particles of coarse aggregate and cement grains fill the spaces between sand grains (average diameter of about 0.1μ *m*). Fig. 4.2 shows the effect of different silica fume dosages on the compressive strength at the age of 28 days of HSC mixes at a constant w/c ratio for different concrete mixes. It can be noted that with the increasing silica fume dosages up to 9.5% by weight of cement, the concrete strength increases by about 5%, i.e., mix 1 and mix 17. This phenomenon also applies to concrete mixes having w/c ratio of 0.28 (mix 3, and mix 4). As the silica fume dosage is increased beyond 9.5% the compressive strength tends to reduce markedly, e.g, at a silica fume content of 11.43% the strength drops by about 14% for Mix 5 compared with Mix 1. These findings agree with the results obtained by Yogendran *et al.*[149] who concluded that a dosage of 20% of silica fume gives a much lower compressive strength than that of a 15% dosage. Fig. 4.3 also shows the development of cube strength for ages of 1, 7 , 28, and 90 days with silica fume dosages of 5%, 6%, 10%, and 11.43%, and different w/c ratios. It is apparent from this Figure that the development of strength is broadly similar irrespective of the silica fume dosage. However, from these test results it appears that the optimum silica fume dosage is 9.5% by weight of cement for achieving the highest f_{cu} for a concrete mix.

(ii) Effect of W/(C+SF) on strength

The effect of W/(C+SF) ratio on concrete strength at various ages is shown in Fig. 4.4. In this investigation, by using silica fume as an additive, the highest strength of concrete attained at 90 days was 120 *MPa* (mix 3). For this mix the W/(C+SF) ratio was 0.256 and the slump was 60 *mm*. A similar result was obtained for a concrete mix with W/(C+SF) ratio of 0.258 with a slump of 115 *mm* (mix 4).

In general the following observation could be made from the results shown in Table 4.1 and Figs. 4.2 to 4.4. Silica fume had the most significant effect when the dosage was about 10% by weight of cement. This appears to be the optimum dosage percentage to achieve the maximum cube compressive strength. Also, the optimum percentage of superplasticizer to obtain a medium slump concrete mix with highest compressive strength was 1.27% by weight of cement content and the optimum cement content appeared to be 450 kg/m^3.

Fig. 4.1- Effect of superplasticizer on workability of concrete

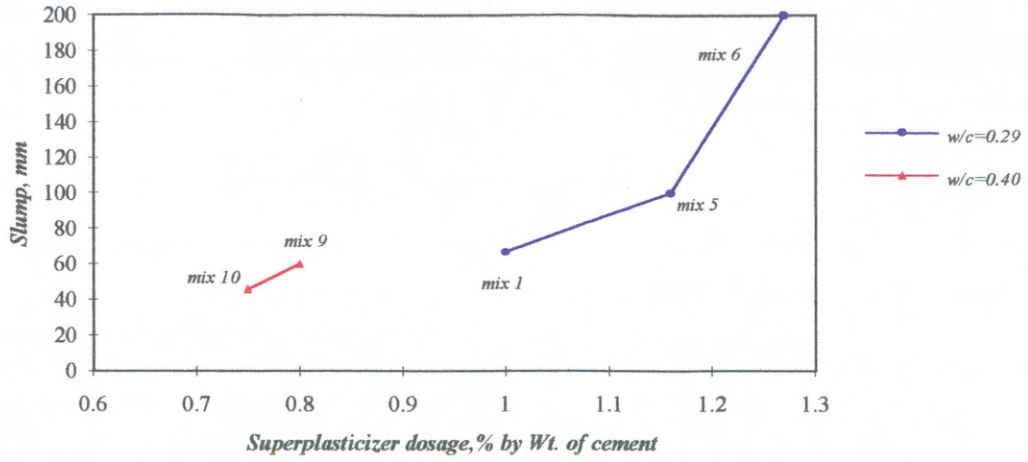

Fig.4.2- Effect of silica fume dosages on concrete strength

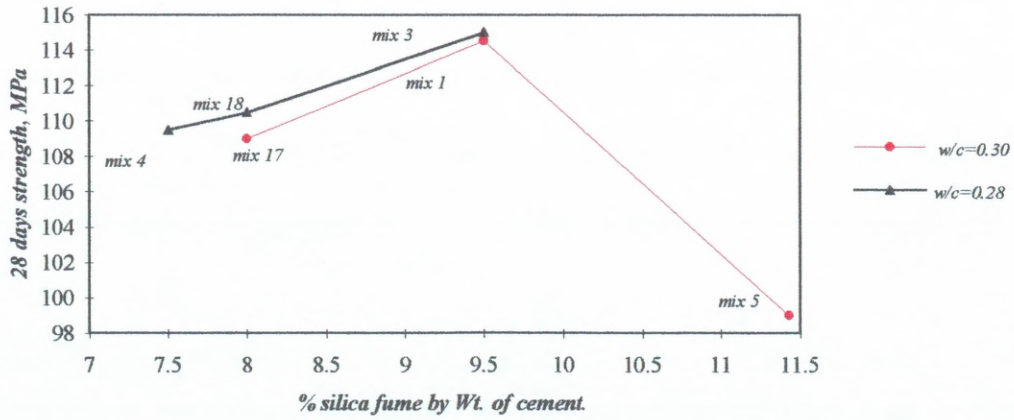

Fig. 4.3- Development of strength with age as a function of silica fume content

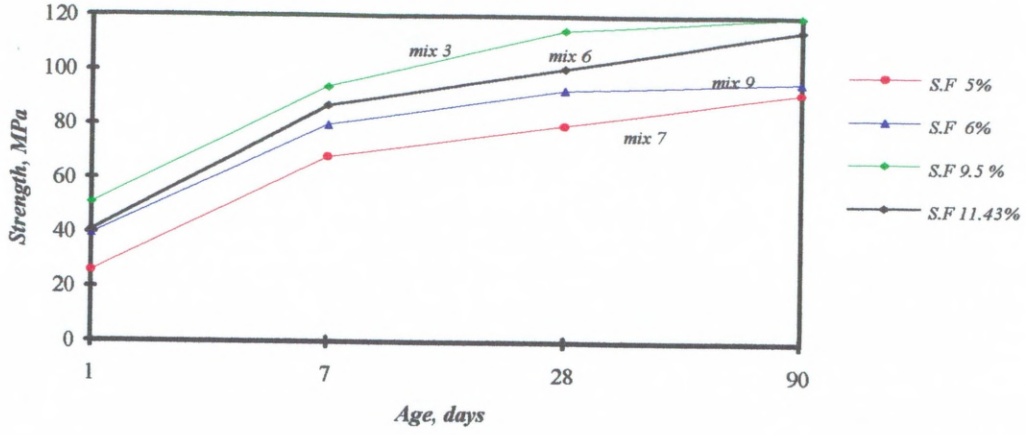

Fig. 4.4 - Effect of W/ (C+S.F) on concrete strength.

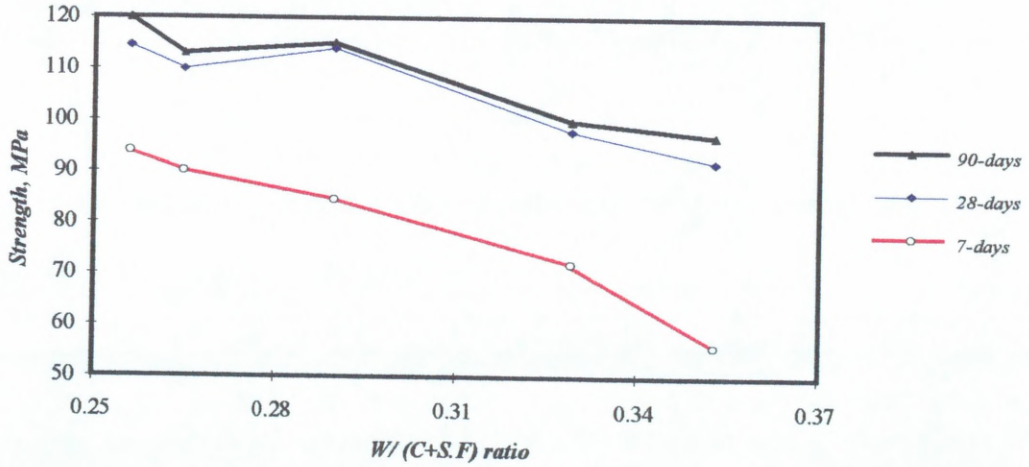

Table 4.1 Experimental Results of Compressive Strength of HSC Mixes

Mix	Slump *mm*	f_{cu}, *(MPa)*				Dry unit weight kg/m^3
		1 day	7 days	28 days	90 days	
1	67	46.9	84.50	114.50	114.50	2492
2	60	51.6	90.00	110.00	113.00	2546
3	60	50.9	94.00	114.50	120.00	2477
4	115	51.0	90.50	109.50	115.50	2529
5	100	50.9	90.50	99.00	106.50	2493
6	shear	40.5	87.00	101.00	114.50	2490
7	shear	25.6	68.00	80.00	92.50	2480
8	shear	23.3*	70.25	80.50	90.00	2474
9	60	39.4	80.00	93.00	96.00	2500
10	46	37.8	66.50	91.50	93.00	2475
11	145	37.6	56.00	92.00	106.00	2490
12	85	37.6	72.00	98.00	100.00	2500
13	35	28.4	60.50	78.00	88.00	2483
14	55	41.1	80.00	99.50	107.00	2455
15	103	44.4	82.50	90.00	105.00	2478
16	60	46.9	91.00	100.50	111.00	2508
17	60	47.4	90.00	109.00	110.00	2507
18	60	36.1	93.00	109.50	110.00	2521

All the results are the average of two test specimens.
** This value represents 2-day test as there was a delay in Setting time of concrete.*
See Table 3.4 for mix compositional details

4.2.3 Splitting cylinder tensile strength

To evaluate the tensile strength of HSC mixes the splitting cylinder tensile tests were carried out, as it has been established by the ACI-ASCE committee[2] that this method provides a more reasonable strength estimation compared with that by the direct tensile test. Table 4.2 presents the splitting tensile strength test results, f_{sp}, along with the corresponding cube compressive strength, f_{cu}, at the age of 28 days for all the concrete mixes.

In spite of the limited number of concrete mixes which were cast, it is obvious from the test results that the concrete splitting tensile strength increases as the compressive strength increases, see mix 3, and mix 13 in Table 4.2. It is also worth noting that concrete mixes possessing the same silica fume dosage (mix 14 and mix 15, at 9.96% silica fume dosage), have different tensile strengths, e.g., 7.07 *MPa* for mix 14, and 6.53 *MPa* for mix 15 respectively. Similar results are seen in mixes 10, 11, 12 and 13 which had the same silica fume dosage. The obvious reason for this phenomenon is that the strength of concrete depends not only on the silica fume content but also on other parameters such as W, C+S.F and their ratios.

However, it can be concluded that the splitting tensile strength of concrete is a function of the compressive strength irrespective of silica fume dosages. For all the concrete mixes tested, the splitting cylinder tensile strengths were found to be approximately 5 to 7.5% of the corresponding compressive strengths at 28 days.

Table 4.2- Splitting Tensile Strength Results

Mix	f_{cu}, *MPa* 28 days	f_{sp}, *MPa* 28 days	Silica fume dosage (%)
1	114.50	5.73	9.49
2	110.00	6.34	9.49
3	114.50	7.22	9.49
4	109.50	7.37	7.46
5	99.00	5.50	11.43
6	101.00	6.47	11.43
7	80.00	5.04	5.00
8	80.50	5.78	8.00
9	93.00	7.00	6.00
10	91.50	6.50	9.96
11	92.00	6.72	9.96
12	98.00	6.31	9.96
13	78.00	5.51	9.96
14	99.50	7.07	9.96
15	90.00	6.53	9.96
16	100.50	6.68	9.96
17	109.00	6.79	8.00
18	109.50	7.77	8.00

All the results are average of two test specimens

4.2.4 Stress-strain relationship

The stress-strain relationships of HSC mixes were determined in compliance with BS 1881: part 115 using standard 100 *mm* x 300 *mm* cylinders at 28 days. Axial and lateral strains were measured using electrical resistance strain gauges (PL -60- 11) with a gauge length of 60 *mm*. From the test results the following observations can be made:

(i). The strain corresponding to maximum stress is approximately 0.003 for the range of concrete tested.

(ii). The slope of the σ-ε curve is fairly linear up to approximately 75% of the compressive strength as compared to the early start of non-linearity of NSC.

(iii). Poisson's ratio was found to be 0.21 which compares well to a range of 0.2 to 0.25 based on all other available published results.

Fig. 4.5-Stress-strain relationships of some HSC mixes

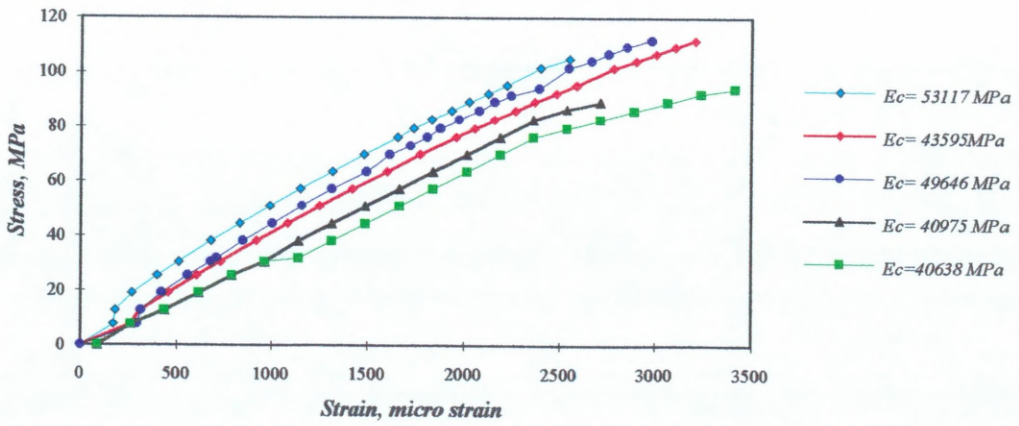

4.3 Behaviour of HSC Beams in Flexure

As described in section 3.2.2 (Chapter 3) the beams were tested under two-point loading and the following data were recorded for each beam: the maximum load attained, the deflection at mid-span and strains in the concrete and in the reinforcement at mid- span for each load increment. For each beam the crack pattern was marked following each load increment. From the measured loads and the specimen dimensions, the applied moment was calculated at each load increment. The measured load-deflection curves for some of the beams tested are shown in Fig. 4.6 to 4.11. The detailed numerical values of the load-deflection are given in Appendix-B . The corresponding diagrams showing strains along the depth of each beam at every significant load increment are presented in Fig. 4.12 through Fig. 4.24. The moment-rotation relationships for all test specimens are presented in Fig. 4.25 through Fig. 4.30.

4.3.1 Load-deflection characteristics

It can be seen from the load versus deflection diagrams Fig. 4.6 to Fig. 4.11, that the initial slope of the curve (pre-cracking portion) is quite steep. During this stage, the behaviour of the beams is essentially linear elastic. As the load increases a change in slope occurs indicating the formation of the first tensile concrete crack. The slopes of load-deflection curves are fairly linear while the strain in steel remains below yield.

For all the groups of beams, initial cracking was observed at similar load level, i.e., about 20 *kN*; this indicates that the initial cracking occurs at a similar load irrespective of the strength of concrete. On the other hand, as a percentage of the ultimate load the initial cracking loads ranged from 26% to 37% for group one, 20% to 25% for group two, 20% for group three, and 8% to 17% for group four respectively, which means that for heavily reinforced sections crack initiation occurs at a smaller percentage of the ultimate load.

As expected, in the post-cracking region the slope of the curve became flatter due to the reduction of the effective second moment of area, i.e, the flexural rigidity (EI) of the cross section. This slope remained steady until the yielding of the tensile reinforcement. The nature of the curves varied for different reinforcement ratios and compressive strength of concrete. For high ρ values the slope changed abruptly leading to an abrupt failure. This phenomenon can be seen in Fig. 4.10. For instance, in comparing beam HSC1-1 (f_{cu} = 107 MPa, ρ = 1.03%), with beam HSC4-1 (f_{cu} = 101 MPa, ρ = 4.04%), which have approximately the same concrete compressive strength but different ρ values, it can be seen that the beam with higher ρ ratio has a stiffer response in terms of load-deflection characteristic. This phenomenon can be attributed to higher second moment of area of beams with higher ρ values and consequent less cracking.

On the other hand, in comparing beam HSC2-2 (f_{cu} = 100 MPa, ρ = 1.42%) with beam HSC2-3 (f_{cu} = 77 MPa, ρ = 1.42%) which have equal ρ values, but different concrete strengths, see Fig. 4.7, it is seen that the beam with the higher strength concrete exhibits less deflection than the other beam with a lower strength concrete at same load levels, i.e, beam HSC2-2 is approximately 32% stiffer than beam HSC2-3. This is expected since higher strength concrete beams are stiffer because of their higher E_c values (E_c = 43595 MPa for HSC2-2, and E_c = 34000 MPa for HSC2-3). However, this behaviour was not observed in all the remaining beams with different compressive strength values but having the same ρ value, e.g., beam HSC1-1 and HSC1-3 in Fig. 4.6, beam HSC3-1 and HSC3-3 in Fig. 4.8, and beam HSC4-1 and HSC4-3 in Fig. 4.9; these discrepancies are not thought to be significant and may be due to experimental error. In summary, it could be stated that, the behaviour of beams in this region (post-cracking) is a function of both the reinforcements ratio ρ and the f_{cu}.

At yielding of the tension reinforcements, the mid-span deflection of the beams varied between 13 to 17 *mm* for group one, 10 to 20 *mm* for group two, 14 to 17 *mm* for group three, and 21 to 23 *mm* for group four. The deflection corresponding to maximum load varied between 25 to 50 *mm* for all the groups of beams.

At the post yielding stage each beam exhibited different load-deflection response depending upon the tensile reinforcement ratio,ρ , and the concrete strength, f_{cu}, but in all cases there was a significant bending of the load-deflection curve towards the horizontal due to the yielding of the tensile reinforcement. When this occurred, cracks propagated upwards into the compression zone causing a reduction in the neutral axis depth as evidenced by the strain diagrams, see Fig. 4.12 to Fig. 4.24. Thereby both the curvature and deflection are increased immediately after yielding. For instance, in comparing any two beams with approximately the same concrete strength, i.e., beam HSC1-1 in Fig. 4.6, and beam HSC3-1 in Fig. 4.8, it can be noted that, the beam with higher steel content exhibits less deformation at the same load. Beams with higher steel content would require larger compressive stress block for equilibrium as evidenced in the strain diagrams shown in Fig. 4.12 to Fig. 4.19; the neutral axis depth of beam HSC3-1 is approximately twice that of beam HSC1-1 at ultimate stage. On the other hand, from the results of beams HSC1-1, HSC2-1, HSC3-1 and HSC4-1, which are illustrated in Fig. 4.10, it can be seen that the increase in stiffness in the post-yield region is more dependent on the increase in steel percentage than on the increase in concrete strength.

Overall, the tensile reinforcement ratio ρ was found to be the dominant factor in determining the shape of the load-deflection curves, rather than the concrete compressive strength, f_{cu}, which has a minor influence. Beams with tensile reinforcement ratios (ρ = 1.03%, 1.42%, and 1.94%) underwent large deformations at relatively constant loads before the maximum load was attained; also, the drop-off in the load-deflection curves was very gradual beyond the maximum load as seen in

Figs. 4.6, 4.7, and 4.8. On the other hand, beams with higher tensile reinforcement content (ρ = 4.04%) exhibited significant drop in load capacity with increasing deflection beyond the peak load, see Fig. 4.9. It is worth mentioning that beam HSC 4-1 failed at the same time when the steel yielded; while the other beams did not; they were able to sustain increasing loads even when the concrete compression fibres were exhibiting crushing.

In doubly reinforced sections the behaviour of all beams in this group was similar, see Fig. 4.11, which shows them to exhibit similar pre-yielding and post yielding characteristics. In addition, the influence of compression steel ratio,ρ', on the load-deflection response could be seen by comparing beams HSC4-1 [f_{cu} = 107 *MPa*; ρ = 4.04%] and DHSC1-2 [f_{cu} = 107 *MPa*; ρ = 4.04% and ρ' = 0.505%]. The beam with 0.505% compression reinforcement has a stiffer response in terms of load-deflection behaviour and a higher load at yielding, for example, the deflections at 100 *kN* load were 16.41 *mm* and 14.2 *mm* for beams HSC4-1 and DHSC1-2 respectively.

Fig. 4.6- Load- Deflection at midspan of group one beams

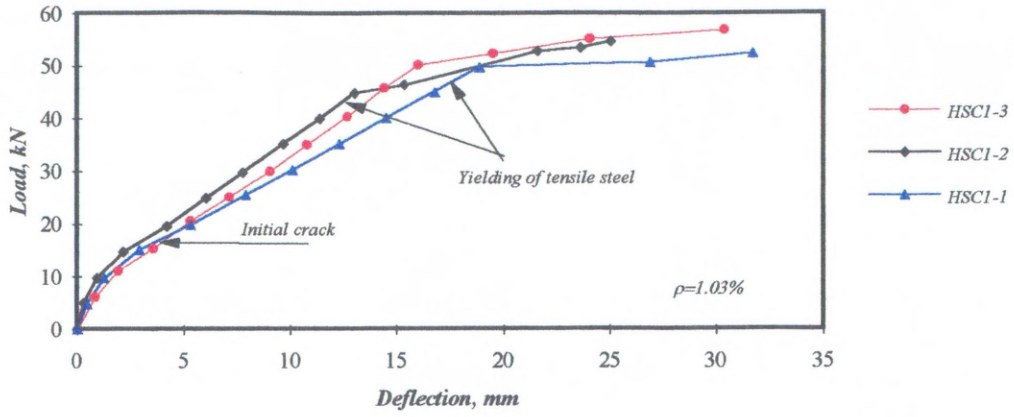

Fig. 4.7- Load - Deflection at midspan of group two beams

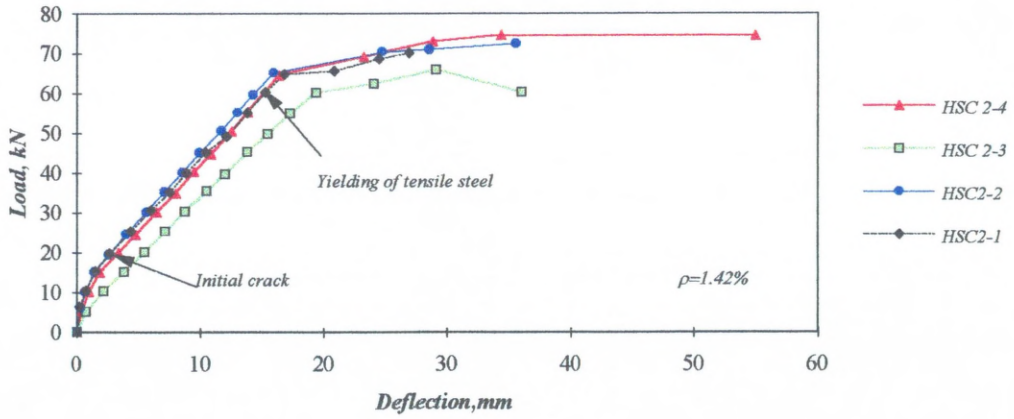

Fig. 4.8- Load - Deflection at midspan of group three beams

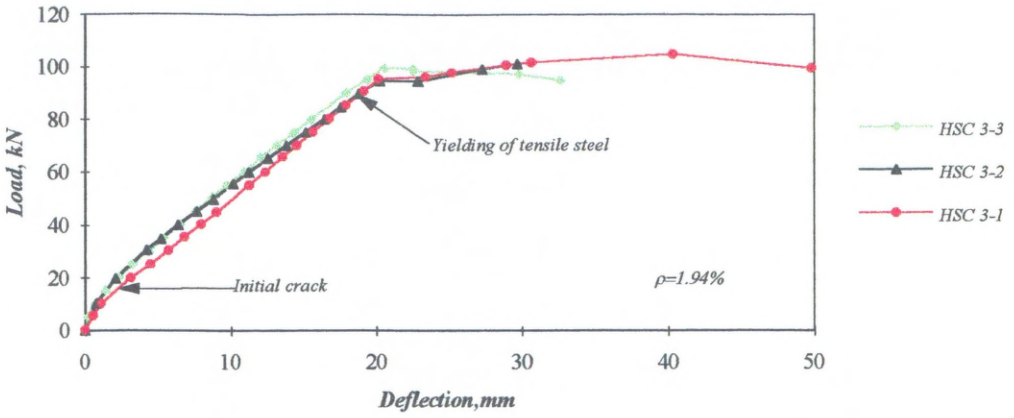

Fig. 4.9- Load -Deflection at midspan of group four beams

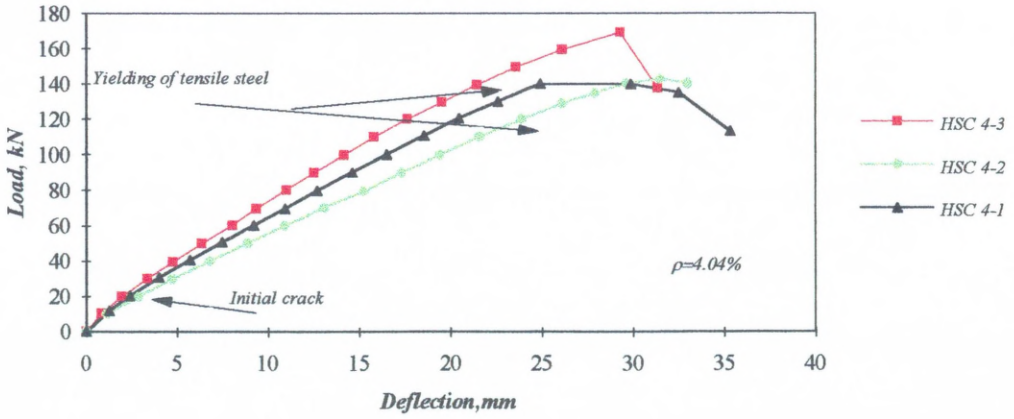

Fig. 4.10- Load-Deflection at different reinforcement ratios

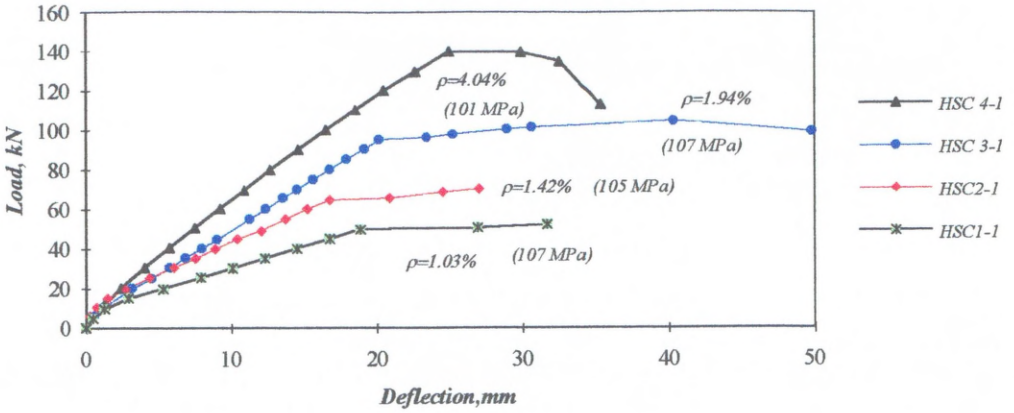

Fig.4.11-Load -Deflection at midspan for doubly reinforced sections

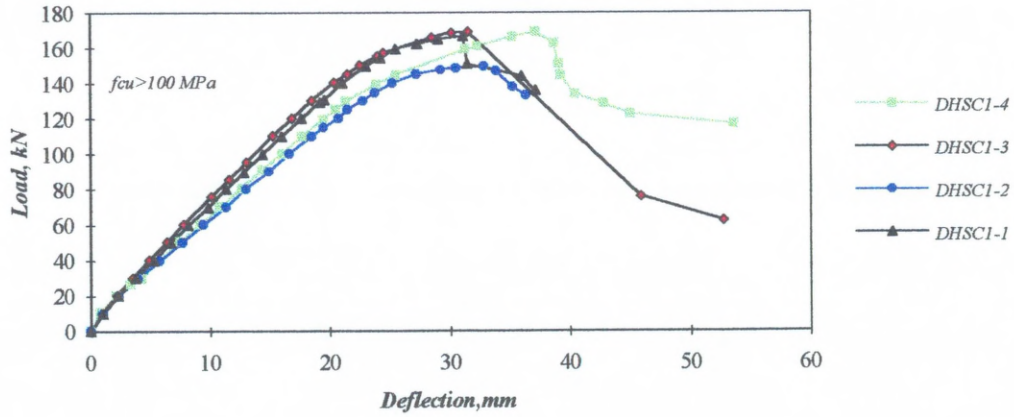

4.3.2. Strain Distribution

Figures 4.12 to 4.24 show the flexural strain variations along the beam depth at mid-span both in the compression zone, and at the tensile reinforcement level for the test beams. The magnitudes of the strains represent the average of the strain readings on each face, front and rear, of the beam. The strains were measured at each incremental load in all beams. At each load stage the neutral axis was located from the strain diagrams. The numerical values of load-strain curves at each load increment are presented in Appendix-A for all the beams tested.

For beams with low tensile reinforcement the neutral axis rose prior to failure, while for heavily reinforced members the neutral axis remained more or less at the same position at failure. It should also be stated that the maximum concrete strain recorded was 0.0037 for beam HSC4-2 at the extreme compression fibre, see Fig. 4.23 and the lowest 0.002 for beam HSC2-4. For all other test specimens the maximum compressive strain recorded varied between 0.0022 to 0.003.

The measured steel strains showed that the yield strength of the reinforcement was attained in all beams prior to crushing of the compression concrete which indicated that all the test specimens were under-reinforced sections. The load-strain curves of the reinforcement at each load increment are presented in Appendix-D for all beam tested.

Fig. 4.12- Strain distrbution along the depth of beam HSC 1-1

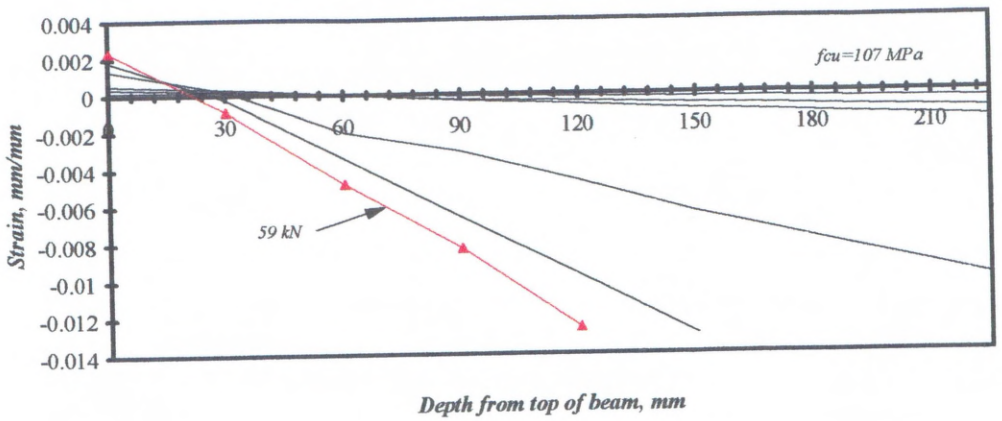

Fig.4.13- Strain distribution along the depth of beam HSC1-2

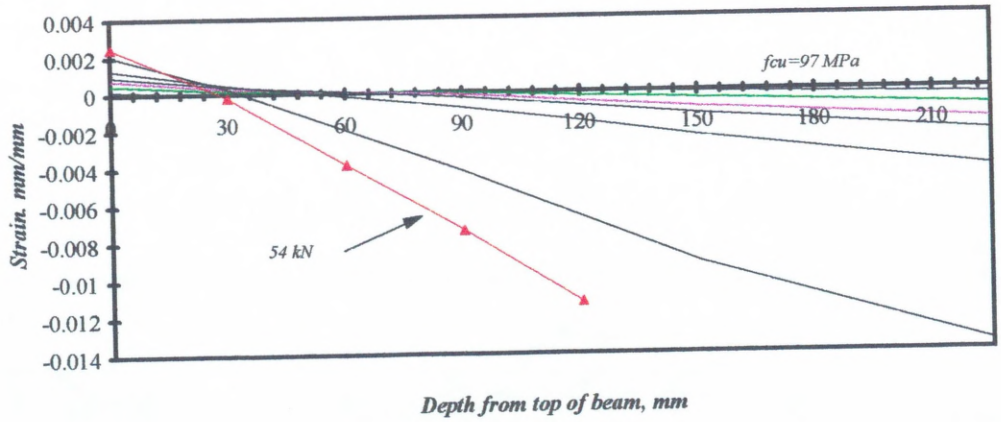

Fig. 4.14- Strain distribution along the depth of beam HSC 1-3

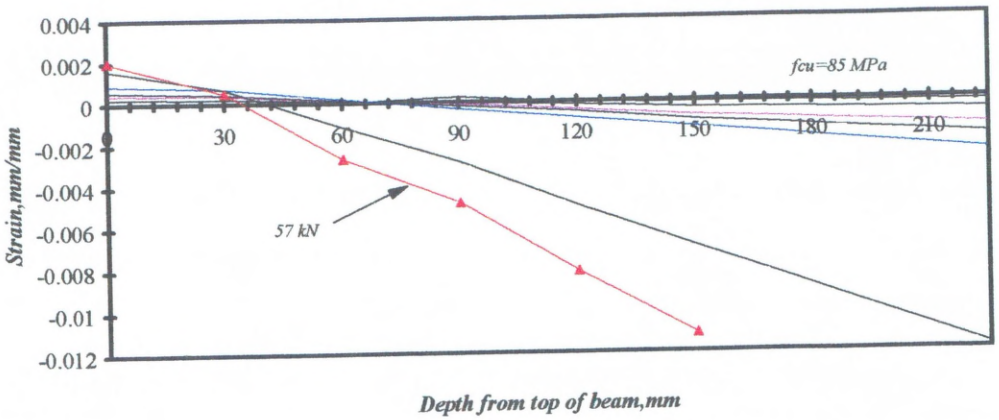

Fig. 4.15- Strain distribution along the depth of beam HSC 2-1

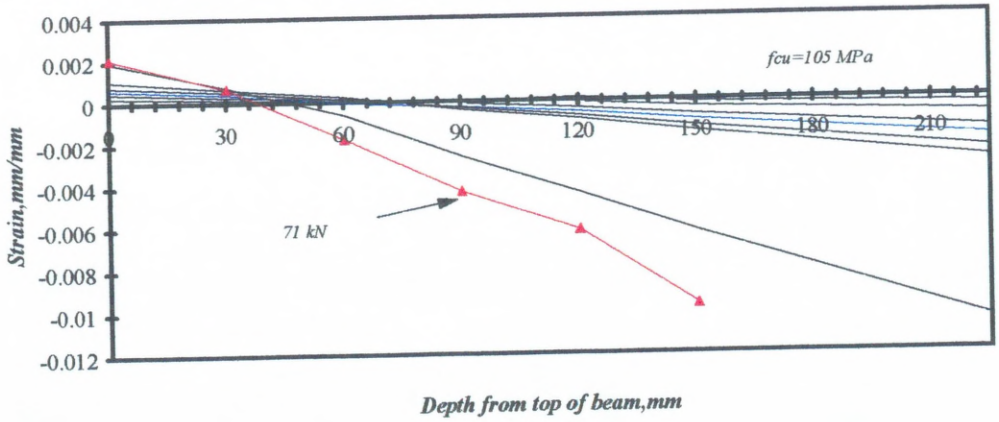

Fig.4.16- Strain distribution along the depth of beamHSC 2-2

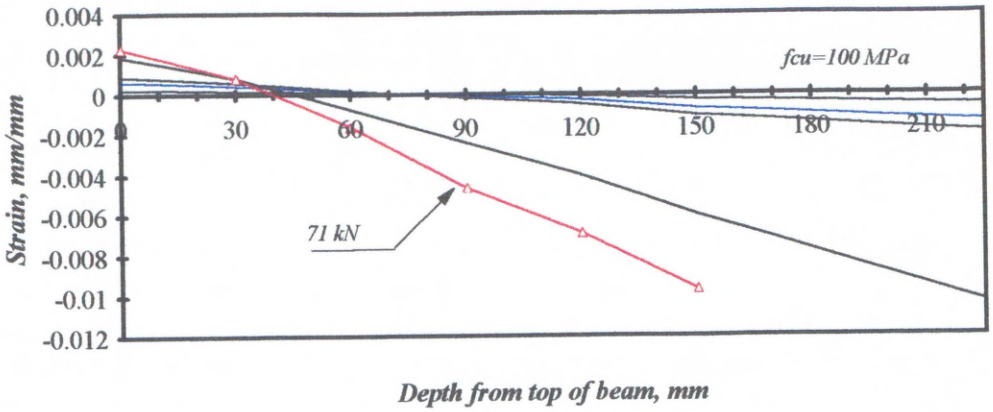

Fig.4.17-Strain distribution along the depth of beam HSC 2-3

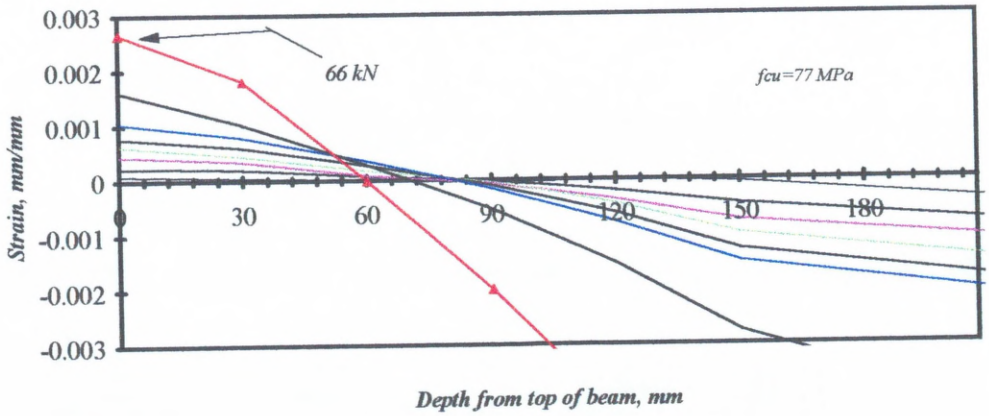

Fig.4.18- Strain distribution along the depth of beam HSC 2-4

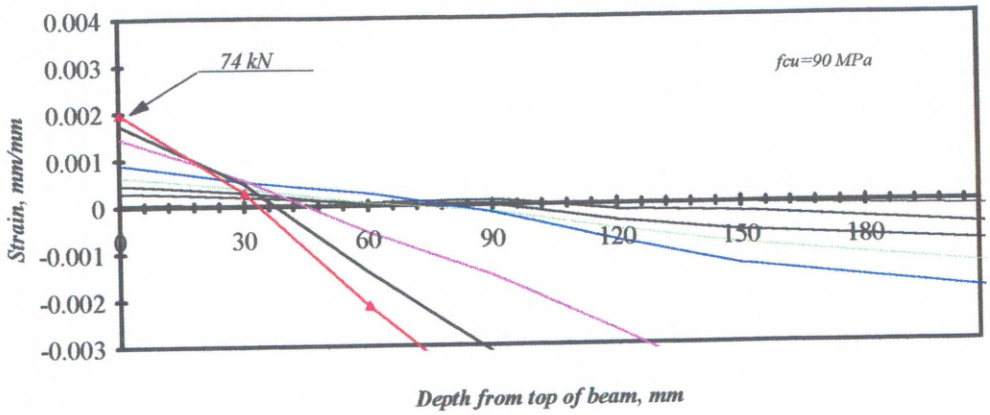

Fig. 4.19-Strain distribution along the depth of beamHSC 3-1

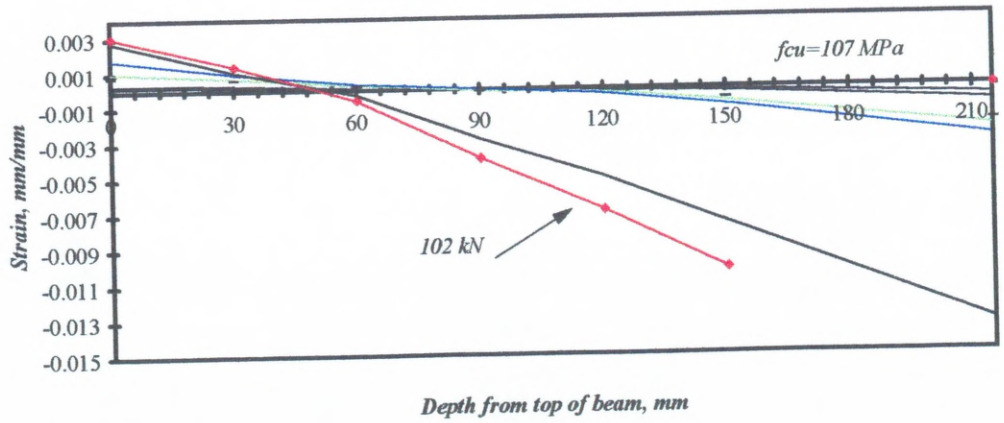

Fig.4.20- Strain distribution along the depth of beam HSC 3-2

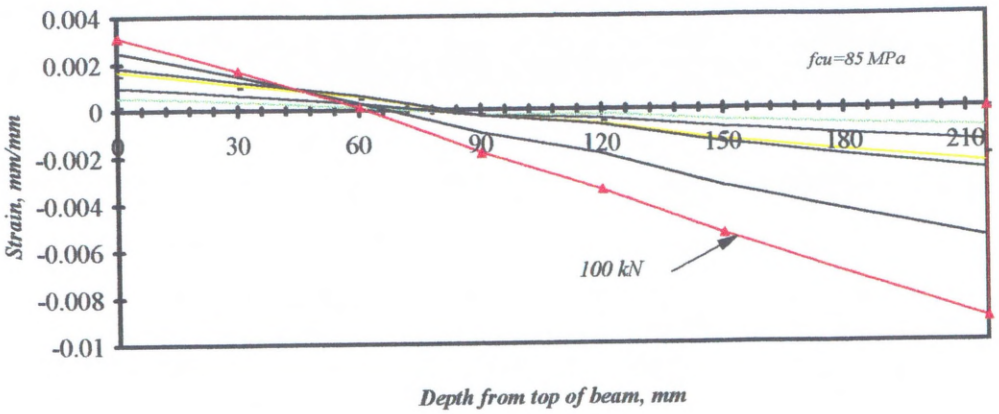

Fig. 4.21- Strain distribution along the depth of beam HSC 3-3

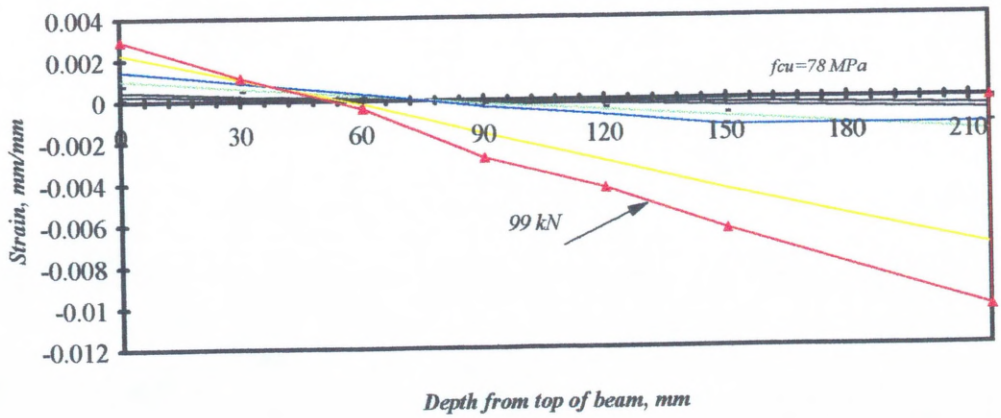

Fig.4.22- Strain distribution along the depth of beam HSC 4-1

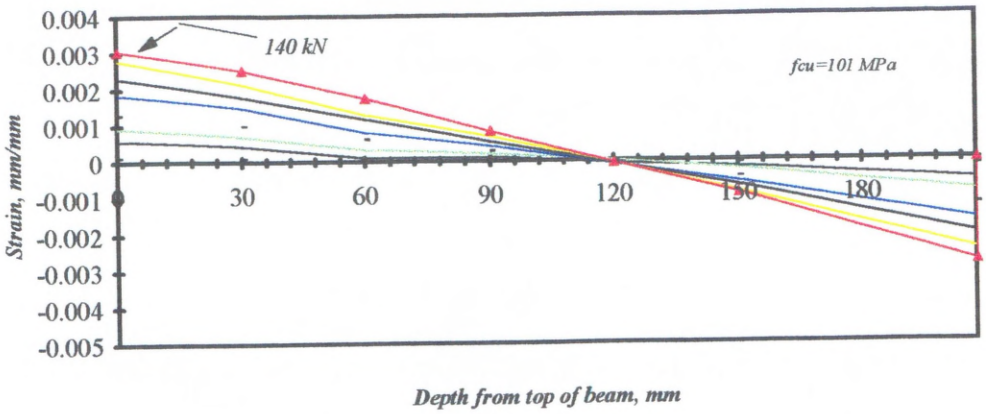

Fig.4.23- Strain distribution along the depth of beam HSC 4-2

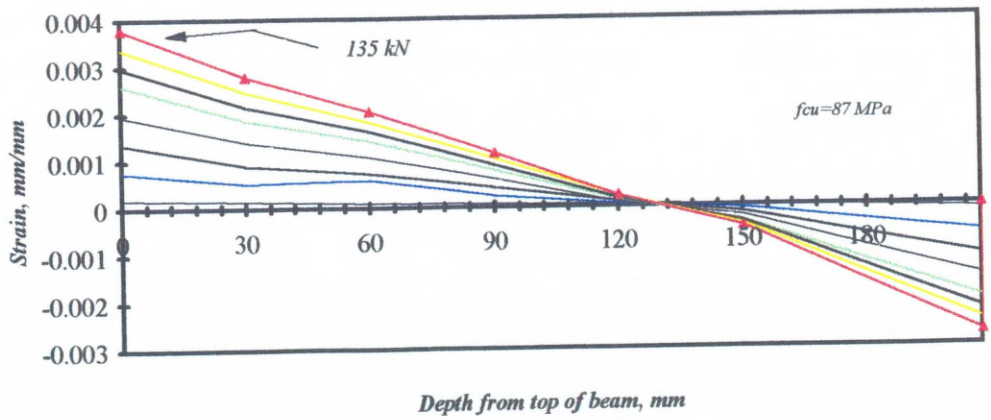

Fig.4.24- Strain distribution along the depth of beam HSC 4-3

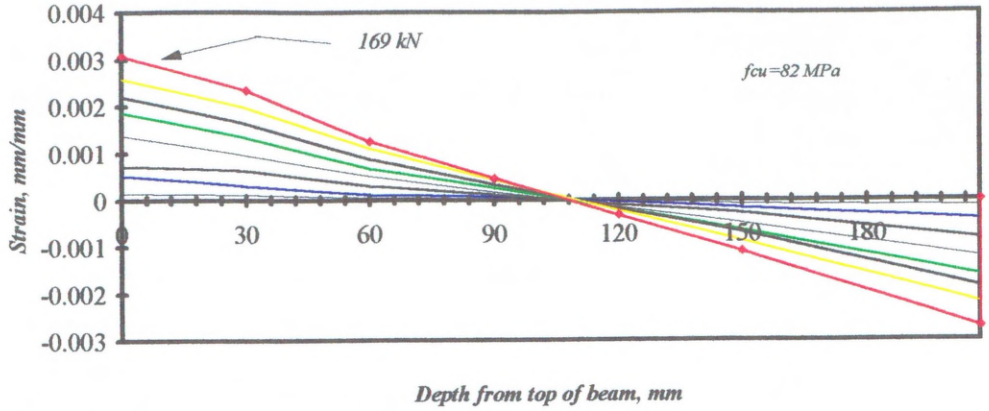

4.3.3 Moment-rotation relationship

In this subsection the moment-rotation relationships at the mid-span section of the beams are provided. The rotations were derived from the flexural strains developed in the extreme compression fibres at mid-span for each load increment. The rotation was calculated as follows:

$$\theta = \left(\frac{\varepsilon_c}{k_d}\right) d \qquad 4.1$$

where,

θ = Rotation, in (radians)

ε_C = strain at extreme compression fibre

k_d = neutral axis depth in (mm)

d = Demec-gauge length, (200 mm)

The mid-span rotations of the beams tested, which were derived using the above expression, are presented in Figs. 4.25 to 4.30. The shape of these curves is basically similar, i.e., they exhibit elasto-plastic behaviour, for the first three groups of beams (ρ = 1.03%, 1.42%, and 1.94%). The curves for the beams with ρ = 4.04% do not exhibit this phenomenon and right up to the failure load the relationship is nearly

elastic. This phenomenon conforms with the well known fact that beams with high reinforcement percentage can not accommodate significant rotation even when approaching the ultimate loads. It is also clear from the graphs in Fig. 4.29 that the slopes of moment-rotation curves for beams with higher ρ ratios are steeper than those with lower ρ ratios. It should also be stated, in comparing beams HSC1-1 and HSC1-2 which have equal ρ values, but different concrete strengths, f_{cu}, as illustrated in Fig. 4.25 and also for beams HSC3-1 and HSC3-2 in Fig. 4.27, that the slopes of moment-rotation curve exhibit stiffer response for beams possessing higher f_{cu}.

Tables in Appendix-C provide the numerical Moment-Rotation results for all the beams tested at each load increment.

4.3.4 Ductility

In a broad sense, ductility is defined as the ability of a structure to sustain deformations beyond the elastic range without a significant variation of the resistance capacity. In this part of study the ductility index is taken in terms of sectional curvature, i.e., the ratio of ultimate to first yield load curvature ($\mu_c = \psi_u / \psi_y$). It has been noticed that the tensile reinforcement percentage, ρ, is the most dominant factor in influencing the ductility indices.

In general, for similar concrete strength the ductility index, μ_c, decreases as the tensile reinforcement ratio, ρ, increases; on the other hand, in spite of the limited range of the compressive strength used in this study it was observed that although HSC is considered to be a less ductile material compared to NSC, the ductility index for a specified reinforcement ratio ρ of an HSRC section in flexure increases with the increase in the compressive strength of concrete, for example, beam HSC1-1 (f_{cu}= 107 *MPa*) had μ_c = 7.4, and beam HSC1-3 (f_{cu}= 85 *MPa*) had μ_c = 4.46. This trend indicates that the ductility index is dependent on the compressive strength (see Table 4.3).

Fig4.25- Midspan moment - rotation for group one beams

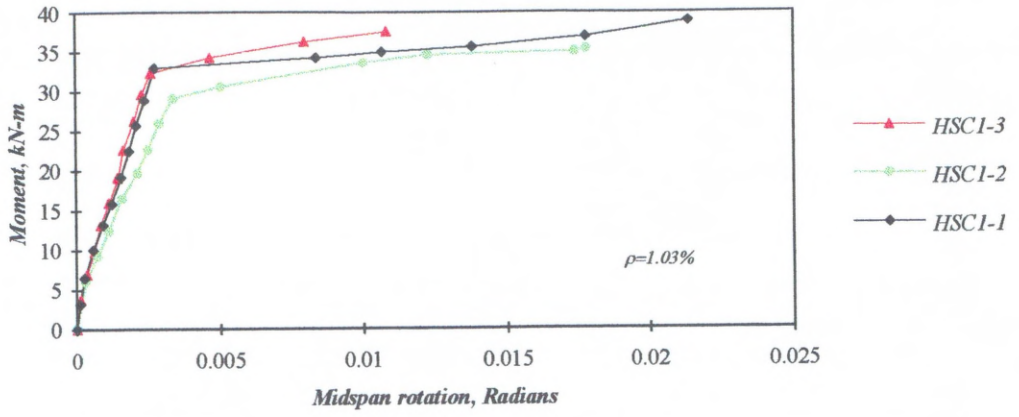

Fig. 4.26- Midspan moment - rotation for group two beams

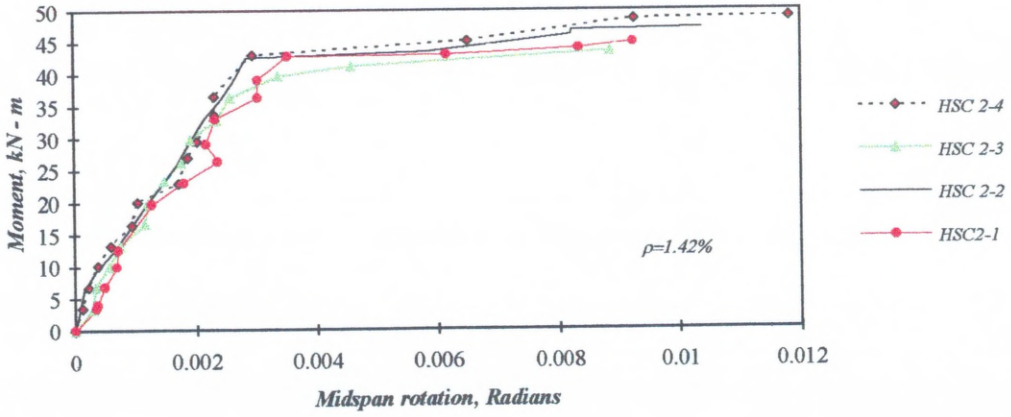

Fig.4.27- Midspan moment - rotation for group three beams

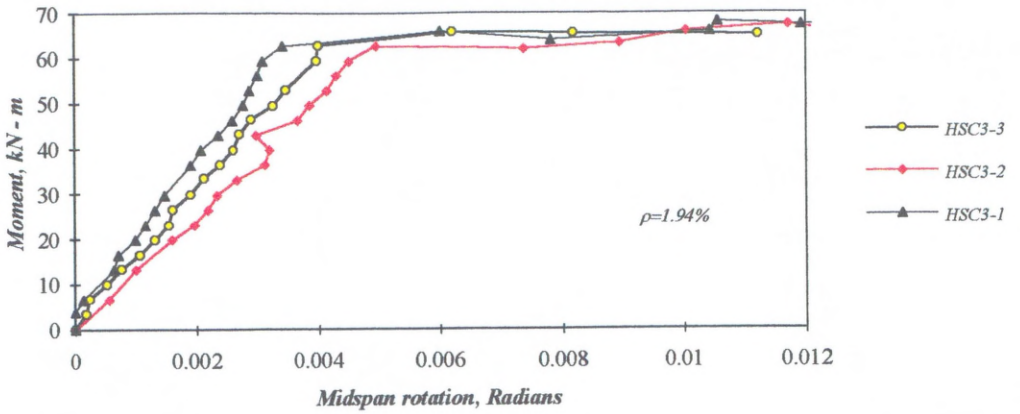

Fig.4.28- Midspan moment - rotation for group four beams

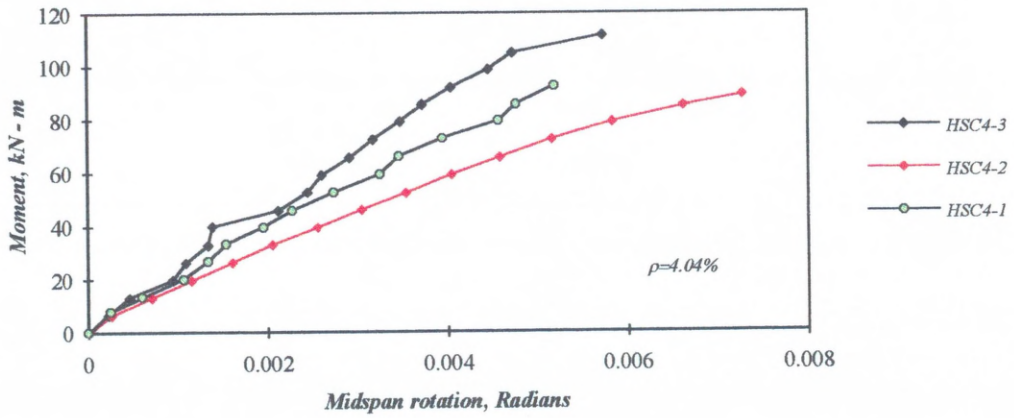

Fig.4.29- Moment - rotation for different reinforcement ratio

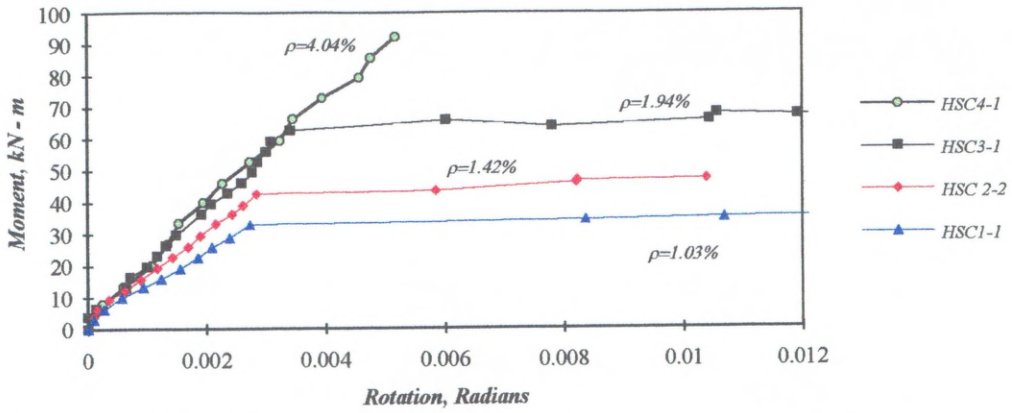

Fig.4.30-Midspan moment- rotation for doubly reinforced sections

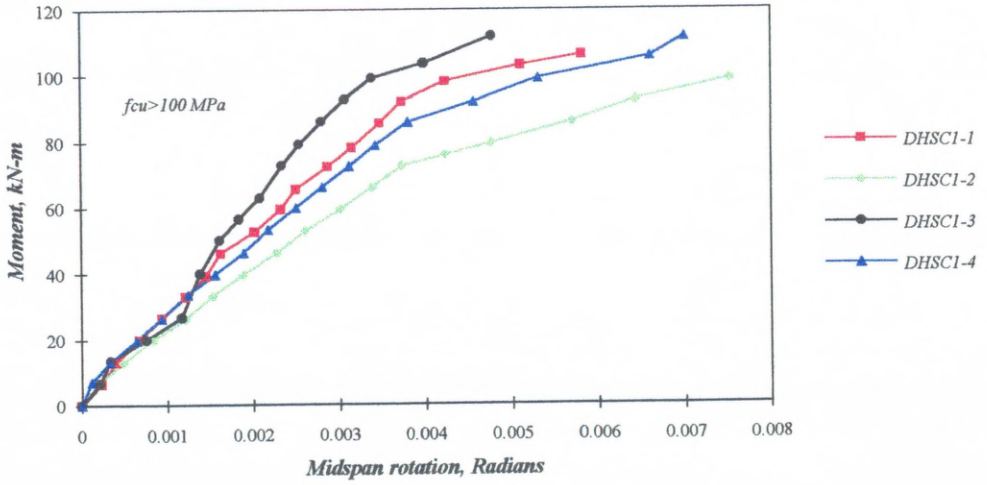

4.3.5 Crack widths and patterns

For all the beams tested the total number of cracks increased with the increase in load, and the crack widths became larger. All the cracks were marked on both sides of each member at each load increment. The cracks in the pure flexure region were predominantly vertical as expected. Crack propagation outside the pure flexure zone was also as for flexural cracks. However, for heavily reinforced beams a joining of an inclined crack to a flexural crack occurred at approximately 70% of the maximum load, which is due the presence of increasing shear stresses. This phenomenon was particularly clear in beam HSC4-3 as cracks propagated towards the vicinity of the end support.

Pictorial views of crack patterns are presented in Appendix-D. The only definite trend in crack propagation appears to be that the crack initiation occurs at a smaller percentage of the maximum load for a certain group of beams. However, as the amount of longitudinal reinforcement increases the percentage decreased, e.g., at 14% for HSC 4-1 beam, whereas at about 37% for HSC 1-1 of the maximum load. It is worth stating that crack propagation was markedly limited for doubly reinforced sections due to the confinement provided by both compression and web reinforcements. On the other hand, the width of the crack is essentially dependent on the main reinforcement ratio, ρ . For instance, the largest crack width at tensile steel level was 2.4 *mm* for beam HSC1-1(f_{cu} = 107 *MPa*, ρ = 1.03%), while only 0.9 *mm* at maximum loads for beam HSC4-1(f_{cu} = 101 *MPa*, ρ = 4.04%). The load and the corresponding crack widths at initial and ultimate stages are presented in Table. 4.4.

Table 4.3 -Summary of Experimental Results at Yield and Ultimate Load Stage

Beam	Yield stage		Ultimate stage		Ductility index	Average measured and calculated crack spacings		
	Load *kN*	ψ_y *rad./ m*	Load *kN*	ψ_u *rad. /m*	$\mu_c = \psi_u / \psi_y$	Measured surface crack, *mm*	Calc. surface crack, *mm*	Ratio
HSC1-1	45.10	0.0119	59.00	0.088	7.40	74.36	81.86	0.91
HSC1-2	44.90	0.0168	54.00	0.089	5.30	132.00	81.86	1.61
HSC1-3	49.00	0.0130	57.00	0.058	4.46	112.27	81.86	1.37
HSC2-1	61.00	0.0118	70.20	0.056	4.75	143.00	79.87	1.79
HSC2-2	63.30	0.0121	71.00	0.058	4.79	N.A	N.A	N.A
HSC2-3	60.00	0.0139	66.00	0.044	3.17	77.64	79.87	0.97
HSC2-4	60.00	0.0147	74.00	0.059	4.01	N.A	N.A	N.A
HSC3-1	82.79	0.0118	103.0	0.053	4.49	93.98	83.44	1.13
HSC3-2	75.00	0.0193	101.0	0.071	3.68	79.61	83.44	0.95
HSC3-3	85.00	0.0198	99.0	0.0561	2.83	108.00	83.44	1.30
HSC4-1	125.00	0.0259	145.0	0.026	1.00	54.60	70.29	0.78
HSC4-2	128.00	0.033	140.46	0.0364	1.10	67.77	70.29	0.96
HSC4-3	140.57	0.024	169.00	0.029	1.20	70.41	70.29	1.00
DHSC1-1	149.00	0.021	166.5	0.0291	1.38	-	-	-
DHSC1-2	140.00	0.032	150.0	0.0376	1.17	-	-	-
DHSC1-3	157.00	0.020	169.31	0.024	1.2	-	-	-
DHSC1-4	139.41	0.029	169.01	0.035	1.21	-	-	-
							mean	1.16
							Std. Deviation	0.31

Table 4.4- Crack Initiation, Propagation and Crushing in Test Beams

	First visible crack			Crack at ultimate load		
Beam	Max. load (kN)	$\frac{load}{Max.load}$ (%)	Width (mm)	Width (mm)	Comp.crushing depth (mm)	Mode of Failure
HSC1-1	59.00	37.28	0.03	2.40	not available	flexure
HSC1-2	54.00	33.33	0.04	4.50	not available	"
HSC1-3	57.00	26.00	0.04	2.90	not available	"
HSC2-1	70.00	21.00	0.04	2.90	not available	"
HSC2-2	71.00	25.00	0.02	4.45	not available	"
HSC2-3*	66.00	22.00	0.01	1.50	42	"
HSC2-4	74.00	20.00	0.02	4.01	37.5	"
HSC3-1	103.00	24.50	0.02	2.60	34.1	"
HSC3-2	101.00	21.00	0.02	3.00	35.5	"
HSC3-3	99.00	20.00	0.02	2.86	43	"
HSC4-1	145.00	13.56	0.02	0.90	58.31	"
HSC4-2	140.46	7.37	0.01	0.34	62.2	"
HSC4-3	169.00	17.73	0.02	0.42	65	"

** Concrete mix was not consistent, thus the beam was repeated*

CHAPTER 5

THEORETICAL CONSIDERATIONS AND COMPARISON WITH EXPERIMENTAL RESULTS IN FLEXURE

5.1 Introduction

In a manner similar to the previous Chapter, the theoretical consideration and comparison with experimental results of some mechanical properties of HSC and HSRC beams in flexure are presented in two parts.

Part one presents the theoretical considerations concerning some mechanical properties of HSC mixes which include, a predictive relationship between the cylinder crushing strength, f_c, and splitting cylinder tensile strength, f_{sp}, of HSC. A comparison is made of some existing equations for relating splitting cylinder tensile strength to concrete compressive strength and an expression is proposed in this study. In addition, a mathematical model which has been developed to predict the concrete compressive strength, f_{cu}, of HSC mixes in terms of their constituents proportions is presented.

Part two concerns with the theoretical considerations of HSRC beams in flexure. This includes a discussion and comparison of the measured load-deflection characteristic with theoretical values; analysis of ultimate flexural capacity by using different models of stress block idealisations of HSRC beams; the BS 8110 design method for flexural strength is evaluated by comparing measured and predicted moments of resistance to determine its applicability to HSC beams. The surface crack width and spacing of cracks of HSRC beams were evaluated; a comparison of the test results with those predicted by some existing formulae and a modified formula is presented in this study. Finally, the ductility and ductility index have been studied.

5.2 Mechanical Properties of HSC Mixes

5.2.1 Splitting cylinder tensile strength

As mentioned earlier in the literature review, the data on the relationship between the splitting tensile strength, f_{sp}, and cylinder crushing strength, f_c, of HSC is quite limited. Therefore, the validity of these relationships has to be checked and improved to be valid for concrete possessing cube compressive strengths up to 120 *MPa*. An accurate prediction of tensile strength of concrete would be helpful in mitigating crack problems, improving shear strength prediction and minimising failure of concrete in tension.

In this study a relationship between the splitting cylinder tensile strength, f_{sp}, and compressive strength, f_c, of HSC is developed. The data of cube strength at 28 days were converted into cylinder strength (f_c = 0.85 f_{cu}; as recommended by ACI Committee 363[16] and Regan et *al.*[109] and as verified in this study) and its relationship with splitting cylinder strength was analysed using a linear regression analysis.

The more commonly used existing relationships between split cylinder tensile strength and compressive strength are as follows: (the author's proposed model is also shown)

$f_{sp} = 0.54 \text{ x}(f_c)^{0.5}$ Carrasquillo *et al.*[33] 5.1

$f_{sp} = 0.59 \text{ x}(f_c)^{0.5}$ ACI committee 363[16] 5.2

$f_{sp} = 0.462 \text{ x}(f_c)^{0.55}$ Ahmad *et al.*[4] 5.3

$f_{sp} = 0.342 \text{ x}(f_c)^{2/3}$ Raphael [111] 5.4

$$f_{sp} = 0.564 \text{ x}(f_c)^{0.55} \quad \text{Proposed model} \qquad 5.5$$

where,

f_{sp} = splitting tensile strength of concrete (*MPa*)

f_c = cylinder compressive strength of concrete (*MPa*)

Fig. 5.1 illustrates the relationship of the concrete cylinder strength, f_c, against the splitting tensile strength, f_{sp}, values which indicates that the splitting tensile strength increased with the increase in the compressive strength, as expected, but with a wide spread of values for a given compressive strength.

Table 5.1 presents all test results and the results of applying the various equations and a proposed model for predicting splitting tensile strength of HSC. It can be concluded from these results that Carrasquillo *et al.*, ACI and Ahmad *et al.* expressions provide a conservative estimate of splitting cylinder strength of HSC mixes (see Fig. 5.1) which can be seen from the average percentage deviations of 23.08%, 15.96% and 17.92% if using Carrasquillo *et al.*, ACI and Ahmad *et al.* equations respectively. On the other hand, the Raphael model exhibits a general agreement with the test results giving an average of error of -3.27% which is very close to that of the proposed model which yields an average error of -0.42%. Overall, it appears that both the Raphael and the proposed expressions are applicable for estimating the splitting cylinder tensile strength of HSC of up to 120 *MPa* concrete compressive strength.

Fig. 5.1- Splitting cylinder tensile strength of HSC

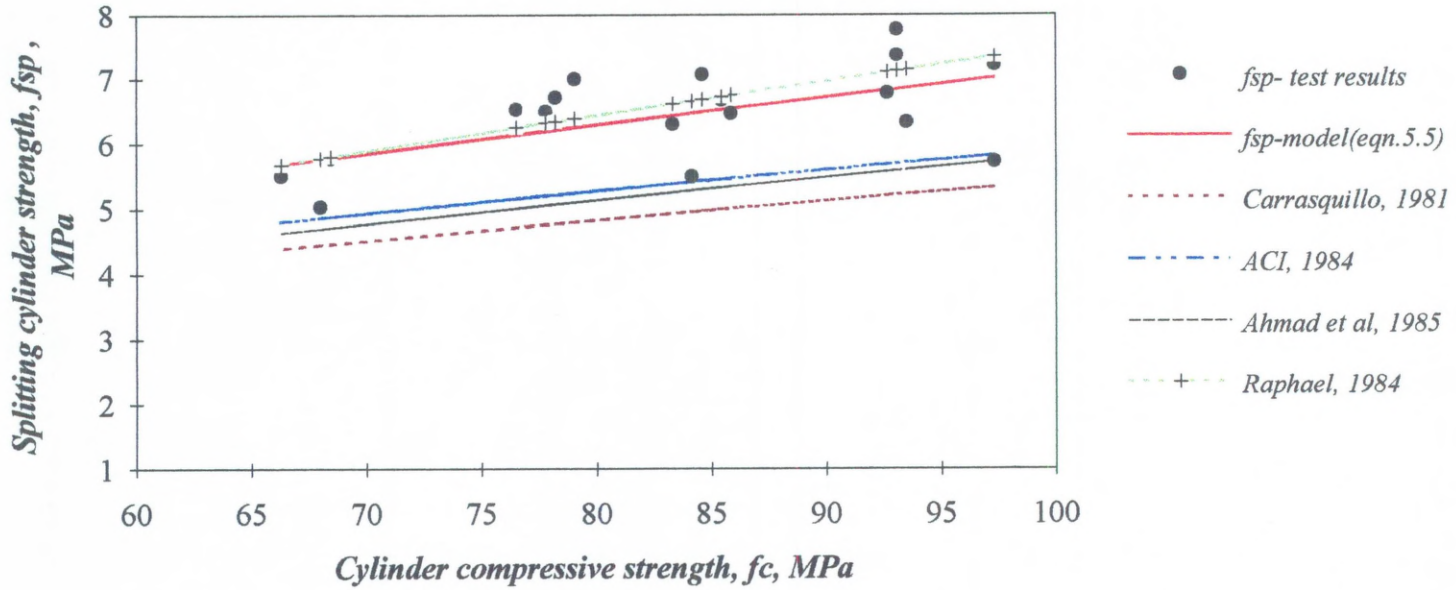

Table 5.1- Comparison Between The Proposed Equation & The Existing Relations for Predicting Splitting Tensile Strength of HSC

Test results				*Carrasquillo et al. eqn.5.1 (1981)*		*ACI, eqn.5.2 (1984)*		*Ahmad et al. eqn. 5.3 (1985)*		*Raphael eqn.5.4 (1984)*		*Proposed eqn. 5.5*	
Mix No.	f_{cu},	f_c,	f_{sp},	f_{sp},	error	f_{sp},	error	f_{sp},	error	f_{sp},	error	f_{sp},	error
	MPa	*MPa*	*MPa*	*MPa*	*%*	*MPa*	*%*	*MPa*	*%*	*MPa*	*%*	*MPa*	*%*
1	114.50	97.33	5.73	5.33	7.03	5.82	-1.58	5.73	-0.003	7.347	-28.23	7.01	-22.36
2	110.00	93.50	6.34	5.22	17.64	5.71	10.02	5.61	11.59	7.15	-12.82	6.86	-8.17
3	114.50	97.33	7.22	5.33	26.21	5.82	19.38	5.73	20.64	7.35	-1.77	7.01	2.89
4	109.50	93.00	7.37	5.21	29.31	5.69	22.77	5.59	24.14	7.13	3.24	6.84	7.17
5	99.00	84.15	5.50	4.95	9.93	5.41	1.60	5.29	3.83	6.67	-21.19	6.47	-17.67
6	101.00	85.85	6.47	5.00	22.67	5.47	15.51	5.348	17.34	6.76	-4.41	6.54	-1.13
7	80.00	68.00	5.04	4.45	11.65	4.87	3.47	4.70	6.65	5.78	-14.65	5.76	-14.19
8	80.50	68.43	5.78	4.47	22.72	4.88	15.56	4.72	18.33	5.80	-0.39	5.77	0.088
9	93.00	79.05	7.00	4.80	31.41	5.25	25.06	5.11	26.99	6.39	8.70	6.25	10.68
10	91.50	77.78	6.50	4.76	26.73	5.20	19.95	5.07	22.08	6.32	2.73	6.20	4.66
11	92.00	78.20	6.72	4.78	28.94	5.22	22.36	5.08	24.40	6.35	5.57	6.22	7.51
12	98.00	83.30	6.31	4.93	21.89	5.38	14.66	5.26	16.64	6.62	-4.91	6.44	-1.99
13	78.00	66.30	5.51	4.40	20.200	4.80	12.81	4.64	15.80	5.68	-3.11	5.68	-3.00
14	99.50	84.58	7.07	4.97	29.76	5.43	23.25	5.30	24.98	6.69	5.41	6.49	8.21
15	90.00	76.50	6.53	4.72	27.67	5.16	20.97	5.02	23.13	6.25	4.24	6.14	5.96
16	100.50	85.43	6.68	4.99	25.28	5.45	18.37	5.33	20.16	6.73	-0.79	6.53	2.31
17	109.00	92.65	6.79	5.20	23.45	5.68	16.36	5.58	17.86	7.11	-4.70	6.82	-0.50
18	109.50	93.10	7.77	5.21	32.95	5.69	26.74	5.59	28.04	7.13	8.23	6.84	11.96
					23.08*		**15.96***		**17.92***		**-3.27***		**-0.42***

** percentages Average error*

5.2.2 Compressive strength prediction of HSC

The design of an HSC mix is a more complex process than the design of normal strength concrete (NSC) mix. Therefore, the conventional mix design techniques are not applicable for HSC. As a result of that, the author has developed an empirical expression for application to HSC mixes with Portland cement, silica fume and superplasticizer in order to predict the concrete compressive strength. This proposed equation is based on a total of 40 HSC mixes, eighteen mixes in current investigation and twenty two mixes from published literature incorporating both silica fume, and superplasticizer. The following equation was obtained using a regression analysis:

$$f_{cu} = 5.26\, e^{7s/c} + 139 e^{sp/c} - 149\, w/c - 20\, FA/TA \qquad 5.6$$

where,

f_{cu} = compressive strength of concrete cubes at 28 days.

s, c, sp, w = The mass of silica fume, cement, superplasticizer, and water in Kg/m^3 of fresh concrete, respectively.

FA, TA = The mass of fine aggregates, and total aggregates in Kg/m^3 of fresh concrete, respectively.

The above equation is valid for concretes with w/c ratios in the range of 0.22 to 0.46 using 20 *mm* maximum size of crushed aggregate. The model could be used to obtain an average concrete strength between 63 to 120 *MPa*. In addition, the accuracy of prediction is estimated at about ± 15 *MPa*. Fig. 5.2 illustrates both predicted and experimental concrete compressive strengths. It should be stated that the correlation coefficient of 0.7 for the proposed formula indicates a positive correlation for all the variables included.

Fig.5.2- Comparsion between actual and predicted strengths

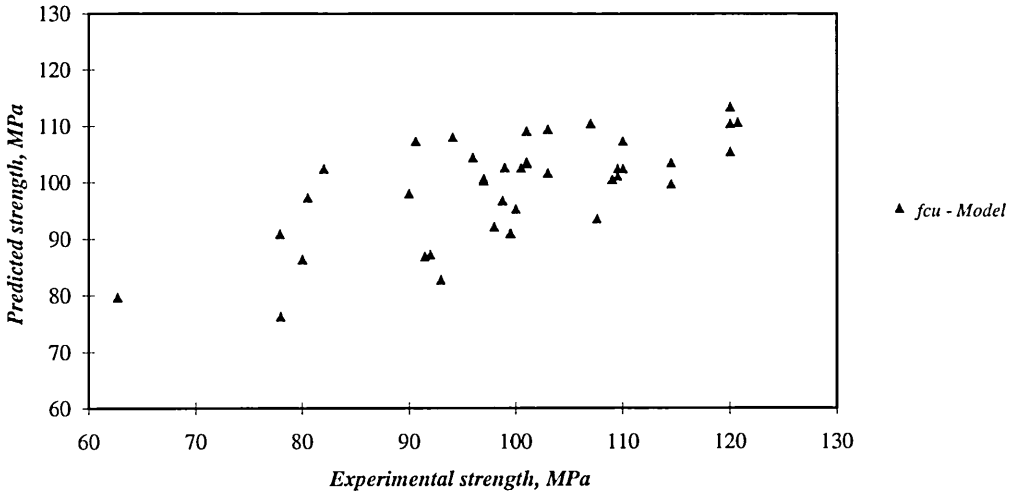

5.4 HSRC Beams in Flexure

5.4.1 Load-deflection characteristics

Deflection calculation in reinforced concrete beams represents an important phenomenon for the following reasons. Firstly, structure serviceability checks, and thereby the control of deformations, are becoming more and more important particularly in the case of high strength concrete because smaller sections are being used. Secondly, comparison between the actually measured and analytically computed deflections can represent an important parameter for field-control of the structure.

The deflection up to the flexural cracking for each beam was calculated using the full uncracked second moment of area of the cross section (I_g). Beyond the cracking stress the beam was treated as a cracked section and the cracked second moment of area was used to calculate the deflection.

$$I_{cr} = \frac{bx^3}{3} + mA_s(d-x)^2 \qquad 5.7$$

where,

I_{cr} = The second moment of area of the cracked transformed area (mm^4)

b = Breadth of the beam (mm)

x = Neutral axis for a cracked section (mm)

A_s = Area of main reinforcement (mm^2)

m = Modular ratio (E_s / E_c)

The position of the neutral axis for a cracked section (x) is obtained by equating the moment of the transformed area about the neutral axis to zero. The following quadratic equation is obtained:

$$b\frac{x^2}{2} - mA_s(d-x) = 0 \qquad 5.8$$

The splitting cylinder tensile strength, f_{sp}, (equation 5.5) was used to estimate the cracking stress. Then the moment at first crack was estimated as follows:

$$M_{cr} = \frac{f_{sp} I_g}{y} \qquad 5.9$$

where,

M_{cr}= Moment at first crack ($N.mm$)

f_{sp}= Splitting tensile strength (MPa)

y= Distance from centroidal axis of cross section neglecting reinforcement (mm).

$$I_g = \frac{bh^3}{12} + (m-1)A_s(d-x)^2$$

As expected, difficulty was experienced in using the elastic theory in estimating the deflections of the beams at post-cracking stages to give a reasonable agreement with the load-deflection results obtained from experiments. For this reason an extensive statistical evaluation of data has been carried out using the back calculation technique. The available data were analysed using the regression analysis with the aim to develop an equation to estimate the effective second moment of area (I_e) of the cracked cross-section. The predicted equation was selected based on the smallest relative residual error which might be obtained in order to predict I_e as a dependent variable. The following equations were obtained;

a- Effective second moment of area for pre-yielding stage works out to be:

$$I_{e1} = 297030 \frac{\left(I_{cr} M_{cr}/M_u\right)^{1.007}}{\left(I_g M_{cr}/M_u\right)^{0.633}} \quad \text{, and} \qquad 5.10$$

b- Effective second moment of area for post-yielding stage:

$$I_{e2} = 2.51\text{x}10^{15} \frac{\left(I_{cr} M_{cr}/M_u\right)^{-0.214}}{\left(I_g M_{cr}/M_u\right)^{0.809}} \qquad 5.11$$

On the basis of the above stated considerations, the deflection at mid-span was estimated for every beam at each incremental load using the Conjugate-beam method given by the equation:

$$\delta = \frac{pl^3}{6EI_e}\left[\frac{3a}{4l} - \left(\frac{a}{l}\right)^3\right] \qquad 5.12$$

where,

δ = Deflection at mid-span due to imposed loads (*mm*)

l= Beam span length between two supports (3240 *mm*)

a= Distance from end support to one loading point (1320 *mm*)

Figs 5.3 to 5.6 show the calculated load-deflection curves of some of the beams tested up to failure. It is obvious that the load-deflection curves can be divided into three portions. The first, from zero load up to first cracking (region 0-1 in Figs. 5.3 and 5.4), is referred to as the pre-cracking portion. The second from the cracking load to the yield load (1-2), is referred to as the post-cracking portion. The third from yield load to the failure load (2-3), is referred to as the post yielding stage.

During the pre-cracking portion, the behaviour is essentially linear-elastic for both observed and predicted values (strains are small and proportional to load). In addition, since flexural cracks have not yet developed, the deformation of concrete is more or less the same as of the tensile reinforcement. At around 20% (for beam HSC1-1) to 14% (for beam HSC4-1) of the ultimate load, flexural cracks occurred and propagated quickly up wards; thereafter, the neutral axis depth decreases from its uncracked transformed section value to a value dependent on the cracked transformed properties of the section. This results in a change in the slope of the load-deflection curve, as it tends to flatten horizontally; this is due to the sudden reduction in the flexural rigidity (EI) of the cross-section which is responsible for the break in load-deflection curve at point-1 (see Fig. 5.4). Beyond the post-cracking point, and up to yielding of the tensile reinforcement, deformations continue to increase linearly with load, but at a faster rate compared with the pre-cracking portion.

After yielding (stage 2-3), the load-deflection curve bends towards the horizontal and the deformation continues to increase linearly with load up to failure. The beginning of the post-yielding stage is characterised by a significant bending of the load-deflection curve towards the horizontal due to yielding of the tensile reinforcement. Once this occurs, cracks propagate upwards into the compression region causing a reduction in the depth of compression block as discussed in Chapter 4 (see Figs. 4.12 to 4.24).

As expected and discussed in Chapter 4, the theoretical calculations showed that beams with higher ρ value have stiffer response in terms of load-deflection characteristic which is because the higher ρ value increases the flexural rigidity (EI) of the section. This aspect is clearly seen in comparing beam HSC1-1 with beam HSC4-1 in Fig. 5.3.

Overall, it can be stated for all the beams that both measured and calculated load-deflection response showed satisfactory agreement at both post-cracking and post-yielding stages for all load stages,e.g., the ratios of actual to calculated deflections work out to be 0.98 at a load of 35 kN for beam HSC2-2 and 1.14 at a load of 100 kN for beam HSC4-2. The load-deflection curves for all beams tested are presented in Appendix B.

Fig. 5.3- Theortical load-deflection at midspan for different beams

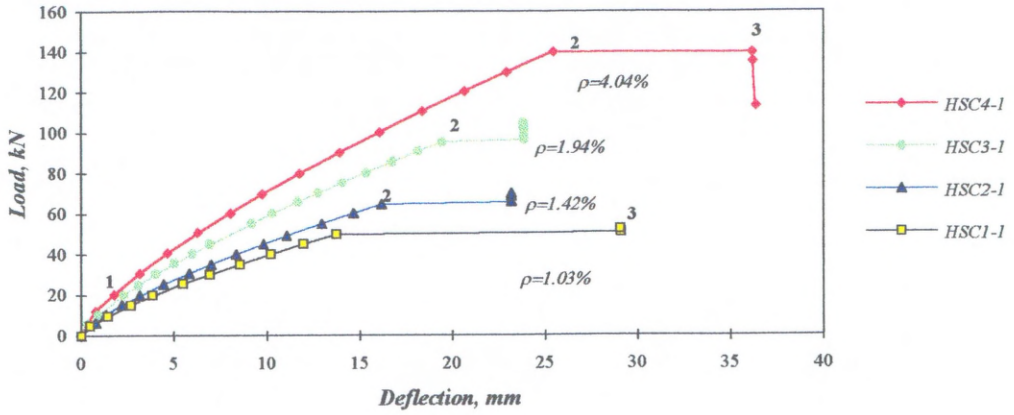

Fig.5.4- Theortical load-deflection at midspan for group three

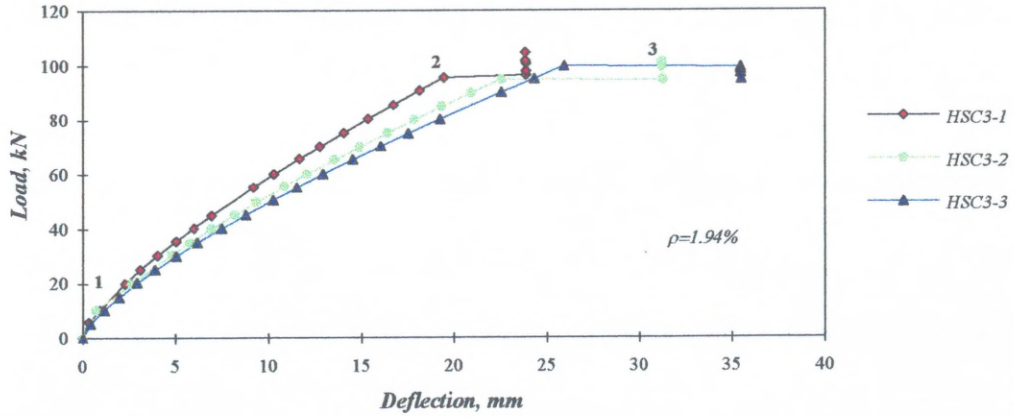

Fig. 5.5- Load- Deflection of HSC 2-2 beam

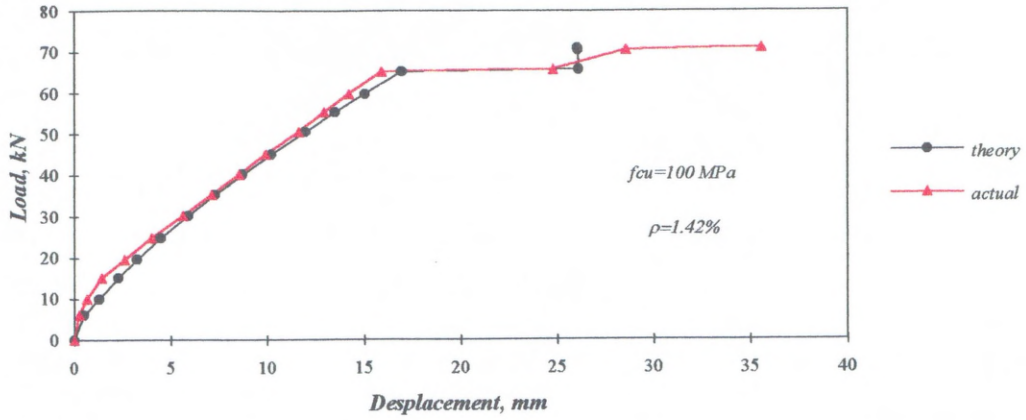

Fig. 5.6- Load-Deflection of HSC4-2 beam

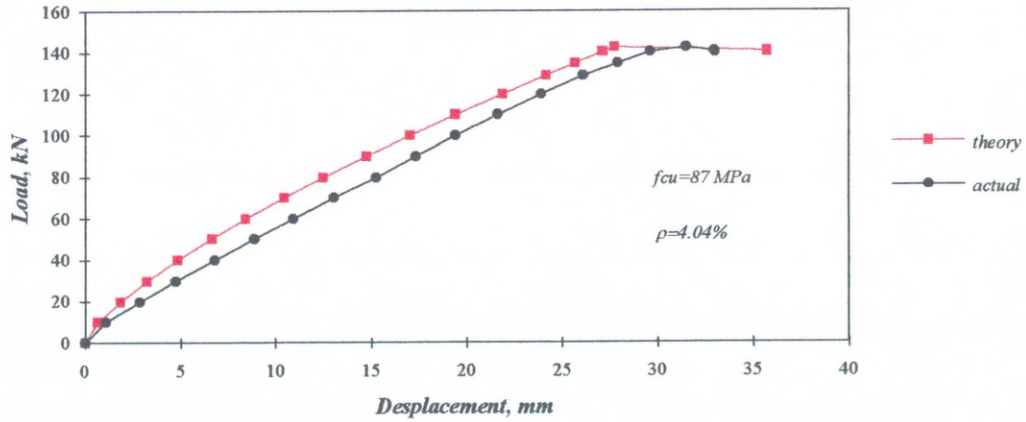

5.4.2 Analysis for Ultimate Flexural Capacity

5.4.2.1 Introduction

Many theories on the computation of flexural strength of reinforced concrete sections have been published, the ultimate limit state method based on tests on beams having concrete strength of up to 50 *MPa* are in use. The provisions in many codes of practice are based on these; however, the applicability of these provisions on HSRC beams need to be investigated. In order to achieve this, a proper modelling of stress block has to be established, for the purpose of flexural strength computation of HSRC beams. The idealisation should preferably be valid in the range of concrete cube strength up to 110 *MPa*, and would hopefully predict the ultimate flexural strength in reasonable agreement with the experimental test results.

5.4.2.2 General equation of ultimate flexural capacity

Fig. 5.7 shows the conditions at ultimate load,i.e., the extreme compression fibre concrete strain attaining a value of ε_u, the ultimate value, for a concrete section reinforced in tension and subjected to flexure. Using the well known form of equations, the force and moment equilibrium equations for the cross section of the beam can be written as follows :

$$k_1 k_3 f_c b x = A_s f_y \qquad 5.13$$

giving $$x = \frac{A_s f_y}{k_1 k_3 f_c b} \qquad 5.14$$

and, $$Mn = k_1 k_3 f_c b x(d - k_2 x) \qquad 5.15$$

where, k_1, k_2 and k_3 are characteristic ratios of stress block (see Fig. 5.7)

x = neutral axis depth

By substituting the value of x from equation 5.14 into equation 5.15 the following expression is obtained for M_n :

$$M_n = A_s f_y [1-(\rho k_2 f_y)/(k_1 k_3 f_c)\ ]\, d \qquad 5.16$$

In the presence of compression reinforcement equation 5.16 becomes

$$M_n = A_s f_y [1-(\rho k_2 f_y)/(k_1 k_3 f_c)\ ]\, d + A'_s f'_s (d - d') \qquad 5.17$$

The ratio k_2/k_1k_3 can be directly obtained from beam test results, the value of this ratio varies from 0.53 to 0.64 for HSC according to Kaar, Hanson and Capell[69]. It was observed from their investigation that the value of k_2/k_1k_3 increased with the increase of concrete strength up to 83 *MPa*. Thus, referring to equation 5.16, it can be seen that the contribution of concrete to flexural strength decreases with the increase of concrete strength.

5.4.2.3 BS 8110 stress block

As a result of the extensive research work in the past decades, the ultimate load behaviour of reinforced normal concrete beams is now well understood. The current BS 8110 design method for estimating the flexural strength of a reinforced concrete section is based on the following essential assumptions (Fig. 5.8):

i. Strains in both concrete and steel reinforcement are directly proportional to the distance from the neutral axis.

ii. The ultimate concrete strain at the extreme compression fibre is 0.0035 and the parabolic part of the stress block ends at a strain of $\varepsilon = \sqrt{f_{cu}}/5000$.

iii. Tensile strength of concrete is neglected in all flexural calculations for reinforced concrete.

Further, as an alternative to the stress block shown in Fig. 5.8, BS 8110 states that the ultimate moment can be determined from a simplified rectangular stress block of

intensity $0.45 f_{cu}$ in concrete with a depth of $0.9x$. Accordingly, equation 5.16 can be modified as follows:

$$M_n = A_s f_y \left(1 - \rho \frac{k_2 f_y}{k_1 f_{cu}}\right) d \qquad 5.18$$

where,

$$k_1 = 0.45\left(1 - \sqrt{f_{cu}}/52.5\right) \qquad 5.19$$

$$k_2 = \frac{\left(2 - \sqrt{f_{cu}}/17.5\right)^2 + 2}{4\left(3 - \sqrt{f_{cu}}/17.5\right)} \qquad 5.20$$

and the values of k_1 and k_2 will be 0.405, and 0.45 respectively using the simplified stress block technique.

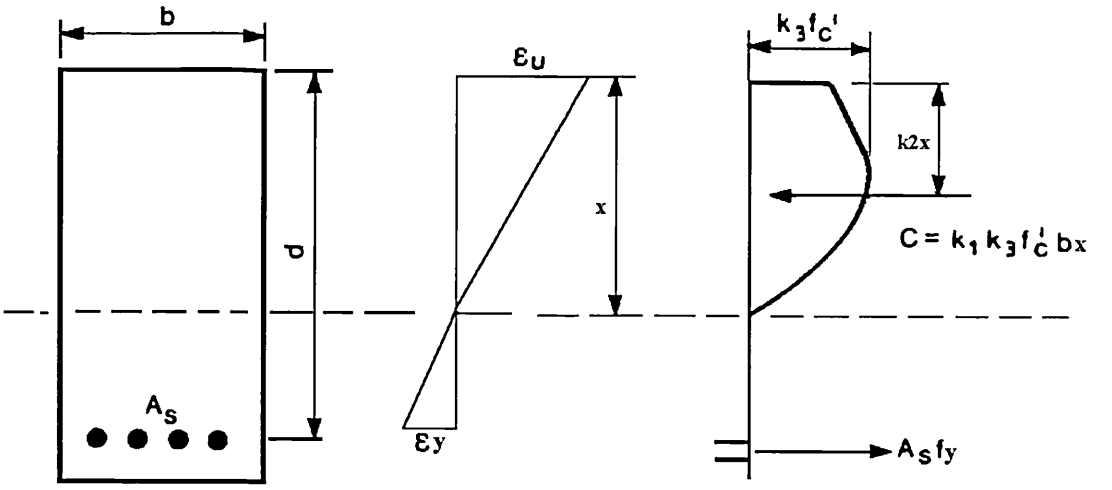

Fig. 5.7- Condition at ultimate load, Beam reinforced in tension

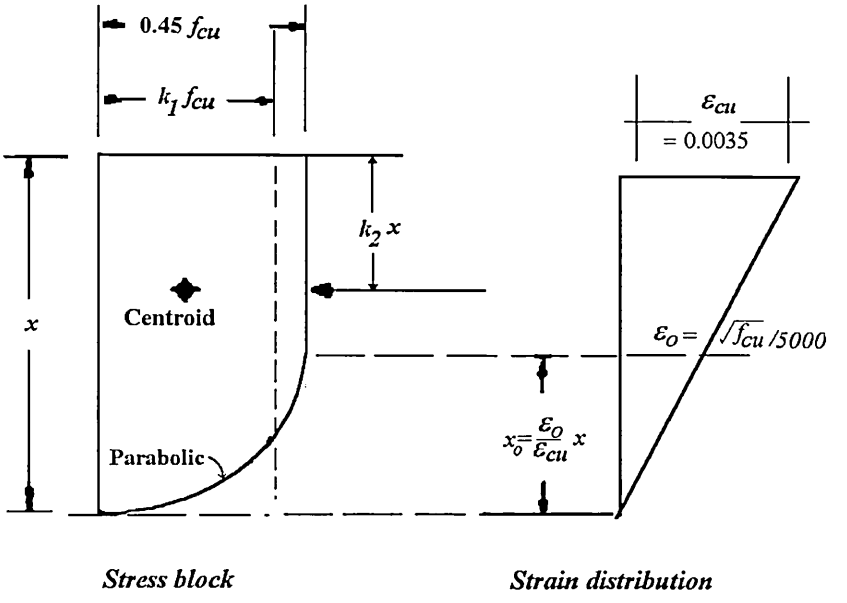

Fig.5.8- Ultimate limit state-BS 8110

5.4.2.4 Current Investigation

The most important factors in any strength estimation procedure are the assumptions of a suitable compression stress block, the value of the ultimate compression strain (ε_u) at the extreme compression fibre of the beam and the value of E_c. The values of E_c were obtained from direct compression test on cylinders.

Some different approaches have been proposed for the prediction of flexural strength of HSRC members as stated earlier in the literature review. However, there is still little agreement on a comprehensive stress block to be used in predicting adequately the ultimate strength of HSRC beams in flexure. In this study four approaches are tried along with BS 8110 method. The results of application of these approaches are compared with measured test results. The proposed approaches to strength computation can be summarised as follows:

(i). Method one

For all the beams tested the flexural concrete strains along the depth of the beams were measured at each load increment. The average strain values from the readings on each face of the beam were determined and then the neutral axis was located at each load stage. The stresses corresponding to these strains are calculated using the experimental cylinder stress-strain data. Based on all the stress-strain data obtained in this study an equation was developed by employing the regression analysis technique in order to obtain the stress values at different distances measured from the neutral axis. The equation of this curve was then used to obtain the area of the stress block and the location of its centroid by integration. The results of this exercise are presented below. The equation of the stress block works out to be:

$$\sigma_c = 32144 \left(f_c / f_{c\,max} \right) (\varepsilon)^{0.96} \qquad 5.21$$

In addition, from the ultimate strain distribution curve (see Fig. 5.9. i), the strain along the beam depth in the compression zone can be written as:

$$\varepsilon = \frac{\varepsilon_u}{n} y \qquad 5.22$$

where,

ε_u = flexural ultimate strain

y= distance from neutral axis to the given fibre (*mm*).

n = neutral axis depth at ultimate load (*mm*).

Substituting Eqn. (5.22) into Eqn. (5.21) yields:

$$\sigma_c = A \left(f_c / f_{c\,\max} \right) \left(\frac{\varepsilon_u}{n} y \right)^{0.96} \qquad 5.23$$

where, A is constant and $f_{c\,\max}$ = Maximum compressive strength of concrete cylinder.

The area under the curve is obtained by integrating equation (5.23) between the neutral axis and the top of the beam. This can be written as follows:

$$C = \int_0^n \sigma_c dy = \int_0^n \left\{ A \left(f_c / f_{c\,\max} \right) \left(\frac{\varepsilon_u}{n} y \right)^{0.96} \right\} dy \qquad 5.24$$

where, C= Compression force / *mm* width of beam.

The location of the centroid of C is then obtained by taking its moment about the neutral axis as given below:

$$\xi = \frac{1}{C} \int_0^n (\sigma_c . y)\, dy \qquad 5.25$$

Then the distance from the extreme compression fibre to the resultant force λ is given by:

$$\lambda = (n - \xi) \qquad 5.26$$

giving the ultimate nominal moment capacity of the beam, Mn:

$$M_n = C\, b\, (d - \lambda) \qquad 5.27$$

Moreover, in the presence of compression reinforcement equation 5.27 is modified to:

$$M_n = C\,b\,(d-\lambda) + A'_s f'_s\,(d-d') \qquad 5.28$$

where, b and d are the width and the effective depth.

For all beams tested the above procedures were applied in order to determine the ultimate moment capacity; a sample calculation for beam HSC1-1 is presented in appendix-D as an example.

(ii). Method two

In this approach, a triangular stress block was used, the maximum stress at the extreme compression fibre is taken as (f_{cu}). The resulting compressive force, the depth of the neutral axis and then the nominal ultimate moment is calculated as follows:

$$T = C \qquad 5.29$$

$$C = f_{cu}\frac{bn}{2} \qquad 5.30$$

$$T = A_s f_y \qquad 5.31$$

The neutral axis depth is given by

$$n = \frac{2A_s f_y}{f_{cu} b} \qquad 5.32$$

Then the nominal ultimate moment is given by

$$M_n = T\left(d - \frac{n}{3}\right) \qquad 5.33$$

In the presence of compression reinforcement equation 5.33 is modified to:

$$M_n = T\left(d - \frac{n}{3}\right) + A'_s f'_s (d-d') \qquad 5.34$$

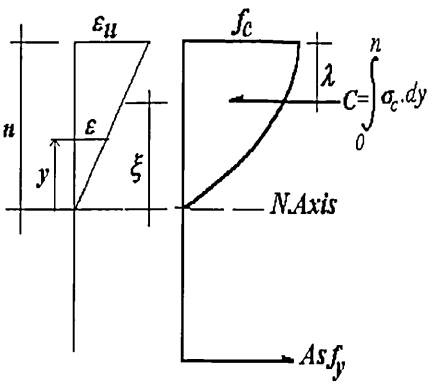

(i) *Method one*

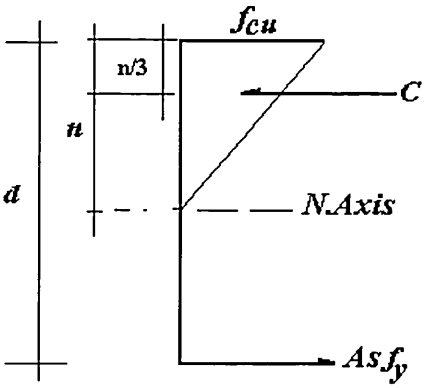

(ii) *Method two*

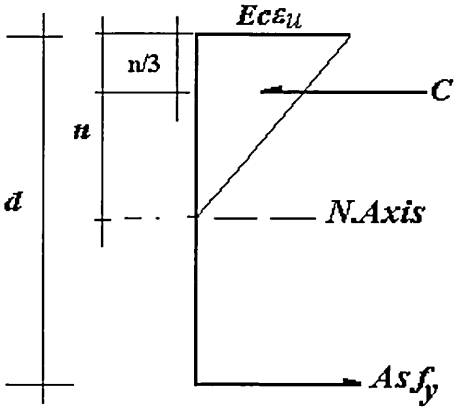

(iii) *Method three*

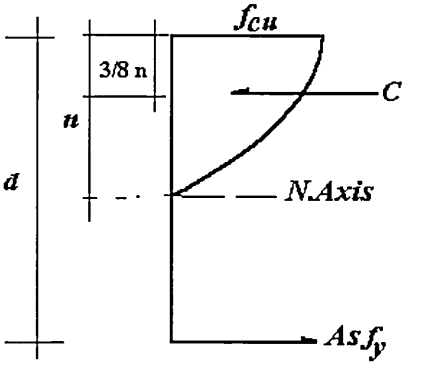

(iv) *Method four*

Fig.5.9- Different stress blocks of HSC beam in flexure

(iii). Method three

This method is inherently similar to method two but using (E_c * ε_{cu}) as the maximum compressive stress at the extreme fibre. The ultimate flexural strain,ε_u, of each beam was obtained from the respective beam test. The modulus of elasticity (E_c) for every beam was also calculated using the expression proposed by Carrasquillo *et al.*[33] and modified by Nilson.[101]

$$E_c = \left(3320\sqrt{f_c} + 6900\right) + \left(\rho/2320\right)^{1.5} \qquad 5.35$$

It should be noted that, approaches two and three implies a linear stress-strain relationship all the way up to ultimate strain value. Moreover, in view of the observed shape of the stress-strain curves of HSC, which are shown in the previous Chapter (see Fig. 4.5), the ascending branch of the curve is almost linear, and a descending branch is almost non-existent

(iv). Method four

A 2^{nd} degree parabolic stress block was used with f_{cu} at the extreme compression fibre. The compressive force (C) is computed as two-thirds of the area under the parabola times the width of the beam. The value of nominal ultimate strength capacity can then be found as follows:

$$T = C \qquad 5.36$$

$$T = A_s f_y \qquad 5.37$$

$$C = \frac{2}{3} f_{cu}.b.n \qquad 5.38$$

$$n = \frac{A_s f_y}{2/3 f_{cu} b} \qquad 5.39$$

Therefore, the nominal ultimate moment capacity can be determined as follows:

$$M_n = T\left(d - \frac{3}{8}n\right) \qquad 5.40$$

In the presence of compression reinforcement equation 5.40 yields;

$$M_n = T\left(d - \frac{3}{8}n\right) + A'_s f'_s\left(d - d'\right) \qquad 5.41$$

Fig. 5.9(i,ii,iii,iv) illustrates the different block idealisations. Also, Table 5.2 presents the measured and calculated ultimate moment capacity of all beams tested using the above four methods and also according to BS 8110 ultimate state design method.

It is apparent from the results that the moment capacity of singly and doubly reinforced HSC beams is realistically but conservatively predicted by all methods presented, particularly the triangular and parabolic stress blocks, i.e., methods 2, 3 and 4. It should be also stated that method one shows good correlation with the experimental ultimate moment capacity M_u, the mean and standard deviation being 1 and 0.13 respectively. However, in using this method the worst discrepancies were observed in the case of beams HSC3-2 and HSC4-3 which were 20% and 22% respectively. These discrepancies could be due to the discrepancies in measuring the ultimate strains and the consequent evaluation of the depths of the neutral axes.

Additionally, the tabulated results confirm the adequacy of the BS 8110 stress block approach for concrete having strength up to 110 *MPa* since it shows good correlation with experimental ultimate moment capacity but generally underestimating the strength,the mean and standard deviation being 1.13 and 0.09 respectively. However, the worst discrepancies were again observed in the case of beams HSC3-2 and HSC4-3, i.e., 25% and 29% respectively. It can ,therefore, be concluded that all the methods presented provide an adequate and safe basis for the prediction of the

ultimate moment capacities of HSRC beams with f_{cu} up to 110 MPa, and particularly, the BS 8110 design method provides a safe basis for the prediction of M_u of HSRC beams. In summary, all methods presented are reasonably applicable in predicting the ultimate moment capacity of HSRC beams.

Table 5.2- Measured Vs. Calculated Ultimate Strength of Test Beams

Beam	M_u, test *kN.m*	Method 1 M_n, *kN.m*	Ratio	Method 2 M_n, *kN.m*	Ratio	Method 3 M_n, *kN.m*	Ratio	Method 4 M_n, *kN.m*	Ratio	BS8110 M_n, *kN.m*	Ratio
HSC1-1	38.94	38.32	1.02	32.00	1.22	31.96	1.22	32.17	1.21	33.24	1.17
HSC1-2	35.64	42.86	0.83	31.90	1.12	31.97	1.11	32.08	1.11	33.06	1.08
HSC1-3	37.62	37.83	0.99	31.73	1.19	31.89	1.18	31.94	1.18	32.79	1.15
HSC2-1	46.33	53.58	0.86	42.17	1.10	41.93	1.10	42.47	1.09	41.87	1.11
HSC2-2	46.86	55.02	0.85	42.08	1.11	41.96	1.12	42.39	1.11	41.71	1.12
HSC2-3	43.56	52.15	0.84	41.48	1.05	41.99	1.04	41.88	1.04	40.71	1.07
HSC2-4	48.84	40.93	1.19	41.85	1.17	41.60	1.17	42.20	1.16	41.34	1.18
HSC3-1	67.32	61.66	1.09	54.40	1.24	54.80	1.23	54.90	1.23	54.18	1.24
HSC3-2	66.00	54.86	1.20	53.57	1.23	54.69	1.21	54.20	1.22	52.81	1.25
HSC3-3	64.68	62.36	1.04	53.20	1.22	54.48	1.19	53.89	1.20	52.21	1.24
HSC4-1	92.42	98.31	0.94	101.70	0.91	104.30	0.89	103.83	0.89	92.01	1.00
HSC4-2	89.60	96.03	0.93	99.52	0.90	104.47	0.86	101.98	0.88	88.39	1.01
HSC4-3	111.63	91.52	1.22	98.55	1.13	103.43	1.08	101.17	1.10	86.80	1.29
DHSC1-1	106.20	114.24	0.93	117.13	0.91	119.77	0.89	119.25	0.89	102.51	1.04
DHSC1-2	98.69	106.79	0.92	107.75	0.92	111.54	0.88	109.62	0.90	95.27	1.04
DHSC1-3	111.74	114.25	0.98	116.37	0.96	118.00	0.95	118.39	0.94	103.40	1.08
DHSC1-4	105.10	102.87	1.08	107.79	0.98	108.56	0.97	109.44	0.96	96.59	1.09
		Mean	**1.00**		**1.08**		**1.09**		**1.06**		**1.13**
		Std.Dev.	**0.13**		**0.13**		**0.13**		**0.13**		**0.09**

5.5 Surface crack spacing

The experimental cracks spacing of some beams are compared with predicted values according to the CEB- EC2.[51] expression which is as follows:

$$s_{rm} = 50 + 0.25\, k_1\, k_2\, \phi/\rho \qquad 5.42$$

where,

s_{rm}= The average final spacing between cracks, *mm*

ϕ= the bar size, k_1= the coefficient which takes account of the bond properties (0.8); k_2= a coefficient which takes account of the form of the strain distribution (0.5 for bending).

The measured and calculated values of the crack spacings of beams are presented in Table 4.3. It can be stated that there is somewhat reasonable agreement between the measured and theoretical values (i.e., means = 1.16 and Std. deviation = 0.31). The worst discrepancies were noticed in the case of beams HSC1-2 and HSC2-1(ratio of 1.61 and 1.79 respectively). This may be due to the fact that CEB-EC2 expression (equation 5.42) is expressed in terms of the geometric properties of the beam cross-section and independent of concrete compressive strength, f_{cu}.

In summary, it may be stated that the CEB-EC2 equation predicts the surface crack spacing of HSRC beams ,in the pure bending region, reasonably well.

5.6 Surface Crack Width

The existing formulae[27,35] for estimating the width of cracks on the concrete surfaces are subject to relatively large number in the variables, which makes it difficult to say which equation is the best for predicting crack width. The author has endeavoured critically to examine some of the existing formulae and establish a suitable crack width formula in the context of HSRC beams based on a statistical

analysis of all experimental data. Below are given two expressions generally used to predict the maximum crack width, w_{max} , at the level of the centroid of the tensile reinforcement:

$$w_{max} = 3.3\ c\ \varepsilon_m \qquad \text{BS 8110: part}^{[27]} \qquad 5.43$$

where,

$$\varepsilon_m = \varepsilon_1 - \frac{b(h-n)}{3EsAs} \text{ and}$$

$$\varepsilon_1 = \frac{M}{(\frac{1}{2}E_c)I_c} h_1$$

$$w_{max} = (4.5 + \frac{0.4}{\rho_e})\frac{\phi f_s}{k} \qquad \text{CEB-FIP}^{[35]} \qquad 5.44$$

where,

c= bottom cover measured from the centre of the lowest bar; k= constant; ϕ = nominal bar diameter ; f_s= steel stress ; ε_c= average strain in the concrete at the level of the centroid of the reinforcement

$\rho_e = A_s/A_e$, where A_s= area of tension reinforcement and $A_e = 2b(h-d)$, area of concrete having the full width of the beam and having the same centroid as the main reinforcement (see Fig. 5.10).

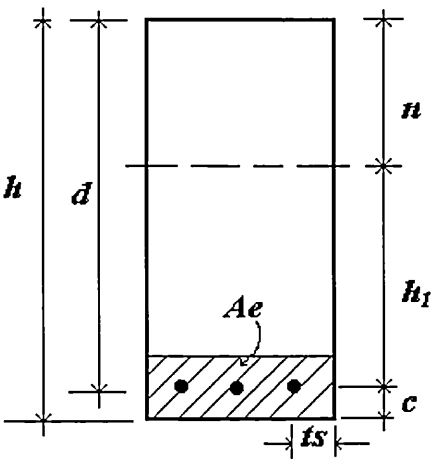

Fig. 5.10- Cross- section of beam

Two considerations were kept in mind to establish an empirical relationship to predict the average crack width at the level of the steel reinforcement in the zone of pure flexure: firstly, the expression has to be acceptable within the experimental data obtained and secondly, it should have a dimension of length. The proposed expression was in line with that proposed by Gergely and Lutz[56] and is as follows;

$$w_{avg} = 2.131 \frac{\sqrt[3]{ts\,A}}{1 + {}^{ts}/_{h_1}} \varepsilon_c \qquad 5.45$$

where,

$w_{avg.}$= average crack width at the level of the centroid of the reinforcement, *mm*

ts = side cover measured from the centre of the outer bar, *mm*

$A = {}^{Ae}/_{m}$ = average effective concrete area around a reinforcing bar, mm^2

m= number of tensile reinforcement bars

$h_1 = d - n$,distance from neutral axis to the centroid of reinforcement bars, *mm*

Crack widths obtained from test results were compared with the predicted maximum crack width values at the tensile reinforcement level using the above equations (i.e., 5.43, 5.44 and 5.45). From this analysis it is found that:

i- The BS crack equation grossly overestimated the maximum crack widths for HSRC beams in the pure bending region.

ii- The CEB-FIP crack expression gives a close correlation with the observed crack widths.

iii- The proposed empirical expression gives satisfactory agreement with existing test data with a correlation coefficient of 0.85 (see Fig. 5.11).

Fig.5.11- Comparsion between measured and predicted crack width

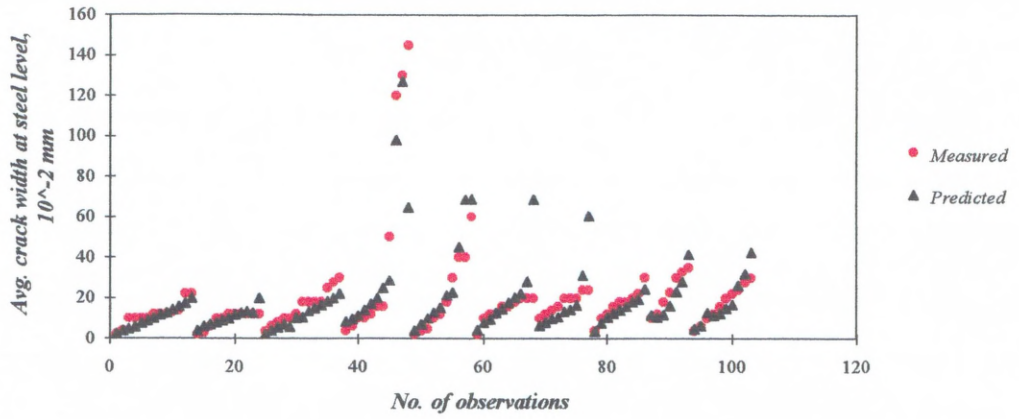

5.6 Ductility and Ductility Indices

5.6.1 Introduction

In a broad sense, ductility is defined as the ability of structure to sustain deformations beyond the elastic range without significant variation of the resistance capacity. Therefore, if the amount is small or negligible, the response is said to be brittle, but if the deformation is significant, the response is said to be ductile. Ductility can be quantitatively expressed by either member deformation or by sectional curvature. It is usually of significance in limit design or earthquake resistant design.

Member ductility is obtained from load-deflection relationships and can be expressed as follows:

$$\mu_d = \Delta_u / \Delta_y \qquad 5.46$$

where,

μ_d = displacement ductility index.

Δ_y = deflection at first yield of tensile reinforcement.

Δ_u = deflection at ultimate load.

Similarly, if the sectional curvature is considered, the ratio is obtained from moment -curvature relationships and can be expressed as:

$$\mu_c = \psi_u / \psi_y \qquad 5.47$$

where,

μ_c = Curvature ductility index.

ψ_y = Curvature at first yield of the tensile reinforcement.

ψ_u = Curvature at ultimate load.

It is logical that both indices are related to each other as the deflection is a function of the second integral of the curvature along a structural member. In this study curvature ductility index was considered.

5.7.2 Derivation of curvature ductility equation

Consider Fig. 5.12 where strain-stress condition is assumed elastic as shown for doubly reinforced beam at first yield of the tensile reinforcement.

$$\psi_y = \frac{fy}{d(1-k)Es} \qquad 5.48$$

From the properties of the transformed sections, the net area of transformed section can be written as follows:

$$b(kd) + mAs + (m-1)A'_s \qquad 5.49$$

The distance of the neutral axis from the top compressive fibres (*kd*) can be established for a rectangular section by setting the moments of the transformed area about the neutral axis equal to zero.

Then, $\frac{b(kd)^2}{2} + (m-1)\rho' bd(kd - d') - m\rho bd(1-k)d = 0$ 5.50

where, $d' = (d - k'd)$

Rearranging equation 5.50 and recognising that $bd^2 \neq 0$ we have:

$$\frac{k^2}{2} + (m-1)\rho'[k-(1-k')] - m\rho(1-k) = 0 \quad 5.51$$

Rearranging this equation

$$\frac{k^2}{2} - m\rho + m\rho k + (m-1)\rho' k - (m-1)\rho'(1-k') = 0$$
$$\frac{k^2}{2} + k(m\rho + (m-1)\rho') - [m\rho + (1-K')\rho'(m-1)] = 0,$$

and solving for k we get,

$$k = -(m\rho + \rho'(m-1)) + \sqrt{[m\rho + \rho'(m-1)]^2 + 2[m\rho + (1-k')(m-1)\rho']} \quad 5.52$$

Similarly, for singly reinforced section

$$k = -m\rho + \sqrt{(m\rho)^2 + 2m\rho} \quad 5.53$$

$$m = \frac{Es}{Ec}; \quad \rho = {As}/{bd}\ ; \text{ and } \rho' = {As'}/{bd}$$

Writing the equilibrium equation at ultimate limit state

$$k_1 f_{cu} b\, k_d = Asfy - As'f's \quad \text{giving,}$$

$$k_d = \frac{(\rho fy - \rho' f's)d}{k_1 f_{cu}}$$

k_d for singly reinforced sections can be written as follows;

$$k_d = \frac{\rho fy\, d}{k_1 f_{cu}}$$

Then, $\psi_u = \frac{\varepsilon_{cu}}{k_d}$; 5.49

and $\psi_y = \frac{fy}{d(1-k)Es}$ 5.50

Hence for doubly reinforced section

$$\mu_c = \frac{\psi_u}{\psi_y} = \frac{\varepsilon_{cu}\, k_1 f_{cu}(1-k)Es}{fy\ (\rho fy - \rho' f's)}, \text{ and} \qquad 5.51$$

for singly reinforced sections

$$\mu_c = \frac{\psi_u}{\psi_y} = \frac{\varepsilon_{cu}\, k_1 f_{cu}\ (1-k)Es}{\rho fy^2} \qquad 5.52$$

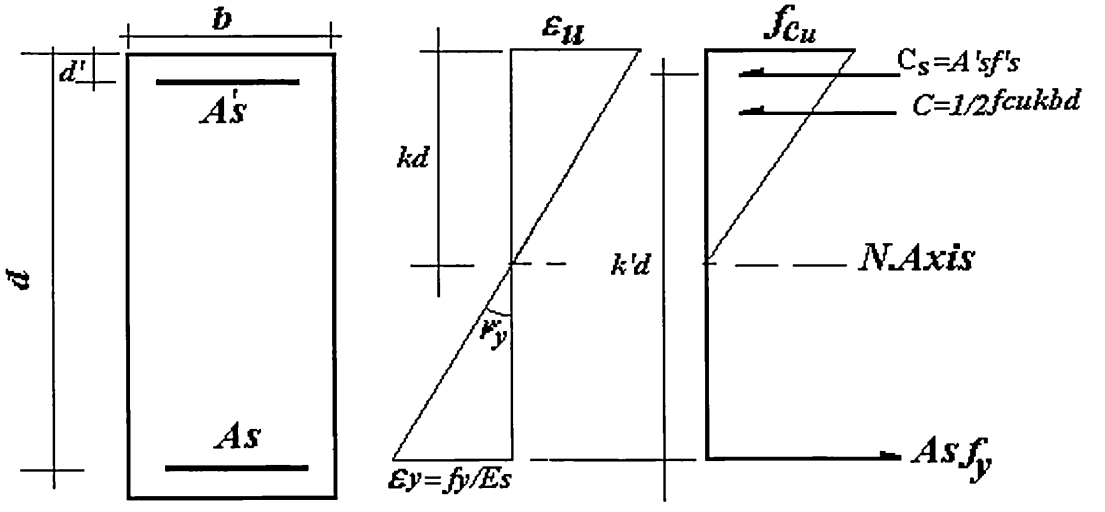

Fig 5.12-Stress-strain conditions in doubly reinforced section at yield.

In the light of test results the following major parameters which affect the ductility indices are discussed below:

1. Amount of tensile reinforcement

As it has been established from the definition of the curvature ductility increasing the amount of tensile steel decreases the ultimate curvature. Consequently, it decreases the ductility curvature index. This is experimentally confirmed as comparing two beams with same concrete compressive strength and different tensile steel ratio (see Table. 4.3; in Chapter 4) the ductility indices decrease drastically as the tensile steel ratio increases. Furthermore, In the light of the experimental results it seems that this factor is the most dominant factor influencing the magnitudes of the ductility indices.

2. Concrete strength

Theoretically, μ_c is directly proportional to concrete strength (f_{cu}). Consequently, keeping all other variables constant, increasing concrete strength (f_{cu}) would increases the magnitude of μ_c. Experimentally, in spite of the limited range of concrete strength (f_{cu}) in this research study, it was noticed for beams having constant tensile steel ratio, and varied concrete strength an increase in curvature ductility index,e.g., the curvature ductility indices for HSC1-1, HSC1-2, and HSC1-3 beams which were of different concrete strength, f_{cu}, are 7.4, 5.3 and 4.46 respectively.

3. Confinement reinforcement

The test results did clearly show the expected beneficial effect of web and compression reinforcements on ductility. In short, providing web reinforcement slightly increased the ductility index (see Table. 4.3), the ductility indices for HSC4-1 and DHSC1-2 beams which are of same concrete strength and tensile reinforcement, but DHSC1-2 has $\rho' = 0.504\%$, are 1 and 1.17 respectively.

CHAPTER 6

EXPERIMENTAL PROGRAMME IN SHEAR

6.1 Introduction

One of the objectives of this study is to investigate experimentally if the present codes of practice for concrete shear design can be extended to include HSC having a nominal compressive strength ranging up to 120 *MPa*. An experimental programme was carried out to study the shear strength of high strength reinforced concrete beams. A total of 17 beams were cast and tested in this experimental programme, in addition to the six beams tested previously in flexure, the ends of which were retested in shear. The experimental programme aimed to examine the effects of the following variables on the shear strength of high strength reinforced concrete beams:

(i). Concrete strength

(ii). longitudinal reinforcement

(iii). Shear span to depth ratio

(iv). Aggregate interlock

6.2 Specimen Details

All specimens tested in this study were rectangular beams with different length varying between 1180 *mm* and 1800 *mm*. The tensile reinforcement consisted of 20 *mm* ϕ bars and the reinforcement ratios were 1.94%, 2.92%, 4.04% and 4.4%. The shear span to depth ratio,*a/d*, was varied by changing the location of the load point on the beam surface; ratio of 1.5, 1.75, 2 and 2.6 were used. Tables 6.1 to 6.3 and Figs. 6.1 to 6.4 give specimen details. The specimens were divided into four series. The beams of HSRC (*group I*) had no stirrups and were used to investigate the effects of tensile reinforcement,ρ, and concrete strength,f_{cu}, on the concrete shear capacity of

reinforced concrete beams. The shear span to depth ratio was 2 for this series, and all beams were 1300 *mm* long, and 150 *mm* wide, see Table 6.1.

The beams of HSRW1-1 to HSRW1-9 (*group II*) had stirrups and were designed to investigate the effect of both f_{cu} and *a/d* ratio on the shear capacity of HSC. The concrete strength varied from 35 *MPa* to 111 *MPa* while the shear span varied from 1.5 to 2.6, see Table. 6.2. Another series of beams were cast, beams HSRW1-10 to HSRW12 (*group III*) since most of the beams in groups I and II failed in the long span side, i.e., the ultimate diagonal crack had occurred in the long span of the beam. In this series the shear reinforcements were provided from the supports up to the loading points of the beam. Both groups II and III contained one each of normal strength concrete beam for reference purposes (NSRC1-5 and NSRW1-1).

Additionally, three more beams (*group IV*) were cast with preformed inclined cracks were cast using the same details as the beams with shear reinforcement up to loading point. They were identical to those of group III except that the aggregate interlock mechanism was eliminated by introducing preformed shear cracks, thus enabling assessment of the contribution of aggregate interlocking,V_a, to the ultimate shear strength by comparison of the two series.

The beams of group IV were identical to beams of group III except that a smooth diagonal crack was introduced in the beam by using a thin steel plate of 0.8 *mm* thickness in order to eliminate the aggregate interlock. The width of the plate was the same as that of the beams, i.e., 150 *mm*, and each beam had preformed crack in the short side of the beam's span. Thus, theoretically the only difference between the corresponding beams of group III and IV is the shear contribution due to the aggregate interlock mechanism. The position of the diagonal crack was determined from the diagonal failure cracks observed in the beams of group III. Fig. 6.5 shows the position and detail of the preformed crack.

All beams in groups III and IV were 1800 *mm* long, 150 *mm* wide and 250 *mm* deep with 225 *mm* effective depth. The shear span to depth ratio, a / d, was 2.

6.3 Testing Procedure

All beam tests were performed using a hydraulic jack through a single loading point to provide the required *a/d* ratio. Loads were increased monotonically at 10 *kN* intervals up to failure, i.e., shear ultimate capacity. At each load increment the deflection at the loading point, strain reading along the beam's depth, concrete cracking patterns and the development of diagonal cracking were recorded. In addition, cube tests were carried out to determine the concrete compressive strength.

6.4 Materials and Their Properties

6.4.1 Concrete

In this part of study three nominal concrete strengths 40, 80 and 120 *MPa* were required. A superplasticizer and silica fume were used to obtain the required HSC. The fine aggregate was a natural sand with a wet relative density of 2.61. The coarse aggregates, 10 *mm* and 20 *mm*, were air dried crushed porphyritic andesite stone. The quantities of ingredients used for the different strengths are given in Table. 6.4.

6.4.2 Reinforcement

High yield deformed steel of 20 *mm* having f_y = 442 *MPa* were used in this part of the investigation. The reinforcements were bent at the end according to the BS 4466 clause 3.12.8.4 to provide sufficient anchorage and to ensure that beams did not fail due to insufficient bond. The shear stirrups were fabricated using plain 6 ϕ @ 150 *mm*, 8 ϕ @ 150 *mm* and 6 ϕ @ 100 *mm* for groups II and III respectively.

Table. 6.1- HSRC beams Without Shear Reinforcement(group I)

Beam	Cross-section	*d* *(mm)*	Rein-forcing bars	A_s, (mm^2)	ρ (%)	*a/d*	f_{cu}, *MPa*
HSRC1-1+	150 x 250	225	3ϕ 20	942.50	2.92	2	97.00
HSRC1-2+	150 x 250	225	2ϕ 20	628.32	1.94	2	102.00
HSRC1-3+	150 x 250	195	4ϕ 20	1257	4.04	2	107.00
HSRC1-4*	150 x 250	225	3ϕ 20	942.50	2.92	2	85.00
NSRC1-5*	150 x 250	225	3ϕ 20	942.50	2.92	2	42.33

+ The variable is steel reinforcement while a/d ratio is constant.

** The variable is concrete strength while ρ is constant.*

Table. 6.2- HSC Beams with Shear Reinforcement(group II)

Beam	Cross-section	*d* *(mm)*	Rein-forcing bars	A_s, (mm^2)	ρ (%)	ρ_v+ (%)	*a/d*	f_{cu}, *MPa*
NSRW1-1	150 x 250	225	3ϕ 20	942.50	2.92	0.126	1.75	35.00
HSRW1-2	150 x 250	225	3ϕ 20	942.50	2.92	0.126	1.75	102.00
HSRW1-3	150 x 250	225	3ϕ 20	942.50	2.92	0.126	1.75	82.30
HSRW1-4*	150 x 250	207.5	4ϕ 20	1257	4.04	0.22	2.6	111.00
HSRW1-5*	150 x 250	207.5	4ϕ 20	1257	4.04	0.22	2	109.00
HSRW1-6*	150 x 250	207.5	4ϕ 20	1257	4.04	0.22	1.5	108.00
HSRW1-7*	150 x 250	207.5	4ϕ 20 1ϕ 12	1370	4.4	0.22	2	103.00
HSRW1-8*	150 x 250	207.5	4ϕ 20 1ϕ 12	1370	4.4	0.22	2	104.00
HSRW1-9*	150 x 250	207.5	4ϕ 20 1ϕ 12	1370	4.4	0.22	2	104.00

**These beams are adopted from the doubly reinforced sections in flexure.*

$+\rho_v = A_v / b\,s$; *where,* A_v *is the area of web reinforcement within a distance(s).*

Table. 6.3-HSRC Beams with Shear Reinforcement up to Loading point (group III)

Beam	Cross-section	*d* (*mm*)	Rein-forcing bars	A_s, (mm^2)	ρ (%)	ρ_v (%)	*a/d*	f_{cu}, *MPa*
HSRW1-10	150 x 250	225	3ϕ 20	942.50	2.92	0.188	2	111.00
HSRW1-11	150 x 250	225	3ϕ 20	942.50	2.92	0.188	2	95.00
NSRW1-12	150 x 250	225	3ϕ 20	942.50	2.92	0.188	2	37.50

Note; Group IV beams were identical to the above except for the preformed crack, see Fig. 6.4.

Table. 6.4- Concrete Mix Proportions for the Shear Test Programme

Mix	C kg/m^3	S kg/m^3	C/A kg/m^3	SF L/m^3	SP L/m^3	W L/m^3	W/C	f_{cu}, *MPa*
1	528.88	663.4	1561.33	65.6	14.05	66.07	0.23	110
2	528.88	663.4	1561.33	65.6	14.05	107.77	0.31	85
3	371.26	814.37	1221.77	-	-	234.22	0.63	40

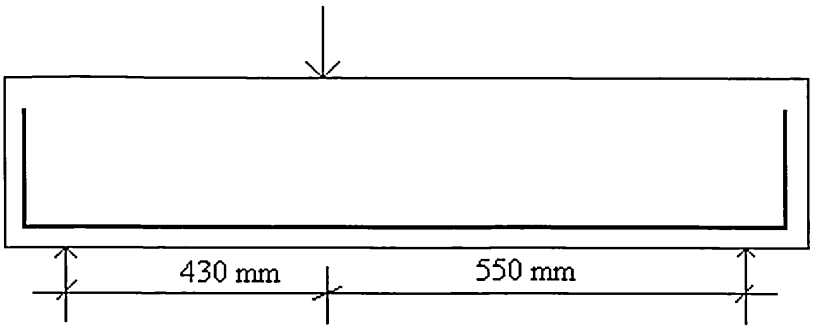

Fig. 6.1- Specimen Details for Group I Beams

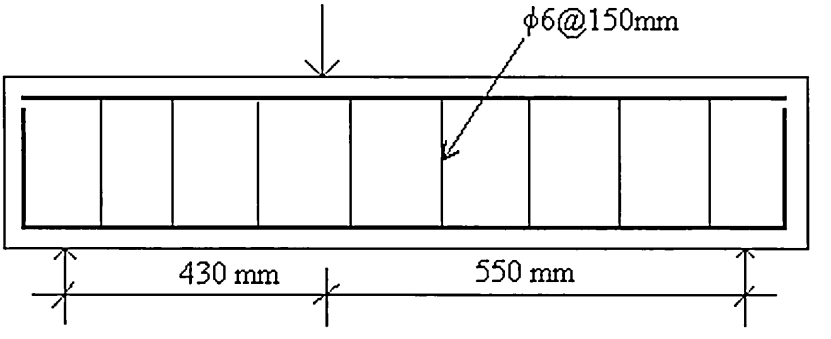

Fig. 6.2- Specimen Details for Group II Beams

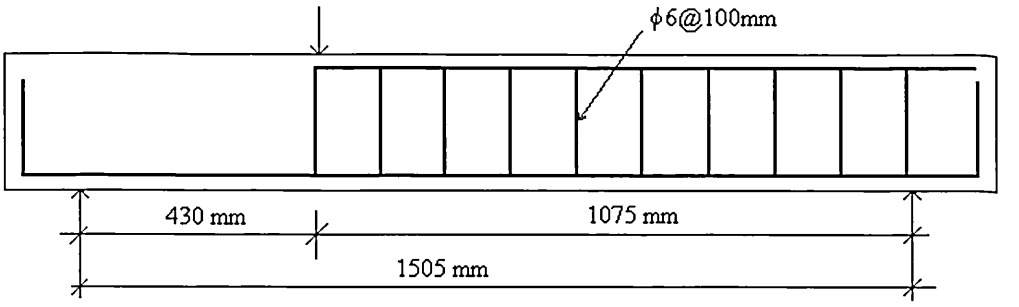

Fig. 6.3- Specimen Details of Group III and IV Beams

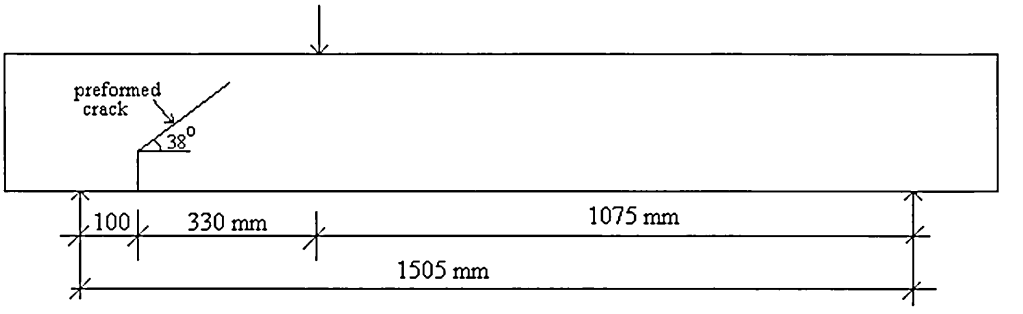

Fig.6.4- Specimen Details of Group IV Beams-Position of the preformed crack

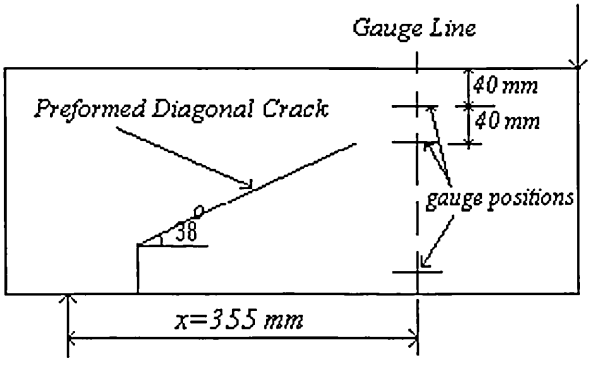

Fig. 6.5- Details of Preformed Crack and Location of Dial Gauges

CHAPTER 7

PRESENTATION OF EXPERIMENTAL RESULTS IN SHEAR

7.1 Introduction

As described in chapter 6, a total of 23 beams were cast and tested for this part of investigation. These beams can be classified into the following groups:

(i). Group I: Five reinforced concrete beams without web reinforcement. The main objective of this series of tests was to investigate the influence of f_{cu} and ρ ratio on the shear capacity of HSC beams.

(ii). Group II: Nine reinforced concrete beams with web reinforcement. The objectives of this series were to investigate the influence of *a/d* ratio in addition to other variables on shear capacity of HSRC beams.

(iii). Group III: Three reinforced concrete beams with web reinforcement in the longer sections from the loading point to the support. These beams were tested to supplement the findings from the tests of group I beams which exhibited some uncharacteristic failure pattern.

(iv). Group IV: Three reinforced concrete beams with a preformed diagonal crack. These beams were identical to beams in group III and were intended to assess the contribution of the aggregate interlocking mechanism,V_a.

In addition, three plain concrete beams were tested to estimate and compare flexural tensile strengths of HSC and NSC.

For all the beams tested, as well as the diagonal cracking load, V_{cr}, the ultimate shear failure loads,V_u, deflections under the point loading and concrete crack patterns were recorded at each load increment.

7.2 General Behaviour and Crack Patterns

At the early stages of loading the beams were free of cracks. With further increase of load flexural cracks were observed in the region of high bending moment and these cracks tended to curve towards the loading point with the increase of load. After this the behaviour of the beams was dependent upon f_{cu}, ρ and a/d and was influenced by the presence or absence of web reinforcement. Further load caused extensions of all previous cracks.

It is worth noting that, at failure longitudinal splitting along the main reinforcement was prevalent in most of the tested beams having $a/d = 2$, although, careful observation of the actual progress of failure indicated that the longitudinal splitting did not trigger the final failure. These cracks developed suddenly at or after the ultimate load had been reached. It was also noticed that short horizontal cracks developed near failure load just above the level of the longitudinal reinforcement. The peculiar cracking characteristics of beams without and with shear reinforcement are discussed in the following sections.

(i) Beams without shear reinforcement (Group I beams)

The general cracking pattern for all beams in this group was very similar. It was relatively easy to follow the sequential progress of the cracks once the first flexural cracks had been detected. All the beams tested in this group failed in shear, either in diagonal tension or in tension combined with arching action depending on the concrete compressive strength (Fig. 7.1).

Beams with $f_{cu} \geq 85$ *MPa* failed in diagonal tension and generally developed significant arch action such as beams HSRC1-1 and HSRC1-2 where a wide diagonal crack parallel to the first diagonal crack developed, after a significant amount of additional load had been applied from when the major diagonal crack had developed.

Also, beams with normal strength concrete failed in diagonal tension but the final failure accompanied with a horizontal splitting failure along the longitudinal reinforcement. This may be attributed to the significance of shear bond induced by higher strength concrete to the reinforcement.

Fig. 7.1 shows typical failure crack patterns for beams tested. These crack patterns show, the initial flexural crack loads were much higher in beams possessing high concrete strength. Also, the behaviour showed that HSRC beams were have much less vertical flexural cracking. For these beams, the failure loads were substantially higher, varying from 120% to 150% of the diagonal cracking loads. This reveals that a significant amount of load (i.e., reserve shear capacity) could be carried after the development of the major diagonal crack.

Up to the cracking load, shear is resisted mostly by shear stresses in the concrete. After cracking, shear is resisted by aggregate interlocking, dowel action of the main reinforcement and resistance of the uncrarcked concrete at the top of the beam as discussed in the following sections. The percentage carried by each mechanism strongly depends on factors such as f_{cu} and ρ . Examination of the crack widths of the beams in this investigation confirmed that the low strength concrete beams had wider cracks compared with the higher strength concrete beams at the same applied loads.

(ii) Beams with shear reinforcement (Groups II & III beams)

Web reinforcement increases the shear capacity of all reinforced concrete beams but, it has little or almost no effect on the crack pattern development of the beam or on its diagonal cracking load. As expected, all beams tested in these groups failed in diagonal tension, except for beams HSRW1-7, HSRW1-8 and HSRW1-9 which failed in shear compression with some destruction of the concrete in the compression zone; this is essentially because the latter possess higher web reinforcement ratio compared to the former. Generally the cracking patterns of these beams were very

similar to those of group I; once again it was quite easy to follow the progress of the crack once the first flexural cracks were developed. The final failure behaviour of the beams tested in this group were not as sudden and as explosive as those in group I beams without shear reinforcement. Also, the failure loads were 127% to 145% higher than the diagonal cracking loads. The pattern and development of the cracks of some beams in groups I I& III are shown in Fig. 7.2.

It was also noticed at about a third of the ultimate load that the cracks developed were flexural in group III beams. Above this load diagonal cracks started to develop. As expected, the failure diagonal crack in group III beams was in the short side of each beam tested. The ultimate failure loads were between 150% to 213% of the diagonal cracking loads. Once again, although all the beams in this series failed in diagonal tension, the final failure of the normal strength concrete beam (NSRW1-12) was accompanied by a horizontal splitting failure along the flexural reinforcement.

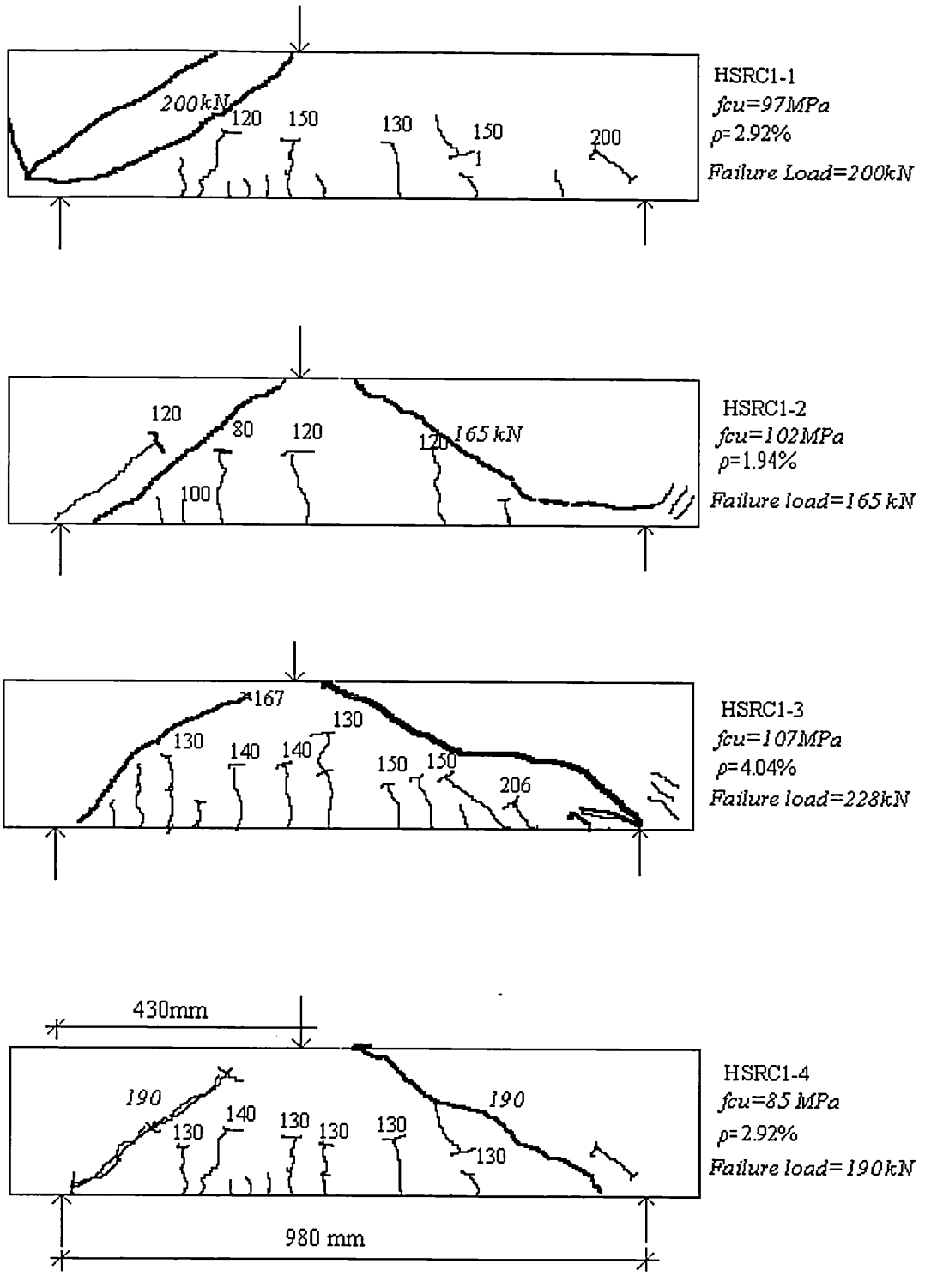

Fig. 7.1 Cracking Patterns of Beams Group I (a/d=2)

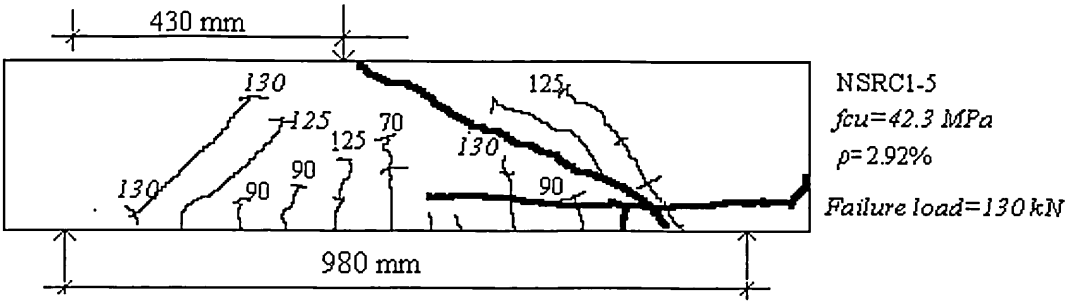

Fig. 7.1 Continued: Cracking Patterns of Beams Group I (a/d=2)

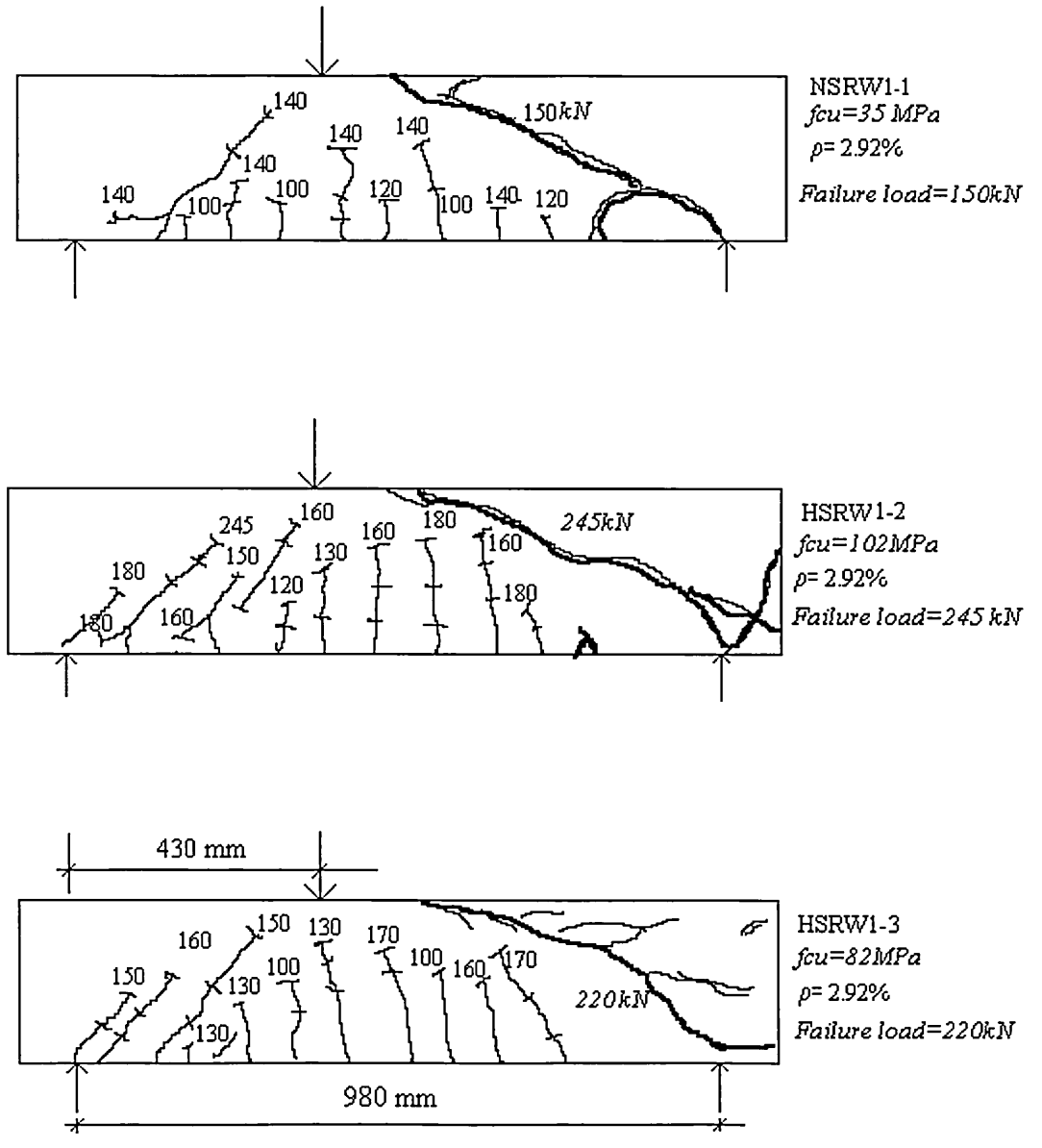

Fig. 7.2 Cracking patterns of some Beams in Group II & III (a/d=1.75)

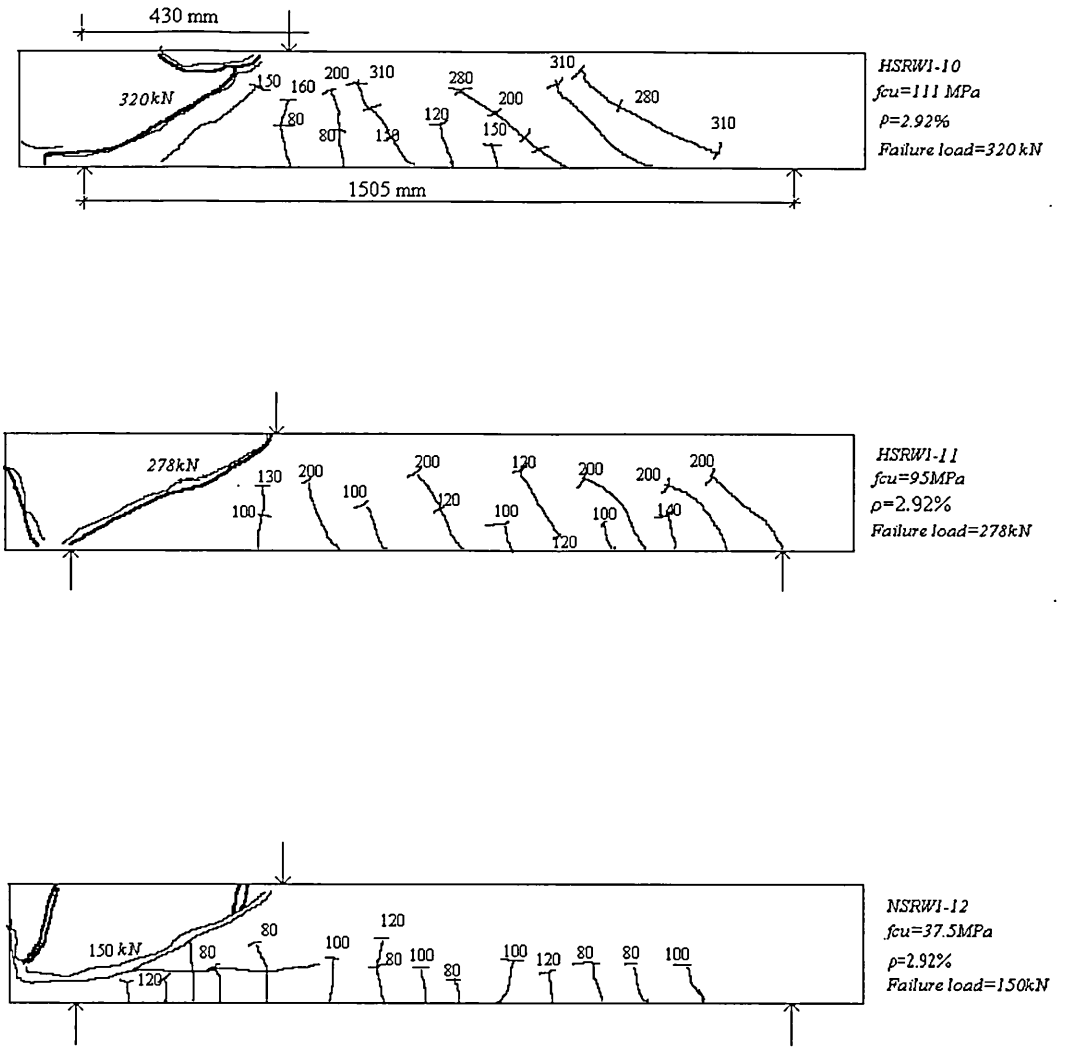

The numbers in the figures represent the applied load

Fig. 7.2 Continued:Cracking patterns of some Beams in Group II & III (a/d=1.75)

7.3 Diagonal Critical Crack and the Ultimate Shear Capacity

In this study the diagonal cracking stress, v_{cr}, is defined as the shear stress at which the diagonal crack crossed the mid-depth of a beam. In most cases the first diagonal crack eventually developed into the final failure crack. Tables 7.1, 7.2 and 7.3 show that the diagonal cracking stresses, as estimated from the observation of the concrete cracking patterns, were quite low compared with the measured ultimate shear stresses. However, in most of the tests, the diagonal cracking stress were higher than the values predicted by the BS 8110, ACI 318 codes and well below those given by the CEB-FIP shear expression.

The values of v_c obtained from equations 8.12, 8.13 and 8.14 were compared with the diagonal cracking stresses, v_{cr}, as shown in Table 7.2; the averages of the ratios of v_{cr} to v_c obtained from BS 8110, ACI 318 and CEB-FIP equations work out to be 1.12, 1.10 and 0.87 with standard deviations of 0.14, 0.18 and 0.2. These demonstrate that BS and ACI equations give good prediction of v_{cr} while the CEB-FIP expression overestimates it.

The values of v_n predicted by Zsutty's expression (equation 8.11) were also compared with the measured ultimate shear strengths, v_u, as shown in Tables 7.1 and 7.2; the averages of the ratios of v_u to v_n work out to be 1.09 and 1.04 with standard deviations of 0.05 and 0.16 which indicate a very close agreement between the predicted and the test results.

7.4 Effect of Concrete Strength

As expected, the ultimate shear stress, v_u, of the test beams increased with increase in f_{cu} but at a slower rate than the increase in concrete strength.

Also, the diagonal cracking shear capacity tended to increase with f_{cu}. This trend was consistent for all the beams tested, for example, v_{cr} = 3.54 and 2.88 *MPa* for beams HSRW1-10 and HSRW1-11 respectively which had the same design criteria but f_{cu}=94.4 and 80.8 *MPa* respectively. The ratio of f_{cu}/v_{cr} for these two beams were 26.67 and 28.09 respectively.

It was noticed from the test results that the ultimate shear stress, v_u, (at different f_{cu} values and constant ρ and a/d ratios) followed a reasonable trend and gave general agreement with the values predicted by Zsutty's expression (equation 8.11). In that respect, as far as the final cracking patterns and the ultimate shear strengths are concerned it could be stated that good reproducibility in the data was obtained. The effects of f_{cu} on the shear stresses v_{cr} and v_u are shown in Fig. 7.3.

On the other hand, the tests on the plain concrete beams indicated that the flexural tensile strength for 107 *MPa* concrete was 6.43 *MPa* and for 40 *MPa* concrete 3.47 *MPa* which were in reasonable agreement with the tensile strength results obtained using splitting cylinder tests.

Fig.7.3-Effect of fcu on shear stress at constant a/d

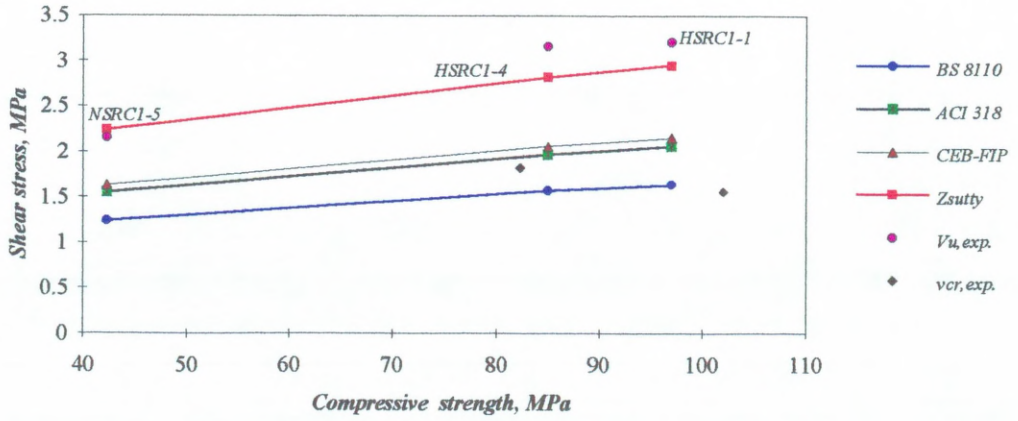

7.5 Effect of Flexural Reinforcement Ratio, ρ

The effect of ρ on the shear stress of test beams is shown in Fig. 7.4 from which it can be seen that ρ has a significant effect on the ultimate shear stress of HSC beams. For all beams tested with and without web reinforcement, increasing ρ increased the shear stress capacity. For instance, by comparing the beams HSRC1-2 and HSRC1-3 which had approximately the same f_{cu}, but ρ of 1.94% and 4.04% respectively, it is seen that the ultimate shear strength of beam HSRC1-3 was about 36% greater than that of beam HSRC1-2 (see Fig. 7.4).

Fig. 7.4- Effect of Flexural Reinforcement on Shear Stress

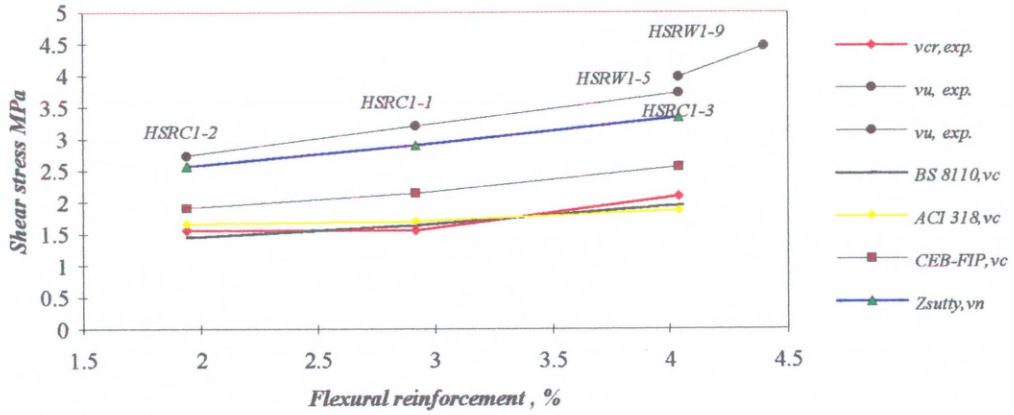

It can be seen from the limited test results given in Table 2 that the diagonal cracking stresses, v_{cr}, compared quite favourably with stresses predicted by the BS 8110 and ACI 318 expressions; the BS 8110 expression gave a safer prediction compared to that by ACI one. It should be further stated that the ACI 318 expression (equation 8.2) is restricted to beams possessing lower values of ρ. From Table 7.2 it can be seen that the CEB-FIP expression(equation 8.3) gave unsafe design shear capacities at different ρ values for all beams tested (i.e., $v_{cr}/v_c < 1$).

In conclusion, the BS 8110 expression generally gave safe shear diagonal stress predictions whereas the ACI code expression gave slightly conservative values for

beams with web reinforcement; the CEB-FIP generally gave unsafe shear predictions for all beams tested. In comparing these values the writer is very aware that the number of tests in this programme was limited and the comparison of v_{cr} against v_c could be somewhat subjective in that the accuracy of v_{cr} depended on the skill of the observer. Additionally, it was noticed that the test results of ultimate shear stress (at different ρ values) followed a reasonable trend and were in general agreement with the values predicted by Zsutty's expression (equation 8.11).

7.6 Effect of *a/d* Ratio

The effect of *a/d* ratio on shear strength is shown in Fig. 7.5. Generally, the shear strength decreased dramatically with an increase of *a/d*, all other variables remaining constant. For the same applied load on the beams higher *a/d* means larger bending moment in the shear span; thus, the depth of penetration of the flexural cracks increases. Therefore, the flexural stresses near the crack tip increase. By increasing *a/d*, the possibility grows that a flexural crack will develop into a diagonal one. For instance, the beams HSRW1-4 & HSRW1-6 are compared which had approximately the f_{cu} and ρ values and *a/d* = 2.6 and 1.5 respectively; it was found that increasing *a/d* from 1.5 to 2.6 resulted in a reduction in shear strength of about 42% (see Table 7.2). However, it was noted that the shear strength of the beams was also affected by the reinforcement ratio, ρ , which can be seen by comparing the beams HSRW1-5 & HSRW1-8 which had approximately the same f_{cu} and *a/d* ratio but values of ρ = 4.04% and 4.4% respectively. For beam HSRW1-5 with ρ of 4.04% the ultimate shear strength was reduced by 35% lower than that of beam HSRW1-8 (ρ = 4.4%). This substantial reduction could be attributed to yielding of the longitudinal reinforcement near to failure.

As stated earlier the values of v_c obtained from equations 8.12, 8.13 and 8.14 were compared with the diagonal cracking stresses, v_{cr}, as shown in Table 7.2; the ratios

of v_{cr} to v_c obtained from BS 8110 were slightly conservative and in very close agreement (i.e., v_{cr}/v_c = 1.06,1.16 and 1.02 for beams HSRW1-4 and HSRW1-5 and HSRW1-6 respectively). It was also found that the ACI equation gave a safe prediction of shear diagonal stress values for different *a/d* ratios. It was of interest to note that the ratio of measured to predicted shear strength employing the ACI equation decreased with increasing *a/d* ratio (compare HSRW1-4 and HSRW1-6 beams, Table 7.2), whereas these ratios showed a relative increase with higher *a/d* ratios when BS 8110 code equation was employed. As before, the CEB-FIP equation was found to be unsafe in predicting the design shear stress of HSRC beams.

It was further noted from the test results that the ultimate shear stress at different *a/d* ratios followed a reasonable trend and these were in general agreement with the values predicted by Zsutty's expression (equation 8.11). Additionally, it is worth stating to state that the higher ultimate shear strength of a beam having lower *a/d* ratio may be attributed to arch action as part of the load is transmitted by means of diagonal compression towards the supports.

Fig. 7.5- Effect of a/d on Shear Stress of Beams with Constant fcu

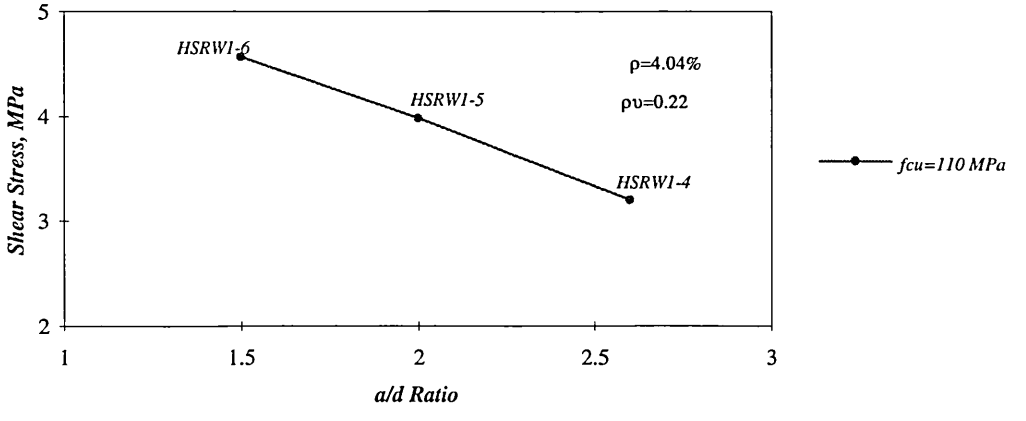

Table 7.1-Experimental and Predicted Shear Stress of Beams without Shear Reinforcement (group I)

Specimen design criteria					*Measured shear stress, MPa*				*Predicted shear stress, MPa*				*Ratio of* v_{cr}/v_c			*Ratio* v_u/v_n
									v_c			v_n				
Beam	f_{cu} *MPa*	f_c ♣ *MPa*	ρ %	*a/d*	v_{cr}	f_{cu}/v_{cr}	v_u	f_{cu}/v_u	*BS8110*	*ACI 318*	*CEB-FIP*	*Zsutty*	$v_{cr}/$*BS8110*	$v_{cr}/$*ACI 318*	$v_{cr}/$*CEB-FIP*	$v_u/$*Zsutty*
HSRC1-1	97.00	82.45	2.92	2.00	1.56	62.18	3.21	30.22	1.64	1.70	2.56	2.89	0.95	0.92	0.61	1.11
HSRC1-2	102.00	86.70	1.94	2.00	1.56	65.38	2.74	37.23	1.45	1.66	2.15	2.57	1.07	0.94	0.73	1.07
HSRC1-3	107.00	90.95	4.04	2.00	2.10	50.95	3.72	28.76	1.95	1.87	1.91	3.33	1.07	1.12	1.10	1.12
HSRC1-4	85.00	72.25	2.92	2.00	1.82	46.70	3.16	37.28	1.57	1.61	2.06	2.77	1.16	1.13	0.89	1.14
NSRC1-5	42.33	35.98	2.92	2.00	1.66	25.50	2.25	18.81	1.24	1.21	1.63	2.19	1.34	1.37	1.02	1.03
												Avg.	***1.12***	***1.10***	***0.87***	***1.09***
												Std. Dev.	***0.14***	***0.18***	***0.20***	***0.05***

♣ f_c = *cylinder strength assumed to be 0.85 of* f_{cu}

Table 7.2-Experimental and Predicted Shear Stress of Beams with Shear Reinforcement (group II)

Specimen design criteria						*Measured shear stress, MPa*				*Predicted shear stress, MPa*				*Ratio of* v_{cr}/v_c			*Ratio* v_u/v_n
										v_c			v_n				
Beam	f_{cu} *MPa*	f_c ♣ *MPa*	ρ %	ρ_v %	*a/d*	v_{cr}	f_{cu}/v_{cr}	v_u	f_{cu}/v_u	*BS8110*	*ACI 318*	*CEB-FIP*	*Zsutty*	$v_{cr}/$ *BS8110*	$v_{cr}/$ *ACI 318*	$v_{cr}/$ *CEB-FIP*	$v_u/$ *Zsutty*
NSRW1-1	35	29.75	2.92	0.13	1.75	1.66	21.08	2.37	14.77	1.65	1.48	1.92	2.78	1.01	1.13	0.87	0.85
HSRW1-2	102	86.70	2.92	0.13	1.75	2.24	45.54	4.07	25.06	2.22	2.09	2.60	3.83	1.01	1.07	0.86	1.06
HSRW1-3	82.3	69.96	2.92	0.13	1.75	2.24	36.74	3.55	23.18	2.15	1.94	2.52	3.59	1.04	1.15	0.89	0.99
HSRW1-4	111	94.35	4.04	0.22	2.60	2.17	51.15	3.21	34.58	2.05	2.14	2.89	2.93	1.06	1.02	0.75	1.10
HSRW1-5	109	92.65	4.04	0.22	2.00	2.89	37.72	3.98	27.39	2.49	2.20	3.08	3.90	1.16	1.31	0.94	1.02
HSRW1-6	108	91.80	4.04	0.22	1.50	3.20	33.75	4.57	23.63	3.12	2.31	3.33	5.45	1.02	1.38	0.96	0.84
HSRW1-7	103	87.55	4.40	0.22	2.00	2.58	39.92	3.90	26.41	2.50	2.19	3.11	3.93	1.03	1.18	0.83	0.99
HSRW1-8	104	88.40	4.40	0.22	2.00	2.45	42.45	5.36	19.40	2.51	2.20	3.12	3.94	0.98	1.11	0.79	1.36
HSRW1-9	104	88.40	4.40	0.22	2.00	2.59	40.15	4.46	23.32	2.51	2.20	3.12	3.94	1.03	1.18	0.83	1.13
													Avg.	***1.04***	***1.17***	***0.86***	***1.04***
													Std. Dev.	***0.05***	***0.11***	***0.07***	***0.16***

♣ f_c *=cylinder strength assumed to be 0.85 of* f_{cu} *and* $v_u = v_c + v_s$, *where;* $v_s = \dfrac{A_v f_y}{b\,s}$, *(MPa)*

Table 7.3-Experimental and Predicted Shear Stress of Beams (group III)

Specimen design criteria					*Measured shear stress, MPa*				*Predicted shear stress, MPa*				*Ratio of* v_{cr}/v_c			*Ratio* v_u/v_n
									v_c			v_n				
Beam	f_{cu} *MPa*	f_c ♣ *MPa*	ρ %	*a/d*	v_{cr}	f_{cu}/v_{cr}	v_u	f_{cu}/v_u	*BS8110*	*ACI 318*	*CEB-FIP*	*Zsutty*	$v_{cr}/BS8110$	$v_{cr}/ACI\ 318$	$v_{cr}/CEB-FIP$	$v_u/Zsutty$
HSRW1-10	111.00	94.35	2.92	2.00	3.54	31.36	7.08	15.68	1.73	1.81	2.27	3.02	2.04	1.96	1.56	2.34
HSRW1-11	95.00	80.75	2.92	2.00	2.88	32.99	6.16	15.42	1.64	1.69	2.16	2.87	1.75	1.70	1.34	2.14
HSRW1-12	37.50	31.88	2.92	2.00	2.21	16.97	3.32	11.30	1.21	1.16	1.59	2.11	1.83	1.91	1.39	1.58
												Avg..	***1.87***	***1.86***	***1.43***	***2.02***
												Std. Dev.	***0.15***	***0.14***	***0.12***	***0.40***

♣ f_c = *cylinder strength assumed to be 0.85 of* f_{cu}

7.7 Unusual Cracking Pattern

While testing the beams in shear an unusual phenomenon was observed which was: diagonal shear cracks developed in the long span of beams HSRC1-3, NSRC1-5, NSRW1-1 and HSRW1-2 near the failure loads. At early stages of loading flexural cracks appeared; on increasing the load one of these cracks near the support tended to curve towards the loading point. With further application of load, a diagonal crack, different from the others, suddenly appeared in the short span of each beam. The crack tended to widen with the increase of load.

With further increase of the load a diagonal crack suddenly appeared in the longer side of each beam tested; the diagonal shear crack in the short side stopped developing. The failure of the beam occurred after the full development of a diagonal crack in the long side of the beam which was accompanied by the development of a wide horizontal crack near to and parallel with the main reinforcement.

The failure was adjudged to be either bond diagonal tension or bond diagonal compression failure. As no clear explanation of this phenomenon could be offered, it was decided to cast another three beams providing web reinforcements in the long side of the beams to prevent this phenomenon from occurring. (See Figs 7.1 and 7.2).

7.7.1 Beams with stirrups in the long side

Three reinforced concrete beams with nominal concrete strength of 40, 80 and 120 *MPa* were cast and tested. The reinforcement and *a/d* ratios were 2.92% and 2 respectively. The observed cracking behaviour of these beams under load was almost the same at low loads when flexural vertical cracks developed up to 160 *kN* for HSRW1-10, 130 *kN* for HSRW1-11 and 100 *kN* for NSRW1-12 respectively. After that the cracks tended to widen until ultimate diagonal shear failure occurred in the short side.

The values of v_c and v_u obtained from equations 8.11, 8.12, 8.13 and 8.14 were compared with the diagonal cracking stresses, v_{cr}, and the ultimate shear strength, v_u, as shown in Tables 7.3.

It has further been noted that the addition of web reinforcement significantly affected the ultimate failure loads as compared with the previous beams. The ultimate failure load for beam HSRW1-10 was 330 *kN* (f_{cu} = 111 *MPa*), 290 *kN* for beam HSRW1-11(f_{cu} = 95 *MPa*) and 150 *kN* for beam NSRW1-12 (f_{cu} = 37.5 *MPa*).

Table 7.4- Experimental Results: Diagonal Crack and Ultimate Loads

Beam	*fcu, MPa*	ρ , %	ρ v, %	*a/d*	*Vcr, kN*	*Vu, kN*
HSRC1-1	97.00	2.92	-	2.00	93.81	193.04
HSRC1-2	102.00	1.94	-	2.00	93.81	164.77
HSRC1-3	107.00	4.04	-	2.00	126.29	223.71
HSRC1-4	85.00	2.92	-	2.00	109.45	190.00
NSRC1-5	42.33	2.92	-	2.00	99.83	135.31
NSRW1-1	35.00	2.92	0.13	1.75	99.83	142.52
HSRW1-2	102.00	2.92	0.13	1.75	134.71	244.76
HSRW1-3	82.30	2.92	0.13	1.75	116.74	220.00
HSRW1-4	111.00	4.04	0.22	2.60	120.35	178.02
HSRW1-5	109.00	4.04	0.22	2.00	160.28	220.73
HSRW1-6	108.00	4.04	0.22	1.50	177.47	253.45
HSRW1-7	103.00	4.40	0.22	2.00	143.08	216.29
HSRW1-8	104.00	4.40	0.22	2.00	135.87	297.26
HSRW1-9	104.00	4.40	0.22	2.00	143.64	247.35
HSRW1-10	111.00	2.92	-	2.00	167.27	334.53
HSRW1-11	95.00	2.92	-	2.00	136.08	291.06
NSRW1-12	37.50	2.92	-	2.00	104.42	156.87
HSRW1-13	122.00	2.92	-	2.00	-	206.96
HSRW1-14	95.00	2.92	-	2.00	-	168.68
NSRW1-15	37.50	2.92	-	2.00	-	108.20

7.8 Load-Deflection Behaviour

The structural behaviour of a beam under load can be described by observing the characteristics of the load-deflection curve of a beam. Figs. 7.6 to 7.10 show the applied load versus deflection at loading point of beams tested. The behaviour of the beam was initially linear as can be seen in Figs 7.6 to 7.10 but as the loading increased non-linear behaviour dominated due to the formation of flexure and shear cracks. As expected the beams with higher flexural reinforcement ratio,ρ, demonstrated a stiffer response to loading, see Fig. 7.6.

The effect of concrete strength f_{cu} and the reinforcement ratio ρ can be seen clearly by comparing the beams (i) HSRC1-1 and HSRC1-3 (see Fig. 7.6) which had approximately the same concrete strength, 97 and 107 *MPa*, but values of ρ = 2.92% and 4.04% respectively; beam HSRC1-3 was approximately 20% stiffer than beam HSRC1-1; (ii) HSRC1-4 and NSRC1-5 (see Fig. 7.7) which had the same reinforcement ratio ρ= 2.92% but different f_{cu} value 85 and 42 *MPa* respectively. Beam HSRC1-4 was approximately 30% stiffer than beam NSRC1-5.

The effect of *a/d* ratio on deflection can be seen in Fig. 7.9, the load deflection curve being relatively linear. Beams HSRW1-5 and HSRW1-6 with *a/d* ratio of 1.5 and 2 generally showed a significant increase in stiffness after formation of the major inclined crack compared with beam HSRW1-4 with *a/d*= 2.6. It was also noticed that providing shear (web) reinforcement increases the load capacity of beams, for example, beam HSRC1-1 in Fig. 7.6 and beam HSRW1-2 in Fig. 7.8 both had same ρ and f_{cu} but the latter with web reinforcement failed at a load of 245 *kN* compared 190 *kN* for the former. Additionally, the slope of the load-deflection curve is much steeper demonstrating greater stiffness when web reinforcement is present.

Fig. 7.6-Load-Deflection at Loading Point of Beams with Different Reinforcement

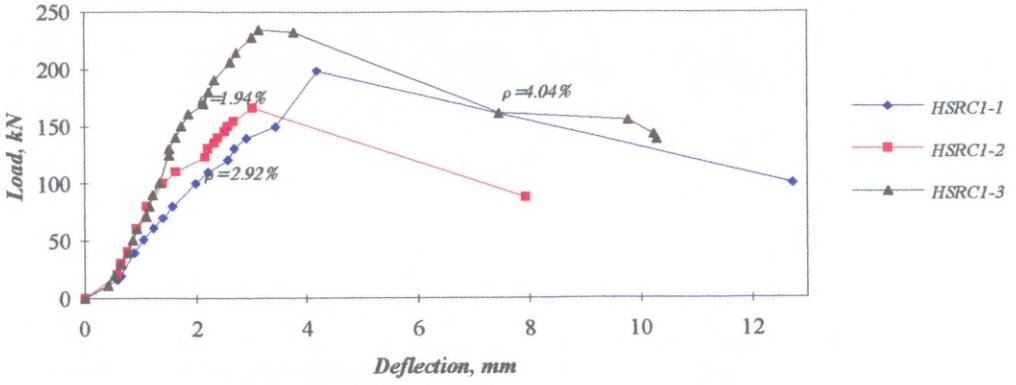

Fig. 7.7-Load-Deflection at Loading Point of Beams with Different fcu

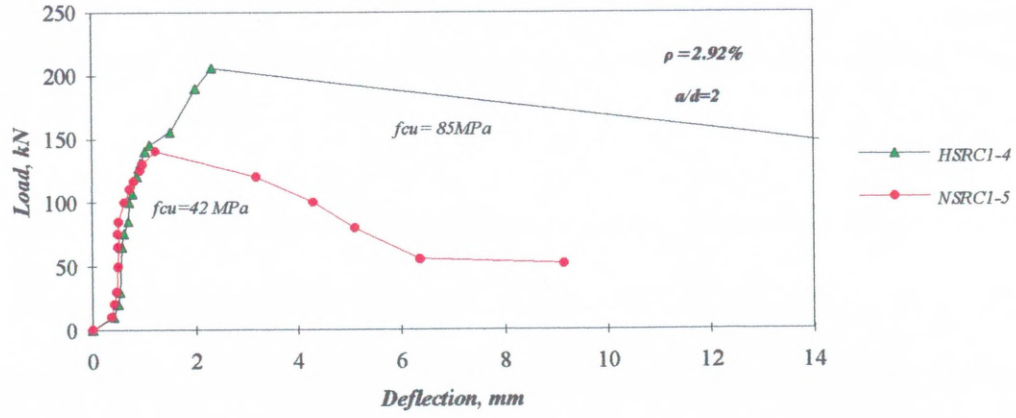

Fig. 7.8-Load-Deflection at loading point of Beams with Different fcu

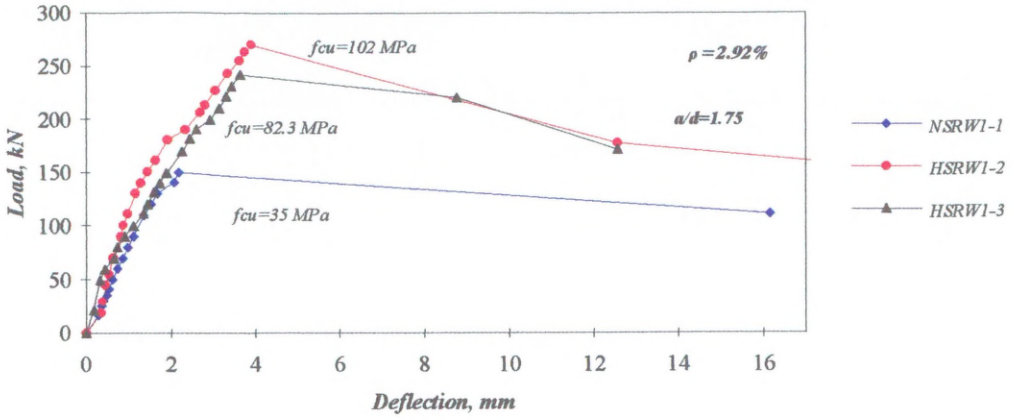

Fig. 7.9- Load-Deflection at Loading Point of Beams with Different a/d

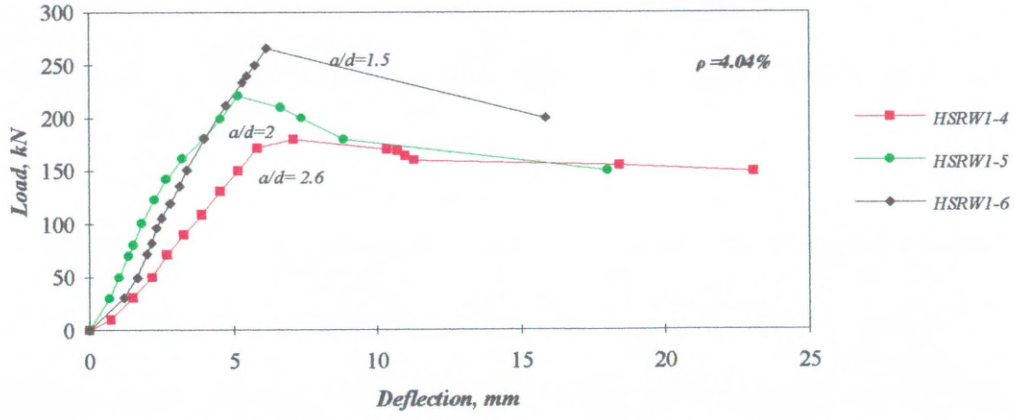

Fig. 7.10-Load-Deflection at Loading Point of Some Beams

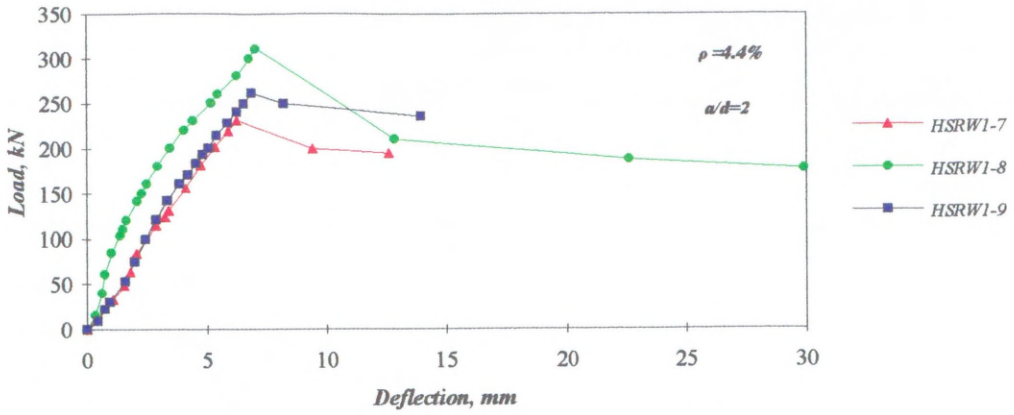

7.9 Tests of Beams with Preformed Diagonal Crack

This subsection reports the effect of concrete strength on aggregate interlock. Three reinforced concrete beams with web reinforcement up to loading point in the long section and having preformed diagonal cracks in the short section were tested to study the influence of the concrete strength on the aggregate interlock shear transfer mechanism,V_a. The beams were made of concrete having nominal strengths of 40, 80 and 120 *MPa* and were tested under single point loading using the same *a/d* ratio of 2. The ultimate shear failure load ,V_u, deflections at loading point, concrete cracking patterns and the longitudinal surface strains in the compression zone concrete were recorded at selected load stages.

7.9.1 Crack pattern development and general behaviour

The crack pattern in beams having preformed diagonal crack differed markedly from beams without preformed diagonal cracks. The preformed diagonal cracks opened early during the test, i.e., 70 *kN* for HSRW1-13 and 40 *kN* for HSRW1-14 beams. This affected the subsequent formation of flexural cracks. Most flexural cracks in these beams remained vertical throughout the test up to load of 110 *kN*. The propagation of the flexural cracks was limited by the development of cracks in the

preformed diagonal crack region unlike in beams without preformed diagonal crack where the flexural cracks propagated extensively and tended to incline towards the loading point during the later stages of the load.

It was also noticed, that horizontal cracks developed along the main reinforcement during later stages of the tests. All the beams in this series had almost identical crack patterns, (see Fig. 7.11 for the crack patterns). In beams without preformed crack, flexural cracks were the first cracks to be seen whereas, in beams with preformed crack, flexural cracks were noticed after separation at the inclined portion of the diagonal crack. Flexural cracks then formed along both the short and long sections. As the load increased the preformed diagonal crack continued to propagate both towards the loading point and the support point. Moreover, additional loads did not seem to change the vertical flexural cracks very much. Eventually, the failure was sudden and explosive, all beams in this series failing in shear tension.

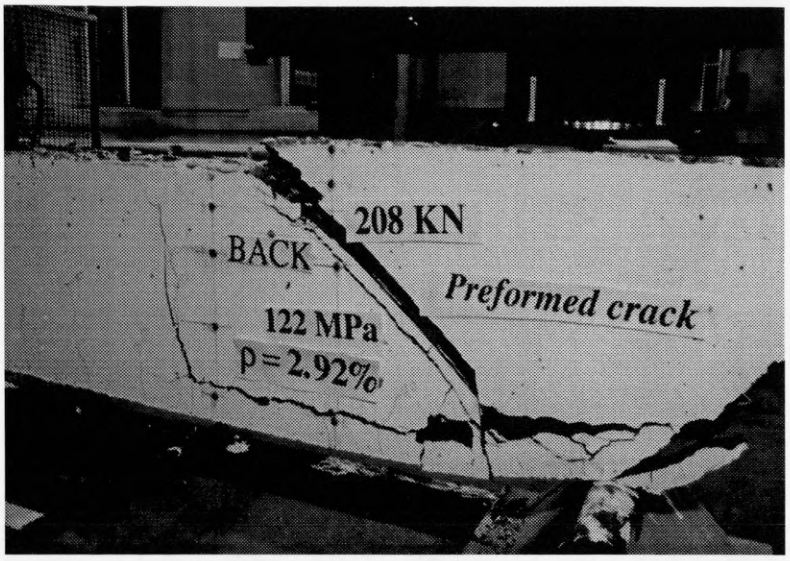

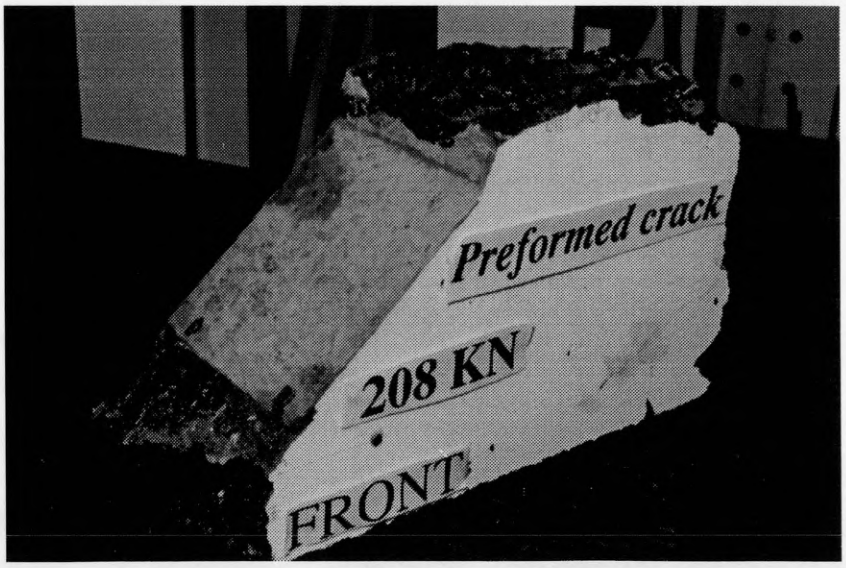

Fig. 7.11 Cracking Patterns of Beam HSRW1-13 (a/d=2)

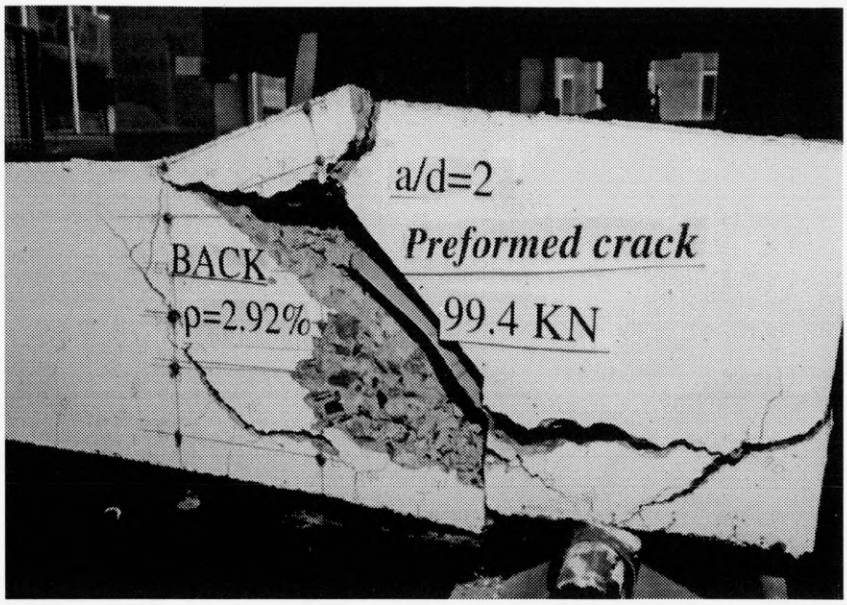

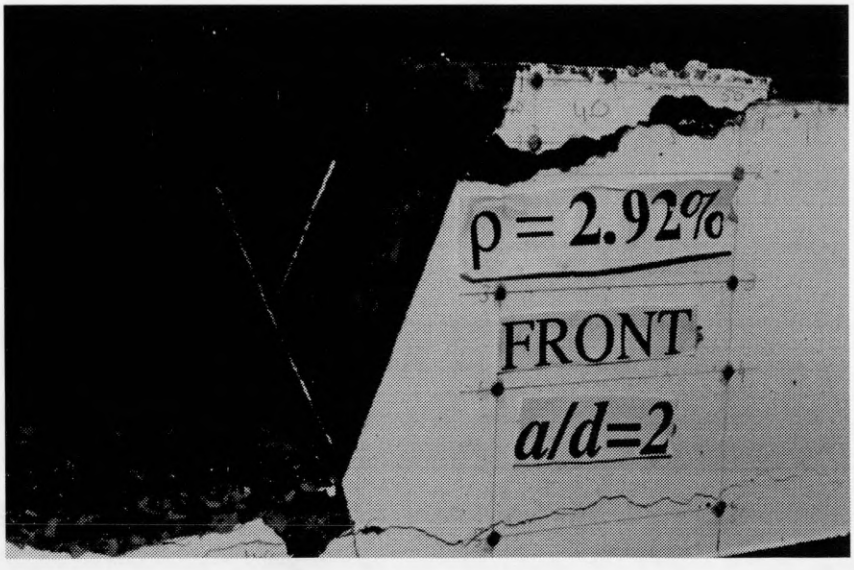

Fig. 7.11 Continued: Cracking Patterns of Beam HSRW1-14 (a/d=2)

7.9.2 Estimation of Shear Transfer Carried by Different Mechanisms

7.9.2.1 Shear capacity carried by compression zone

A semi-empirical method, which was originally developed by Taylor[131] was employed to estimate the shear strength carried by the compression zone, v_{cz}, from strain readings taken at different levels along the beam's depth. The analytical procedures are presented in Chapter 8.

7.9.2.2 Shear capacity carried by aggregate interlock

As described earlier in Chapter 6, the aggregate interlocking forces were removed from all beams of group IV by preforming smooth diagonal cracks. Therefore, in order to determine the shear resisted by the aggregate interlock mechanism, the ultimate shear capacities of these beams (group IV) were compared with those of group III, which had no diagonal preformed cracks.

7.9.2.3 Shear carried by dowel action

The compression zone shear stress, v_{cz}, was computed analytically from the longitudinal strain readings taken in the compression zone of a beam. Thence, the dowel resistance, v_d, was postulated to be equal to the numerical difference between the total applied shear and the compression zone mechanism contribution, i.e.,

$$V_d = V_u - V_{cz} \qquad 8.5$$

Following the procedures proposed by Taylor[131] which are presented in details in Chapter 8 concerning the estimation of the shear force resisted by the concrete compression zone, V_{cz}, the dowel action, V_d, was determined at every load stage. As it can be seen from Figs. 7.12 to 7.14, the dowel action was the more predominant shear mechanism in all beams tested compared with the concrete compression zone contribution (i.e., v_d = 72, 73 and 81% of the ultimate shear strength, v_u, for beams HSRW1-13, HSRW1-14 and HSRW1-15).

Fig. 7.12 - Applied versus Calculated Shear Stress

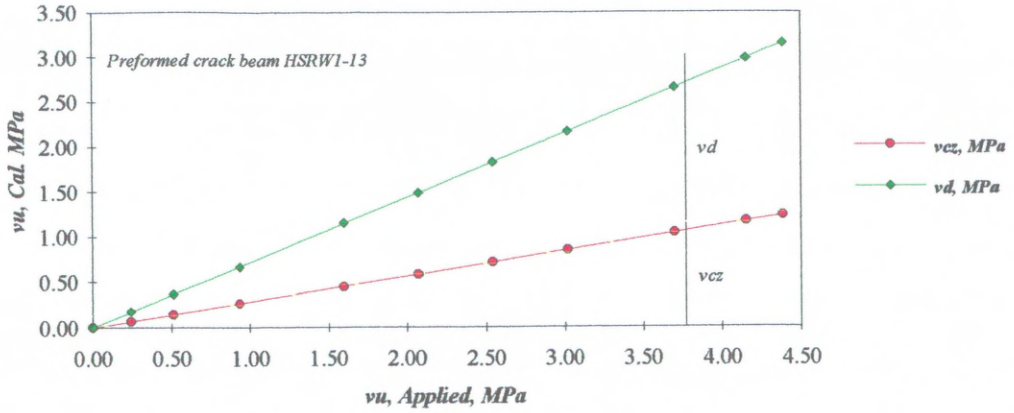

Fig.7.13- Applied versus Calculated Shear Stress

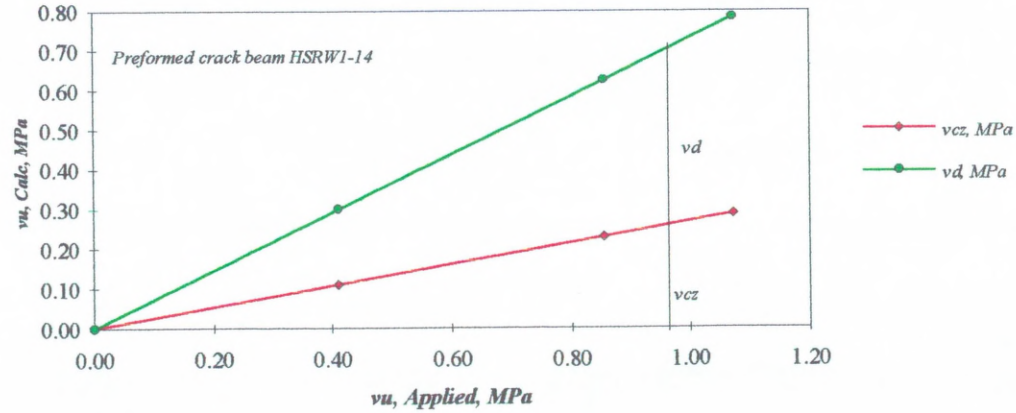

Fig.7.14- Applied versus Calculated Shear Stress

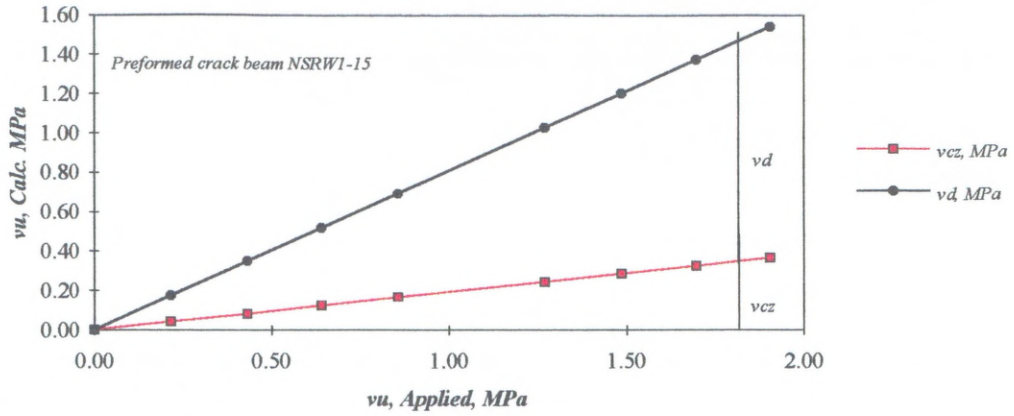

7.10 Contribution of Shear Mechanisms to Beam Shear

Fig. 7.15 represents the ultimate strength capacities of group III and IV beams. The shear contribution by aggregate interlock at any f_{cu} should be the difference between the curves representing group III and IV. The shear strength contributed by the compression zone, v_{cz}, and dowel action, v_d, are also presented in Fig. 7.16. The percentage contributions of various shear transfer mechanisms in terms of the total concrete shear strength, V_u, are given in Table 5.

7.10.1 Significance of aggregate interlock

From the analysis of test data at low and higher concrete strengths the aggregate interlock mechanism was a significant contributor to the total shear carried by the beam, i.e., 34 percent for a beam having 40 *MPa* concrete strength and about 42 percent for beams having concrete strength of 110 *MPa*. The results did clearly indicate that the role of this mechanism at higher strengths is slightly increased. Moreover, this mechanism had a predominant influence on the ultimate load carried by the beam. In other words, the contribution of this mechanism to the total shear strength of the beam was approximately 42 percent for higher concrete strength beams.

7.10.2 Significance of compression zone shear

The test results did clearly indicate that the shear carried by the compression zone showed a slight increasing trend with increasing f_{cu}, see Fig. 7.16 and Table 7.5. However, for practical purposes v_{cz} can be considered to be fairly constant with increasing f_{cu} .

It is worth noting that the compression zone shear depends on E_c and the strain conditions, i.e., at a constant level of applied load on the beam, as f_{cu} and E_c increase the neutral axis rises and thus strain decreases. Therefore, the compression zone shear does not seem to vary markedly as the foregoing factors have nullifying effects.

7.10.3 Significance of Dowel Action

As a result of the flexural rotation of the compression zone, shear displacement is created along the critical horizontal and diagonal cracks. The vertical displacement at the level of the flexural reinforcement can not develop unless either the flexural reinforcement or the surrounding concrete deforms. Therefore, a resistance is induced at the level of the flexural reinforcement which is known as the dowel action. Moreover, this action introduces tensile stresses in the concrete surrounding the flexural reinforcements. As this stress exceeds the tensile strength in the concrete, splitting of concrete occurs along the reinforcement.

The results did clearly indicate that v_d is a predominant contributor to the ultimate shear load carried by a beam. However, as f_{cu} increased from 40 to 110 *MPa*, the shear carried by dowel action did not increase but rather decreased as a percentage from 53% of total shear for a beam having 40 *MPa* to 44% of total shear for a beam having 110 *MPa* concrete strength (see Fig. 7.16). Table 7.6 also presents the contribution of different shear mechanisms at ultimate strength condition for different concrete strength.

Fig.7.15- Effect of Concrete Strength on va

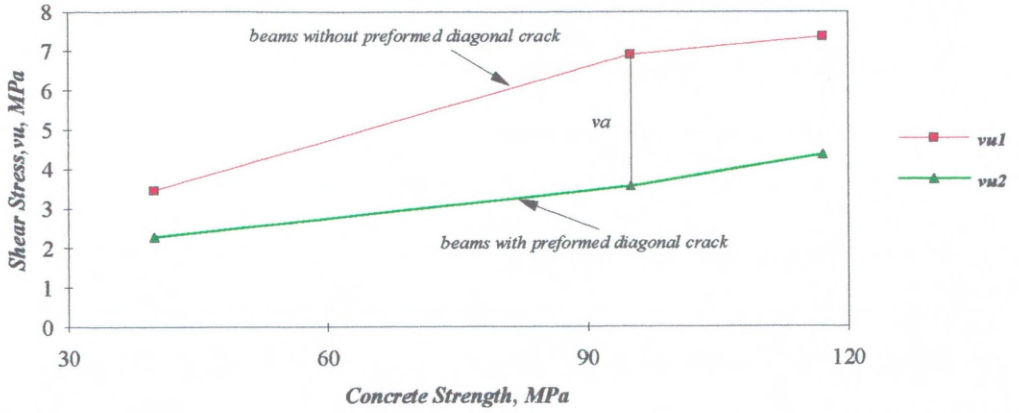

Fig. 7.16- Contribution of Shear Mehansims at Ultimate State

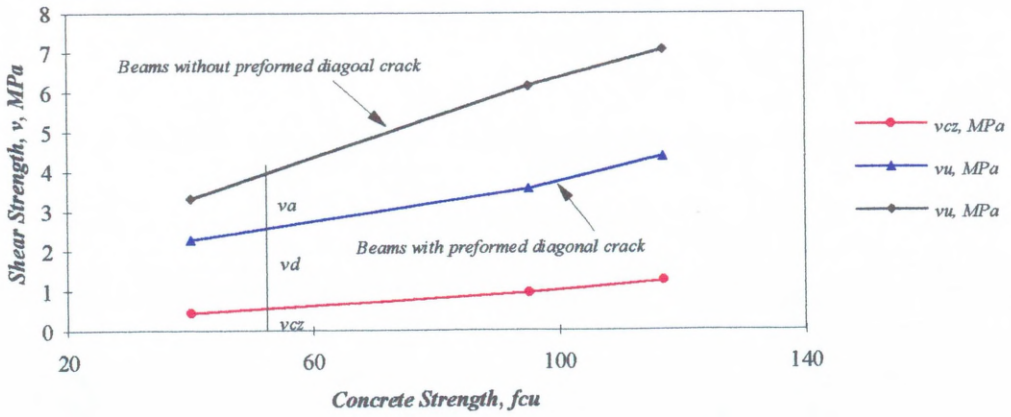

Table 7.5- Ultimate Shear Capacity and Their Element Shear Contribution

Specimen criteria		*Beams without preformed diagonal crack*	*Beams with preformed diagonal crack*		
Beam	f_{cu}, *MPa*	v_u, *MPa*	v_u, *MPa*	v_{cz}, *MPa*	v_d, *MPa*
HSRW1-10	111-122*	7.08	4.38	1.24	3.14
HSRW1-11	95	6.16	3.57	0.94	2.63
NSRW1-12	40-37.5*	3.32	2.29	0.44	1.85

**The first number represents fcu of Group III Beams whereas the second for Group IV Beams*

Table 7.6-Percentage Contribution of Different Shear Mechanisms to Beam Strength at Ultimate Capacity

Shear Strength	*Percentage of V_u* contributed by each mechanism*	*Concrete Strength (f_{cu})*
V_a	34-40%+	$40 < f_{cu} < 111$ *MPa*
V_{cz}	13-17 % +	$40 < f_{cu} < 111$ *MPa*
V_d	53-43%+	$40 < f_{cu} < 111$ *MPa*

** V_u was calculated from beams without preformed crack*
+The first number represents the percentage contribution at lower of f_{cu} and the second represents the upper limit of f_{cu}

7.11 Shear Ductility and Ductility Index

Adequate flexural ductility is necessary for structures in high seismic regions. Many serious problems pertaining to the structural behaviour of reinforced concrete structures under seismic action can be attributed to the poor characteristics of reinforced concrete when subjected to shear. In that respect, the shear ductility is discussed in this sub-section.

Ductility can be defined as the ability of a structure to sustain deformation beyond the elastic range without a significant variation of the resistance capacity. To quantify this definition, the shear ductility index,μ_s, is defined as the ratio of the load-deflection characteristics area at $P_{max.}$ (area A_1) plus $0.75P_{max}$(area A_2) in the descending portion of the area to $P_{max.}$(area A_1), i.e.,

$$\mu_s = \frac{A_1 + A_2}{A_1} \qquad 7.6$$

where; μ_s= shear ductility index, A_1= area of load-deflection up to $P_{max.}$and A_2= area of load-deflection up to $0.75P_{max.}$. Fig. 7.17 represents the schematic diagram for the definition of the shear ductility ratio,μ_s. Based on this definition, the shear ductility indices were calculated from the test results of 14 beams, i.e., group I and II, and these results are presented in Table 7.7. These results clearly indicate a slight increase in the shear ductility index as the tensile reinforcement decreases, i.e.,μ_s= 1.49 for beam HSSRW1-5 and μ_s= 1.14 for beam HSSRW1-9. It appears that the most desirable steel ratio for high shear ductility index,μ_s, is ρ = 2.92%.

The influence of *a/d* ratio on the shear ductility index is shown in Fig. 7.18 which indicates that the shear ductility index increases with *a/d* ratio.

Additionally, one should state that providing web reinforcement significantly increases the shear ductility index particularly for beams made with normal strength concrete.

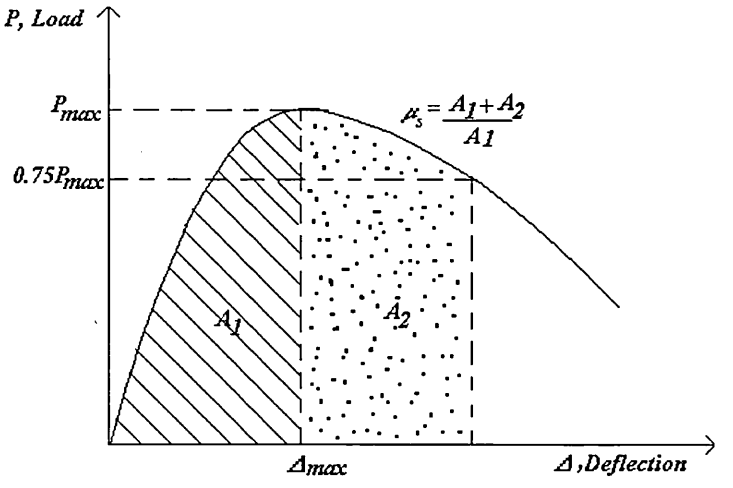

Fig. 7.17-Schematic diagram for definition of deflection shear ductility ratio

Fig. 7.18- Effect of a/d ratio on shear ductility of beams with web reinforcement

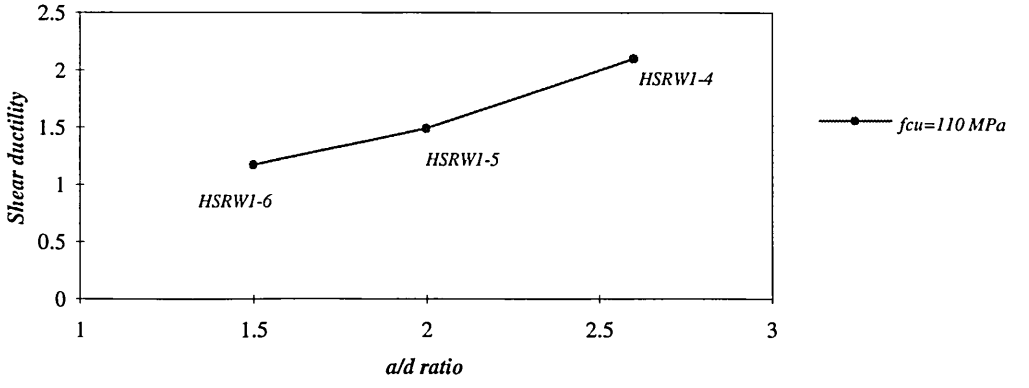

Table 7.7- Test Results of HSRC Beams on Shear Ductility

Beam	$P_{max.}$ *kN*	Δ_{max} *mm*	μ_s
HSRC1-1	200	3.00	4.15
HSRC1-2	165	3.00	2.59
HSRC1-3	228	3.33	2.40
HSRC1-4	190	3.5	1.90
NSRC1-5	135	2.44	2.12
NSRW1-1	150	4.00	4.28
HSRW1-2	245	4.50	2.94
HSRW1-3	220	5.50	1.80
HSRW1-4	180	11.32	2.10
HSRW1-5	220	13.95	1.49
HSRW1-6	255	13.16	1.17
HSRW1-7	220	12.50	1.48
HSRW1-8	300	10.00	1.29
HSRW1-9	250	12.50	1.14

Δ_{max} = *deflection corresponding to maximum load*

CHAPTER 8

THEORETICAL CONSIDERATIONS IN SHEAR

8.1 Introduction

As described earlier in the literature review the problem of shear capacity of reinforced concrete members has been engaging the attention of many researchers. Despite this, it has not yet been fully solved simply because of the fact that the stress condition in concrete structures under different loads are quite complex. In addition, to the writer's best knowledge very little information , in the area of shear on HSRC members, is available in terms of shear contribution of different elements in the beams and failure mechanisms. In this chapter, an attempt has been made to discuss in some detail both the above aspects in the context of HSRC beams failing in shear.

8.2 Analytical Methods of Shear Capacity

Many researchers have attempted to develop rational solutions to the problem of shear in reinforced concrete. These approaches can be classified under the following categories: (i) Tooth analogy (ii) Arch analogy (iii) Compression theory (iv) shear-compression theory (v) Rigid elasto-plastic model (vi) Statistical analysis (vii) Code of practices. These are briefly described in the following subsections.

8.2.1 Tooth analogy

It is assumed that the concrete between adjacent flexural cracks behaves as a cantilever fixed to the compression zone of the beams under the action of the bond stresses. This model was proposed by Kani[71] and Fenwick *et al.*[53]. Kani considered an isolated tooth which was subjected to a bond force,ΔT,which

represented the difference in tension forces in the flexural reinforcement at the two sides of the tooth, see Fig. 8.1. It was further assumed that the force in steel varied linearly from a maximum under the loading point to zero at the supports. Kani also considered the average tooth rather than the longest and weakest one and neglected any shear transfer across the crack caused by aggregate interlock or by dowelling action. This rational theory indicates that the flexural stresses at the root of the concrete tooth due to the bond force,ΔT, can be substantially larger than the diagonal tensile stresses. If a straight line is assumed to act at the root of the tooth (see Fig. 8.1) as a variation of the flexural stresses, then the magnitude of the flexural stress at the extreme fibre of tooth is given by:

$$f = \frac{6\,\Delta T\,s}{b\,(\Delta x)^2} \qquad 8.1$$

and the maximum shear stress by:

$$v_{max} = 3/2\frac{\Delta T}{b\,\Delta x} \qquad 8.2$$

One should state that despite different investigations relating to the stress condition of a concrete tooth cantilever analogy by researchers such as Taylor[131], the approach does not clearly explain why the diagonal shear crack initiate near the tip of the flexural crack. Even though this analogy provided some insight into the probable mechanism of failure it did not lead to a comprehensive method of analysis or design as most codes of practice have chosen the ultimate shear stress as the parameter for determining the shear of a beam and consider it of primary importance, whereas this approach employs the bond force intensity as the main indicator of design failure. Thus, it can be stated that the tooth analogy did not find favour with the various codes of practice as a design method.

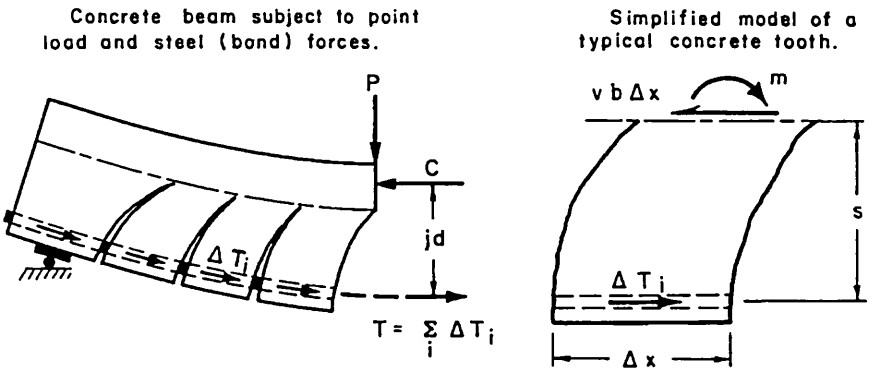

8.1-Concrete Tooth Analogy.[73]

Legend:

ΔT = horizontal loading on concrete tooth caused by main reinforcement
Δx = depth of crack tooth
s = average crack length
jd = lever arm of internal moment

8.2.2 Arch analogy

This analogy ,attributed to Kani[73], has been used to represent internal stress conditions in beams subjected to shear and flexure. The main objective of this analogy was to reduce the complexity and indeterminacy of the actual cracked beam and an element between adjacent cracks is isolated and treated as a tied arch free body as shown in Fig. 8.2.

In this approach, the dowel action of the main reinforcement is neglected and the transverse shear is carried by components of shear and compressive stresses along the arbitrary arch boundaries in the uncracked parts of the beam. The arch ribs are capable of resisting transverse loads as long as they act essentially in compression and not in bending. One should state that without web reinforcement only short beams can develop a tied arch action. As the length of the shear span increases, bending moment develops in the rib which leads to collapse. Fig. 8.2 shows the mechanism of arch analogy approach. Three arches are indicated by I,II and III in Fig. 8.2, Arch I supported by reactions (Fig. 8.2 b) and Arch II is a hanging arch without direct support from reactions (Fig. 8.2 c). Arch III (Fig. 8.2 a) is like Arch II, but arch III has first to transfer its hanging reaction to Arch II which then transfers these reactions together with its own to Arch I and eventually to the support of the beam. With further increase of loads and after flexural cracking develops, the cracks reduce the area for hanging support forces more and more so that less and less can be carried by Arch II. Kani again considers the load carrying capacity of an arch depends mainly on ΔT, the horizontal reaction. Fig. 8.2 f shows the force resultants acting on Arch III. If the small force (H_3) is neglected, two couples remain: ΔC_3 and ΔT_3 and couple V_T and V_{cz} , which are equal and opposite to preserve equilibrium. That is :

$$\Delta C_3 z_3 = V_T x_3 \qquad 8.3$$

where, V_T = Shear force at the cross section.

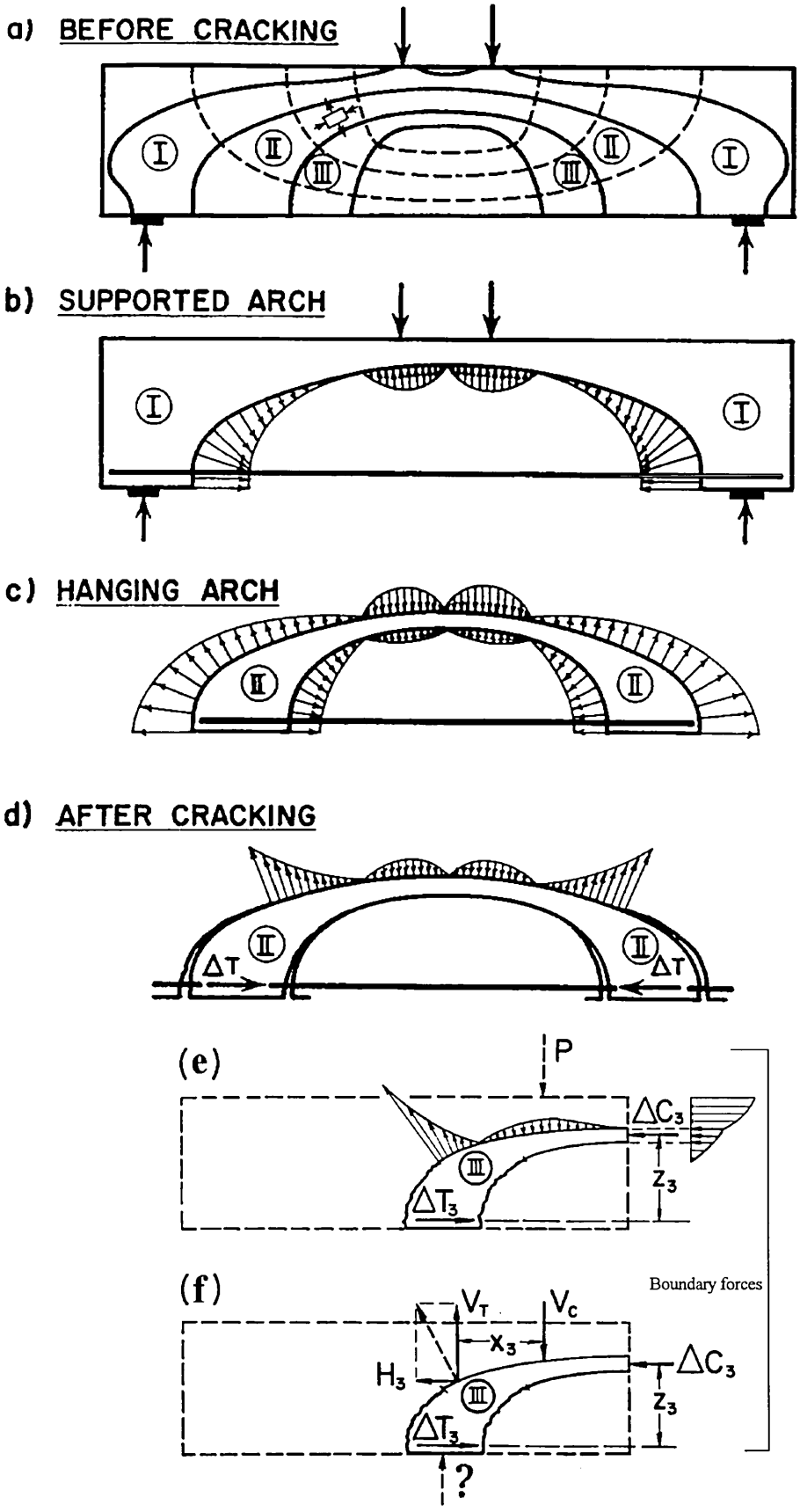

Fig.8.2- Arch Analogy Approach.[73]

Overall, this approach is a qualitative one which provides some insight into the behaviour of beams without stirrups but remains impractical for design purposes.

8.2.3 Compression theory

Many researchers have accepted the concept that reinforced concrete beams with shear reinforcement could behave like trusses known as truss analogy. Collins's[40,41] compression field theory is also based on the truss analogy, but is more sophisticated and is applicable to beams with and without shear reinforcement. Basically, this approach is based upon the two following assumptions:

(i). The concrete in a reinforced concrete member after cracking can carry no tension and the shear is carried by a field of diagonal compression.

(ii). The reinforced concrete member with diagonal cracks can be treated as a macroscopic continuous body and average strains and stresses are calculated by the global compatibility and equilibrium conditions by using Mohr's Circle, as shown in Fig. 8.3.

From the Mohr's circle the magnitude of the average transverse compressive stress, σ_t required in the concrete is:

$$\sigma_t = v \tan \theta \qquad 8.4$$

while the magnitude of the average longitudinal compressive stress, σ_l , is :

$$\sigma_l = \frac{v}{\tan\theta} \qquad 8.5$$

In addition, the magnitude of the average principal compressive stress, f_d, in the concrete is:

$$f_d = \left(\tan\theta + \frac{1}{\tan\theta} \right) \qquad 8.6$$

in which θ= the angle of inclination of the principal compressive stress:

$$\tan^2 \theta = \frac{\varepsilon_l + \varepsilon_d}{\varepsilon_t + \varepsilon_d} \qquad 8.7$$

where, ε_l is the average longitudinal compressive strain, ε_t is the average transverse tensile strain and ε_d is the average principal compressive strain.

Provided the stress-strain relationship and the failure criteria of the materials are known,i.e., using the compatibility and equilibrium conditions the full behavioural response of a member can be calculated. Since the strains in this approach are the average strains in the cracked member it is not appropriate simply to apply the failure criteria obtained from cylinder compression tests. Therefore, Collin's *et al.* defined new failure criteria by using semi-empirical approach.

Based on this theory the angle θ can be calculated by satisfying the global compatibility and equilibrium conditions. In addition, the average strains and stresses can be determined. Finally, the failure is considered to occur when the average stress in the diagonal strut reaches a certain limiting value. Overall, the compression field theory is also capable of predicting not only the failure load but also the complete load-deformation response.

8.2.4 Shear compression theory

In this approach the moment equilibrium condition about a point in the shear compression zone above the end of the diagonal shear crack is considered. Further, most of the authors considered the shear failure employing this approach as a premature flexural compression failure because of the consideration that the presence of shear stresses reduces the compressive strength. Therefore the effect of shear stresses in the shear compression zone is considered.

One of the most comprehensive approaches using shear-compression theory to develop design methods is the one which was developed by Regan[107,108]. He stated that actual failure is caused by the normal stresses in the compression zone of the

beam. He calculated these stresses using both the equilibrium equations and the compatibility condition.

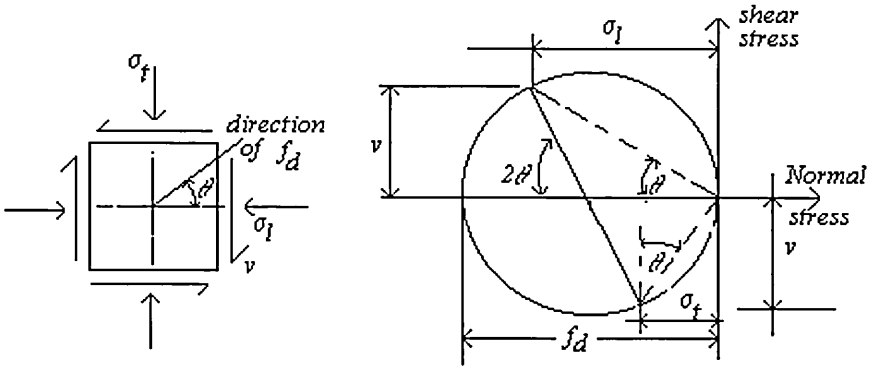

(a) Equilibrium condition for average stresses in concrete

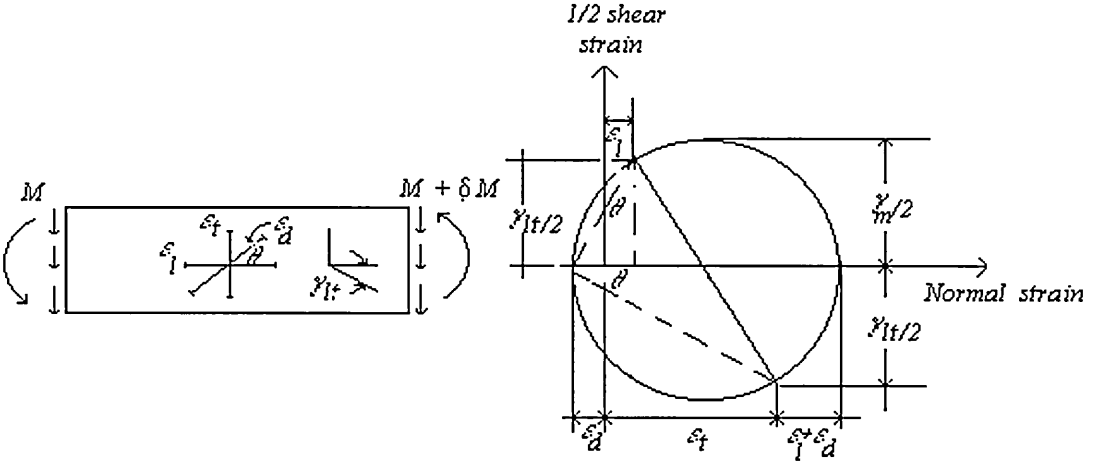

(b) Compatibility condition for average strains in concrete

Fig 8.3.- Collins's Compression Field Theory. [40]

legend: ε_d = average value of principal compressive strain;

ε_l = average value of longitudinal compressive strain;

ε_t = average value of transverse tensile strain;

γ_m = average value of maximum shear strain;

γ_{lt} = average shear strain between longitudinal and transverse lines;

v = average shear stress;

σ_t = average value of transverse compressive stress in concrete;

σ_l = average value of longitudinal compressive stress in concrete;

fd = average principal compressive stress in concrete

Firstly, he calculated the neutral axis factor $\bar{n}$ at section A-A (see Fig. 8.4) by the simple compatibility condition as follows:

$$\frac{\Delta_{cc}}{\Delta_{st}} = \frac{\bar{n}}{1 - \bar{n}} \qquad 8.8$$

where, Δ_{cc} = deformation of the top fibre along AB; Δ_{st} = deformation of the main steel along A-B, and $\bar{n}$ = neutral axis factor at A-A.

Both Δ_{cc} and Δ_{st} were determined by numerical integration. In determining $\bar{n}$, the concrete strains above the diagonal crack were integrated along the finite length A-B, and the diagonal crack was assumed to be a straight line. Furthermore, the stress-strain curve of concrete in the compression zone was assumed to be a parabola. (see Fig. 8.4).

Having determined $\bar{n}$, equilibrium equations were used to predict the ultimate capacity as follows:

$$M_u = \tfrac{2}{3} f_c \, b \, d^2 \, \bar{n} \left(1 - \tfrac{3}{8} \bar{n}\right) \qquad 8.9$$

and,

$$V_u = v_u \, b \, d \, \bar{n} \qquad 8.10$$

where, v_u = critical average shear stress in the compression zone.

As numerical integration was employed in determining $\bar{n}$ for different situations, the final equation of the ultimate shear is quite complex to be practical. Therefore, Regan suggested a graphical approach or other simplified approach. Overall, the shear-compression theory always estimates failures by crushing of concrete. However, from the practical point of view large number of beams fail in a mode different from that assumed by this theory.

8.2.5 Rigid elasto-plastic model

This model developed by Moore[92] for beams shear analysis is a rigid elasto-plastic model consisting of three rigid bodies joined by a hinge as shown in Fig. 8.5. The

rigid bodies are further connected by an elasto-plastic spring representing the compression zone, by elasto-plastic links representing the longitudinal and transverse steel reinforcement and by elastic threads representing the concrete in tension. This model has two degrees of freedom representing the rotations between each pair of adjacent rigid elements. The solution is obtained by using the minimum energy principle together with a yield or failure criterion for the connecting elements.

Although there are a number of the limitations to this model , such as , ignoring the variation in the position of the neutral axis, bond slip development and assuming the geometry of the crack, a number of studies have used it. In addition, this model explained why long span members do not have residual (reserve) strength resistance beyond the shear diagonal load as reported by Bresler and MacGregor[25].

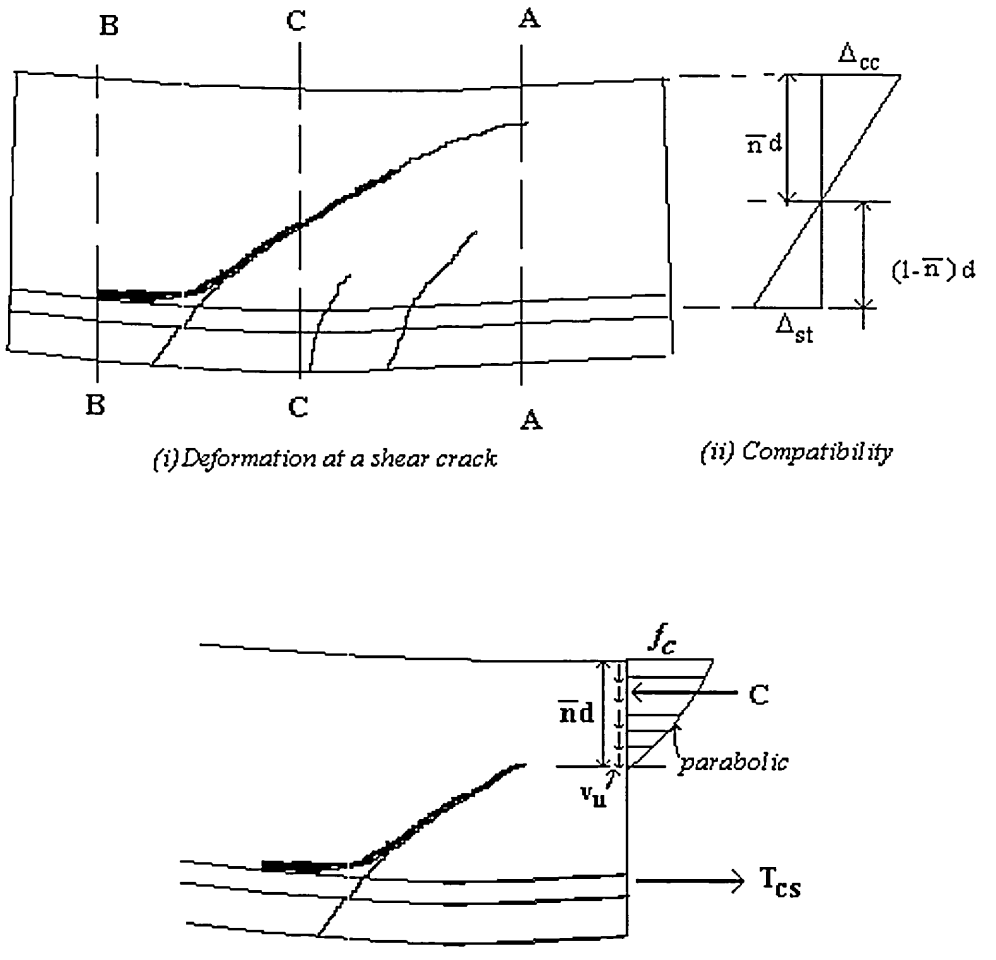

Fig. 8.4 -Regan's Shear-Compression Theory.[107]

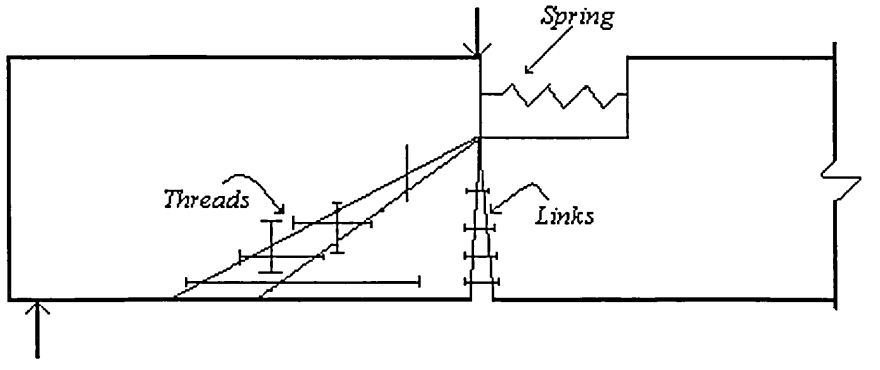

Fig. 8.5-Rigid Elasto-Plastic Model Approach. [92]

8.2.6 Statistical analysis

Many researchers presented statistical studies of the factors affecting the shear failure capacity of reinforced concrete beams. The statistical studies of tests of reinforced concrete beams suggest that the most predominant variables affecting the shear at flexural-shear cracking are the tensile strength of concrete, f_t, the main reinforcement ratio,ρ, and the moment to shear ratio (M/Vd or a/d). It should be pointed out that the best one proposed to date is Zsutty's[152] for reinforced concrete beams without web reinforcement. Zsutty used the techniques of dimensional analysis,i.e., Buckingham's theorem, and the unknown coefficient was determined by statistical regression analysis. He classified the beams into slender beams (a/d >2.5) and short beams (a/d<2.5). The nominal ultimate shear strength ,v_n, for beams having $a/d \geq 2.5$ is given to be :

$$v_n = 2.18\left(f_c \rho \, d/a\right)^{1/3} \qquad 8.11$$

For beams having $a/d < 2.5$ the equation 8.11 is modified by multiplying it by the factor $\left(2.5 d/a\right)$.

To date, the above equation has been considered to be among the best formulae for estimating the shear capacity of the reinforced concrete beams without web reinforcement.

8.2.7 Shear according to codes of practice

The provisions in most of codes of practice like BS, ACI and CEB-FIP for calculating the shear capacity of reinforced concrete beams are based on the assumption that the load which causes the diagonal shear capacity can be taken as the shear capacity of the beam.

These code design provisions, namely the BS 8110 and ACI 813 equations and the CEB-FIP model, have been selected for comparison with the test results. The code design equations include partial safety factors for materials and therefore they are inherently conservative. These equations are as follows:

(i). BS 8110:

$$\text{For } a/d \geq 2, \quad v_c = \frac{0.79}{\gamma_m}(100\,\rho)^{1/3}\left(\frac{400}{d}\right)^{1/4}\left(\frac{f_{cu}}{25}\right)^{1/3} \qquad 8.12$$

where, γ_m = partial safety factor for materials =1.25.

For $a/d < 2$ the shear stress is estimated by multiplying equation 8.12 by the factor $2d/a$.

(ii). ACI- 813:

$$\text{For } a/d \geq 2.5, \quad v_c = 0.16\sqrt{f_c} + 17.25\ \rho\ (d/a) \qquad 8.13$$

For $a/d < 2.5$ the equation 8.13 is modified by multiplying it by the factor $(3.5 - 2.5a/d)$.

(iii). CEB-FIP:

$$v_c = 0.15\,(3d/a)^{1/3}\left[1 + \sqrt{200/d}\right](100\,\rho f_c)^{1/3} \qquad 8.14$$

In this investigation both the measured diagonal cracking and the ultimate shear capacities (i.e., the failure load)were studied.

8.3 Mechanism of Failure

In this section the initiation and development of cracks leading to the final shear crack formation and failure mechanism are discussed . It was felt worthwhile to define some terminology relating to types of cracks which normally occur in RC members failing in shear (see Fig. 8.6).

(i) Flexural cracks: these cracks can be categorised into three types.

(a) Vertical flexural cracks: these develop in the pure bending moment zone.

(b) Inclined flexural cracks: these develop in the shear span zone. These cracks become inclined because the concrete section is subjected to shear force and bending moment.

(c) Critical flexural crack: this is the crack in the vicinity of the diagonal shear crack and horizontal crack.

(ii). Diagonal shear crack: this is the major crack which leads to the beam collapse.

(iii). Horizontal crack: this is the crack which forms along the flexural reinforcing bars.

8.3.1 Theoretical failure mechanism

Referring to the load case which was adopted in this part of study (see Fig. 8.7), theoretically the shear failure could occur either near the support where maximum shear force and negligible bending moment exist or at the loading point where the shear force and bending moment are maximum. However, the experiments which were carried out in this part of investigation concerning shear critical condition have shown that the critical section for shear failure was predominantly the section just adjacent to the load points as discussed in details in Chapter 7.

Immediately after the diagonal cracks develop, after the development of flexural crack, the first redistribution of stresses occurs in the compression zone of concrete. At this stage the shear stresses are partially transferred by the flexural reinforcement by dowel action, V_d, and the rest is carried by the V_{cz} and V_a as discussed earlier in the literature review of this investigation section 2.3.3.5.

It is conjectured that a second redistribution of the stresses occurs as the load approaches failure so that the transferred shear stresses get themselves redistributed. According to Neville *et al.*[99,100] that dowel shear stress, v_d, is negligible before the formation of diagonal crack, but it increases to a significant value just at the

formation of diagonal crack but then drops down to a negligible value at the time of collapse. It was further stated by Neville *et al.* that the contribution due to dowel effect to shear strength is of least importance in the analysis of shear capacity of concrete beams.

Since the entire shear force then gets transferred to the compression zone of concrete, the shear stress in the compression zone is assumed to attain a plastic state. The influence of the normal stress present in the concrete is to reduce this effect. Thus the most critical location for shear failure is at the level of the neutral axis (N.A) where the influence of normal stresses on shear is minimum. The concrete element at the level of N.A is subjected to a state of simple shear,i.e., the shear stresses at this location will yield two equal and unlike principal stresses. The critical concrete element would then fail when these two principal stresses fulfil a failure criterion for concrete under compressive-tensile stresses. Also, the depth of the compression zone of concrete is reduced significantly even for very small increments in load with the development of the diagonal crack.

If the failure does not occur by the above mode then the beam transforms into the so called tied-arch mechanism as described by Kani[73] by which other diagonal cracks form parallel to the existing one with the increase in load (see Fig. 8.2). The portion of the concrete in between the diagonal cracks I, II, III and so on will loose its support, thus reducing the depth of compression zone by a small amount.

The process of this mechanism will continue along the beam,i.e., more diagonal cracks will form until the last diagonal crack finds an un-yielding base near the supports, in this case crack III. One should state here that the critical section at failure of the transformed arch-action is at the loading point where the depth of the arch is minimum. Accordingly, the critical point in the structure at failure is influenced by the following stresses:

(i). A horizontal normal compressive stress, due to the external bending moment.

(ii). A vertical normal stress, due to the external loads.

(iii). A shear stress, due to the shear forces.

All the above stresses interact with each other and cause major principal stresses which are compressive. In addition, the failure of the arch mechanism will occur when these principal stresses fulfil the failure criterion of concrete under biaxial compressive stresses.

Based on the above observations, the objective of this part of investigation is to carry out a study regarding shear transfer via aggregate interlock and shear failure mechanisms of rectangular HSRC beams with an emphasis on tackling the following issues:

(i). The mechanism by which the inclined diagonal shear cracks are initiated.

(ii). The behaviour by which the diagonal shear crack is propagated.

(iii). The contribution of aggregate interlock to shear strength.

The underlying difficulties in developing a theoretical expression for the shear strength of RC beams stem from the following :

(i) The non-linearity of concrete stress-strain relationship.

(ii) The non-homogeneity of the reinforced concrete members; and

(iii) The uncertainty of the quantitative values of internal forces system after the formation of the cracks.

Diagonal shear cracks in the web of a concrete member can develop prior to or after a flexural crack occurs as shown in Fig. 8.6. One type of diagonal crack is normally called a web-shear crack and the other type is identified as a flexural-shear crack; of which the latter one is the most common type. In the following section an attempt

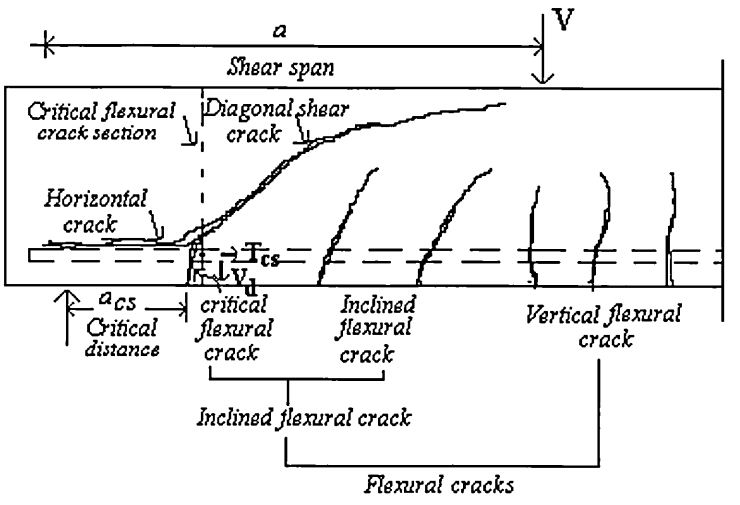

Fig. 8.6- Definition of Cracks Terminology

Legend:

a_{cs}= *Critical distance : is the distance from the support section to the critical crack section.*

T_{cs}= *dowel tension, rebar tension, is the tension force in the reinforcing bar at the critical flexural crack.*

V_d= *dowel shear section , rebar shear, is the shear force carried by the steel portion at critical flexural crack section.*

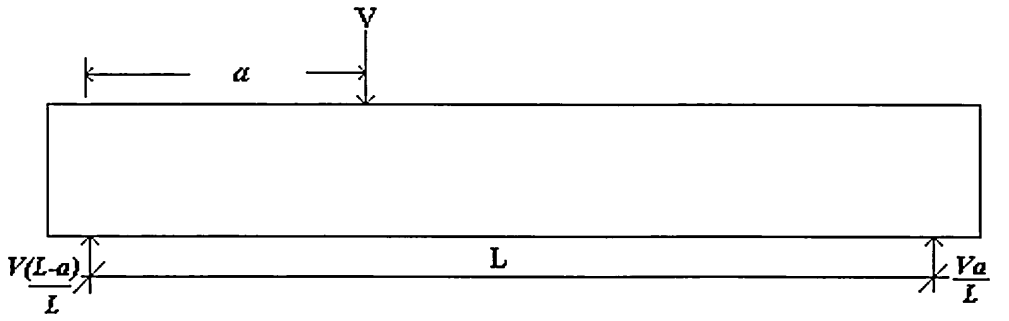

Fig.8.7- Idealised Case of Loading in Shear

will be made based on the information obtained from this investigation as well as from the available literature, to contribute to a better understanding of the fundamental nature of shear behaviour in the context of HSRC beams.

8.4 Physical Failure Mechanism of Beams in Shear

In this section a hypothesis of the mechanism of shear failure in beams without shear reinforcement is suggested based on the experimental findings and the information obtained from literature search of published work like Fenwick[53] and Mathey[86], and utilising the fundamental principles of fracture mechanics Karihaloo[75], Ngo[98] and Wells[146].

Since the beam shear failure is mainly characterised by the occurrence of the diagonal shear crack, attention is focused on the general behaviour of the diagonal shear crack. The major cause of the diagonal shear cracking is the tensile stress concentrations at the critical zone after the formation of the flexural crack. Further, the propagation of these is mainly due to the diagonal tensile stress concentration at the crack tip.

8.4.1 Stress condition at the critical zone

After the formation of flexural cracks highly concentrated shear stresses develop in the zone next to the critical flexural crack along the main reinforcement. These localised shear stresses at the critical zone is the major cause of the diagonal shear crack initiation. The following discussions are focused on the stress state at the critical zone after formation of a critical flexural crack.

8.4.1.1 Free body diagram

Fig. 8.8-a shows a typical point loaded beam after flexural and shear cracks have developed. The free body diagram of the end section of the beam including the critical zone is shown in Fig. 8.8-b.

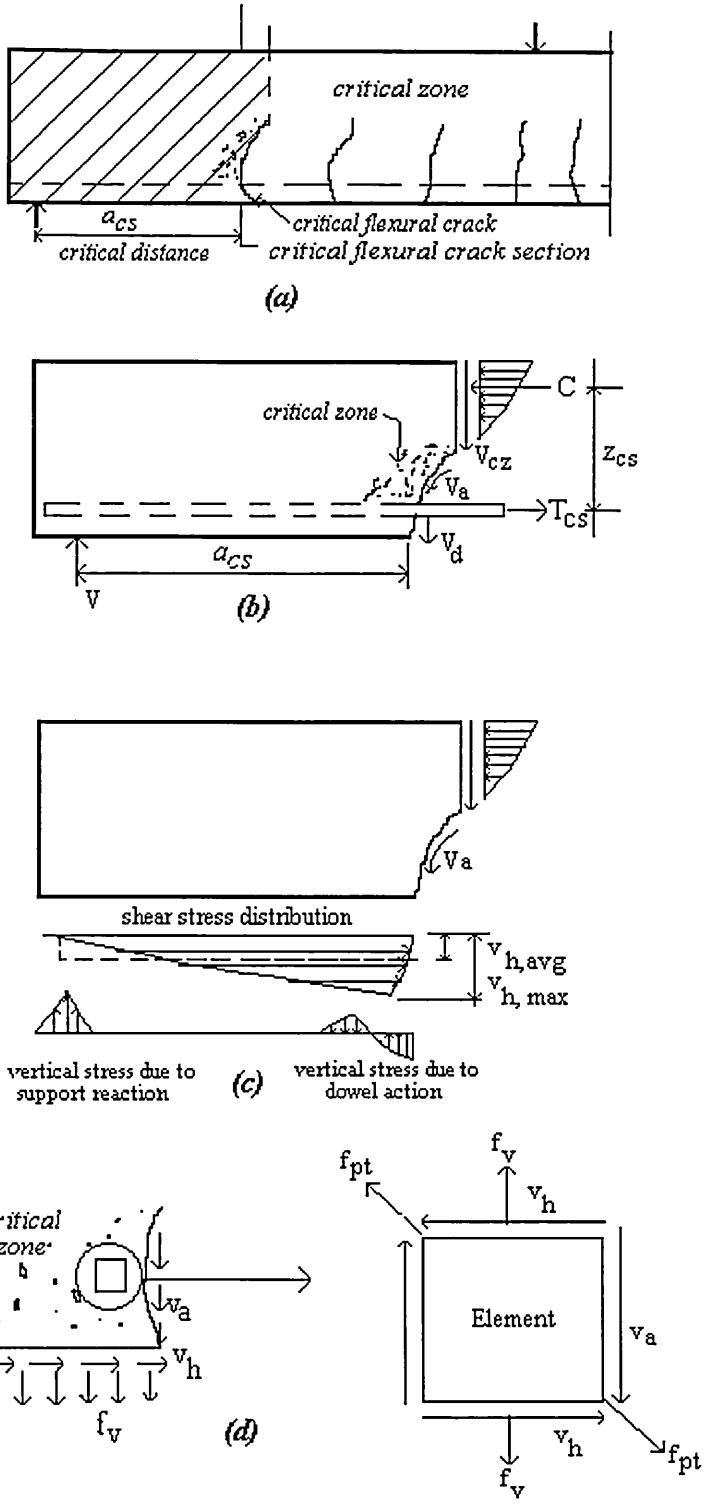

Fig. 8.8- Free Body Diagram of Beam End Part

$f_{pt} = 0.5 f_v + \sqrt{(0.5 f_v)^2 + (v_h + v_a)^2}$ *where;* f_{pt} *= principal tensile stress,* f_v *=vertical normal stress,* v_h *=bond induced shear stress and* v_a *= shear stress due aggregate interlocking.*

By applying the equilibrium condition, the following equations can be obtained:

$$C = T_{cs} \qquad 8.15$$

$$M = T_{cs}\, z_{cs} \qquad 8.16$$

$$V = V_{cz} + V_a + V_d \qquad 8.17$$

where,

C = Normal compression force in concrete

T_{cs} = Critical section rebar tension;

V_{cz} = Shear carried by concrete;

V_a = Aggregate interlock shear;

V_d = Rebar shear force;

V = Support reaction

It should be stated that none of the above forces can be accurately calculated because of the non-homogeneity of the R.C members, i.e., composite action of two different materials (concrete & steel). Therefore, a free body can be modified to have only one material of concrete by cutting away the bottom part of the beam end section. Fig. 8.8 d shows the modified free body diagram. The forces acting on this free body diagram are the same as those on the free body in Fig. 8.8 c except for some substitutions on the bottom surface. These substituted forces on the bottom surface T_{cs} , V_d and V are ignored in the new modified free body diagram. It is believed that the magnitude and distribution of T_{cs}, V_d along the bottom of the beam are quite complex. The remaining stresses as shown in the free body diagram (see Fig. 8.8 d) which act upon an element in the critical zone are as follows:

(i). The bond induced shear stress, v_h .

(ii). The shear stress due to the aggregate interlock, v_a.

(iii). The Vertical tensile normal stress due to the dowel shear action, f_v.

When the principal tensile stress resulting from the above stresses reaches a certain limit of stress a diagonal shear crack should appear at some point in the critical zone signalling the start of a diagonal shear crack.

The following subsections describe the methods of evaluation of these stresses.

8.4.1.2 Bond induced shear stress

As stated earlier, the bond induced shear stresses, v_h, are created by the horizontal shearing action due to T_{cs}-C forces, see Fig. 8.8 b. However, since the steel force, T_{cs}, is transferred to concrete through bond the distribution of v_h on the horizontal shear surface is quite complex and varies within the length and width of the beam as stated by Mains[81], Mathey[86] and Mirza[90]. To evaluate the state of stress in the critical zone the following assumptions are made:

(i). The intensity of the bond induced shear stress is uniform along the width of the beam;

(ii). The area of nominal average bond shear stress at the critical zone is assumed to be a uniform stress field within the zone;

Using these assumptions the average bond induced shear stress, $v_{h,avg}$, along the horizontal critical shear surface can be obtained as follows:

$$v_{h,avg} = \frac{T_{cs}}{b.\ a_{cs}} \qquad 8.18$$

where,

T_{cs} = The critical section rebar tension

b = width of a beam

a_{cs} = critical distance

8.4.1.3 Shear stress due to aggregate interlock

As described earlier in the literature review around 50% of the total shear force is transferred through the crack in a beam failing in shear. However, no comprehensive theory is available yet because of the complexity of the behaviour of aggregate interlock.

Earlier investigations[53&131] indicated that aggregate interlocking capacities are mainly dependent on: width of the crack, size of aggregate, concrete strength and *a/d* ratio. The most critical factor among these is the crack width which affect the interlocking stresses. It was also confirmed that the aggregate interlocking shear stress, v_a is inversely proportional to the crack width. In addition, the previous experimental studies concerning the flexural crack width have demonstrated the following:

(i).Crack widths are proportional to the stress in the main reinforcement.

(ii).Crack widths are dependent on how well the tension reinforcements are distributed over the concrete tension zone.

However, as far as the shear problem is concerned, v_a at the critical zone can not exceed the nominal shear stress calculated by $V_{cr}/b\,d$, where V_{cr} is the diagonal shear cracking force. Therefore, it can be said that after the critical flexural crack develops v_a is much smaller than the nominal value.

As it has already been described in chapter 6 the aggregate interlock contribution to shear, V_a was removed from the beams of group IV by preforming a smooth diagonal shear crack in the short shear span of the beams. The aggregate interlock contribution,V_a, was then determined by comparing the ultimate shear capacities, V_u, of the beams in group IV with those of group III which had no preformed crack. As a result, the shear contribution carried by aggregate interlock was determined as:

$$Va = V_{uIII} - V_{uIV} \qquad 8.19$$

8.4.1.4 Vertical tensile stress due to dowel action

Dowel shear force, V_d, acts on the reinforcement and results in high stresses under the bar. In this sub-section the vertical tensile stress, f_v, at the critical zone before the development of the horizontal crack is calculated.

Many Investigator like Taylor[133] and Gergely[56] have showed that V_d varies with the length of the critical flexural crack, and even when this crack is completely developed, V_d does not exceed 25% of the total shear, V_u.

On the other hand, Baumann and Rush[21] investigated the problem of dowel action in a series of RC beams and they evaluated their results on the basis of what is called an elastic foundation model. They proposed the following empirical equation to determine the dowel shear force, V_d:

$$V_d = 1.64\, b\, \Phi \sqrt[3]{f_c}, \qquad \text{(N)} \qquad 8.20$$

where,

b= width of beam, *mm*

Φ= diameter of main reinforcement, *mm*

8.5 Propagation Mechanism of Diagonal Shear Crack

In this section an attempt is made to highlight how a diagonal shear crack propagates and causes a failure of a beam. It has been known that the bond induced shear stress, due to the horizontal shearing action, v_h, has a key role not only in the initiation of the diagonal shear crack but also in triggering the horizontal crack [81,86] as the horizontal crack is just a downward extension of the diagonal shear crack.

8.5.1 Redistribution of shear stress

As the diagonal cracks develop and the horizontal cracking occurs at the level of the main reinforcement, the physical mechanism of beam shear failure is considered as a

modification of the internal forces accompanied by the deformation for the altered geometry of the member. Additionally, as the horizontal crack occurs along the main reinforcement, the crack opening displacement (COD) at the mouth of the diagonal shear crack zone increases (see Fig. 8.9). This increase of the COD is proportional to the length of the horizontal cracks,i.e., a longer horizontal crack yields larger increase of the COD. The increase of the COD at the diagonal shear crack results in two major changes in shear compression zone above the diagonal shear crack tip which are:

(i). Shear stress in the compression zone, v_c, increases. This is due to the reduction of the aggregate interlock resistance, v_a, as the crack width increases.

(ii). The shape of diagonal stress distribution along the compression zone, at the tip of the diagonal shear crack, tends to be non uniform and concentrated at the tip of shear crack (see Fig. 8.9). This may be because the elements at the crack tip experience quite high strains as the COD at the crack mouth widens*.

8.5.2 Concentration of shear stress at crack tip

From a comprehensive review of the work of previous investigators like[75,143] it was revealed that statement (i) in the foregoing section has been found to be correct whereas statement (ii) has been ignored. However, after the diagonal shear crack reaches above the neutral axis of a beam a diagonal tensile stress (f_{dt}) is created in the compression zone due to V_c and C. With further increase in load f_{dt} at the tip of the diagonal shear crack reaches a certain limit stress causing the concrete to reach

* *COD in fracture mechanics is an alternative measurement of crack tip stress as stated by Wells*[146]. *This is because the crack tip strain is a function of COD which is a measurable value.*

the maximum permissible plastic strain. The diagonal shear crack would then propagate continually causing failure.

8.5.3 Variation of reserve shear capacity with *a/d* ratio

It is believed that the shear span to depth ratio,*a/d,* is a crucial factor on the overall behaviour in RC beams after shear cracking develops. This statement can be conceptually checked by verifying the results of beams HSRW series (see Chapter 7). For a beam having $a/d > 6$ the failure was pure flexure. For the rest of the beams having $1.5 < a/d < 2.6$ an approximately 30% reserve shear strength obtained.

On the other hand, beams having $a/d = 1.5$ the horizontal crack along main reinforcement could not develop well because the support confinement stress prevented it. This small horizontal crack resulted in very small increase in the tip stress of the diagonal shear crack but not enough for the crack to extend. Therefore, the diagonal shear crack was stable after reaching slightly above the neutral axis. As a consequence, failure occurred by crushing of the concrete above the diagonal shear crack and considerably higher reserve strength was obtained. The same shear failure mechanism also occurred for beams having intermediate shear span (a/d=2 to 2.6) but they were accompanied by horizontal cracking along the main reinforcement in most of the beams.

Overall, it appears that *a/d* ratio is a key factor governing the shear failure modes in high strength rectangular concrete beams. This observation fully agrees with the conventional knowledge which demonstrated similar phenomenon for normal strength reinforced concrete beams. Additionally, it could be stated that both ultimate and diagonal shear capacities of HRC beams having constant ρ and f_{cu} are inversely proportional to the value of *a/d* ratio as exemplified in Fig. 8.10.

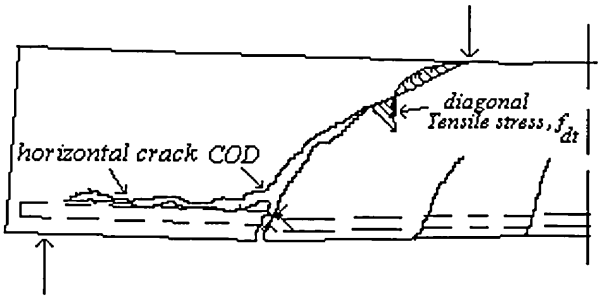

Fig. 8.9- Tensile Stress Concentration on Diagonal Tip Crack. [146]

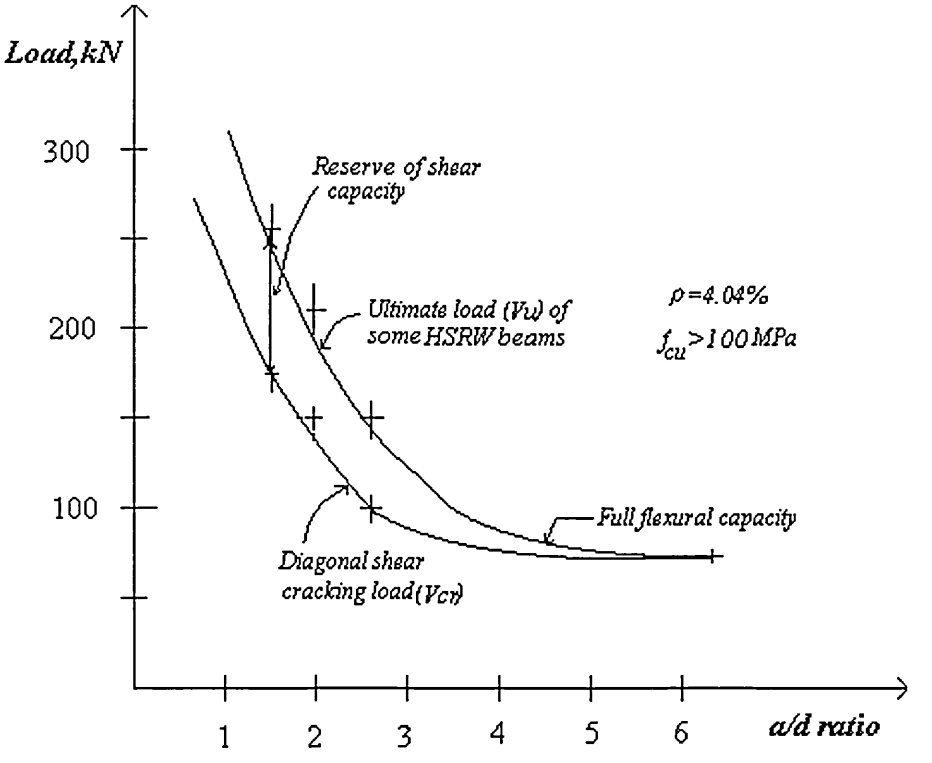

Fig. 8.10- Variation of Shear Capacity with a/d Ratio

8.6 Analysis of Shear Transfer Mechanism

As described earlier ,in Chapter 7, the aggregate interlock mechanism was eliminated from all beams in series IV by preforming smooth diagonal cracks in these beams. Consequently, the difference in strengths between beams with stirrups up to loading point and beams with preformed crack series should be the shear resistance due to the aggregate interlock, V_a. The compression zone shear,V_{cz}, was determined analytically from the concrete strains which were measured along the beam compression zone. Meanwhile, the dowel resistance, V_d, was then assumed to be equal to the difference between the total shear strength, V, and the compression zone shear, V_{cz} .

8.6.1 Shear Stress due to Concrete Compression Zone

The compression zone contribution to shear capacity,V_{cz}, was computed analytically from concrete strain readings measured at different levels of beam depth adopting Taylor's semi-empirical approach[131]. The procedure involves the evaluation of shear stress for which the following expression was used:

$$v_{cz} = \int_0^y \frac{\delta\sigma}{\delta M}\frac{\delta M}{\delta x} dy \qquad 8.21$$

where,

v_{cz} = Shear stress due to compression zone at depth y from the compression face and at distance x from the support.

σ = Longitudinal stress at distance x from the support.

M = Moment at distance x from support.

The calculation of V_{cz} involves the following steps;

(i). Plot ε against M for each gauge level and from this determine the slope $\frac{\delta\varepsilon}{\delta M}$ of the plot at every gauge level.

(ii). Determine the total shear $\frac{\delta M}{\delta x}$ for the load stage under consideration. This is a constant value at any load stage for all the gauge level.

(iii). Determine $\frac{\delta\sigma}{\delta M}\frac{\delta M}{\delta x}$ by multiplying the product of expression (i) and (ii) with the modulus of elasticity of concrete, E_c, which is taken to be constant.

(iv). Integrate expression (iii) from the compression face down to each gauge level to determine the shear stress at that gauge level. Fig. 8.11 represents a typical plot of strain versus applied moment.

8.6.2 Shear carried by dowel action

Having computed the compression zone shear, V_{cz}, from the strain readings taken in the beam compression zone the dowel resistance, V_d, was assumed to be equal to the numerical difference between the total applied shear and the compression zone shear resistance, i.e, $V_d = V_u - V_{cz}$.

Fig. 8.11-Typical Plot of Strain Versus Moment

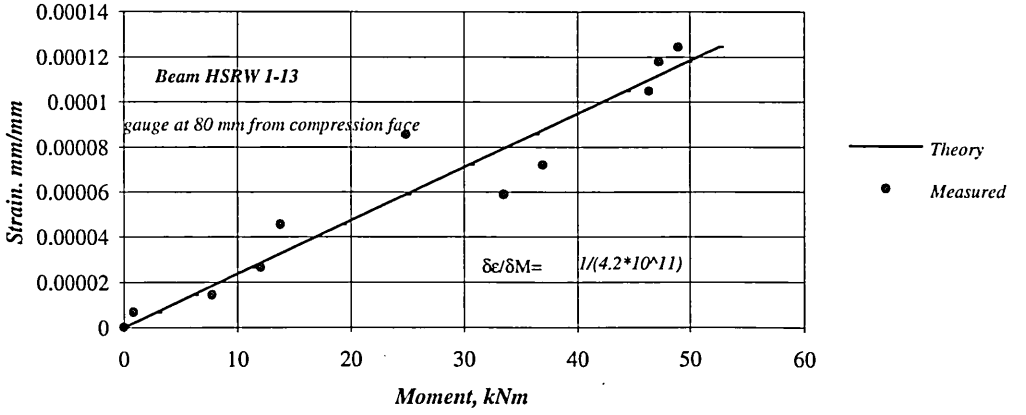

8.7 Proposed formulae for predicting ultimate shear strength

So far the conceptual mechanism of shear failure has been discussed. In this section an attempt is made quantitatively to estimate the ultimate shear strength, v_u, of HSC beams without web reinforcement.

As all the design code provisions were based upon the assumption that the useful shear capacity of a reinforced concrete member is exhausted once a diagonal cracking develops and because to the author's best knowledge no equations are available for predicting the ultimate shear strength of HSC beams without web reinforcement, the author has developed and proposed some empirical expression in order to predict the nominal ultimate shear strength of HSRC beams. These expressions are based on the results of a total of 134 test beams (current investigation & published literature work). These expressions are in line with those proposed by Zsutty[152] but in the context of HSRC beams using a multiple regression analysis. It was further decided to consider the ultimate shear strength of a reinforced concrete beam, v_u, rather than the diagonal shear strength, v_{cr}.

Basically, the available data have been classified into two categories,viz., beams having $a/d \leq 2.5$ and beams having $a/d > 2.5$. The general form of the ultimate shear equation for beams without web reinforcement considered is as follows:

$$v_n = \beta \ (f_c * \rho * d/a)^n \qquad 8.22$$

where, v_n is the nominal ultimate shear strength and β is a constant related to the concrete. The expressions are:

(i) Beams having $a/d \leq 2.5$;

$$v_n = 3.9 \ (f_c * \rho * d/a)^{0.65} \ , MPa \qquad 8.23$$

(ii) Beams having $a/d > 2.5$;

$$v_n = 2.45\ (f_c\ *\ \rho\ *\ d/a)^{0.44}, MPa \qquad 8.24$$

The above expressions are considered to be statistically valid for reinforced concrete beams having strength in the range $40<f_c<120\ MPa$ having correlation coefficients of 0.83 and 0.91 for equations 8.23 and 8.24 respectively which indicate a positive correlation. The mean and standard deviation values were found to be 1.04 and 0.29 respectively which are considered to be satisfactory.

Fig. 8.12 and 8.13 represent comparisons between measured and predicted shear stresses for the available test results.

Fig. 8.12-Comparsion Between Measured and Predicted Shear Stress

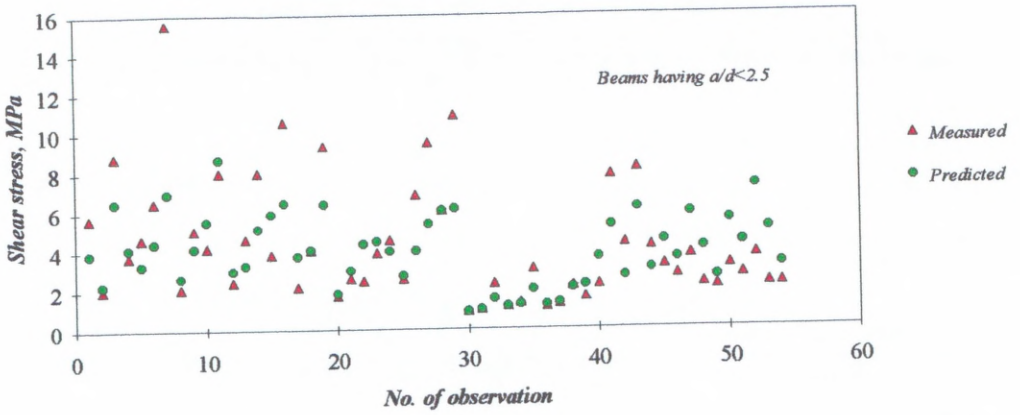

Fig. 8.13-Comparsion Between Measured and Predicted Shear Stress

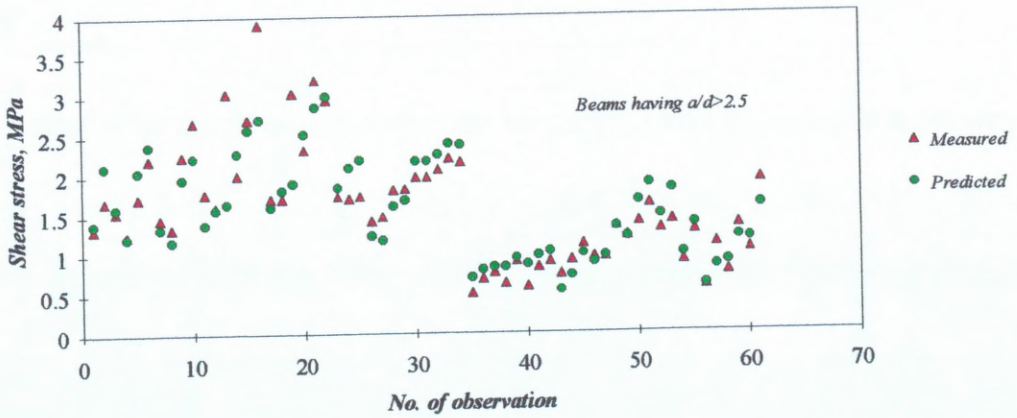

CHAPTER 9

CONCLUSIONS AND RECOMMENDATIONS FOR FURTHER STUDY

9.1 Conclusions

This investigation involved a fundamental study into the engineering properties and structural behaviour of HSRC beams on flexure and shear. Based on the results of this investigation and in view of the experimental evaluations and analytical considerations, previously presented the following conclusions can be drawn

9.1.1 High strength concrete materials

1. The local crushed Ardowney aggregate which was used in this investigation was reliable in order to produce HSC mixes. This aggregate is well graded and sufficiently strong to achieve the optimum required concrete strength.
2. Concrete with compressive strength in the order of 120 *MPa* can be developed by using silica fume with the addition of superplasticizer. A maximum W/(C+S.F) ratio of 0.256 is recommended. The optimum percentages of silica fume and superplasticizer are 10% and 1.27% respectively by weight of cement content to achieve this strength.
3. The expression reported by the ACI[16], Carrasquillo *et al.*[33], and Ahmad *et al.*[4] for estimating the splitting cylinder tensile strength of HSC are too conservative, since they underestimate the splitting tensile values of HSC. On the other hand, the expression reported by Raphael[111] gave a better estimate of the splitting cylinder tensile strength values.
4. On the basis of the test results, a relationship between the splitting cylinder tensile and compressive strength has been developed using the multiple regression analysis technique. The equation is $f_{sp} = 0.564\,(f_c)^{0.55}$.

The proposed equation shows close agreement with the test results obtained and it could be used in predicting the splitting cylinder tensile strength of HSC mixes up to a concrete cube strength of 120 *MPa*.

5. On the basis of the current test results and those available through literature study, an expression has been developed using the regression analysis to predict the cube strength, f_{cu}, of HSC mixes as follows:

$$f_{cu} = 5.26e^{\%} + 139e^{\%} - 149\,w/c - 20\,FA/TA$$

where,

f_{cu} = concrete compressive strength at 28 days.

s, c, sp, w = The mass of silica fume, cement, superplasticizer, and water in kg/m^3 of fresh concrete, respectively.

FA, TA = The mass of fine aggregates, and total aggregates in kg/m^3 of fresh concrete, respectively.

The above equation is valid for concretes with strength between 63 to 120 *MPa* and w/c ratios in the range of 0.22 to 0.46 using 20 *mm* maximum size of crushed aggregate and with silica fume and superplasticizer contents in the range of 5 to 11.5% and 0.67 to 2 % respectively by weight of cement.

6. The shape of the stress-strain curve is much steeper for higher strength concretes. In addition, the ascending part of the curve is quite linear up to about 75% of the maximum compressive strength while the descending part is almost non-existent.This is likely ,however, to be influenced by the loading system used. The strain corresponding to maximum (failure) stress is about 0.003. This value is more or less the same for the different strengths of concrete specimens used.
7. Based on the stress versus lateral and axial strain data from cylinder tests of HSC, Poisson's ratio was found to be range between 0.2 to 0.25 for all test results. The average value was found to be 0.21. There was no consistent variation with compressive strength.

8. Based on the experimental results obtained the moduli of elasticity, E_c of HSC varied between 34 to 53 *GPa*, for compressive strengths in the range of 75 to 115 *MPa*.

9.1.2 High strength concrete beams in flexure

1.For all beams tested, the measured maximum flexural strain at the extreme compression fibre, ε_u varied between 0.002 to 0.0031.

2. Effects of the major test parameters on the serviceability of HSRC reinforced beams in flexure can be summarised as follows:

(i). The tensile reinforcement ratio parameter (ρ) was found to be the dominant factor in determining the shape of load-deflection curves. Beams with low ρ ratio underwent large deformations even at a constant load before the ultimate load capacity was obtained, whereas beams with high ρ ratio often exhibited a dramatic drop-off in the load-deflection curve immediately beyond crushing of the concrete compression zone. On the other hand, while in such beams crushing of the compression zone occurred at the same time as the tensile reinforcements yielded, they were generally able to resist increasing loads beyond that causing crushing of the compression zone.

(ii). At any constant tensile reinforcement ratio,ρ , beams with higher strength concrete exhibited less deflection than similar beams with lower strength concrete at the same load level. This was apparent at both elastic and elasto-plastic stages of the beam tests.

(iii). At a constant ρ value the slope of the moment-rotation curve exhibited a stiffer response for beams having higher concrete compressive strength, indicating the brittleness of higher strength concrete. On the other hand, beams with low ρ ratio exhibited elasto-plastic behaviour, whilst for

beams with high ρ ratio the moment-rotation behaviour was nearly elastic even right up to the failure load.

(iv) For all beams tested, two equations were developed in order to estimate the effective second moment of area, I_e, of the cracked cross-section for pre-yielding and post-yielding stages. The equations are as follows:

(a). Effective second moment of area for pre-yielding stage is:

$$I_{e1} = 297030 \frac{\left(I_{cr}\, Mcr/Mu\right)^{1.007}}{\left(I_g\, Mcr/Mu\right)^{0.633}}$$

(b). Effective second moment of area for post-yielding stage is:

$$I_{e2} = 2.51x10^{15} \frac{\left(I_{cr}\, Mcr/Mu\right)^{-0.214}}{\left(I_g\, Mcr/Mu\right)^{0.809}}$$

All Symbols definitions can be obtained by referring to section 5.3.

3. For all beams tested the width of the cracks at the tensile reinforcement level was found essentially to be dependent on ρ and f_{cu}. An expression is proposed to predict the crack widths at the level of the centroid of the tensile reinforcement which is:

$$w_{avg} = 2.131 \frac{\sqrt[3]{ts\, A}}{1+ts/h_1}\, \varepsilon_c$$

where,

w_{avg} = average crack width at the level of the centroid of the reinforcement

ts = side cover measured from the centre of the outer bar

$A = A_e/m$ = average effective concrete area around a reinforcing bar, (mm^2)

(A_e as defined in section 5.5 and Fig. 5.10)

$h_1 = d - n$, distance from neutral axis to the centroid of reinforcement bars

ε_c= Average strain at the reinforcement level

The proposed expression gave a satisfactory agreement with the existing test data. It also appeared to be significantly better than some of the existing published equations in the context of HSRC beams.

4. For a given amount of tensile reinforcement, the ductility index of HSRC beams increased with increasing compressive strength of concrete.
5. Based on the stress-strain data and the measured flexural strain along the beam's depth a stress block equation is proposed in order to estimate the ultimate moment capacity of HSRC beams in flexure. The expression could be used as a design method to estimate the flexure capacity of HSRC singly and doubly reinforced beam sections in reasonable agreement with the experimental data obtained. In addition, from the analysis the equation appears to be adequately rigorous and provides a basic and realistic approach to ultimate flexure design of HSRC beams. It thus provide a good general approach to the flexure design and a means of determining the internal forces in the context of the compatibility of strain and equilibrium conditions of concrete.
6. It is concluded that the existing BS 8110 design provisions marginally underestimate the ultimate flexural capacity of HSRC beams and thus provide a conservative estimate of the ultimate strength capacity of HSRC members in flexure.
7. Another three alternative idealisations are also suggested, i.e., a triangular and two parabolic stress blocks to estimate the moment capacity of reinforced HSC beams in flexure. These stress blocks are based on f_{cu} and $\varepsilon_{cu} . E_c$ values respectively at the extreme compression fibre. All these approaches provided a very close agreement with the actual measured ultimate moment capacities of all beams tested.

9.1.3 High strength concrete beams in shear

From the experimental data and the theoretical considerations of the shear stress of HSRC beams with and without web reinforcement, the following conclusions have been drawn:

1.The current codes of practice, namely the BS 8110[27] and ACI 318[1] equations for predicting the diagonal shear crack, v_{cr}, are generally conservative, whereas the CEB-FIP[35] expression over-estimates the diagonal shear stress. It was also found that Zsutty's expression[152] estimates the ultimate shear stress, v_u, in a close agreement to the experimental data obtained.

2.As expected the addition of web reinforcement increases the ultimate shear capacity of beams.

3. The mode of failure was sudden and explosive particularly at low *a/d* ratio beams.

4. The diagonal shear crack was distinguishable from diagonal flexural crack since:

   (i) the diagonal shear crack was not necessarily related to the critical flexural crack.

   (ii) for beams having moderate *a/d* ratio,the diagonal shear crack extended at both ends simultaneously; at the upper end it extended along the diagonal line to the loading point, at the bottom end it extended along the main reinforcement.

5.The shear span to depth ratio *a/d* has a major influence on the shear failure mode and the variation of the reserve shear capacities after diagonal shear cracking is developed. The ultimate shear capacity increased with decreasing *a/d* ratio and with the increase in the flexural reinforcement.

6.The ultimate shear capacity of beams increased with increase in the compressive strength of the concrete but at a slower rate than the increase of concrete strength.

7.The significance of the aggregate interlock mechanism of shear transfer was studied along with other mechanisms of shear transfer. Based on the consistent behaviour in the beam series with a preformed diagonal crack, it appeared that the procedure employed to preform the diagonal crack worked well in eliminating the

contribution of aggregate interlocking while allowing the other shear transfer mechanisms to function normally. In that respect it can be concluded that:

(i). The aggregate interlock shear mechanism played a very important role as a shear carrying mechanism both for low and higher strength concrete beams. However, in HSC it had only a slight increase as a shear mechanism contributor.

(ii). The shear resisted by the compression zone remained fairly constant with increasing concrete strength, f_{cu}.

(iii). In the absence of aggregate interlock mechanism at low and higher strength concretes dowel action was a predominant contributing mechanism, although this contribution was of a lesser significance to the ultimate shear strength of HSC beams.

(iv). The contribution of various mechanisms could be numerically expressed for beams having nominal concrete strength in the range of $40 < f_{cu} < 120$ *MPa* as follows:

aggregate interlock,	V_a in the range of 34-40%
concrete compression,	V_{cz} in the range of 13-17%
dowel action,	V_d in the range of 53- 43%

The first number represents the percentage contribution of a mechanism at the lower limit of f_{cu} and the second at the upper limit of f_{cu}.

8.The shear ductility index, μ_s, decreases with an increase in the concrete strength up to f_{cu}= 85 *MPa*. For beams made with concrete having f_{cu}> 85 *MPa*, the shear ductility index, μ_s increased significantly with an increase in f_{cu}.

9.For beams with web reinforcement, the shear ductility index, μ_s increased as the tensile reinforcement,ρ , increased. For beams without web reinforcement the most desirable flexural reinforcement ratio for high shear ductility index was found to be 2.92%.

10.Shear reinforcement increases the shear ductility index particularly for beams made with NSC.

11.It would appear that bond induced shear stress, v_h, plays a key role in the initiation of the diagonal shear crack.

12.Regression equations were developed to improve prediction of ultimate shear stress of HSRC beams. The equations predict v_u with reasonable accuracy and they are better than the existing published equations, particularly with respect to HSRC beams. The equations are shown below:

(i) Beams having $a/d \leq 2.5$;

$$v_n = 3.9\ (f_c\ \rho\ d/a)^{0.65}\ , MPa$$

(ii) Beams having $a/d > 2.5$;

$$v_n = 2.45\ (f_c\ \rho\ d/a)^{0.44}, MPa$$

9.2 Recommendations for Further Research

There is an increasing demand for the use of higher strength concrete as a material that can replace normal strength concrete. Other research in the School has shown that considerable strengths can be obtained without the use of silica fume thus reducing cost. In addition, extensive research efforts are required to bring all theories and specifications together, and it is suggested that the following topics related to the HSC members are worth further study.

1.As this study was limited to a montonically increased static loads, it is highly likely that the mechanisms of resistance and deformation behaviour would be different for those under montonically increased cyclic loads. Little or no information exists on the response of HSC members subjected to repeated load cycles.

2.The behaviour and strength of partially and fully prestressed HSRC beams should be investigated under both short and long-term loading. Such a study will provide valuable information on the use of HSRC long-span precast prestressed girders.

3.The flexural strength of HSRC beams with non-rectangular cross-sections should be studied to determine if the amendments suggested to the current code of practice for rectangular sections are appropriate for these.

4.Experimental and/or theoretical investigations need to be carried out in order to study the shear stress of HSRC deep beams.

5.It is recommended to devote a study of shear mechanism failure of HSC beams under pure torsion and/or combined torsional and shear stresses in order to develop a design method of HSRC members under the combined action of bending, shear and torsion.

6.A comprehensive theory with regard to horizontal crack formation does not yet exist. Further investigations are required with particular emphasis on the mechanism and stability of horizontal cracking.

7.For a comprehensive understanding of HSRC the ductility of HSRC columns and other forms of structural members must be studied. This includes for instance the role of confinement ,i.e., hoop, spiral and steel fibres on the structural behaviour of HSC columns. In addition, a number of parameters could be examined in the light of current national code provisions for structural use of concrete. Such a study would provide a better understanding and amendment ,if any, in the standard code, so the material can be used to its best advantage.

REFERENCES

[1].ACI Committee 318:1995, *''Building Code Requirements for Reinforced Concrete''*, ACI Standard, Detroit, Michigan.

[2].ACI-ASCE Committee 426. (1973),''The Shear Strength of Reinforced Concrete Members", *Journal of the structural division, ASCE*, 99 (June), pp. 1091-1187.

[3].Adwan, O. K., Aljazzar. O. L. (1990), *"Retempering of Fresh Concrete Using Superplasticizer''*, (BSc. Project, Al- Fateh University, Tripoli - Libya), 79pp.

[4].Ahmad, S., Shah, S. (1985), "Properties of High Strength Concrete for Structural Design", *Material Research Symposium Proceeding,* 42, pp. 169-181.

[5].Ahmad, S *et al.*, (1986),"Shear Capacity of Reinforced High Strength Concrete Beams", *ACI Structural Journal*, 83 (March-April), pp. 297-305.

[6].Ahmad, S., Lue, D. (1987), "Flexure-Shear Interaction of Reinforced High Strength Concrete Beams", *ACI Structural Journal* , July -August, pp. 330-358.

[7].Ahmad, S., Barker, R. (1991), "Flexural Behaviour of Reinforced High-Strength Lightweight Concrete Beams", *ACI Structural Journal,* 88 (January-February), No.1, pp. 69-77.

[8].Ahmad, S., Batts, J. (1991), ''Flexural Behaviour of Doubly Reinforced High-Strength Light-weight Concrete Beams with Web Reinforcement", *ACI Structural Journal,* 88 (May-June), No. 3, pp. 351-358.

[9].Ahmad, S *et al.* (1992), "Mechanical Properties of High Strength Concrete", *Proceeding of The 9th conference on Engineering Mechanics*, College Station TX USA, May, pp. 864-867.

[10].Aitcin,P.C. (1980), ''How to Produce High strength Concrete'', *Concrete Construction*, 25, No. 3, pp. 222-230.

[11].Aitcin, P. C *et al.* (1985), ''Very High strength Cement for Very High Strength Concrete'', *Material Research Symposium Proceeding*, V42, pp. 201-210.

[12].Aitcin, P. C *et al.* (1985), ''Development and Experimental Use of a 90 *MPa* Field Concrete'', *Special Publication. SP 87, ACI, Detroit, Michigan*, pp. 51-69.

[13].Aitcin, and Mehta. (1990), ''Effect of Coarse Aggregate Characteristic on Mechanical Properties of High Strength Concrete'', *ACI materials*, 87(March.-April), No. 2, pp. 103-107.

[14].Aitcin,P.,Laplante.P. (1990), ''Long-term Compressive Strength of Silica Fume Concrete'', *Journal of Materials in Civil Engineering*, 2 (August), No. 3, pp.164 -170.

[15].Aitcin, P. C. (1992), ''*High Performance Concrete from Martial to Structure*, The Use of Superplasticizers in High Performance Concrete by Y.Malier'', London: E &FN Spon, pp. 14-33.

[16].AMERICAN CONCRETE INSTITUTE 363. (1984),"State of Art Report on High Strength Concrete'', *ACI Journal,* 81(July-August), pp. 363-411.

[17].Ashour, S. *et al.* (1992), ''Shear Behaviour of High Strength Fiber Reinforced Concrete Beams'', *ACI Structural Journal*, 89 (March-April), No. 2, pp. 176 - 127.

[18].Asselanis, J. *et al.* (1989), ''Effect of Curing Condition on Compressive Strength and Elastic Modulus of Very High-Strength Concrete'',*Cement,Concrete and Aggregate*, 11, pp 80 - 83.

[19].Baalbaki, W. *et al.* (1991), ''Influence of Coarse Aggregate on Elastic Properties of High Strength Concrete'', *ACI Material Journal*, 88 (Sep.-Oct.), No. 5, pp. 499- 503.

[20].Batchelor,B.,Kwun,M. (1981), ''Shear in RC Beams without Web Reinforcement'', *Journal of Structural Division, ASCE*, 107(May), ST5, pp.907-921.

[21].Baumann,R., Rush. H. (1970), ''Versuche zum Studium der Verdubelungswirkung der Biegezugbewehrung eines Stahlbetonbalkens. *Deutscher Ausschuss fur Stahlbeton'', Berlin, No. 210.* (Translation in British Cement Association Library).

[22].Bentur, A.,Goldman, A. (1988), ''Curing Effects, Strength and Physical Properties of High Strength Silica Fume Concretes'', *Journal of Materials in Civil Engineering*, 1(Feb.) No.1, pp. 46 -58.

[23].Bickley, J. *et al.* (1992), ''Some Characteristics of High-Strength Structural Concrete'', *Canadian Journal of Civil Engineering*, 18, pp. 885 - 889.

[24].Bresler, B., Scordelis, A. C. (1963), ''Shear Strength of Reinforced Concrete Beams'', *ACI Journal*, 60(January), No.1, pp.51-72.

[25].Bresler, B.,MacGregor, J.G. (1967), ''Review of Concrete Beams Failing in Shear'', *Journal of the Structural Division, ASCE*, 93 (Feb.), ST1,pp. 343-372.

[26].Brick, R. L. *et al.* (1974), ''Proportioning and Controlling High Strength Concrete'', *SP-46, ACI*, pp.141-163.

[27].BS 8110:1985, ''*Structural Use of Concrete: Part 1*'', Code of Practice for Design and Construction.

[28].Bunett, (1991), ''Silica fume Concrete in Melbourne Australia'', *Concrete International: Design and Construction* , 13 (August), No. 8, pp. 18 -24.

[29].Burge, T.A. (1983), ''14000 Psi in 24 Hours", *Concrete Journal*, September, pp.36-41.

[30].Cabrerra, G., Claisse, P (1990), ''Measurement of Chloride Penetration into Silica Fume Concrete'', *Cement and Concrete Composites*, 12, No. 3, pp.157 - 161.

[31].Carette, G., Malhorta, V. (1982), ''Silica Fume in Concrete-Preliminary Investigation'',*Canada Centre for Mineral and Energy Technology CANMET*, Report No. 82-1E, Feb., 16pp.

[32].Carette, G. G. (1989), ''Preliminary Data On long Term strength Compressive Strength Development of Silica Fume Concrete'', *Third International Conference on Fly Ash, Silica Fume,Slag and Natural Pozzollans in Concrete. Trondhiem*, Supplementary Papers. pp. 597 - 617.

[33].Carrasquillo, R.L. *et al.* (1981), ''Properties of High Strength Concrete Subjected to Long term Loads'', *ACI Journal*, 78 (May-June), pp. 171-178.

[34].CEB Bulletin. (1989), ''Design Aspects of High Strength Concrete'', December, Lausanne, No.193, pp.13-163.

[35].CEB-FIP:1993, ''Model Code'', Switzerland.

[36].Chana, P.S. ''Some Aspects of Modelling The Behaviour of Reinforced Concrete under Shear Loading'', *Cement and Concrete Association*, Technical report No. 543, 22pp.

[37].Chung, W., Ahmad. S. (1995), ''Analytical Model for Shear Critical Reinforced Concrete Members'', *Journal of Structural Engineering*, June, pp.1023-1029.

[38].Clarke, J. L. (1987), ''Shear Capacity of High Strength Concrete Beams'', *Concrete*, March, pp.24-26.

[39].Cohn, M .Z., Ghosh. S. K. (1972), ''The Flexural Ductility of Reinforced Concrete Sections'', *Publications Intentional Association for Bridges and Structural Engineering*, Zurich, A. 32-2, pp.53-83.

[40].Collins, M.P. (1978), ''Toward a Rational Theory for RC Members in Shear'', *Journal of Structural Division, ASCE*, 104 (April), No. ST4, pp.649-666.

[41].Collins, M.P., Mitchell,D. (1980), '' Shear and Torsion Design of Prestressed and Non Prestressed Concrete Beams'', *PCI Journal*, 25 (Sep.-Oct.), No.5, pp.32-100.

[42].Cong, X. *et al.* (1992), ''Role Of Silica Fume in Compressive Strength of Cement Paste, Mortar, and Concrete'', *ACI Material Journal*, 89 (July-August), No. 4, pp. 375- 387.

[43].Corley, W. G. (1966), ''Rotational Capacity of Reinforced Concrete Beams'', *ASCE Journal of Structural Division*, 92, pp.121-146.

[44].De Larrad, F. *et al.* (1987),''Very High Strength Concrete From the Laboratory to The Construction Site'', *Conference on Utilisation of High Strength Concrete, Stavanger, Norway, June 1987*, pp.509-517.

[45].De Larrard, F. (1990), ''A Method for Proportioning High-Strength Concrete Mixtures'', *Cement, Concrete and Aggregate*, Summer Issue, pp. 47 - 52.

[46].De Larrard. F. *et al.* (1991),''On long-term Strength Losses of Silica Fume High-Strength Concretes'', *Magazine of Concrete Research*, 43 (June), No. 155, pp. 109 - 119.

[47].De Pavia, H. R., Siess, C.P. (1965), ''Strength and Behaviour of Deep Beams in Shear'', *Journal of the Structural Division, ASCE*, 91(Oct.), ST5, part 1, pp. 19-41.

[48].Detwiler. R. J.,Mehta. P. K. (1989), ''Chemical and Physical Effect of Silica Fume on the Mechanical Behaviour of Concrete'', *ACI Materials Journal*, 86 (Nov.-Dec.), No.6,pp. 609- 614.

[49].Diaz de Cossio, R., Siess.C.P. (1960), ''Behaviour and Strength in Shear of Beams and Frames Without Web Reinforcement'', *ACI Journal*, 56 (Feb.), No. 8, pp. 695- 736.

[50].Elzanaty *et al.* (1986), ''Shear Capacity of Reinforced Concrete Beams Using High Strength Concrete'', *ACI Journal*, 83 (March- April), pp. 290-296.

[51]. Eurocode No. 2 (1992) Commission of European Communities, Paris.

[52].Ezeldin, A., Aitcin. P. (1991), ''Effect of Coarse Aggregate on The Behaviour of Normal and High Strength Concretes'',*Cement, Concrete and Aggregate*, 13 (Winter) No. 2, pp.121 - 124

[53].Fenwick, R. C., Paulay, T. (1968), ''Mechanisms of Shear Resistance of Concrete Beams'', *Journal of the Structural Division, ASCE*, 94 (Oct.), pp. 2325-2350.

[54].Ferguson, P. M. (1952), ''Discussion of Diagonal Tension in Reinforced Concrete Beams'', *ACI Journal*, 48 (Dec.), part 2, pp. 156-1- 156-3.

[55].Freedam, S. (1970), ''High Strength Concrete'', *Modern Concrete*, October, 34, pp.29-36.

[56].Gergeley, P. (1969), ''Splitting Cracks along The Main Reinforcement in Concrete Members'', *Department of Structural Engineering, at Cornell University, Ithaca, N.Y.*, April, 51pp.

[57].Gjorv, O. E. (1988), ''Properties of Silica Fume Concrete'', *Proceeding concrete workshop 88, International workshop on the use of fly ash, slag, silica fume, and other siliceous materials in concrete, Sydney, Australia*, pp. 230 - 251.

[58].Godfrey, K. (1987), ''Concrete Strength Record Jumps 36%'',*Civil Engineering*, Oct., pp. 84-88.

[59].Haddadin. M. *et al.* (1971),''Stirrup Effectiveness in Reinforced Concrete Beams with Axial Force'', *Journal of the Structural Division, ASCE*, 97(Sep.), ST9, pp. 2277-2297.

[60].Hanson, J.A. (1958), ''Shear Strength of Lightweight Reinforced Concrete Beams'', *ACI Journal*,55 (Sep.), pp. 387-403.

[61].Hassoun, M.N.(1985),''*Design of Reinforced Concrete Structure", U.S.A,PWA,* pp. 166-215.

[62].Heger, F. J., McGrath, T. J. (1982), ''Shear Strength of Pipe, Box Section, and Other One Way Flexural Members'', *ACI Journal*, 79 (Nov.-Dec.), No. 6,pp. 470-483.

[63].Hjorth, L. (1983), ''Micro Silica in Concrete'', *Nordic Concrete Research*, Pub. No.1, Nordic Concrete Federation , Oslo, Paper No. 9, 18pp.

[64].Iyengar, S. R *et al.* (1968),''Some Factors Affecting the Shear Strength of Reinforced Concrete Beams'', *The Indian Concrete Journal*, 42 (December), pp. 499-523.

[65].Jahren, P. (1983),''Use of Silica Fume in Concrete'',SP-79, *ACI*, Detroit, pp.625-642.

[66].Jensen, V.P. (1943), ''The Plasticity Ratio of Concrete and Its Effect on The Ultimate Strength of Beams'', *ACI Journal*,39 (June), No. 6, pp. 565-582.

[67].Jerath, S., Yamane, L. (1987), ''Mechanical Properties and Workability of Superplasticized Concrete'', *Cement, Concrete and Aggregate*, 9 (No.1), pp. 12-19.

[68].Jobse, H. J., Mustafa, E. S. (1981),''Application of High Strength Concrete for Highway Bridges'', *PCI Journal* ,19 (May-June), pp.44-73.

[69].John, K., Henry, R. (1990), ''Shear Strength of High Strength Concrete Beams with Web Reinforcement'', *ACI Structural Journal*, 87 (March- April), No. 2, pp. 191-198.

[70].Kaar, P. H. *et al.* (1978), ''Stress-Strain Characteristics of High Strength Concrete'', *ACI Special Publication,SP-55, Douglas Mchenry International Symposium,*pp. 161-185.

[71].Kani, G. J. (1964), ''The Riddle of Shear Failure and Its Solution'', *ACI Journal, Proc.*61(April), pp. 441-469.

[72].Kani, G. J. (1966), ''Basic Facts Concerning Shear Failure'', *ACI Journal*, 63 (June), pp. 675-692.

[73].Kani, M.W *et al.* (1979), ''Kani on Shear in Reinforced Concrete'',*University of Toronto, Civil Eng. Dept.*, 225pp.

[74].Kazuyuki, T. *et al.* (1991), ''Chloride Permeability and Corrosion of Reinforcement in Concrete Containing Silica Fume'', *Journal of the Society of Materials Science*,40 (Sep), No. 456, pp. 1164 - 1170.

[75].Karihaloo, B.L.(1995), '' *Fracture Mechanics & Structural Concrete*", London, Longman Group, 330 pp.

[76].Kennedy, J. B., Neville, A.M. (1986), ''*Basic Statistical Methods for Engineers and Scientists'',* New York, Harper & Row, third edition, pp. 420-440.

[77].Kim, J., Park, Y. (1994), ''Shear Strength of Reinforced High Strength Concrete Beams without Web Reinforcement'', *Magazine of Concrete Research*,46 (March), No. 166, pp.7-16.

[78].Leslie, K.E *et al.* (1976), ''Flexural Behaviour of High Strength Concrete Beams'', *ACI Journal Proceeding*, 73(Sep.), No. 8,pp. 517-521.

[79].Lin, C. H. *et al.* (1992),''Flexural Behaviour of High Strength Fly Ash Concrete Beams'', *Journal of Chinese Institute of Engineers*, 15, pp.85-92.

[80].MacGregor *et al.* (1960), ''Effect of Draped Reinforcement on Research of Prestressed Concrete Beams'', *ACI Journal,* 57(Dec.), pp. 649-677.

[81].Mains, R.M. (1951), ''Measurement of the Distribution of Tensile and Bond Stresses Along Reinforcing Concrete Beams'', *ACI Journal*,48(Nov.), No.3, pp.225-252.

[82].Mak, S., Sanjayan, G. (1990), ''Mix Proportions for Very High Strength Concretes'', *National Conference Publication-Institution of Engineers, Australia*, No. 90 Pt 10. Published by IE Australia., pp.127 - 130.

[83].Malhorta,V.M.,Carette,G.G. (1983), "Silica Fume Concrete-Properties, Applications and Limitations", *Concrete International: Design & Construction*, 5 (May), pp.40- 46.

[84].Malier, Y. (1992), "*High Performance Concrete from Material to Structure*", London, E & FN Spon, 542pp.

[85].Mark, K. J., Julio. A. R. (1989), "Minimum Shear Reinforcement in Beams with Higher Strength Concrete", *ACI Structural Journa*l, 86 (July-August), No. 4, pp.376-382.

[86].Mathey, R.G.,Watstein.D. (1961), "Investigation of Bond in Beam and Pullout Specimens with High-Yield Strength Deformed Bars", *ACI Journal*,57 (March), No.9, pp.1071-1090 and discussion pp. 1823-1826.

[87].Mattock, A., Hawkins, N. (1972), "Shear Transfer in Reinforced Concrete-Recent Research", *PCI Journal*, 17(April), PT 2, pp. 55-75.

[88].Mattock, K. *et al.* (1961), "Rectangular Concrete Stress Distribution in Ultimate Strength Design", *ACI Journal*, 57 (Feb.), No. 8, pp 875-928.

[89].McCormac, J. C. (1975), "S*tructural Analysis*", U.S.A,Harper & Row, pp. 302-339.

[90].Mirza, S.A., MacGregor, J.G. (1979), "Statistical Study of Shear Strength of Reinforced Concrete Slender Beams", *ACI Journal,*76 (Nov.), No.11, pp.1159-1177.

[91].Moody .K.G *et al.* (1955), "Shear Strength of Reinforced Concrete Beams-Part 1, 2 and 3", *ACI Journal*, 51(Dec.), No. 4, pp. 317-332; No. 5, January 1955, pp. 417-434; No. 6, February 1955, pp. 525-540.

[92].Moore. W. (1964), "An Analytical Study of the Effect of Web Reinforcement on the Strength of Reinforced Concrete Beams Subjected to Combined Flexure and Shear", *Structural Research Series* No. 282, Civil Engineering Studies, Univ. of Illinois, Urbana.

[93].Mor. A. *et al.* (1992), "Fatigue of High Strength Reinforced Concrete", *ACI Materials Journal*, 89(March-April) , No. 2, pp. 197 - 207.

[94].Morrow, J.,Viest, I. M. (1957), "Shear Strength of Reinforced Concrete Frame Members without Web Reinforcement", *ACI Journal*, March, pp. 833-869.

[95].Mphonde, A.G., Frantz, G.C. (1984), "Shear Strength of High Strength Reinforced Concrete Beams", *ACI Journal*, 81(July-August), No.5, pp. 350-356.

[96].Nagataki, S. (1978), "On the Use of Superplasticizers", *Journal of Japanese PSC Eng. Assoc.* V2D, No.5, pp.7-15.

[97]. Nawy, E.G. (1996), " *Fundamentals of High Strength High Performance Concrete''*, London, Longman Group, 340pp.

[98].Ngo, D.,Scordelis,A.C. (1967),''Finite Element Analysis of Reinforced Beams'', *ACI Journal,* 64 (March), No. 3, pp.152-163.

[99].Neville *et al.* (1966), ''Distribution of Shear in R.C Beams-Part I'', *Concrete & Constructional Engineering*, 61(April), pp. 119-130.

[100].Neville *et al.* (1966), ''Distribution of Shear in R.C Beams-Part II'', *Concrete & Constructional Engineering*, 61(May), pp. 157-162.

[101].Nilson, A. (1985), ''Design Implication of Current Research on High-Strength Concrete'', ACI SP. 87-7, High Strength Concrete, pp. 85-117.

[102].Novokshchenov, V. (1992), ''Factors Controlling the Compressive Strength of Silica Fume Concrete in the range 100-150 *MPa*'', *Magazine of Concrete Research*,44 (March), No.158, pp. 53 - 61.

[103].Oluokun, F. A. (1991), ''Prediction of Concrete Tensile Strength from it's Compressive Strength:Evaluation of Existing Relations for Normal Weight Concrete'', *ACI Material Journal*, May-June, pp. 302-309.

[104].Palaskas, M.N. *et al.* (1981), ''Shear Strength of Lightly Reinforced T-Beams'', *ACI Journal*, 78 (November-December), No.6, pp. 447-455.

[105].Radjy, F. F. *et al.* (1985), ''A review Experiences with Condensed Silica Fume Concretes and Products'', *Fly ash, Silica fume, Slag and natural pozzolans in concrete, SP-91, American Concrete Institute, Detroit*, 2, pp. 1135-1152.

[106].Rangan, B. V. (1991), ''Strength of High Strength Concrete Columns'', *Trans. of the Institution of Engineers Australia Civil Engineering*, Vol. CE 33, Part 4, pp.293-298.

[107].Regan, P.E. (1969), ''Shear in Reinforced Concrete Beams'', *Magazine of Concrete Research*,21 (March), No.66, pp.31-42.

[108].Regan, P.E, Placas,A. (1970), ''Limit State Design for Shear in Rectangular and T Beams'', *Magazine of Concrete Research*, 22 (Dec.), No.73, pp.197-208.

[109].Regan, P. E. *et al.* (1993), ''Behaviour of High Strength Concrete Slabs'', *Proceedings of Concrete 2000, held at Dundee University on 7-9(September 1993*), pp.761-773.

[110].Regan. P.E. (1993), ''Research on Shear: A Benefit to Humanity or A Waste of Time?'', *The structural Engineer Journal*, 71(Oct.), No. 19, pp. 337-347.

[111].Rephael. J. M. (1984),''Tensile Strength of Concrete, *ACI Journal*, 81 (March-April), pp. 158-165.

[112].Salandra, M, Ahmad. S. (1989), "Shear Capacity of Reinforced Lightweight High Strength Concrete Beams'', *ACI Structural Journal*, 86 (November-December), No. 6, pp. 697-704.

[113].Sandvik, M, Gjorv, O. E. (1992), ''Prediction of Strength Development for Silica fume Concrete", *Proceedings on fly ash, silica fume, slag, and natural pozzolans in concrete,* Istanbul, Turkey, May, SP-132, pp.987-998.

[114].Sarkar, S. (1964), *''Study of Combined Bending Shear and Torsion on Hollow R.C. Sections''*, (PhD thesis, University of Leeds), pp.131.

[115].Sarkar, S, Adwan, O, Munday, J. (1997), ''High Strength Concrete:An Investigation of The Flexural Behaviour of High Strength RC Beams'', *The Structural Engineer Journal*,75, No. 7, pp. 115-121.

[116].Sarkar, S, Adwan, O, Munday, J. (1997), '' Shear Capacity and Ductility of High Strength Reinforced Concrtete Beams'', *Fourth International Kerensky Conference, Sep. 1997, Hong Kong.*

[117].Sarkar, S. L., Aitcin, P. C. (1987), ''Comparative Study of the Microstructures of Normal and Very High Strength Concretes'', *Cement, Concrete and Aggregate*, 9(2), pp. 57-65.

[118].Sarkar, S. L., Aitcin. P.C. (1987), ''Dissolution Rate of Silica Fume in Very High Strength Concrete", *Cement and Concrete Research,* 17 (No.4), pp.591-601.

[119].Sarsam, K, Al-Musawi, J. (1992), ''Shear Design of High And Normal Strength Concrete Beams With Web Reinforcement", *ACI Structural Journal*, 89 (November-December), No. 6,pp. 658-664.

[120].Saucier, K. (1980), ''High Strength Concrete, Past, Present and Future", *Concrete International,* June, pp. 46-50.

[121].Scott, R. H. (1983), ''The Short Term Moment-Curvature Relationship for Reinforced Concrete Beams'', *Proceeding of the Institute of Civil Engineers,*75 (Dec.) PT.2, pp. 725-734.

[122].Setunge, S. *et al.* (1990), ''Engineering Properties of Very High Strength Concrete'', *Second International Structural Engineering Conference, Australia*, pp.120 -126.

[123].Shah, S, Ahmad, S. (1985), ''Structural Properties of High Strength Concrete and Implications for Precast Prestressed Concrete", *PCI Journal*, (November-December) pp. 93 - 119.

[124].Shah, S .P, Lange, D. A. (1992), ''Properties of Aggregate-Cement Interface for High Performance Concrete", *Proceeding of the 9th Conference on Engineering Mechanics TX.* USA 24th May 1992, pp.852-855.

[125].Sheehn.T.(1991), ''High Strength Concrete-A review of US Expertise", *Concrete*, (Nov.-Dec)., pp. 35-37.

[126].Sing, S.W *et al.* (1989), ''Flexural Ductility of Ultra-High Strength Concrete Members", *ACI Structural Journal*, 86 (July-August), No. 4, pp. 394-400.

[127].Slanicka, S. (1991),"The Influence of Condensed Silica Fume on the Concrete Strength", *Cement and Concrete Research*, 21, pp. 462-470.

[128].Swamy, R .N., Andriopoulos, A. D. (1974), ''Contribution of Aggregate Interlock and Dowel Forces to The Shear Resistance of Reinforced Beams with Web Reinforcement", *ACI Publication, SP-42, ACI, Detroit*, pp. 129-166.

[129].Swamy, R.N., Bahia, H. M., (1979), ''Influence of Fiber Reinforcement on The Dowel Resistance to Shear", *ACI Journal*, 76 (Feb.), pp. 327-355.

[130].Tachibana, D. *et al.* (1990),''High Strength Concrete Incorporating Several Admixture", *Second International Symposium, ACI*, SP-121,pp. 310-326.

[131].Taylor, H.P. (1968),''Shear Stresses in RC Beams without Shear Reinforcement", Technical Report TRA 407, *Cement and Concrete Associations*, London, Feb., 23pp.

[132].Taylor. H.P. (1970), ''Investigation of the Forces Carried Across Cracks in Reinforced Concrete Beams in Shear by Interlock of Aggregate", *Cement and Concrete Association*, TRA 42.447, London, November, 22 pp.

[133].Taylor. H.P. (1970), ''Further Tests to Determine Shear Stresses in Reinforced Concrete Beams", Technical Report TR 42.438, 1970, *Cement and Concrete Associations*, London, 25pp.

[134].Taylor, R. (1960)," Some Shear Tests on Reinforced Concrete Beams without Shear Reinforcement", *Magazine of Concrete Research*, 12 (Nov.), No. 36, pp. 145-154.

[135].Taylor. H. P. (1974),"The Fundamental Behaviour of Reinforced Concrete Beams in Bending and Shear", *ACI Publication SP-42, American Concrete Institute, Detroit*, pp. 43-77.

[136].The Institute of Concrete Technology. (1994)," The 22nd Annual Convention Symposium and Annual General Meeting on High Performance Concrete'', 28th-30th March 1994, Swindon, U.K.

[137].Ting, E. *et al.* (1992),"Compressive Strength Testing of Very High Strength Concrete", *17th Conference on Our Word in Concrete and Structures: 25-27 August, 1992, Singapore,* pp.217-226.

[138].Ting, E., Patnaikuni. I. (1992),"Influence of Mix Ingredients on the Compressive Strength of Very High Strength Concrete", *17th Conference on Our Word in Concrete and Structures, 25-27 August, 1992, Singapore*, pp.207-215.

[139].Tognon, G *et al.* (1980)," Design and Properties of Concretes with Strength Over 1500 kgf/cm^2", *ACI Journal*, May -June, pp. 171-178.

[140].Tu, C. (1988),"*Properties of Micro Silica Concrete*",(M.Sc.Thesis, Aberdeen University).

[141].Tuna, M. *et al.* (1992), ''Interpreting High Strength Concrete as a Design Engineer", *17th Conference on Our Word in Concrete and Structures, 25-27 August 1992, Singapore*, pp.63-66.

[142].Van der Berg, F. J. (1962), ''Shear Strength of Reinforced Beams without Reinforcement", *ACI Journal*,59 (November), pp. 1587-1600.

[143].Walraven, J. (1982)," Shear in Elements without Shear Reinforcement", Bulletind Information No. 146, *Comite Euro-International Du Beton, Jan.1982*, pp.7-41.

[144].Wang, P. T *et al.* (1978). ''High Strength Concrete in Ultimate Strength Design", *Proceedings of American Society of Civil Engineers*, 104 (Nov.), No. ST11, pp 1761-1773.

[145].Watanabe, A. (1981), ''Study on Workability of High Strength Concrete Containing Superplasticizer", *Polymers in Concrete*, Korimaya, 2, pp. 1344-1354.

[146].Wells, A.A. (1961), ''Unstable Crack Propagation in Metal, Cleavage and Fast Fracture", *The Crack Propagation Symposium, Cornfield, U.K*, pp. 210-230.

[147].Wilinson, M. K and Warwaruk, J. (1969), ''Moment Curvature Relationships of Prestressed Concrete Beams with Confined Compressed Concrete", *Report No. 17, Civil Engineering Department, University of Alberta Edmonton, Canada,* January., 54pp.

[148].Wolsiefer, J. (1984), ''Ultra High-Strength Field Placeable Concrete with Silica Fume Admixture", *Concrete International*, 6 (Part 3) , pp 25 - 31.

[149].Yogendran, V *et al.* (1987), "Silica Fume in High Strength Concrete", *ACI Material Journal*, 84 (March- April), No. 2, pp. 124 -129.

[150].Zia, P. (1977), ''Structural Design with High Strength Concrete", *Report No. PZIA-77-01, Department of Civil Engineering, North Carolina State University, Raleigh, U.S.A*, Mar., 66 pp.

[151].Zia.,P. (1983),''Review of ACI Code for design with High-Strength Concrete", C*oncrete International*, August, pp 16-20.

[152].*Z*sutty, T. C. (1968), ''Beam Shear Strength Prediction By Analysis of existing Data*", ACI Journal*, 65 (November) pp. 942-951.

Appendix A

Load-flexural strain data along depth of beams

- ***App.Table 1.1- Load- Strain Data for Beam (HS1-1)†***

Load No.	Load *kN*	Average Strain Gage Readings ($\mu\varepsilon$) 1&8 0 *mm*	2&9 30 *mm*	3&10 60 *mm*	4&11 90 *mm*	5&12 120 *mm*	6&13 150 *mm*	7&14 steel level	N. Axis depth (*mm*)
1	0.00	0	0	0	0	0	0	0	0
2	4.90	43	65	28	-4	-22	-24	-45	86
3	9.80	111	130	47	-12	-53	-109	-142	84
4	15.30	211	191	55	-61	-129	-227	-380	74
5	20.10	310	195	53	-179	-251	-395	-660	67
6	24.10	393	245	38	-263	-380	-571	-937	64
7	29.10	490	285	30	-273	-477	-732	-1184	63
8	34.10	583	324	34	-300	-561	-858	-1415	63
9	39.00	663	377	44	-336	-640	-990	-1665	63
10	43.80	748	414	38	-387	-749	-1143	-1920	63
11	50.00	829	459	12	-486	-934	-1395	-2335	61
12	52.00	1380	221	-1985	-3055	-4680	-6410	-9905	33
13	53.00	1680	154	-2960	-6045	-8595	-12100	-	31
14	54.00	1860	-210	-3405	-6615	-9735	-12950	-	27
15	56.00	2095	-570	-4104	-7735	-11250	-13550	-	24
16	59.00	2350	-853	-4760	-8280	-12550	-	-	23

† Average cube strength = 107 *MPa* and ρ =1.03%

App.Table 1.2- Load- Strain Data for Beam (HS1-2)†

		Average Strain Gage Readings ($\mu\varepsilon$)							
Load No.	Load *kN*	1&8 0 *mm*	2&9 30 *mm*	3&10 60 *mm*	4&11 90 *mm*	5&12 120 *mm*	6&13 150 *mm*	7&14 steel level	N. Axis depth (*mm*)
1	0.00	0	0	0	0	0	0	0	0
2	4.90	56.6	-83	20	97	49	-20	-65	12
3	9.20	198	-12	61	131	28	-83	-320	128
4	14.10	376	80.9	91	81	-89	-220	-580	104
5	19.40	516	160	93	6	-220	-420	-900	91
6	25.00	659	231	87	-26	-340	-620	-1240	83
7	29.80	773	283	80.9	-110	-510	-880	-1660	73
8	34.40	860	348	87	-200	-630	-1060	-1910	69
9	39.50	975	404	80.9	-250	-720	-1230	-2260	67
10	44.30	1096	465	72.8	-360	-820	-1380	-2540	65
11	46.50	1335	489	-150	-790	-1540	-2390	-4140	53
12	51.40	1857	392	-1270	-2860	-4690	-6580	-10440	37
13	52.60	2079	293	-1960	-4180	-6666	-9110	-13520	34
14	53.10	2437	-170	-3760	-7290	-10610	-	-	28
15	53.50	2496	-170	-3810	-7360	-11210	-	-	28

† Average cube strength = 97 *MPa* and ρ =1.03%

App.Table 1.3- Load- Strain Data for Beam (HSC1-3)†

Load No.	Load *kN*	Average Strain Gage Readings ($\mu\varepsilon$) 1&8 0 *mm*	2&9 30 *mm*	3&10 60 *mm*	4&11 90 *mm*	5&12 120 *mm*	6&13 150 *mm*	7&14 steel level	N. Axis depth (*mm*)
1	0.00	0	0	0	0	0	0	0	0
2	5.80	74.8	66.7	48.5	297	-28	-57	-140	117
3	10.60	184	166	93	127	-97	-230	-430	107
4	14.90	293	263	121	16.2	-97	-320	-490	94
5	20.00	374	340	133	-10	-220	-540	-980	88
6	24.30	479	407	148	-40	-340	-700	-1250	84
7	29.10	585	443	150	-73	-390	-820	-1500	80
8	34.30	625	473	158	-130	-440	-910	-1690	76
9	39.80	785	562	178	-120	-640	-1060	-1960	78
10	45.00	872	657	198	-180	-710	-1170	-2280	76
11	49.00	945	740	216	-290	-740	-1240	-2460	73
12	52.00	1300	785	-120	-1320	-2390	-3570	-5990	56
13	55.00	1660	712	-1100	-2830	-4940	-6930	-11780	42
14	57.00	1984	562	-2000	-4490	-7680	-1064	-	37
15	*	2037	542	-2630	-4780	-8090	-11110	-	34

† Average cube strength = 85 *MPa* and ρ =1.03%

App.Table 1.4- Load- Strain Data for Beam (HSC2-1)†

		Average Strain Gage Readings ($\mu\varepsilon$)							
Load No.	Load *kN*	1&8 0 *mm*	2&9 30 *mm*	3&10 60 *mm*	4&11 90 *mm*	5&12 120 *mm*	6&13 150 *mm*	7&14 steel level	N. Axis depth (*mm*)
1	0.00	0	0	0	0	0	0	0	0
2	5.30	48.5	-4	-140	89	36.4	-81	-140	28
3	6.10	93	28.3	-12	97.1	112	-93	-150	51
4	10.40	121	89	-4	40.5	162	-110	-270	51
5	15.20	154	142	-150	4.05	0	-190	-480	45
6	19.10	316	190	121	0	-32	-340	-700	90
7	25.00	518	255	89	-49	-190	-520	-970	52
8	30.00	530	320	186	-53	-310	-690	-1400	83
9	35.00	627	493	93	-180	-410	-840	-1640	70
10	40.00	696	453	-16	-230	-510	-940	-1800	59
11	44.10	793	502	190	-230	-580	-1100	-2070	73
12	50.10	833	558	178	-270	-680	-1240	-2390	72
13	55.10	1092	647	210	-320	-740	-1360	-2530	72
14	59.40	1120	688	303	-350	-840	-1480	-2850	74
15	65.00	1230	748	214	-440	-950	-1690	-3130	70
16	65.20	1634	777	-230	-1610	-2840	-4190	-7300	53
17	66.70	1982	773	-550	-2570	-4340	-6210	-10420	48
18	68.10	2071	760	-780	-3260	-5580	-7640	-12950	45
19	71.00	2160	712	-1720	-4250	-6100	-9660	-	38.8

† Average cube strength = 107 *MPa* and ρ =1.42%

App.Table 1.5 -Load- Strain Data for Beam (HSC2-2)†

Average Strain Gage Readings ($\mu\varepsilon$)									
Load No.	Load *kN*	1&8 0 *mm*	2&9 30 *mm*	3&10 60 *mm*	4&11 90 *mm*	5&12 120 *mm*	6&13 150 *mm*	7&14 steel level	N. Axis depth (*mm*)
1	0.0	0	0	0	0	0	0	0	0
2	6.10	41	36	18	$-7.2\text{x}10^{-13}$	32	-53	-69	90
3	9.80	95	77	38	14	36	-81	-154	129
4	14.20	174	129	59	4	-8	-158	-129	100
5	18.60	263	190	75	-16	-57	-263	-538	85
6	23.80	360	251	91	-36	-113	-360	-752	81
7	29.40	465	311	115	-57	-150	-485	-975	80
8	34.40	558	368	127	-81	-214	-587	-1137	78
9	39.40	659	432	156	-101	-267	-688	-1347	78
10	44.60	732	473	172	-125	-320	-793	-1525	77
11	50.40	825.	538	184	-150	-409	-934	-1525	77
12	55.00	922	582	192	-166	-493	-1036	-1893	76
13	59.00	991	635	216	-194	-562	-1145	-2075	76
14	64.70	1075	707	237	-222	-647	-1125	-2318	75
15	66.00	1553	777	-229	-1270	-2310	-3564	-6205	53
16	70.00	1877	805	-726	-2391	-4102	-5983	-10326	46
17	71.00	1707	805	-1288	-3588	-5133	-8406	-	42
18	71.50	2148	829	-1353	-3709	-6116	-8648	-	41
19	72.50	2310	813	-1600	-4643	-6876	-9668	-	40.1

† Average cube strength = 100 *MPa* and ρ =1.42%

App.Table 1.6 - Load- Strain Data for Beam (HSC2-3)†

Average Strain Gage Readings ($\mu\varepsilon$)									
Load No.	Load *kN*	1&8 0 *mm*	2&9 30 *mm*	3&10 60 *mm*	4&11 90 *mm*	5&12 120 *mm*	6&13 150 *mm*	7&14 steel level	N. Axis depth (*mm*)
1	0	0	0	0	0	0	0	0	0
2	5.18	101	53	24	-53	8	-53	-372	69
3	10.58	174	150	53	73	-93	-279	-643	103
4	15.00	239	210	73	-12	-198	-445	-773	86
5	20..00	328	263	89	-8	-283	-611	-858	88
6	25.46	449	344	93	-61	-364	-752	-1,076	78
7	30.30	445	376	125	-142	-400	-886	-1,290	74
8	35.10	631	453	186	-28	-437	-987	-1,452	86
9	40.10	696	530	218	-117	-560	-1,137	-1,533	80
10	45.38	781	599	279	-101	-611	-1,266	-1,796	82
11	50.10	955	688	320	-123	-684	-1,383	-1,905	82
12	55.40	1,040	793	360	-150	-769	-1,497	-2,051	81
13	60.22	1,428	890	429	-89	-805	-1,634	-2,233	85
14	64.00	1,618	1,023	291	-522	-1,529	-2,747	-4,114	71
15	64.80	2,229	1,234	28	-1,391	-2,310	-5,291	-7,863	61
16	66.00	2,658	1,808	0	-1,978	-4,243	-6,614	-10,606	42

† Average cube strength = 77 *MPa* and ρ =1.42%

App.Table 1.7 - Load- Strain Data for Beam (HSC2-4)†

		Average Strain Gage Readings ($\mu\varepsilon$)							
Load No.	Load *kN*	1&8 0 *mm*	2&9 30 *mm*	3&10 60 *mm*	4&11 90 *mm*	5&12 120 *mm*	6&13 150 *mm*	7&14 steel level	N. Axis depth (*mm*)
1	0.0	0	0	0	0	0	0	0	0
2	5.43	65	49	32	49	-24	-20	-121	110
3	10.31	121	93	20	89	-32	-40	-186	112
4	15.42	202	150	28	85	-53	-109	-295	109
5	20.20	303	194	65	109	-133	-202	-522	104
6	25.02	388	243	40	-12	-267	-222	-716	83
7	30.38	469	299	8	8	-360	-603	-882	91
8	34.90	550	348	12	-73	-461	-773	-1,068	64
9	40.88	643	388	61	-133	-538	-882	-1,363	69
10	44.77	700	421	65	-138	-781	-845	-1,254	70
11	51.03	809	481	81	-158	-926	-1,125	-1,792	70
12	55.57	902	526	259	-158	-785	-1,323	-1,905	79
13	65.18	991	591	65	-202	-926	-1,396	-2,277	67
14	68.48	1,460	558	-558	-1,505	-2,714	-3,980	-6,565	45
15	73.65	1,739	477	-1,416	-3,147	-5,400	-7,439	-11,775	38
16	74.00	1,986	295	-2,132	-4,292	-6,990	-9,639	-12,665	37.5

† Average cube strength = 90 *MPa* and ρ =1.42%

App.Table 1.8 - Load- Strain Data for Beam (HSC3-1)†

		Average Strain Gage Readings ($\mu\varepsilon$)							
Load No.	Load *kN*	1&8 0 *mm*	2&9 30 *mm*	3&10 60 *mm*	4&11 90 *mm*	5&12 120 *mm*	6&13 150 *mm*	7&14 steel level	N. Axis depth (*mm*)
1	0.0	0	0	0	0	0	0	0	0
2	6.04	-12	40	20	-24	20	-4	-89	74
3	10.00	85	77	32	16	12	-32	-170	128
4	20.00	287	198	69	0	-77	-137	-550	90
5	25.00	299	247	77	-16	-129	-198	-718	85
6	30.00	409	316	101	-32	-129	-231	-898	83
7	35.00	489	354	129	-32	-73	-299	-1052	84
8	40.00	542	409	142	-49	-330	-360	-1234	82
9	45.00	615	453	158	-49	0	-417	-1509	83
10	55.00	781	538	194	-73	-20	-554	-1843	82
11	60.00	858	643	214	-69	-113	-619	-2006	83
12	65.00	1003	676	287	-57	-153	-692	-2168	85
13	70.00	1,088	724	275	-69	-202	-760	-2310	84
14	75.00	1,153	785	303	-89	-231	-809	-2435	83
15	80.00	1,226	829	291	-53	-251	-870	-2565	85
16	85.00	1,311	890	328	-32	-283	-932	-2738	87
17	90.00	1,408	963	348	12	-307	-983	-2872	91
18	95.00	1,497	1,011	427	-36	-364	-1084	-3143	88
19	100.00	1,938	1,116	162	-930	-1865	-3240	-6525	64
20	97.00	2,285	1,193	-60	-1958	-3547	-4789	-10299	59
21	100.00	2,811	1,076	-275	-2791	-4975	-7592	-13272	54
22	103.00	2,819	1,347	-380	-3232	-5740	-8689	-6731	35

† Average cube strength = 107 *MPa* and ρ =1.94%

App.Table 1.9 - Load- Strain Data for Beam (HSC3-2)†

Average Strain Gage Readings ($\mu\varepsilon$)									
load No.	Load *kN*	1&8 0 *mm*	2&9 30 *mm*	3&10 60 *mm*	4&11 90 *mm*	5&12 120 *mm*	6&13 150 *mm*	7&14 steel level	N. Axis depth (*mm*)
1	0	0	0	0	0	0	0	0	0
2	10.00	182	77	40	-186	-28	-57	-129	65
3	20.00	360	222	113	-178	-61	-251	-433	72
4	30.00	582	376	150	-206	-182	-485	-845	73
5	35.00	724	429	186	-222	-218	-570	-1,015	74
6	40.00	805	514	194	-239	-279	-633	-1,201	73
7	45.00	886	570	275	-255	-283	-720	-1,347	76
8	50.00	1,015	651	295	-251	-360	-793	-1,452	76
9	55.00	1,226	748	368	-227	-396	-862	-1,574	79
10	60.00	1,278	845	449	-231	-413	-894	-1,743	80
11	65.00	1,383	906	429	40	-441	-934	-1,946	93
12	70.00	1,497	963	502	-190	-502	-1,088	-2,023	82
13	75.00	1,582	1,031	534	-194	-538	-1,254	-2,188	82
14	80.00	1,683	1,088	595	-243	-587	-1,319	-2,350	81
15	85.00	1,764	1,149	627	-227	-627	-1,476	-2,423	82
16	90.00	1,849	1,230	651	-239	-643	-1,436	-2,645	82
17	95.00	2,018	1,315	680	-267	-760	-1,691	-2,985	82
18	94.00	2,500	1,476	344	-971	-1,893	-3,297	-5,562	68
19	96.00	2,900	1,594	267	-1,383	-2,625	-4,272	-7,277	65
20	100.00	3,131	1,699	154	-1,820	-3,438	-5,331	-8,972	35.5

† Average cube strength = 85 *MPa* and ρ =1.94%

App.Table 1.10 - Load- Strain Data for Beam (HSC3-3)†

		Average Strain Gage Readings (με)							
Load No.	Load *kN*	1&8 0 *mm*	2&9 30 *mm*	3&10 60 *mm*	4&11 90 *mm*	5&12 120 *mm*	6&13 150 *mm*	7&14 steel level	N. Axis depth (*mm*)
1	0.0	0	0	0	0	0	0	0	0
2	5.33	61	16	28	-73	-8	4	-77	68
3	10.46	129	40	57	28	-20	-57	-142	108
4	15.30	198	101	77	-69	-44	-93	-247	76
5	20.49	299	146	89	-57	-89	-182	-421	78
6	25.38	396	210	105	-117	-133	-267	-643	74
7	30.64	481	251	109	-146	-190	-348	-635	73
8	35.14	635	287	113	-40	-243	-433	-773	82
9	40.23	623	336	146	-105	-295	-518	-938	77
10	45.45	720	372	150	-142	-324	-591	-1,088	75
11	50.94	805	498	170	-158	-392	-692	-1,246	76
12	55.53	858	485	182	-287	437	-756	-1,375	72
13	60.13	991	554	227	-194	-461	-813	-1,505	76
14	65.60	1,064	603	255	-158	-510	-870	-1,646	79
15	69.15	1,145	671	271	-158	-554	-963	-1,772	79
16	75.03	1,226	720	287	-279	-615	-1,060	-1,905	75
17	80.00	1,327	769	316	-259	-639	-1,129	-2,055	76
18	90.37	1,497	890	352	-332	-740	-1,315	-2,289	75
19	95.12	1,610	971	595	-283	-785	-1,363	-2,455	80
20	98.00	1,978	1,044	129	-898	-1,832	-2,864	-4,769	64
21	100.00	2,306	1,064	-146	-1,622	-2,981	-4,429	-7,168	56
22	98.00	2,949	1,133	-372	-2,791	-4,288	-6,298	-10,135	43

† Average cube strength = 78 *MPa* and ρ =1.94%

App.Table 1.11 -Load- Strain Data for Beam (HSC4-1)†

		Average Strain Gage Readings ($\mu\varepsilon$)							
Load No.	Load *kN*	1&8 0 *mm*	2&9 30 *mm*	3&10 60 *mm*	4&11 90 *mm*	5&12 120 *mm*	6&13 150 *mm*	7&14 steel level	N. Axis depth (*mm*)
1	0.0	0	0	0	0	0	0	0	0
2	11.00	150	109	8	32	4	-61	-174	122
3	20.00	348	198	10	57	-8	-113	-348	116
4	30.00	587	429	107	125	-61	-178	-538	110
5	40.00	765	582	237	154	-32	-243	-708	115
6	50.00	934	700	342	210	16	-235	-849	122
7	60.00	1,133	882	508	255	-36	-405	-1,056	116
8	70.00	1,298	995	617	283	-65	-453	-1,238	114
9	80.00	1,557	1,125	730	316	-77	-510	-1,436	114
10	90.00	1,861	1,485	807	417	-89	-570	-1,634	115
11	100.00	2,018	1,541	989	473	-61	-623	-1,760	117
12	110.00	2,302	1,784	1,179	550	-69	-680	-2,018	117
13	120.00	2,609	1,970	1,211	611	-142	-773	-2,200	114
14	130.00	2,799	2,136	1,300	692	-57	-829	-2,463	118
15	140.00	3,062	2,520	1,745	829	-49	-894	-2,787	58.5

† Average cube strength = 101 *MPa* and ρ =4.04%

App.Table 1.12 - Load- Strain Data for Beam (HSC4-2)†

		Average Strain Gage Readings ($\mu\varepsilon$)							
Load No.	Load *kN*	1&8 0 *mm*	2&9 30 *mm*	3&10 60 *mm*	4&11 90 *mm*	5&12 120 *mm*	6&13 150 *mm*	7&14 steel level	N. Axis depth (*mm*)
1	0.0	0	0	0	0	0	0	0	0
2	9.95	202	158	97	73	53	40	-85	160
3	19.67	493	316	263	158	53	-28	-344	140
4	29.48	773	518	587	239	53	-57	-578	134
5	39.74	1,060	692	566	320	69	-97	-805	132
6	48.76	1,359	906	732	417	101	-138	-1,064	133
7	58.49	1,654	1,137	898	498	89	-182	-874	130
8	68.50	1,966	1,404	1,076	603	93	-210	-1,497	129
9	79.76	2,298	1,626	1,238	688	138	-279	-1,549	130
10	90.16	2,617	1,869	1,416	781	150	-324	-1,978	129
11	100.21	2,981	2,156	1,622	894	174	-332	-2,200	130
12	110.91	3,369	2,463	1,808	1,023	218	-380	-2,439	131
13	120.24	3,794	2,791	2,047	1,145	231	-441	-2,702	130
14	129.56	4,352	3,159	2,306	1,311	295	-477	-2,961	131
15	135.76	4,781	3,442	2,504	1,416	307	-502	-3,272	62.2

† Average cube strength = 87 *MPa* and ρ =4.04%

App. Table 1.13 - Load- Strain Data for Beam (HSC4-3)†

		Average Strain Gage Readings ($\mu\varepsilon$)							
Load No.	Load *kN*	1&8 0 *mm*	2&9 30 *mm*	3&10 60 *mm*	4&11 90 *mm*	5&12 120 *mm*	6&13 150 *mm*	7&14 steel level	N. Axis depth (*mm*)
1	0.0	0	0	0	0	0	0	0	0
2	10.42	138	109	44	40	0	-89	-129	120
3	19.92	263	214	81	57	-12	-105	-303	115
4	30.02	522	303	121	69	-28	-174	-413	111
5	38.80	582	417	231	89	-65	-218	-534	107
6	49.89	704	518	243	97	-89	-251	-696	106
7	60.53	728	631	303	109	-101	-279	-821	106
8	70.08	1,116	728	372	133	-121	-356	-938	106
9	80.35	1,290	845	433	150	-133	-457	-1,068	106
10	90.35	1,375	963	506	170	-154	-498	-1,218	106
11	100.40	1,561	1,064	534	202	-150	-142	-1,335	107
12	110.34	1,699	1,197	607	227	-170	-174	-1,464	107
13	120.48	1,865	1,339	667	259	-186	-643	-1,614	107
14	129.67	2,014	1,480	789	303	-194	-663	-1,739	108
15	140.08	2,209	1,634	874	336	-182	-688	-1,857	109
16	150.02	2,443	1,792	975	392	-202	-760	-1,723	110
17	160.00	2,589	1,978	1,100	425	-222	-870	-2,188	110
18	169.14	3,074	2,338	1,250	465	-328	-1,100	-2,710	65

† Average cube strength = 82 *MPa* and ρ =4.04%

App. Table 1.14 - Load- Strain Data for Beam (DHSC 1-1)†

		Average Strain Gage Readings ($\mu\varepsilon$)							
Load No.	Load *kN*	1&8 0 *mm*	2&9 30 *mm*	3&10 60 *mm*	4&11 90 *mm*	5&12 120 *mm*	6&13 150 *mm*	7&14 steel level	N. Axis depth (*mm*)
1	0.00	0	0	0	0	0	0	0	0
2	9.84	146	101	61	49	12	-49	-162	126
3	19.73	287	202	133	77	376	-129	-340	142
4	30.04	461	340	182	101	336	-222	-538	138
5	40.00	639	465	283	133	311	-259	-736	136
6	49.75	805	582	360	162	275	-376	-926	133
7	59.20	951	801	405	194	267	-453	-1104	131
8	69.80	1052	833	522	227	251	-530	-1311	130
9	79.64	1298	959	603	263	235	-587	-1489	129
10	89.99	1468	1096	684	299	218	-801	-1667	126
11	99.15	1582	1181	773	348	206	-724	-1877	127
12	109.61	1804	1331	837	320	190	-773	-2059	126
13	118.39	1966	1460	922	417	178	-870	-2253	125
14	129.61	2164	1610	1031	421	170	-898	-2480	125
15	139.35	2316	1731	1104	481	162	-959	-2674	124
16	148.52	2565	1897	1165	485	49	-1007	-3252	121
17	156.10	2864	2095	1258	433	-154	-1319	-4017	112
18	160.92	3074	2294	1270	227	-206	-1840	-4627	65

† Average cube strength = 107 *MPa* and ρ =4.4%

Table 1.15 - Load- Strain Data for Beam (DHSC 1-2)†

		Average Strain Gage Readings ($\mu\varepsilon$)							
Load No.	Load *kN*	1&8 0 *mm*	2&9 30 *mm*	3&10 60 *mm*	4&11 90 *mm*	5&12 120 *mm*	6&13 150 *mm*	7&14 steel level	N. Axis depth (*mm*)
1	0.00	0	0	0	0	0	0	0	0
2	9.45	129	81	57	36	8	-16	-117	130
3	19.09	291	231	142	69	4	-69	-372	122
4	28.40	481	364	231	97	-16	-125	-647	116
5	39.35	692	526	332	125	-28	-206	-942	114
6	48.39	866	655	409	154	-44	-380	-1137	113
7	58.30	1060	801	493	194	-69	-348	-1367	112
8	68.36	1258	942	570	214	-97	-421	-1764	111
9	78.04	1444	1088	684	255	-109	-481	-1796	111
10	88.66	1671	1258	797	291	-125	-550	-2035	111
11	98.06	1849	1404	870	271	-146	-627	-2253	110
12	108.33	2083	1574	979	372	-142	-756	-2508	112
13	119.12	2342	1780	1108	417	-182	-797	-2840	111
14	128.11	2573	1946	1197	413	-267	-959	-3293	108
15	136.11	2965	2200	1315	384	-437	-1254	-3952	104
16	141.92	3289	2403	1383	437	-627	-1602	-4725	102
17	143.64	3641	3216	1480	392	-1359	-2799	-7079	97

† Average cube strength = 100 *MPa* and ρ =4.04%

App. Table 1.16 - Load- Strain Data for Beam (DHSC 1-3)†

		Average Strain Gage Readings ($\mu\varepsilon$)							
Load No.	Load *kN*	1&8 0 *mm*	2&9 30 *mm*	3&10 60 *mm*	4&11 90 *mm*	5&12 120 *mm*	6&13 150 *mm*	7&14 steel level	N. Axis depth (*mm*)
1	0.00	0	0	0	0	0	0	0	0
2	9.84	133	85	57	20	0	-28	-138	120
3	19.73	239	180	113	28	-24	-109	-352	106
4	30.04	522	384	227	53	-101	-299	-789	100
5	40.00	797	566	324	49	-202	-489	-1650	96
6	49.75	918	680	390	61	-247	-603	-1489	96
7	59.20	1056	781	457	73	-275	-676	-1691	96
8	69.80	1189	874	510	89	-558	-765	-1893	94
9	79.64	1339	967	566	93	-344	-866	-2116	96
10	89.99	1476	1056	619	109	-368	-934	-2302	97
11	99.15	1606	1169	684	113	-396	-1015	-2488	97
12	109.61	1760	1278	744	142	-453	-1145	-2827	97
13	118.39	1917	1383	809	150	-461	-1185	-2912	97
14	129.61	2107	1509	866	121	-546	-1367	-3317	95
15	139.35	2476	1715	866	-89	-999	-2111	-3970	87
16	148.52	2896	2079	-239	-2196	-2710	-3539	-5586	57

† Average cube strength = 100 *MPa* and ρ =4.4%

App. Table 1.17 - Load- Strain Data for Beam (DHSC 1-4)†

		Average Strain Gage Readings ($\mu\varepsilon$)							
Load No.	Load *kN*	1&8 0 *mm*	2&9 30 *mm*	3&10 60 *mm*	4&11 90 *mm*	5&12 120 *mm*	6&13 150 *mm*	7&14 steel level	N. Axis depth (*mm*)
1	0.00	0	0	0	0	0	0	0	0
2	10.99	69	77	65	24	0	-24	-117	120
3	20.23	182	166	129	44	-24	-101	-344	109
4	30.27	320	275	178	44	-89	-243	-651	100
5	39.78	449	380	235	36	-146	-352	-858	96
6	50.49	599	498	303	53	-190	-364	-1088	97
7	60.17	744	615	332	57	-247	-158	-1707	96
8	70.04	906	696	409	69	-295	-659	-1497	96
9	80.19	1036	805	473	73	-340	-769	-1658	95
10	90.03	1193	926	538	89	-396	-878	-1954	96
11	100.03	1347	1019	611	109	-429	-983	-2047	96
12	110.00	1497	1133	667	117	-461	-1100	-2237	96
13	118.40	1638	1226	716	125	-510	-1222	-2427	96
14	129.94	1820	1359	785	138	-562	-1290	-2698	96
15	138.95	2095	1501	825	51	-777	-1626	-3454	92
16	145.62	2358	1675	862	-36	-1007	-1982	-4174	89
17	157.46	2743	1832	853	-255	-1460	-2662	-5517	62.5

† Average cube strength = 100 *MPa* and ρ =4.04%

Appendix B

Characterstic of midspan load-deflection curves for beamns in flexure

App.Table 1.18- The Characteristic of Load-Deflection Curve for HSC1-1 Beam

Stage	*Load (kN)*	*Test Results (mm)*	*Analysis (mm)*	*Actual / Theory*
1	0.00	0.00	0.00	0.00
2	4.90	0.45	0.49	0.92
3	9.70	1.25	1.45	0.86
4	15.10	2.90	2.66	1.09
5	19.80	5.30	3.86	1.37
6	25.50	7.90	5.47	1.44
7	30.20	10.09	6.90	1.46
8	35.20	12.30	8.52	1.44
9	40.20	14.53	10.23	1.42
10	45.10	16.76	11.98	1.40
11	49.80	18.88	13.72	1.38
12	50.70	26.90	29.11	0.92
13	52.40	31.69	29.08	1.09

App.Table 1.19- The Characteristic of Load-Deflection Curve for HSC1-2 Beam

Stage	*Load (kN)*	*Test Results (mm)*	*Analysis (mm)*	*Actual / Theory*
1	00	0.0	0.00	0.00
2	5.00	0.31	0.61	0.51
3	9.80	0.92	1.49	0.62
4	14.70	2.18	2.60	0.84
5	19.60	4.19	3.87	1.08
6	24.90	6.03	5.37	1.12
7	29.80	7.74	6.88	1.13
8	35.20	9.64	8.65	1.12
9	40.00	11.38	10.31	1.10
10	44.90	13.00	12.08	1.08
11	46.40	15.35	12.64	1.21
12	52.80	21.58	27.15	0.79
13	53.50	23.63	27.14	0.87
14	54.70	25.03	27.13	0.92

App.Table 1.20- The Characteristic of Load-Deflection Curve for HSC1-3 Beam

Stage	*Load (kN)*	*Test Results (mm)*	*Analysis (mm)*	*Actual / Theory*
1	0.0	0.00	0.00	0.00
2	6.10	0.84	1.02	0.82
3	11.10	1.92	1.86	1.03
4	15.30	3.56	2.89	1.23
5	20.50	5.32	4.31	1.23
6	25.10	7.10	5.70	1.25
7	30.00	9.02	7.28	1.24
8	35.10	10.77	9.03	1.19
9	40.40	12.67	10.95	1.16
10	45.80	14.44	13.02	1.11
11	50.20	16.01	14.76	1.08
12	52.40	19.51	27.33	0.71
13	55.20	24.04	27.30	0.88
14	56.90	30.36	27.28	1.11

App.Table 1.21- The Characteristic of Load-Deflection Curve for HSC2-1 Beam

Stage	*Load (kN)*	*Test Results (mm)*	*Analysis (mm)*	*Actual / Theory*
1	0.00	0.00	0.00	0.00
2	6.30	0.23	0.79	0.29
3	10.40	0.73	1.31	0.56
4	15.20	1.47	2.21	0.67
5	19.80	2.68	3.17	0.84
6	25.30	4.35	4.44	0.98
7	30.70	6.03	5.79	1.04
8	35.10	7.50	6.97	1.08
9	40.00	8.87	8.34	1.06
10	45.10	10.40	9.83	1.06
11	49.20	12.06	11.08	1.09
12	55.10	13.76	12.94	1.06
13	60.30	15.22	14.65	1.04
14	64.80	16.77	16.17	1.04
15	65.70	20.84	23.19	0.90
16	68.70	24.49	23.17	1.06
17	70.20	26.94	23.16	1.16

App Table 1.22- The Characteristic of Load-Deflection Curve of HSC2-2 Beam

Stage	*Load (kN)*	*Test Results (mm)*	*Analysis (mm)*	*Actual / Theory*
1	0.00	0.00	0.00	0.00
2	6.10	0.27	0.48	0.56
3	10.00	0.67	1.29	0.52
4	15.10	1.41	2.27	0.62
5	19.50	2.60	3.23	0.81
6	24.70	4.00	4.46	0.90
7	30.20	5.61	5.88	0.95
8	35.30	7.11	7.29	0.98
9	40.20	8.54	8.72	0.98
10	45.10	9.92	10.21	0.97
11	50.60	11.65	11.96	0.97
12	55.30	12.93	13.51	0.96
13	59.80	14.22	15.04	0.95
14	65.20	15.89	16.94	0.94
15	65.70	24.77	26.09	0.95
16	70.40	28.54	26.05	1.10
17	71.00	35.55	26.04	1.37

App.Table 1.23- The Characteristic of Load-Deflection Curve of HSC2-3 Beam

Stage	*Load (kN)*	*Test Results (mm)*	*Analysis (mm)*	*Actual / Theory*
1	0.0	0.0	0.00	0.00
2	5.11	0.72	0.52	1.39
3	10.33	2.16	1.05	2.06
4	15.17	3.81	1.67	2.29
5	20.20	5.49	3.45	1.59
6	25.31	7.16	5.40	1.33
7	30.26	8.76	7.23	1.21
8	35.45	10.48	9.05	1.16
9	39.77	11.96	10.49	1.14
10	45.22	13.76	12.25	1.12
11	49.86	15.41	13.71	1.12
12	55.06	17.27	15.31	1.13
13	60.24	19.36	16.89	1.15
14	62.41	24.08	17.54	1.37
15	66.00	29.12	18.61	1.56
16	60.36	36.01	16.92	2.13

App.Table 1.24 - The Characteristic of Load-Deflection Curve of HSC2-4 Beam

Stage	*Load (kN)*	*Test Results (mm)*	*Analysis (mm)*	*Actual / Theory*
1	0.00	0.00	0.00	0.00
2	5.43	0.39	0.39	0.99
3	10.10	0.97	1.39	0.70
4	15.02	1.87	2.39	0.78
5	20.05	3.35	3.56	0.94
6	24.51	4.74	4.69	1.01
7	30.23	6.47	6.25	1.04
8	34.90	7.99	7.61	1.05
9	40.34	9.47	9.29	1.02
10	44.64	10.82	10.68	1.01
11	50.56	12.46	12.67	0.98
12	55.42	13.82	14.37	0.96
13	64.63	16.36	17.75	0.92
14	69.18	23.25	28.01	0.83
15	72.91	28.83	27.98	1.03
16	74.56	34.33	27.96	1.23

App.Table 1.25- The Characteristic of Load-Deflection Curve of HSC3-1 Beam

Stage	*Load (kN)*	*Test Results (mm)*	*Analysis (mm)*	*Actual / Theory*
1	0.00	0.00	0.00	0.00
2	5.89	0.54	0.32	1.69
3	10.30	1.10	0.91	1.20
4	20.00	3.13	2.27	1.38
5	25.05	4.50	3.10	1.45
6	30.36	5.74	4.03	1.42
7	35.53	6.83	5.01	1.36
8	40.37	7.97	5.97	1.34
9	44.95	9.03	6.92	1.31
10	55.26	11.27	9.19	1.23
11	60.12	12.39	10.31	1.20
12	65.79	13.57	11.67	1.16
13	70.10	14.54	12.74	1.14
14	75.29	15.61	14.05	1.11
15	80.29	16.76	15.35	1.09
16	85.44	17.89	16.72	1.07
17	90.76	19.11	18.16	1.05
18	95.42	20.16	19.46	1.04
19	96.39	23.37	23.88	0.98
20	97.95	25.15	23.87	1.05
21	100.72	28.89	23.85	1.21
22	101.75	30.61	23.85	1.28
23	104.73	40.28	23.83	1.69

App.Table 1.26- The Characteristic of Load-Deflection Curve of HSC3-2 Beam

Stage	*Load (kN)*	*Test Results (mm)*	*Analysis (mm)*	*Actual / Theory*
1	0.0	0.0	0.00	0.00
2	10.35	0.76	0.73	1.05
3	19.88	2.08	2.64	0.79
4	30.57	4.24	4.77	0.89
5	34.90	5.21	5.72	0.91
6	40.02	6.38	6.90	0.92
7	45.11	7.64	8.13	0.94
8	49.78	8.77	9.31	0.94
9	55.59	10.14	10.84	0.94
10	60.01	11.24	12.04	0.93
11	65.33	12.57	13.53	0.93
12	70.06	13.85	14.90	0.93
13	75.20	15.14	16.42	0.92
14	80.00	16.42	17.87	0.92
15	84.77	17.53	19.35	0.91
16	89.80	18.79	20.95	0.90
17	94.70	20.20	22.54	0.90
18	94.64	22.88	31.25	0.73
19	99.22	27.24	31.22	0.87
20	101.16	29.65	31.21	0.95

App.Table 1.27- The Characteristic of Load-Deflection Curve of HSC3-3 Beam

Stage	*Load (kN)*	*Test Results (mm)*	*Analysis (mm)*	*Actual / Theory*
1	0.00	0.00	0.00	0.00
2	5.28	0.14	0.42	0.34
3	10.25	0.67	1.14	0.59
4	15.09	1.37	1.94	0.71
5	20.28	2.29	2.91	0.79
6	24.99	3.22	3.87	0.83
7	30.15	4.36	5.01	0.87
8	34.99	5.36	6.15	0.87
9	40.23	6.48	7.45	0.87
10	45.28	7.55	8.77	0.86
11	50.71	8.72	10.25	0.85
12	55.21	9.69	11.51	0.84
13	60.01	10.93	12.91	0.85
14	65.46	12.03	14.55	0.83
15	70.32	13.18	16.06	0.82
16	74.92	14.29	17.52	0.82
17	80.18	15.54	19.23	0.81
18	90.05	17.9	22.55	0.79
19	95.12	19.32	24.31	0.79
20	99.62	20.54	25.91	0.79
21	99.24	22.5	35.45	0.63
22	98.52	22.52	35.45	0.64
23	97.23	29.72	35.46	0.84
24	94.81	32.54	35.48	0.92

App.Table 1.28- The Characteristic of Load-Deflection Curve of HSC4-1 Beam

Stage	*Load (kN)*	*Test Results (mm)*	*Analysis (mm)*	*Actual / Theory*
1	0.00	0.00	0.00	0.00
2	11.94	1.25	0.76	1.65
3	20.26	2.39	1.79	1.34
4	30.62	4.01	3.15	1.27
5	40.59	5.71	4.64	1.23
6	50.63	7.47	6.29	1.19
7	60.3	9.20	7.99	1.15
8	69.75	10.92	9.76	1.12
9	79.87	12.67	11.76	1.08
10	90.22	14.61	13.90	1.05
11	100.32	16.50	16.08	1.03
12	110.61	18.54	18.39	1.01
13	120.46	20.47	20.68	0.99
14	129.88	22.60	22.93	0.99
15	140.04	24.91	25.43	0.98
16	139.70	29.85	36.18	0.83
17	135.12	32.50	36.21	0.90
18	113.29	35.33	36.36	0.97

App.Table 1.29- The Characteristic of Load-Deflection Curve of HSC4-2 Beam

Stage	*Load (kN)*	*Test Results (mm)*	*Analysis (mm)*	*Actual / Theory*
1	0.00	0.00	0.00	0.00
2	9.95	1.09	0.66	1.64
3	19.76	2.86	1.84	1.56
4	29.67	4.71	3.21	1.47
5	39.98	6.77	4.84	1.40
6	50.24	8.88	6.62	1.34
7	59.86	10.91	8.42	1.30
8	70.04	13.04	10.45	1.25
9	79.61	15.24	12.46	1.22
10	89.90	17.32	14.72	1.18
11	99.90	19.41	17.02	1.14
12	109.89	21.59	19.40	1.11
13	119.89	23.88	21.87	1.09
14	128.80	26.09	24.13	1.08
15	134.76	27.90	25.68	1.09
16	140.23	29.60	27.12	1.09
17	142.49	31.48	27.72	1.14
18	140.46	32.96	35.69	0.92
19	139.89	32.98	35.69	0.92

App.Table 1.30- The Characteristic of Load-Deflection Curve of HSC4-3 Beam

Stage	*Load (kN)*	*Test Results (mm)*	*Analysis (mm)*	*Actual / Theory*
1	0.00	0.00	0.00	0.00
2	10.42	0.83	0.72	1.16
3	19.92	1.96	1.82	1.07
4	30.02	3.36	3.21	1.05
5	39.66	4.76	4.70	1.01
6	49.89	6.35	6.44	0.99
7	60.37	7.99	8.37	0.95
8	69.68	9.35	10.19	0.92
9	80.01	10.97	12.33	0.89
10	89.92	12.51	14.47	0.86
11	99.90	14.15	16.72	0.85
12	109.98	15.81	19.09	0.83
13	120.24	17.64	21.57	0.82
14	129.67	19.52	23.93	0.82
15	139.49	21.43	26.46	0.81
16	149.57	23.59	32.19	0.73
17	159.25	26.10	32.14	0.81
18	169.14	29.27	32.09	0.91
19	137.57	31.33	32.25	0.97

App.Table 1.31- The Characteristic of Load-Deflection Curve of DHSC1-1 Beam

Stage	*Load (kN)*	*Test Results (mm)*	*Analysis (mm)*	*Actual / Theory*
1	0.00	0.00	0.00	0.00
2	9.92	0.99	0.64	1.55
3	19.99	2.24	1.75	1.28
4	29.90	3.70	3.04	1.22
5	39.78	5.22	4.50	1.16
6	50.12	6.68	6.18	1.08
7	59.72	8.15	7.87	1.04
8	69.80	9.79	9.75	1.00
9	80.07	11.32	11.77	0.96
10	89.76	12.85	13.77	0.93
11	99.89	14.38	15.95	0.90
12	109.84	16.00	18.17	0.88
13	119.98	17.65	20.52	0.86
14	129.46	19.18	22.78	0.84
15	130.68	19.53	23.07	0.85
16	140.18	21.03	25.41	0.83
17	149.66	22.97	27.80	0.83
18	154.42	24.19	29.02	0.83
19	159.57	25.47	30.36	0.84
20	162.28	27.19	31.07	0.88
21	164.71	28.94	31.71	0.91
22	166.51	31.06	32.19	0.96
23	150.81	31.44	38.15	0.82
24	144.04	35.93	38.19	0.94
25	135.90	37.10	38.24	0.97

App.Table 1.32- The Characteristic of Load-Deflection Curve of DHSC1-2 Beam

Stage	*Load (kN)*	*Test Results (mm)*	*Analysis (mm)*	*Actual / Theory*
1	0.00	0.00	0.00	0.00
2	10.02	0.99	0.69	1.43
3	19.83	2.28	1.83	1.25
4	29.86	3.93	3.26	1.20
5	39.75	5.75	4.90	1.17
6	50.18	7.63	6.82	1.12
7	60.00	9.40	8.79	1.07
8	70.04	11.28	10.95	1.03
9	80.01	12.98	13.23	0.98
10	90.13	14.92	15.67	0.95
11	99.97	16.63	18.16	0.92
12	109.88	18.51	20.76	0.89
13	114.99	19.48	22.15	0.88
14	120.28	20.73	23.61	0.88
15	125.07	21.47	24.96	0.86
16	130.25	22.74	26.44	0.86
17	134.82	23.75	27.76	0.86
18	140.10	25.17	29.32	0.86
19	145.13	27.16	30.83	0.88
20	147.61	29.21	31.58	0.93
21	148.66	30.47	31.90	0.96
22	149.53	32.80	32.16	1.02
23	147.15	33.83	31.44	1.08
24	138.09	35.19	28.72	1.23
25	133.08	36.33	27.26	1.33

App.Table 1.33- The Characteristic of Load-Deflection Curve of DHSC1-3 Beam

Stage	*Load (kN)*	*Test Results (mm)*	*Analysis (mm)*	*Actual / Theory*
1	0.00	0.00	0.00	0.00
2	10.05	0.94	0.65	1.46
3	20.45	2.14	1.80	1.19
4	30.23	3.49	3.09	1.13
5	40.20	4.89	4.56	1.07
6	50.52	6.37	6.25	1.02
7	60.29	7.75	7.97	0.97
8	75.91	10.09	10.93	0.92
9	85.57	11.55	12.89	0.90
10	95.40	13.06	14.97	0.87
11	110.31	15.26	18.27	0.84
12	119.96	16.83	20.50	0.82
13	130.43	18.49	23.00	0.80
14	140.51	20.35	25.48	0.80
15	145.29	21.46	26.68	0.80
16	150.24	22.52	27.93	0.81
17	155.37	23.98	29.25	0.82
18	157.12	24.46	29.71	0.82
19	166.03	28.41	32.05	0.89
20	168.72	30.07	32.76	0.92
21	169.31	31.47	32.92	0.96

App.Table 1.34- The Characteristic of Load-Deflection Curve of DHSC1-4 Beam

Stage	*Load (kN)*	*Test Results (mm)*	*Analysis (mm)*	*Actual / Theory*
1	0.00	0.00	0.00	0.00
2	10.84	0.79	0.69	1.15
3	19.99	2.11	2.15	0.98
4	27.00	3.24	3.25	1.00
5	29.79	4.22	3.71	1.14
6	39.94	5.63	5.54	1.02
7	50.80	7.43	7.70	0.96
8	60.25	9.12	9.73	0.94
9	70.11	10.78	11.97	0.90
10	80.63	12.61	14.49	0.87
11	90.84	14.35	17.06	0.84
12	100.34	16.04	19.54	0.82
13	110.00	17.70	22.16	0.80
14	119.46	19.44	24.81	0.78
15	125.05	20.48	26.41	0.78
16	129.99	21.33	27.84	0.77
17	139.41	23.89	30.64	0.78
18	144.67	25.46	32.23	0.79
19	159.14	31.20	36.72	0.85
20	160.92	32.27	37.28	0.87
21	166.23	35.17	38.98	0.90
22	169.01	37.08	39.87	0.93

Appendix C

Characteristic of midspan moment-rotation curves

Moment-rotation at midspan of HSC 1-1 beam

load, kN	*Moment, kN.m*	*Rotation, (10^{-5} Radians)*
0.00	0.00	0
4.90	3.23	10
9.80	6.47	26
15.30	10.10	57
20.10	13.27	92
24.10	15.91	123
29.10	19.21	155
34.10	22.51	185
39.00	25.74	209
43.80	28.91	239
50.00	33.00	273
52.00	34.32	836
53.00	34.98	1,067
54.00	35.64	1,380
56.00	36.96	1,777
59.00	38.94	2,135

Moment-rotation at midspan of HSC 1-2 beam

load, kN	*Moment, kN.m*	*Rotation, (10^{-5} Radians)*
0.00	0.00	0
4.90	6.07	31
9.20	9.24	72
14.00	12.41	114
18.80	16.50	159
25.00	19.67	213
29.80	22.70	249
34.40	25.94	290
39.30	29.11	337
44.10	30.56	503
46.30	33.66	1,001
51.00	34.58	1,226
52.40	35.05	1,737
53.10	35.31	1,780

Moment-rotation at midspan of HSC 1-3 beam

load, kN	*Moment, kN.m*	*Rotation, (10^{-5} Radians)*
0.00	0.00	0
5.80	3.83	13
10.60	7.00	34
14.90	9.83	62
20.00	13.20	85
24.30	16.04	115
29.10	19.21	146
34.30	22.64	164
39.80	26.27	202
45.00	29.70	230
49.00	32.34	260
52.00	34.32	465
55.00	36.30	795
57.00	37.62	1,085

Moment-rotation at midspan of HSC 2-1 beam

load, kN	*Moment, kN.m*	*Rotation, (10^{-5} Radians)*
0.00	0.00	0
5.30	3.50	35
6.10	4.03	36
10.40	6.86	48
15.20	10.03	69
19.10	12.61	70
25.00	19.80	127
30.00	23.10	179
35.00	26.40	236
40.00	29.11	216
44.10	33.07	231
50.10	36.37	303
55.10	39.20	303
59.40	42.90	352
65.00	43.03	614
65.20	44.02	834
66.70	44.95	924
68.10	46.86	1,113

Moment-rotation at midspan of HSC 2-2 beam

load, kN	*Moment, kN.m*	*Rotation, (10^{-5} Radians)*
0.00	0.00	0
6.10	4.03	9
9.80	6.47	15
14.20	9.37	35
18.60	12.28	62
23.80	15.71	88
29.40	19.40	116
34.40	22.70	142
39.40	26.00	169
44.60	29.44	189
50.40	33.26	216
55.00	36.30	242
59.00	38.94	261
64.70	42.70	285
66.00	43.56	584
70.00	46.20	820
71.00	46.86	822
71.50	47.19	1,038
72.50	47.85	1,152

Moment-rotation at midspan of HSC 2-3 beam

load, kN	*Moment, kN.m*	*Rotation, (10^{-5} Radians)*
0.00	0.00	0
5.11	6.88	29
10.33	13.15	34
15.17	19.81	56
20.20	26.18	75
25.31	32.93	115
30.26	39.84	120
35.45	45.99	147
39.77	52.81	175
45.22	59.35	190
49.86	65.93	234
55.06	72.59	256
60.24	79.36	337
62.41	85.58	457
66.00	92.06	886

Moment-rotation at midspan of HSC 2-4 beam

load, kN	*Moment, kN.m*	*Rotation, (10^{-5} Radians)*
0.00	0.00	0
5.43	3.58	12
10.31	6.80	22
15.42	10.18	37
20.20	13.33	59
25.02	16.51	93
30.38	20.05	104
34.90	23.03	171
40.88	26.98	185
44.77	29.55	201
51.03	33.68	231
55.57	36.68	229
65.18	43.02	295
68.48	45.20	649
73.65	48.61	926
74.00	48.84	1,180

Moment-rotation at midspan of HSC 3-1 beam

load, kN	*Moment, kN.m*	*Rotation, (10^{-5} Radians)*
0.00	0.00	0
6.04	3.99	0
10.00	6.60	13
20.00	13.20	64
25.00	16.50	71
30.00	19.80	99
35.00	23.10	117
40.00	26.40	132
45.00	29.70	148
55.00	36.30	191
60.00	39.60	207
65.00	42.90	236
70.00	46.20	259
75.00	49.50	277
80.00	52.80	287
85.00	56.10	300
90.00	59.40	309
95.00	62.70	342
100.00	66.00	601
97.00	64.02	781
100.00	66.00	1,043
103.00	67.98	1,056
102.00	67.32	1,192
102.00	67.32	1,392

Moment-rotation at midspan of HSC 3-2 beam

load, kN	*Moment, kN.m*	*Rotation, (10^{-5} Radians)*
0.00	0.00	0
10.00	6.60	56
20.00	13.20	100
30.00	19.80	160
35.00	23.10	197
40.00	26.40	219
45.00	29.70	234
50.00	33.00	266
55.00	36.30	312
60.00	39.60	320
65.00	42.90	299
70.00	46.20	366
75.00	49.50	386
80.00	52.80	414
85.00	56.10	430
90.00	59.40	451
95.00	62.70	495
94.00	62.04	737
96.00	63.36	894
100.00	66.00	1,005
102.00	67.32	1,171
94.00	62.04	1,419

Moment-rotation at midspan of HSC 3-3 beam

load, kN	*Moment, kN.m*	*Rotation, (10^{-5} Radians)*
0.00	0.00	0
5.28	3.48	18
10.25	6.77	24
15.09	9.96	52
20.28	13.38	76
24.99	16.49	107
30.15	19.90	132
34.99	23.09	155
40.23	26.55	161
45.28	29.88	191
50.71	33.47	213
55.21	36.44	239
60.01	39.61	260
65.46	43.20	271
70.32	46.41	290
74.92	49.45	326
80.18	52.92	347
90.05	59.43	397
95.12	62.78	401
99.62	65.75	620
99.24	65.50	818
98.52	65.02	1,122

Moment-rotation at midspan of HSC 4-1 beam

load, kN	*Moment, KN.m*	*Rotation, (10^{-5} Radians)*
0 .00	0.00	0
12	7.88	25
20	13.37	60
31	20.21	106
41	26.79	133
51	33.42	153
60	39.80	195
70	46.04	227
80	52.71	273
90	59.55	324
100	66.21	346
111	73.00	395
120	79.50	456
130	85.72	476
140	92.43	517

Moment-rotation at midspan of HSC 4-2 beam

load, kN	*Moment, kN.m*	*Rotation, (10^{-5} Radians)*
0.00	0.00	0
9.95	6.57	25
19.76	13.04	71
29.67	19.58	115
39.98	26.39	160
50.24	33.16	205
59.86	39.51	255
70.04	46.23	304
79.61	52.54	354
89.90	59.33	404
99.90	65.93	458
109.89	72.53	515
119.89	79.13	582
128.80	85.01	662
134.76	88.94	728

Moment-rotation at midspan of HSC 4-3 beam

load, kN	*Moment, kN.m*	*Rotation, (10^{-5} Radians)*
0.00	0.00	0
10.42	6.88	23
19.92	13.15	46
30.02	19.81	94
39.66	26.18	109
49.89	32.93	133
60.37	39.84	138
69.68	45.99	211
80.01	52.81	244
89.92	59.35	260
99.90	65.93	291
109.98	72.59	317
120.24	79.36	347
129.67	85.58	372
139.49	92.06	404
149.57	98.72	445
159.25	105.11	472
169.14	111.63	571

Moment-rotation at midspan of DHSC1-1 beam

load, kN	*Moment, kN.m*	*Rotation, (10^{-5} Radians)*
0.00	0.00	0
9.84	6.49	23.11
19.73	13.02	40.36
30.04	19.83	66.81
40.00	26.40	93.72
49.75	32.84	121.35
59.20	39.07	144.99
69.80	46.07	162.25
79.64	52.56	201.98
89.99	59.39	232.28
99.15	65.44	249.75
109.61	72.34	286.53
118.39	78.14	314.30
129.61	85.54	346.88
139.35	91.97	372.51
148.52	98.02	422.56
156.10	103.03	510.77
160.92	106.21	581.68

Moment-rotation at midspan of DHSC1-2 beam

load, kN	*Moment, kN.m*	*Rotation, (10^{-5} Radians)*
0.00	0.00	0
10.02	6.61	19.91
19.83	13.09	47.88
29.86	19.71	83.20
39.75	26.24	120.85
50.18	33.12	152.85
60.00	39.60	188.99
70.04	46.23	227.38
80.01	52.81	260.19
90.13	59.49	301.09
99.97	65.98	337.59
109.88	72.52	372.89
114.99	75.89	422.45
120.28	79.38	475.47
130.25	85.97	569.97
140.10	92.47	642.81
149.53	98.69	752.79

Moment-rotation at midspan of DHSC1-3 beam

load, kN	*Moment, kN.m*	*Rotation, (10^{-5} Radians)*
0.00	0.00	0.00
10.05	6.63	21.19
20.45	13.50	33.54
30.23	19.95	75.60
40.20	26.53	116.86
60.29	39.79	138.42
75.91	50.10	161.03
85.57	56.48	183.47
95.40	62.96	208.27
110.31	72.80	233.56
119.96	79.17	253.59
130.43	86.08	279.47
140.51	92.74	306.54
150.24	99.16	337.81
157.12	103.70	398.21
169.31	111.74	477.22

Moment-rotation at midspan of DHSC1-4 beam

load, kN	*Moment, kN.m*	*Rotation, (10^{-5} Radians)*
0.00	0.00	0
10.84	7.15	11.46
19.99	13.19	33.27
29.79	19.66	63.91
39.94	26.36	93.54
50.80	33.53	124.07
60.25	39.77	155.71
70.11	46.27	189.42
80.63	53.22	217.33
90.84	59.95	249.90
100.34	66.22	280.36
110.00	72.60	311.53
119.46	78.84	341.57
129.99	85.79	379.63
139.41	92.01	456.33
150.00	99.00	531.23
160.00	105.60	660.03

Appendix D

1. Sample calculations of ultimate moment capacity of beam HSC1-1
2. Cracking patterns of some HSRC beams
3. Average load -strain curves reinforcements of beams
4. Calculated versus measured shear stress of HSRC beams

1. Sample Calculation for The Ultimate Moment Capacity Of Beam HSC 1-1

The neutral axis of the beam at ultimate was (c = 23.6 *mm*), and the flexural ultimate strain at the extreme compression fibre was (ε_u = 0.0024).

The equation of the stress block at ultimate load which developed using regression analysis can be written as :

$$\sigma c = 32144 \left(fc/fc\ \max\right)(\varepsilon)^{0.96}$$

The strain along the beam depth in the compression zone can be written as;

$$\varepsilon = \frac{\varepsilon_u}{n} y$$

where, ε_u = flexural ultimate strain

y= distance from neutral axis to the given fibre, *mm.*

n = neutral axis depth at ultimate load, *mm.*

$fc\ \max$= maximum cube strength, *MPa.*

Therefore, the above equation can be written as:

$$\sigma c = A \left(fc/fc\ \max\right)\left(\frac{\varepsilon u}{n} y\right)^{0.96}$$

where, A is constant.

The area under the curve is obtained by integrating between the neutral axis (n) and the top of the beam. This can be written as follows:

$$C = \int_0^n \sigma c.\ dy = \int_0^{23.6} \left\{ A \left(fc/fc\ \max\right)\left(\frac{0.0024}{23.6} y\right)^{0.96} \right\} dy$$

Where;

C= Compression force / mm width of beam.

$fc/fc\ \max$ = 1 for HSC beam.

A= 32144

On integation

$$C = 32144\left[\frac{0.0024}{23.6}\right]^{0.96}.\left[\frac{y}{1.96}\right]_0^{23.6}$$

$$C = 1182.38$$

The location of the centroid of C is then obtained by taking its moment about the neutral axis as given below:

$$\xi = {}^{1}\!/_{C}\int_0^n (\sigma c.y)\,dy$$

$$\xi = \frac{32144}{1182.38}\left[\left(\frac{0.0024}{23.6}\right)^{0.96}\ \frac{y^{2.96}}{2.96}\right]_0^{23.6}$$

$$\xi = 15.63\ mm$$

Then the distance from the extreme compression fibre to the resultant force (λ) is given by

$$\lambda = (n - \xi)$$

$$\lambda = (23.6 - 15.63) = 7.97\ mm$$

giving the ultimate nominal moment capacity of the beam, Mn:

$$M_n = C\ b\ (d - \lambda)$$

where, b and d are the width of the beam and the distance from the extreme compression fibre to the centroid of the tension reinforcement respectively.

$$M_n = 1182.38 * 150\ (220 - 7.97)\ *10^{-6}$$

$$M_n = 37.6\ kN.m$$

The actual moment capacity of the beam (M_u=38.94 $kN.m$)

Therefore; $$\frac{M_u}{M_n} = \frac{38.94}{37.60} = 1.03$$

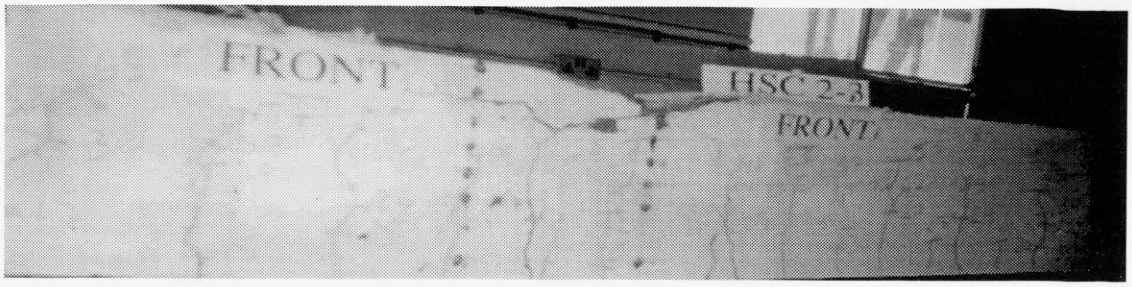

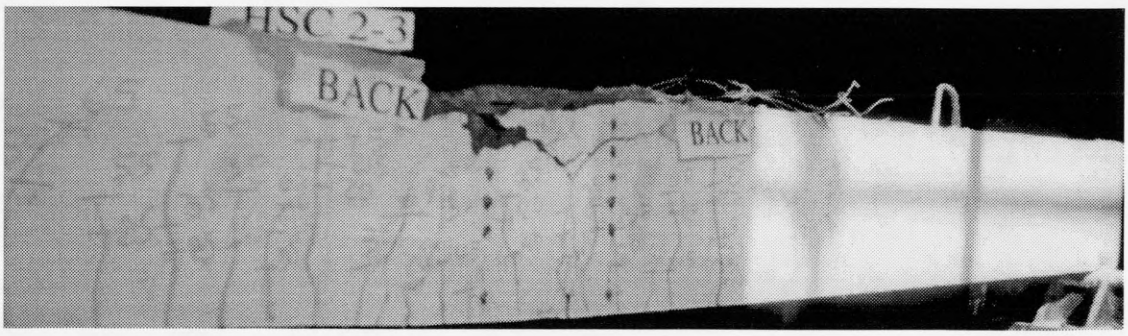

2.- Cracking Patterns of HSRC Beams in Flexure

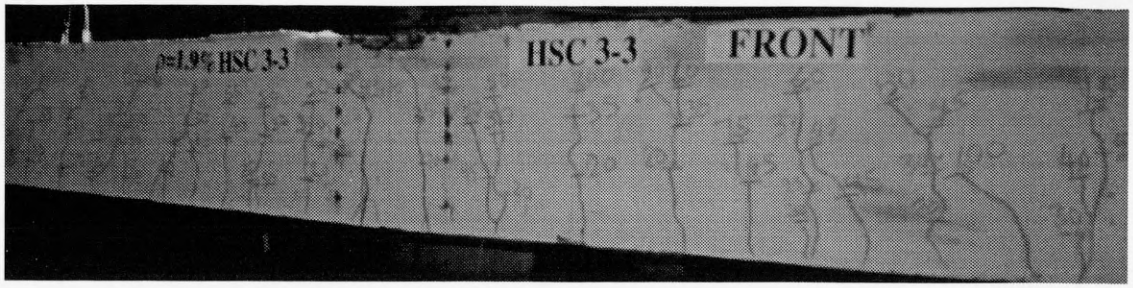

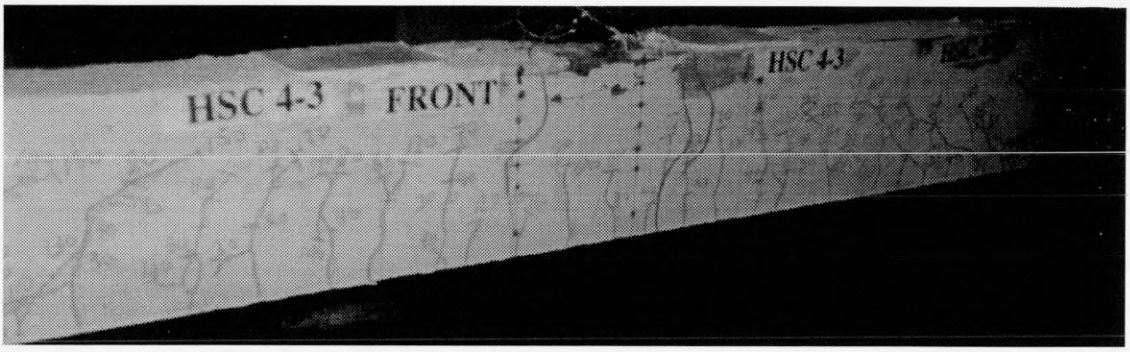

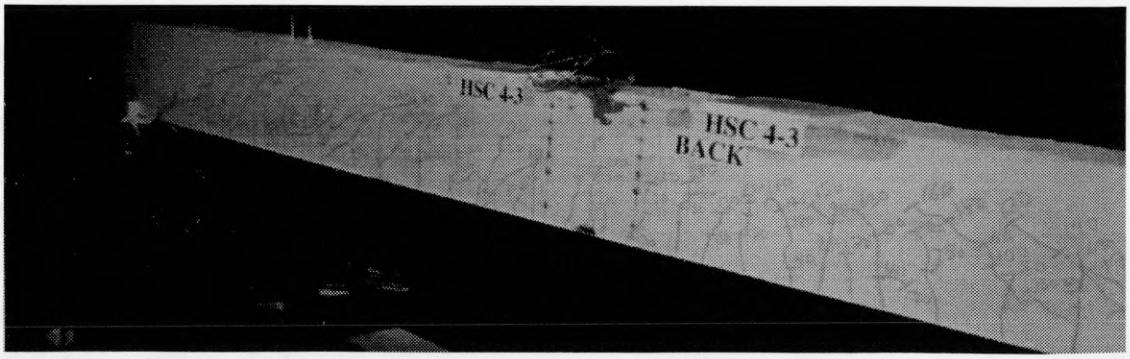

2.- Continued: Cracking Patterns of HSRC Beams in Flexure

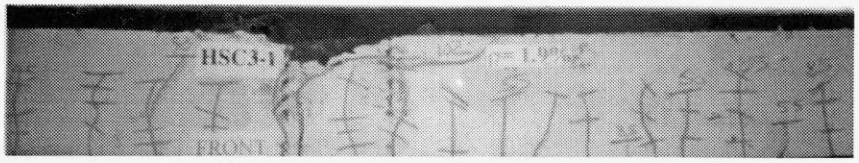

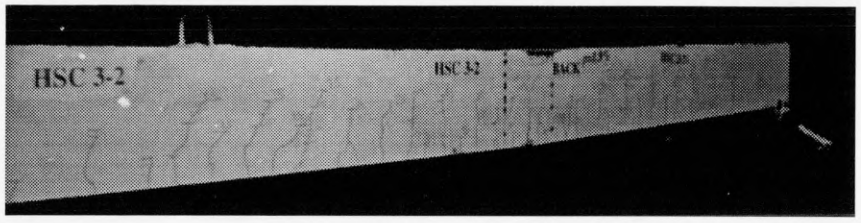

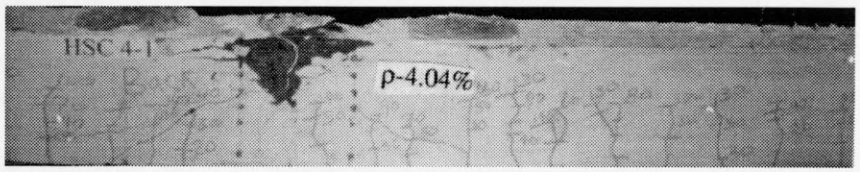

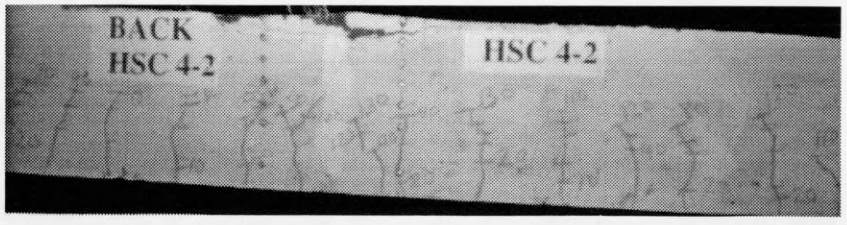

2.- Continued: Cracking Patterns of HSRC Beams in Flexure

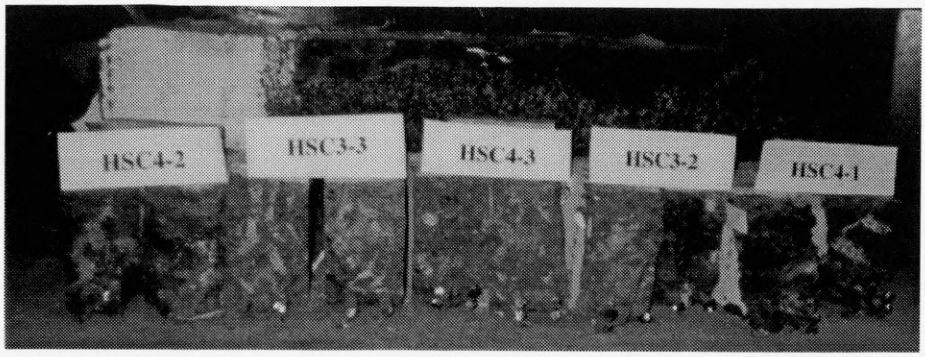

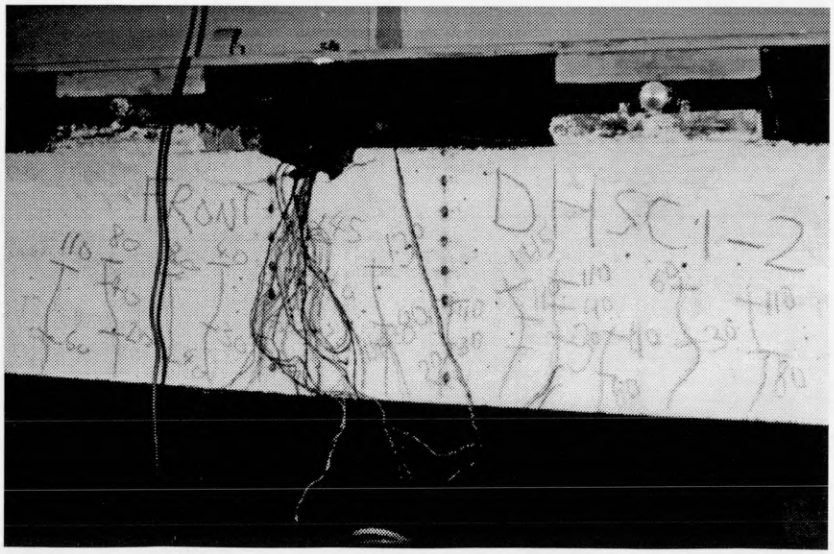

2.- Continued: Cracking Patterns of HSRC Beams in Flexure

Load -Avg. Strain of tensile reinforcement of group one

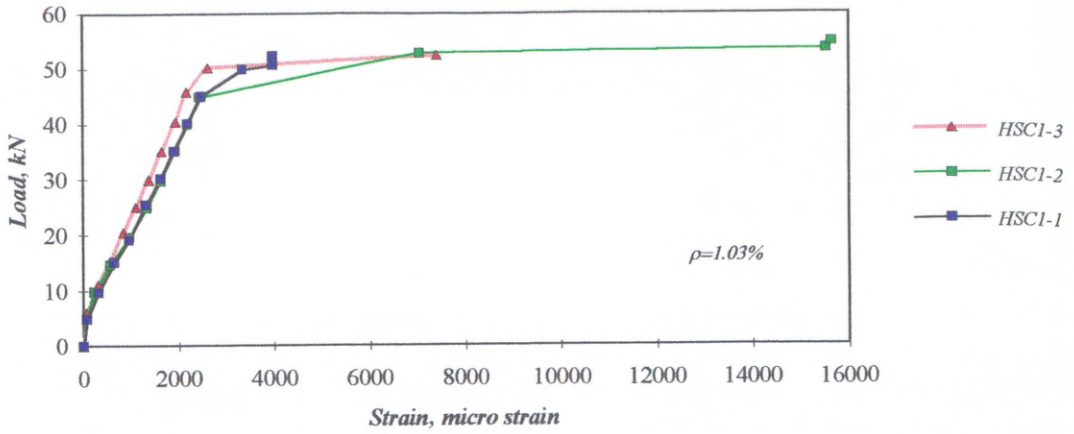

Load - Avg. strain of reinforcement of group two beams

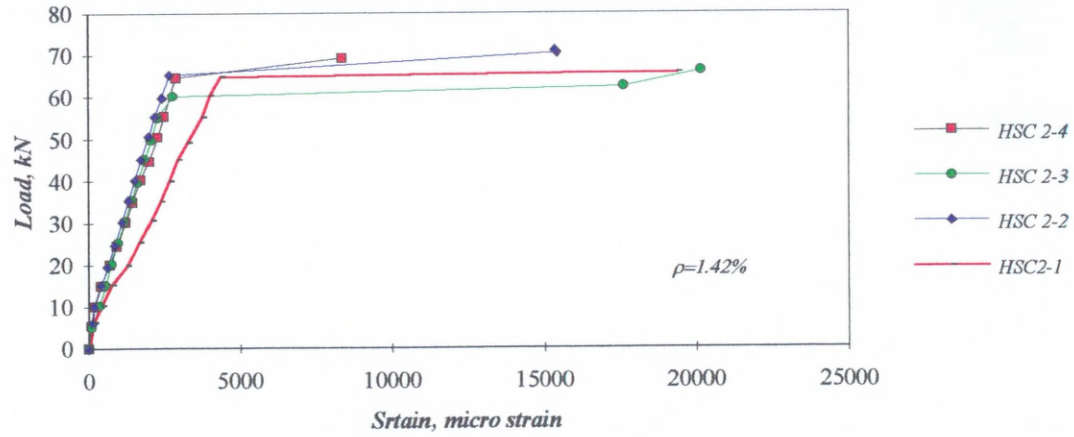

Load - Avg.Strain of tensile reinforcement of group three beams

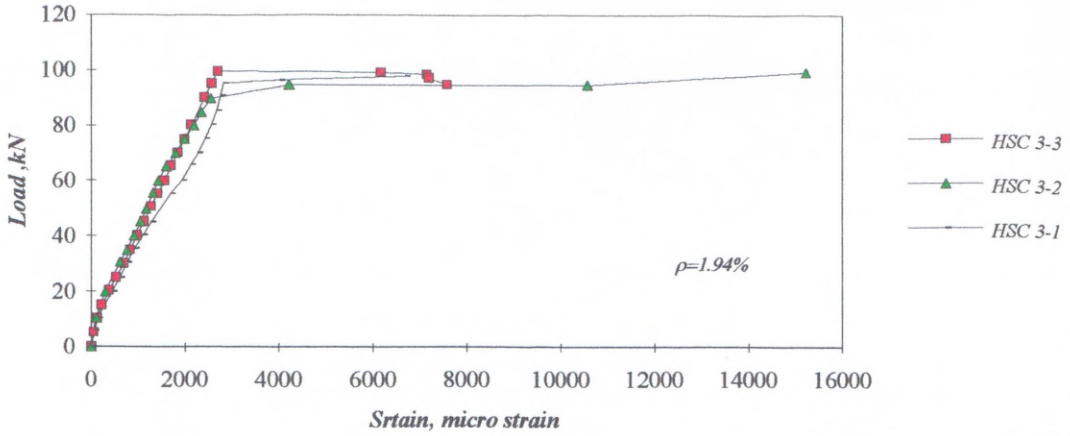

Load - Avg.Strain curve of tensile reinforcement of group four beams

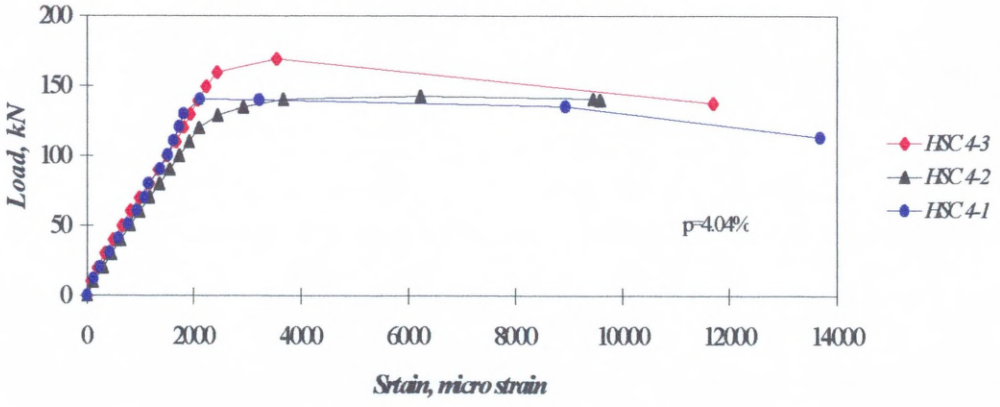

Comparsion of Test value with Calculated values; Proposed Equations 8.22, 8.23 and Zsutty's Equation(Eqn. 8.11)

fc, MPa	*fcu, MPa*	*d,mm*	*a/d*	*ρ*	*vu, Test MPa*	*vn, Calc. MPa*	*vn Cal./vu, Test*	*vn, Zsutty MPa*	*Zsutty/Test*
47.00	55.29	216	1	0.0207	5.68	3.83	0.67	5.40	0.95
41.34	48.64	216	2	0.0207	2.07	2.25	1.09	2.05	0.99
103.76	122.07	216	1	0.0207	8.80	6.41	0.73	7.03	0.80
103.36	121.60	216	2	0.0207	3.71	4.07	1.10	2.79	0.75
60.00	70.59	270	1.5	0.0187	4.62	3.23	0.70	3.30	0.71
61.00	71.76	203.2	2	0.0393	6.46	4.39	0.68	2.89	0.45
61.00	71.76	203.2	1	0.0393	15.52	6.88	0.44	7.29	0.47
61.00	71.76	208	2	0.0177	2.11	2.61	1.24	2.22	1.05
61.00	71.76	208	1	0.0177	5.06	4.10	0.81	5.59	1.10
67.00	78.82	201.68	2	0.0504	4.17	5.48	1.31	3.24	0.78
67.00	78.82	201.68	1	0.0504	8.00	8.60	1.08	8.17	1.02
67.00	78.82	208	2	0.0225	4.63	3.25	0.70	2.48	0.54
67.00	78.82	208	1	0.0225	8.00	5.09	0.64	6.25	0.78
64.40	75.76	184.15	2	0.0664	10.56	6.39	0.61	3.51	0.33
64.40	75.76	206.5	2	0.0326	4.07	4.02	0.99	2.77	0.68
64.40	75.76	206.5	1	0.0326	9.34	6.32	0.68	6.98	0.75
25.10	29.53	298.45	1.5	0.0336	2.55	2.68	1.05	3.00	1.18
45.49	53.52	298.45	1.5	0.0336	6.85	3.95	0.58	3.66	0.53
71.51	84.13	298.45	1.5	0.0336	9.51	5.30	0.56	4.25	0.45
86.42	101.67	298.45	1.5	0.0336	6.07	5.99	0.99	4.53	0.75
88.39	103.99	298.45	1.5	0.0336	10.88	6.08	0.56	4.56	0.42
66.12	77.79	203.2	2	0.00352	1.00	0.96	0.96	1.33	1.33
66.12	77.79	203.2	1	0.00352	2.31	1.51	0.65	3.35	1.45
72.86	85.72	208.03	2	0.0047	1.33	1.24	0.93	1.51	1.14
72.86	85.72	208.03	1	0.0047	3.05	1.94	0.64	3.81	1.25
70.00	82.35	212.85	2	0.0053	1.28	1.30	1.02	1.55	1.21

70.00	82.35	212.85	1	0.0053	2.16	2.05	0.95	3.92	1.81
69.00	81.18	279.4	2	0.012	1.60	2.20	1.37	2.03	1.27
69.00	81.18	279.4	2	0.025	2.23	3.54	1.59	2.59	1.16
55.00	64.71	171.45	0.52	0.0145	7.79	5.15	0.66	12.08	1.55
57.00	67.06	171.45	1.56	0.0145	4.34	2.58	0.59	2.83	0.65
70.38	82.80	171.45	0.52	0.0145	8.17	6.04	0.74	13.12	1.61
71.83	84.51	171.45	1.56	0.0145	4.17	3.00	0.72	3.05	0.73
82.45	97.00	220	2	0.0292	3.21	4.40	1.37	2.90	0.90
86.70	102.00	220	2	0.0194	2.74	3.48	1.27	2.57	0.94
90.95	107.00	220	2	0.0404	3.72	5.79	1.56	3.34	0.90
72.25	85.00	220	2	0.0292	2.28	4.04	1.77	2.77	1.22
35.98	42.33	220	2	0.0292	2.15	2.57	1.19	2.20	1.02
114.12	134.26	225	2	0.0292	3.21	5.43	1.69	3.23	1.01
120.00	141.18	225	2	0.0194	2.74	4.30	1.57	2.87	1.05
125.88	148.10	225	2	0.0404	3.72	7.15	1.92	3.72	1.00
100.00	117.65	225	2	0.0292	2.28	4.99	2.19	3.09	1.36
49.76	58.55	225	2	0.0292	2.25	3.17	1.41	2.45	1.09
69.00	81.18	230	2	0.012	1.69	2.20	1.30	2.03	1.20
69.00	81.18	230	2	0.025	2.43	3.54	1.46	2.59	1.07
39.72	46.73	216	3	0.0207	1.33	1.39	1.04	1.42	1.07
104.18	122.56	216	3	0.0207	1.67	2.12	1.27	1.95	1.17
60.00	70.59	270	3	0.0187	1.55	1.59	1.03	1.57	1.01
60.00	70.59	272	3	0.0101	1.25	1.21	0.97	1.28	1.02
60.00	70.59	267	3	0.0335	1.72	2.05	1.19	1.91	1.11
60.00	70.59	255	3	0.0467	2.20	2.38	1.08	2.13	0.97
60.00	70.59	270	4.5	0.0187	1.45	1.33	0.92	1.37	0.95
60.00	70.59	270	6	0.0187	1.33	1.17	0.88	1.25	0.94

61.00	71.76	203.2	4	0.0393	2.24	1.96	0.87	1.84	0.82
61.00	71.76	203.2	3	0.0393	2.67	2.22	0.83	2.02	0.76
61.00	71.76	203.2	2.7	0.0393	2.67	2.33	0.87	2.10	0.78
61.00	71.76	203.2	2.3	0.0393	3.62	4.01	1.11	2.40	0.66
61.00	71.76	208	4	0.0177	1.77	1.38	0.78	1.41	0.80
61.00	71.76	208	3	0.0177	1.60	1.56	0.98	1.55	0.97
61.00	71.76	208	2.7	0.0177	3.03	1.64	0.54	1.61	0.53
61.00	71.76	208	2.3	0.0177	3.03	2.39	0.79	1.84	0.61
67.00	78.82	201.68	4	0.0504	2.00	2.27	1.14	2.06	1.03
67.00	78.82	201.68	3	0.0504	2.70	2.58	0.96	2.27	0.84
67.00	78.82	201.68	2.7	0.0504	3.90	2.70	0.69	2.35	0.60
67.00	78.82	201.68	2.3	0.0504	5.60	5.01	0.89	2.69	0.48
67.00	78.82	208	4	0.0225	1.70	1.59	0.94	1.58	0.93
67.00	78.82	208	3	0.0225	1.70	2.49	1.47	1.73	1.02
67.00	78.82	208	2.7	0.0225	3.03	2.67	0.88	1.80	0.59
67.00	78.82	208	2.3	0.0225	2.43	2.96	1.22	2.06	0.85
64.40	75.76	184.15	4	0.0664	2.32	2.52	1.09	2.23	0.96
64.40	75.76	184.15	3	0.0664	3.20	2.86	0.89	2.45	0.77
64.40	75.76	184.15	2.7	0.0664	2.95	3.00	1.02	2.54	0.86
64.40	75.76	184.15	2.3	0.0664	3.80	3.67	0.96	2.91	0.77
64.40	75.76	206.5	4	0.0326	1.73	1.84	1.07	1.76	1.02
64.40	75.76	206.5	3	0.0326	1.70	2.09	1.23	1.94	1.14
64.40	75.76	206.5	2.7	0.0326	1.73	2.19	1.27	2.00	1.16
64.40	75.76	206.5	2.3	0.0326	2.17	2.31	1.06	2.30	1.06
22.57	26.55	298.45	3.6	0.0336	1.42	1.23	0.87	1.30	0.91
29.51	34.72	298.45	3.6	0.0232	1.47	1.33	0.90	1.25	0.85
40.97	48.20	298.45	3.6	0.0336	1.81	1.60	0.89	1.58	0.87
45.27	53.26	298.45	3.6	0.0336	1.82	1.68	0.92	1.64	0.90

81.50	95.88	298.45	3.6	0.0336	1.97	2.17	1.10	1.99	1.01
81.18	95.51	298.45	3.6	0.0336	1.97	2.17	1.10	1.99	1.01
88.45	104.06	298.45	3.6	0.0336	2.06	2.25	1.09	2.05	0.99
101.90	119.88	298.45	3.6	0.0336	2.20	2.40	1.09	2.14	0.97
99.89	117.52	298.45	3.6	0.0336	2.15	2.38	1.10	2.13	0.99
22.39	26.34	298.45	2.5	0.0336	1.71	1.79	1.04	1.46	0.85
49.12	57.79	298.45	2.5	0.0336	2.60	2.98	1.15	1.90	0.73
86.23	101.45	298.45	2.5	0.0336	2.45	4.29	1.75	2.29	0.93
91.10	107.18	298.45	2.5	0.0336	3.91	4.45	1.14	2.33	0.60
75.50	88.82	298.45	2.5	0.0336	4.53	3.94	0.87	2.19	0.48
66.12	77.79	203.2	4	0.00352	0.50	0.70	1.40	0.85	1.69
66.12	77.79	203.2	3	0.00352	0.68	0.80	1.17	0.93	1.37
66.12	77.79	203.2	2.7	0.00352	0.76	0.79	1.04	0.96	1.27
66.12	77.79	203.2	2.3	0.00352	0.91	0.88	0.97	1.02	1.12
72.86	85.72	208.03	4	0.0047	0.62	0.83	1.34	0.96	1.55
72.86	85.72	208.03	3	0.0047	0.91	0.94	1.04	1.06	1.16
72.86	85.72	208.03	2.7	0.0047	1.00	0.99	0.99	1.10	1.10
72.86	85.72	208.03	2.3	0.0047	1.15	1.13	0.98	1.26	1.09
70.00	82.35	212.85	4	0.0053	0.58	0.86	1.48	0.99	1.70
70.00	82.35	212.85	3	0.0053	0.83	0.98	1.18	1.09	1.31
70.00	82.35	212.85	2.7	0.0053	0.90	1.02	1.14	1.13	1.25
70.00	82.35	212.85	2.3	0.0053	1.13	1.19	1.05	1.29	1.14
20.70	24.35	279.4	4	0.006	0.74	0.41	0.55	0.69	0.93
20.70	24.35	279.4	4	0.012	0.92	0.72	0.78	0.86	0.94
20.70	24.35	279.4	4	0.025	1.12	1.00	0.89	1.10	0.99
40.02	47.08	279.4	4	0.01	0.95	0.89	0.94	1.01	1.07
40.02	47.08	279.4	4	0.012	0.96	0.96	1.00	1.08	1.12
40.02	47.08	279.4	4	0.025	1.34	1.33	0.99	1.37	1.03

Appendix-D , Continued

66.00	77.65	279.4	4	0.012	1.21	1.20	0.99	1.27	1.05
66.00	77.65	279.4	4	0.025	1.39	1.66	1.19	1.62	1.17
66.00	77.65	279.4	4	0.033	1.62	1.88	1.16	1.78	1.10
79.35	93.35	279.4	4	0.016	1.31	1.48	1.13	1.49	1.14
79.35	93.35	279.4	4	0.025	1.41	1.80	1.28	1.73	1.22
63.50	74.71	279.4	6	0.012	0.90	0.99	1.10	1.10	1.22
63.50	74.71	279.4	6	0.025	1.28	1.36	1.07	1.40	1.09
35.88	42.21	260	5.76	0.0065	0.58	0.60	1.03	0.75	1.29
37.32	43.91	235	6.38	0.0144	1.12	0.82	0.74	0.96	0.85
57.50	67.65	259	5.79	0.0101	0.76	0.89	1.17	1.01	1.33
56.03	65.92	231	6.46	0.0226	1.35	1.20	0.89	1.27	0.94
75.76	89.13	257	5.82	0.0145	1.05	1.18	1.12	1.25	1.19
75.97	89.38	229	6.55	0.0326	1.92	1.60	0.83	1.58	0.82
57.00	67.06	171.45	2.59	0.0145	1.53	1.48	0.97	1.49	0.97
52.11	61.31	171.45	3.63	0.0145	1.25	1.23	0.98	1.29	1.03
70.50	82.94	171.45	2.59	0.0145	1.71	1.63	0.95	1.60	0.94
72.73	85.56	171.45	3.63	0.0145	1.15	1.42	1.24	1.44	1.26
56.00	65.88	220	3.1	0.0249	1.32	1.72	1.31	1.67	1.27
65.55	77.12	230	4	0.012	1.21	1.20	0.99	1.27	1.05
65.55	77.12	230	4	0.025	1.40	1.65	1.18	1.62	1.15
65.55	77.12	230	4	0.033	1.64	1.87	1.14	1.78	1.08
80.04	94.16	230	4	0.016	1.34	1.48	1.11	1.49	1.12
77.97	91.73	230	4	0.025	1.41	1.79	1.26	1.72	1.21
63.48	74.68	230	6	0.012	0.92	0.99	1.08	1.10	1.20
63.48	74.68	230	6	0.025	1.29	1.36	1.06	1.40	1.08
						Mean	***1.04***		***1.00***
						St.Dev.	***0.29***		***0.27***